NOVEL DENDRIMER-BASED NANOCARRIERS TARGETING HER2 RECEPTOR AND ENCAPSULATION IN ALGINATE MICROPARTICLES BY MICROFLUIDICS FOR THE TREATMENT OF BREAST CANCER

Giordana Maria Stella Mateko Peregrino

A thesis submitted in partial fulfilment of the requirements of the University of Brighton for the degree of Doctor of Philosophy

February 2024

ABSTRACT

Breast cancer is one of the most common cancers in the world, diagnosed in 2.3 million women last year, 15-20 % of which have been reported to be HER2 positive. This molecular subtype is caused by an overexpression of the human epidermal growth factor (HER2) receptors on breast cancer cells that cause rapid and uncontrolled cell growth leading to a more aggressive type of cancer.

In this work, selective nanoparticles for the HER2 receptor were prepared. The vectors used were dendrons, novel peptides composed of hyperbranched poly-L-lysine dendrons or linear (K16) versions with or without a HER2 targeting sequence (LSYCCK) or a scrambled version (SGen3K) were synthesised and tested. Hyperbranched peptides electrostatically bind the negative charges of nucleic acids thus, are capable of carrying either DNA or small interfering RNA (siRNA) molecules.

Different behaviours were identified based on the nature of the nucleic acid cargo when tested in MDA-MB-231 and SKBR3 cells. In the case of DNA delivery, experiments were conducted on cells overexpressing the target receptor (HER2). Both the selective peptide (TGen3K) and the branched and linear controls were found to be inadequate for efficient transfection. However, the addition of a small quantity of lipids (DOTMA:DOPE) was necessary to achieve high levels of transfection. In this case, the lipid helper (DOPE) likely facilitated endosomal-escape. Furthermore, TGen3K was shown to be selective for the receptor. However, the scramble control (SGen3K) proved to be even more effective (twice/three times more) than the reference peptide, possibly due to better DNA packaging resulting from the different arrangement of amino acids.

In the case of siRNA delivery, on the other hand, the presence of lipids was found to be unnecessary. Confocal microscopy has revealed how the structure itself has an anti-proliferative effect and how the target sequence (KCCYSL) is selective for the HER2 receptor. It has also shown that peptides, particularly RGen3K and TGen3K, are capable of internalising the siRNA.

Finally, the nanocarriers were encapsulated in alginate microparticles following various studies that optimised the gelation of alginate microparticles. As a result, the chosen preparation for the encapsulation of the nanocarriers will be based on in-chip gelation.

The encapsulation of the nanocarriers highlighted the ability of the microparticles to retain and protect the nanocarriers during the washing of the microparticles to remove the oily phase following emulsion rupture. The nanocarriers are subsequently released within 24 hours when placed in an environment simulating the extracellular environment.

CONTENTS

LIST OF TABLES

LIST OF FIGURE

List Of Abbreviations

ADCC	Cell-Mediated Dependent Antibody Cytotoxicity
ADCC	Antibody-Drug Conjugate
AGO2	Argonaute
AKT	Protein Kinase
ALAS1	Amino Levulinate Synthase 1
ASCVD	Clinical Atherosclerotic Cardiovascular Disease
ASGPR	Asialoglycoprotein Receptor
ASOS	Inhibitory Antisense Oligonucleotides
ATM	Ataxia Telangiectasia Mutated
ATP	Adenosine Triphosphate
BBB	Blood Brain Barrier
BCA	Ad Bicinchoninic Acid
Bcl2	B-Cell Lymphoma 2
Boc	Terbutyloxycarbonyl
BRCA1	Breast Cancer 1
BRCA2	Breast Cancer 2
BSA	Bovine Serum Albumin
Ca	Capillary Number
$CaCl_2$	Calcium Chloride
$CaCO_3$	Calcium Carbonate
CD3	Cluster Of Differentiation 3
CD34	Transmembrane Phosphoglycoprotein Protein
CD47	Cluster Of Differentiation 47
CDK	Cyclin Inhibitor
CH_3COOH	Acetic Acid
CHEK2	Checkpoint Kinase 2
CI	Integrated Circuits
CM	Cell Membrane

CM	Cellular Membrane
CME	Clathrin-Mediated Endocytosis
CRISPR/Cas9	Clustered Regularly Interspaced Short Palindromic Repeats
DAPI	4',6-Diamidino-2-Phenylindole
DCIS	Ductal Carcinoma In Situ
DCM	Dichloromethane
DIPEA	Diisopropylethylamine
DLS	Dynamic Light Scattering
DMF	Dimethylformamide
DMRIE	N-(2-Hydroxyethyl)-N,N-Dimethyl-2,3-Bis(Tetradecyloxy)Propan-1-Aminium Bromide
DNA	Deoxyribonucleic Acid
DOPE	1,2-Dioleoyl-Sn-Glycero-3-Phosphoethanolamine
DORI	N-(2-Hydroxyethyl)-N,N-Dimethyl-2,3-Bis(Oleoyloxy)Propan-1-Aminium Bromide
DORIE	N-(2-Hydroxyethyl)-N,N-Dimethyl-2,3-Bis(((Z)-Octadec-9-En-1-Yl)Oxy)Propan-1-Aminium Bromide
DOTAP	1,2-Dioleoyl-3-Trimethylammonium-Propane (Chloride Salt))
DOTMA	N-[1-(2,3-Dioleyloxy)Propyl]-N,N,N-Trimethylammonium Chloride
DSPC	1,2-Distearoyl-Sn-Glycero-3-Phosphocholine
dsRNA	Double-Stranded Rna
EAC	Ehrlich Ascites Carcinoma
ECM	Extracellular Matrix
EDC	N-(3-Dimethylaminopropyl)-N'ethycarbodiimide Hydrochloride
EDTA	Ethylenediaminetetraacetic Acid
EGFR	EGF Receptor

EMT	Epithelial-Mesenchymal Transition
EPR	Enhanced Permeability And Retention
ER	Oestrogen Receptor
ERBB1 or EGFR	Human Epidermal Growth Factor Receptor 1
ERBB2 or HER2	Human Epidermal Growth Factor Receptor 2
ERBB3 or HER3	Human Epidermal Growth Factor Receptor 3
ERBB4 or HER4	Human Epidermal Growth Factor Receptor 4
ERK1	Extracellular Signal Regulated Kinases 1
ERK2	Extracellular Signal Regulated Kinases 2
FBS	Foetal Bovine Serum
FDA	Food And Drug Administration
FTIR	Fourier Transform Infrared Spectroscopy
GalNAc	N-Acetylgalactosamine
HAO1	Hydroxy Acid Oxidase 1
HBTU	O-(1h-Benzotriazole-1-YI)-N,N,N0,N0-Tetramethyluronium Hexafluorophosphate
HDI	High Development Index
HPLC	High Pressure Liquid Chromatography
IARC	International Agency For Research On Cancer
IDC	Infiltrative Ductal Carcinoma
IGF-1R	Insulin-Like Growth Factor 1
III Rnase/Dicer	3' Two-Nucleotides Overhangs By A Ribonuclease
IJM	Impingement Jet Mixer
K16	16 Poly-Ɛ-Lysine
L2K	Lipofectamine 2000
L3K	Lipofectamine 3000
LDH	Lactate Dehydrogenase
LDL-C	Lipoprotein-Cholesterol
LNP	Liposomes And Lipid Nanoparticles

LPD	Lipopolyplexes - Lipid:Peptide:Dna
LPR	Lipopolyplexes - Lipid:Peptidesirna
LSYCCK	Leu-Ser-Cys-Cys-Lys
mAb	Monoclonal Antibody
MAO	Monoamine Oxidase
MAP	Multiple Antigen Peptide
MAPK	Mitogen Activated Protein Kinases
MEK1	Mitogen Protein Kinase
MEK2	Mitogen Protein Kinase 2
MEMS	Micro Electro Mechanical Systems
miRNA	MicroRNA
MMPS	Matrix Mononuclear Phagocyte System
MPS	Mononuclear Phagocyte System
MPs	Microparticles
mRNA	Messenger RNA
MS	Mass Spectrometer
NAD+	Oxidase Nicotinamide-Adenine-Dinucleotide
NADH	Nicotinamide-Adenine-Dinucleotide
NHS	N-Hydroxysuccinimide
NIH	National Cancer Institute
NP	Nanoparticle
O/W	Oil In Water
PALB2	Partner And Localiser Of Brca2
PAMAM	Poly(Amide Amide)
PBS	Phosphate Buffered Saline
PCR	Polymerase Chain Reaction
PCSK9	Proprotein Convertase Subtilisin/Kexin Type 9
PD	Polyplexes-Peptide:Dna
PDI	Polydispersity Index
PDMS	Dimethylpolysiloxane Or Dimethicone

pDNA	Plasmid DNA
PEG	Polyethylene Glycol
PEI	Poly(Ethylene Imine)
PFA	Paraformaldehyde
PGB	Porphobilinogen
PgR	Progesterone Receptor
PH1	Primary Hyperoxaluria Type 1
Pi	Isoelectric Point
PI3	Phosphatidylinositol 3,4,5-Trisphosphate
PI3K	Phosphatidylinositol 3,4,5-Trisphosphate Kinase
PLA	Poly Lactic Acid
PLGA	Poly(Lactic-Co-Glycolic Acid)
PLL	ε-Poly-L-Lysine
PPI	Poly(Propylene-Imine)
pRB1	Proline Rich Protein Bstni
PR	Polyplexes - Peptide:Sirna
PTEN	Homologous Tensin Phosphatase
RAF	Rapidly Accelerated Fibrosarcoma
RAS	Rat Sarcoma Virus
Rb	Retinoblastoma
Rb1	Retinoblastoma
Re	Reynolds Number
RES	Reticuloendothelial System
RGen3K	Arg-K16
RISC	RNA-Induced Silencing Complex
RLU	Relative Light Units
RNA	Ribonucleic Acid
SGen3K	CSCYLK(Gen3k)
siRNA	Short Interference RNA

SIRPa	Signal-Regulatory Protein Alpha
SPPS	Solid Phase Synthesis
TAE	Tris-Acetate-EDTA
TDLU	Terminal Ductal-Lobular Unit
T-DM1	Trastuzumab Emtansine1
TFA	Trifluoroacetic Acid
TGen3K	LSYCCK(Gen3k)
TIPS	Trisopropyl Silane
TK16	LSYCCK(K16)
TNBC	Triple Negative Breast Cancer
TRPM8	Transient Receptor Potential Cation Channel Subfamily M Member 8
v_c	Flow Velocity
VEGF	Vascular Endothelial Growth Factor
W/O	Water In Oil
γ_{cd}	Interfacial Energy
μ_c	Fluid's Viscosity

ACKNOWLEDGEMENTS

First and foremost, I would like to thank my brilliant supervisors. Professor Marco, I have never really understood physics, and I don't think that it will change in the future. However, when you explain it, you manage to instil all the passion you have for this science. Professor Laila, you are my source of inspiration, and thank you for all the support in the lab. I have treasured all your suggestions and hope to pass them on in the future with the same care and attention.

Finally, Professor Matteo, thank you for all the patience you have shown me and, most importantly, for guiding me over these three years. Additionally, I thank you for being my mentor for both professional and personal growth.

A huge thank you to the entire "Cool Lab" group (Aryako, Narjes, Shirin, and Alex) and others (Shima). Finally, room H415 is no longer quiet! You have been a tremendous help and have managed to comfort me even in the most challenging moments. Take care of my pipettes!

Heartfelt thanks to all my Brighton/London friends, including Cri, Gui, Picco, Luca, Marianna, Roma, Thias, Berna, Fadi, Maria, Enrico, Camila, and Anjuman. You have shown me the funny side of the city and continually inspire me to push my limits. To Pierre, Ismail, Milad, Kapil, Roya, and Nancy: you have made me feel like a part of the group.

Thanks to my lifelong friends scattered across Europe but always close at heart.

Lastly, a special thank you to Mamuska, Emma, Pietro, Nonna, and Federico. Without you, I couldn't have even imagined completing all of this.

Giordana

DECLARATION

I declare that the research contained in this thesis, unless otherwise formally indicated within the text, is the original work of the author. The thesis has not been previously submitted to this or any other university for a degree, and does not incorporate any material already submitted for a degree.

Signed

Date

INTRODUCTION AND LITERATURE REVIEW

1.1 TARGETED MEDICINE

Targeted medicine is a branch of medicine that aims to be achieve higher efficacy than traditional medicine through the development of drugs and carriers for the controlled release of therapeutics that considers heterogenicity in patients' populations. Currently, many medicines, despite being extremely advanced, are inefficient on a high percentage of patients. It is estimated that the top ten best-selling drugs in America have the desired effect on only one in four patients, at worst one in twenty-five. Some drugs are potentially harmful to certain ethnicities that are often not considered in clinical trials [1].

In a society increasingly attentive to the needs of the individual, targeted medicine also changes direction and focuses on genetic variability, individual differences, allowing to sew *ad hoc* treatment for the individual. Targeted medicine is supported by the huge developments in genetics, genomics, transcriptomics, proteomics and metabolomics that allow to determine the heterogeneous nature of many diseases [2].

Like many diseases, neoplasms have also shown a deep connection with genomic mutations that become the new targets of pharmacological treatments. Identifying new targeted therapies avoids exposing the patient to unnecessary side effects that can have long-term effects in terms of prognostic, safety, relapse and cost implications [3].

To date, the "histological" model has prevailed in the field of oncology and thus the initial localisation and origin of the tumour as well as the subsequent choice of the drug have been based on the outcome of histological examinations. Recently, with the "mutational" model

becoming available, the key point is the identification of the molecular alterations that cause the development of the neoplasm, hence the drug therapy is chosen regardless of the location of the tumour, the sex of the patient or age [4].

1.2 CARCINOGENESIS

The process leading to the development of cancer, known as carcinogenesis, does not have a definite trend. On the contrary, it can be said that each cancer has its own history, which can take place in a short time or over the years or even decades. In general, cancer begins when the cells that make it up no longer respond to the normal restrictions that regulate, among other factors, proliferation and cell death.

The growth of the tumour does not occur all at once, but it usually requires a prolonged period of time and complex genetic changes that cause the transformation first into a benign tumour and then into a malignant one [5]. Three phases that characterise the development of the tumour and can be distinguished as it follows [6]:

- *Initiation*: when starting agents (physical, chemical or biological) alter the structure or expression of DNA.
- *Promotion*: promoting agents reversibly affect proliferating activity, increasing or decreasing gene expression by binding to the membrane or nuclear receptors, or by modifying signal transduction by inducing micro-traumas or chronic inflammation.
- *Progression*: infiltration of tissue metastases.

1.2.1 Initiation

The initiation phase represents the first stage of changes and chemical alterations of the genetic material in cells capable of proliferating and

surviving throughout the patient's life. Cell's genetic alteration, can be considered as mutations, amplifications and decreased efficiency of DNA repair mechanisms [7].

Typically, initiating agents are cellular electrophilic compounds that alter the structure of DNA (nucleophile). Direct initiating agents are those that do not require chemical activation, indirect agents require metabolic activation in vivo that gives rise to electrophilic compounds with transforming abilities genomic structure [8].

However, only 5%/10% of cancers are related to genetic heredity, it is estimated in fact the majority of tumours (about 95%) are caused by environmental factors [9]. Indeed, "environmental factors" as tobacco use, alcohol, diet habits, daily work conditions and related stresses, sunlight irradiation and infections are also included. Many of these "environmental pitfalls" can act together increasing the risk of cancer [10, 11].

1.2.2 Promotion

The second phase in the development of a tumour is called promotion. This phase involves the multiplication of initialised cells, and the number of accumulated alterations will be proportional to the number of duplicates. The agents that cause promotion (promoters) can be substances spread in the environment or even some drugs and hormones [12,13]. Unlike carcinogens, the promoters do not cause the tumour on their own, but rather allow initiation cells to become cancerous. Promotion does not affect cells that have not been subjected to initiation [14]. Therefore, the tumour develops by the action of several factors, including, often, the association of a sensitive cell and a carcinogen [15].

1.2.3 Progression

Progression is the malignant phenotypic expression of the tumour and acquires aggressive characteristics over time. Cells begin to compete with each other for survival leading to a further increase in the number of mutations that make them aggressive. As the tumour grows, so does the genetic heterogeneity between cells. Cancer can grow directly in the surrounding tissue or spread to tissues or organs, near or far, moving away from the primary tumour site. Fundamental for cellular mobility is the increased activity of the cytoskeleton and the matrix as a result of mutations, which allow the tumour cell to migrate. Another necessary factor for cancer cell is escape from apoptosis (programmed cell death) [16, 17]. Ultimately, during tumour growth, nutrients come from the blood stream. Local growth is fostered by enzymes (e.g., proteases) which degrade adjacent tissues. As the tumour mass increases, tumours produce angiogenic factors, such as the growth factors for the vascular endothelium (e.g. Vascular endothelial growth factor, VEGF), that promote the formation of new vessels, necessary for a further growth of the tumour. Although most circulating cancer cells die in the intravascular compartment, occasionally individual cells can adhere to the vascular endothelium and penetrate the surrounding tissues generating tumour masses independent of the primitive tumour (metastases). Metastases grow in the same way as primitive cancer and can later originate other metastases [18].

1.2.4 Intracellular Control

While the proliferation of youth cell is under strict control, abnormal cells are constantly being produced and could turn into malignant cells. It has been estimated that, to ignore control systems, the cell will have to undergo four to seven independent genetic or epigenetic events [19].

Cellular homeostasis, lost due to mutations in genes that control proliferation, causes an uncontrolled growth of the tumour.

Uncontrolled growth can be a direct consequence of a mutation on genes which control proliferation or increased genetic instability that raise the mutation rate leading to a high probability of losing cell control proliferation. Cell proliferation control depends on two gene groups: some support cell division (oncogenes), while others inhibit the proliferation (onco-suppressor).

1.2.5 Proto-Oncogenes

Proto oncogenes are genes that regulate important events in cellular life such as growth and differentiation and, if mutated, can favour the appearance of tumours. Mutation of these genes can lead to changes in the activity of cell surface receptors for growth factors, intracellular signal transduction pathways and transcription factors, controlling cell division and growth, cellular metabolism, DNA failure duplication, angiogenesis, and other physiological processes. By losing cellular homeostasis and not controlling cell duplication, the chances of genetic errors on the DNA strand increase, especially on oncogenes [20,21].

However, following the accumulated mutations, not all cells are suitable for survival and reproduction, only some will be able to adapt to the surrounding environmental conditions, but sufficient to initiate tumour growth [22].

In the human body, approximately hundred oncogenes potentially capable of contributing to the neoplastic transformation process are known. For example, the RAS gene encodes RAS protein, which triggers signals from receptors anchored to the plasma membrane along the RAS-MAP kinase pathway to the nucleus of the cell regulating cell division. For

example, an RAS effector is RAF that when activated, phosphorylates and activates proteins called proteins Mitogen Protein Kinases (MEK1 and MEK2) which, on their turn, phosphorylate Mitogen Activated Protein Kinases (MAPKs) and ERK1/ERK2 (Extracellular Signal Regulated Kinases) responsible for cell cycle progression and cell growth [23]. The RAS protein is altered in about 25% of human neoplasms [24,25].

1.2.6 Tumour Suppressors

Onco-suppressors, are genes that constantly monitor the integrity of the genome and control onco-gene activity. A mutation on tumour suppressor genes causes tumour development. It can be divided into two classes: gate-keeper type and care-taker type. Care-takers are those genes that maintain the integrity of genetic information, constantly repairing the damage suffered by DNA by genotoxic agents. Therefore, care-takers avoid carcinogenesis in an "indirect" way, reducing the risk of the cell developing mutations in oncogenes and onco-suppressants [26].

A malfunction of onco-suppressor genes resulting in inherited or acquired mutations, leads to an inefficiency of the genome integrity monitoring system, the persistence and proliferation of cells with spontaneous mutations and the formation of tumours.

An example of a care-taker onco-suppressor gene is the important regulatory protein, p53 encoded by TP53 gene, prevents the replication of damaged DNA in normal cells and promotes programmed cell death (apoptosis) in cells with altered DNA and detects and corrects possible errors on the genetic strand following cell replication. Impaired or inactive p53 allows cells with damaged DNA to survive and divide, nonetheless TP53 is frequently inactivated in many human neoplasms, including lymphomas, sarcomas, brain tumour and colon, lung and breast

carcinomas. Furthermore, according to recent studies it has been shown that changes on a single allele cause similar outcomes in patients with no TP53 variations and have good response to drug treatment, slow progression and higher survival rates [27,28].

Gate-keepers are tumour suppressor genes that have the ability to counteract directly the acquisition of the neoplastic phenotype by opposing the acquisition of fundamental characteristics such as: uncontrolled reproduction, insensitivity to anti-proliferative stimuli, resistance to apoptosis, resistance to senescence, metastasis and angiogenesis [29]. Gatekeepers therefore perform an opposite action to that of oncogenes which instead promote the acquisition of cancer hallmarks.

An example of cancer caused by malfunctioning tumour suppressor genes is Retinoblastoma (Rb), a malignant eye tumour that develops from retina cells and which can occur at any age, but onset is more common in childhood before age five. Hereditary retinoblastoma is due to the transmission of the diseased Rb1 gene from parent to child. Patients with the mutation will have a strong predisposition to the onset of the disease and risk developing the disease much more quickly.

In the case of Sporadic Retinoblastoma, the disease begins when the cells of the retina operate a genomic deletion or a mutation occurs on both alleles of the tumour suppressor gene RB1, located on chromosome 13 [30,31].

The Rb1 gene synthesises for a 110 kDa phosphoprotein, pRb1/p105, which regulates the cell cycle. To transform a normal retinal cell into neoplastic, it is necessary and sufficient that both homologous genes coding for the protein are altered. Mutations or deletion of the RB1 gene are responsible for the inactivation of the two alleles and are crucial

events in tumour development. Lack of the protein results in a lack of cell growth regulation and rapid and uncontrolled division [32].

1.2.7 Organism Defence

Genetic defects acquired by cancer DNA are also reflected on the extracellular environment. Surrounding tissue exerts strong control over new cancer cells and may cause cell death or metastasis [33]. Genetic defects are not driven by only the inner cell environment, in fact the extracellular area can regulate the tumour growth. The micro-environment constantly communicates and evolves according to the needs of adjacent cells thus, determining the fate of the tumour.

The microenvironment changes based on the surrounding organs, but the key components are the extracellular matrix (ECM) which is rich in proteoglycans, hyaluronic acid, fibrous proteins and stromal cells. The latter include fibroblasts, adipocytes, vascular and immune system cells. Finally, small molecules such as growth factors and metabolites [34,35].

A fundamental event in the formation and progression of the tumour is represented by the formation of a peculiar tumour microenvironment and, in particular, by the interaction of the cancer cells that are part of the invasive carcinoma and its stromal component. Cancer cells stimulate the *de novo* formation of connective tissue, in order to provide stromal support for the development of tumour [36].

Nonetheless, crowding and lack of resources should help to contain (self-limiting) clonal expansion. The state of latency (pre-malignant) would be characterised by the fact that the increased proliferative potential is counterbalanced by the limitation of resources. This is a well-known factor, which dictates a strong selective pressure within an ecosystem in which each population is affirmed, contracts or extinguishes in function of

energy availability. The situation of overcrowding establishes a toxic environment for normal cells (hypoxia, acidosis), while neoplastic cells can ensure greater absorption of nutrients, by amplifying the expression of glucose transporters on the surface of cancer cells, or by using anaerobic glycolysis (the Warburg effect) [37,38].

In these conditions it is also favoured to get the degradation of the extracellular matrix and the cell junction's relaxation is a key step in the acquisition of invasive capability, that enables cancer cells to encroach tissues escaping the high population density and causing further deterioration of the local conditions. Under the pressure of the various limiting factors and thanks to the relaxation of the tissue connections, some cells can enter the circulatory or lymphatic stream to colonise new healthy tissues (metastases). Moreover, the transition to the most malignant state is marked by necessity of acquiring nutrients and this can be achieved even through another expedient, i.e. stimulating the formation of new blood vessels (neo-angiogenesis)[39,40]. In fact, the supply of oxygen and nutrients is constantly assured by the network of the bloodstream in tumours like any growing tissue. However, after a certain point, tumour will have a critical mass that will no longer allows all cells to receive an adequate intake from existing vessels, nor to remove waste substances efficiently [41]. This suffering situation represents an intrinsic limitation to growth: cells can neither multiply nor survive unless a new microcirculation is created. Thus, there would be a competition/selection phase with the expansion of some subpopulations and the contraction of others, at least until the tumour begins to produce angiogenin, a molecule that recruits healthy cells to form new vessels and support tumour growth [42].

1.3 BREAST CANCER

1.3.1 Mammary Gland Anatomy

The mammary gland, Figure 0.1, is an even apocrine gland situated in the superficial fascia of the pectoral region, it is extremely variable and dynamic but characterised by some constant elements. The upper limit of the mammary gland is at the anterior arch of the 2nd -3rd rib, while the lower limit is at the anterior arch of the $6^{th}/7^{th}$ rib. The median limit is represented by the sternal margin line, the lateral coincides with the average axillary line. There is a great individual variability in shape and size also in relation to the different constitutional types: in the same woman, then, the mammary gland changes in the different stages of the menstrual cycle, in the different ages, in a possible pregnancy.

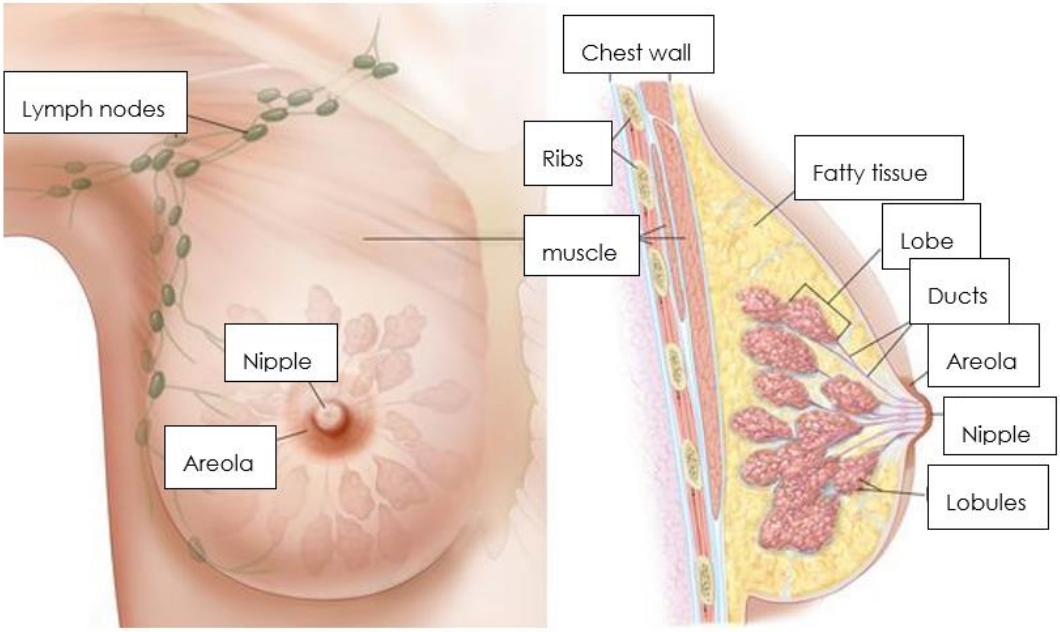

Figure 0.1 Anatomy of female Breast. From: https://www.cancer.gov/publications/dictionaries/cancer-terms/def/mammary-gland.

The anatomy of the gland can be divided in three tissues: the skin, the parenchyma and the stroma. The skin comprehends the nipple and the areola [43]. The *nipple* usually conically protrudes for 6-10 millimetres but there is great individual variability sometimes it can be umbilicated or even introflexed. On the nipple are located 15/20 lactiferous orifices, which constitute the outlets of the lactiferous ducts. The nipple is rich of circular and longitudinal smooth muscles and nerves. The *areolar region* (differently pigmented than the surrounding skin varying from pink to brown) consists of skin, poor subcutaneous tissue and a layer of smooth muscle that allows the complex areola-nipple to contract, especially during lactation. On the areola there are small protrusions called tubercles of Montgomery, which represent the excretion pores of sebaceous glands located in the retro-areolar subcutaneous, to which are attributed

bactericidal and odoriferous functions, the latter to make the milk more pleasant for the new born [43].

The *parenchyma* is a glandular tissue made up of branching ducts, called lactiferous ducts that drain all the terminal secretory lobules which varies from 15 to 20 lobes. The ducts expand to form the lactiferous sinus where the milk is collected and open individually into the nipple.

Finally, the *stroma* is the supporting matrix surrounding the parenchyma. The fatty stroma is the main tissue in the mammary gland and the percentage varies individually while its weight may differ from 30 g to more than 1000 g. In the fibrous stroma there are septa called suspensory ligaments of Cooper, which suspend the gland from the pectoral fascia and separates lobes. The glandular tissue is supported by a massive arterial, venous and lymphatic system.

- *Arterial blood* is derived from five arteries: internal thoracic artery, lateral thoracic artery, superior thoracic artery, acromion-thoracic artery and branches of posterior intercostal artery.
- The *venous system* forms a circular system (anastomotic) around the nipple and is divided into: (i) internal thoracic veins and superficial veins of the lower neck (both superficial); (ii) internal thoracic vein, axillary and posterior intercostal veins (deep veins).
- *Lymphatic drainage* can be divided in two subgroups of lymph nodes. The first is the axillary nodes and are made up of the: pectoral group, the subscapular group (posterior), lateral group, central and apical group. The second cluster, the parasternal nodes, which drains almost 20/25% of the lymph from the breast region through the internal thoracic mammary lymph nodes located along the edge of the sternum body, while the axillary group drains 75/80% of breast lymph [44].

1.3.2 Histology and Physiology

The mammary gland is composed from the histological point of view of ducts and berries immersed in a stromal tissue that represents the majority of the parenchyma of the adult breast and is composed of a variable percentage of fibrous and adipose tissue. The glandular structure proper has instead a "tree in flower" structure, with the major galactophore ducts that branch from the nipple into ductal structures progressively smaller up to the ducts of the so-called TDLU, acronym for Terminal Ductal-Lobular Unit [45]. The TDLU consists of:

- Terminal ductuli or acini, the epithelium of which undergoes secretory changes during pregnancy and lactation, forming secretory berries or lactation glands;
- intralobular collector duct;
- specialised intra-lobular stroma

Ducts, ductuli and acini are therefore tubular structures with an empty lumen and a wall composed of a double layer of cells: an internal layer composed of epithelial cells that stand towards the lumen of the tubules, called therefore "luminal cells", which have a cuboidal or low columnar shape; an outer layer composed of myoepithelial cells, which are therefore the "basal cells".

These two types of tubule wall cells differ not only in their shape and position, but also because they express different markers, which can be identified with specific immuno-histochemical stains. TDLU is the functional unit of the mammary gland and represents the site from which most carcinomas originate (both in situ and invasive forms).

If the ductal structures are characterised by a substantial stability, the TDLU are instead dynamic structures, which follow the phases of the menstrual cycle and under oestrogen hormonal stimulus undergo proliferation, while

in the progestin phase they undergo regression. For instance, the mammary gland in the post-pubertal period is extremely compact and, whether investigated with mammography, would appear very dense and it will be difficult to identify its components. Fertile women are prone to hormonal variations of the menstrual cycle, i.e., to the oestrogen stimulation in the first part of the cycle (1st-14th day), induces proliferation of the epithelium of the ducts. Afterwards, during the ovulation phase, the progestin causes hyperplasia and oedema of the stroma by the prevalence hydro-saline retention. While, with menopause the gland undergoes atrophy, with shrivelling of the stroma and disappearance of glandular tokens. On the contrary, during pregnancy circulating hormones induce hypertrophy of the gland, suitable for lactation. While during the late pregnancy stage, prolactin hormones induce the sinuses to be filled with milk that will shrink and decrease in number when lactation ends. Otherwise, there is an inversion of the gland-stromal ratio and the breast at the end of the pregnancy consists predominantly of glandular lobules and poor stroma [43].

As for the stromal component of the mammary parenchyma, it is possible to identify a stroma rich in collagen between the lobules (the so-called "inter-lobular stroma") and a stroma that is instead located within the single lobule (the "intra-lobular stroma").

The intra-lobular stroma is loose and with a rich fibrovascular component, and is populated by lymphocytes, plasma cells, macrophages and mast cells; this stroma is reactive to hormonal changes and, for example, under the stimulus of oestradiol becomes very oedematous.

Hormones also have effects on the glandular component of the parenchyma: oestrogen, progesterone and androgens promote differentiation and proliferation of luminal cells, while oxytocin causes contraction of myoepithelial cells. Hormone receptors, namely the

oestrogen receptor (ER) and the progesterone receptor (PgR) are expressed in the normal breast, but at low levels and in a heterogeneous way between one lobe and the other (in addition, in the ducts they are even less expressed than in the lobules).

The glandular component produces milk and is active only during pregnancy and lactation, that is, when the development of the breast is complete. In this period of adult life the proliferation of epithelial cells starts again under the stimulus of ER, PgR, prolactin and growth hormone: as a result, we see an increase in the number of lobules at the expense of the stroma, both intra-lobular and inter-lobular.

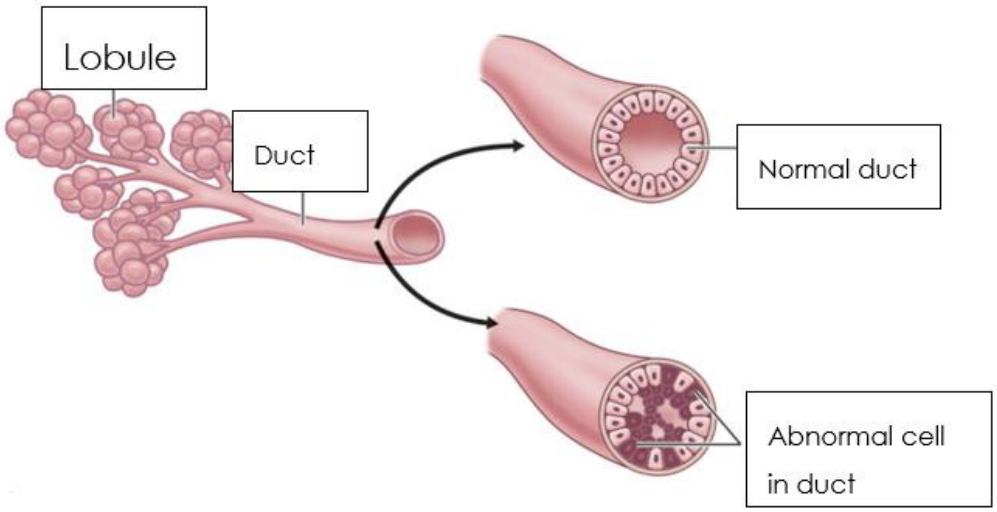

Figure 0.2 Ductal carcinoma in situ. From: https://thoracickey.com/11-breast-anatomy./.

The mammary gland also undergoes secretory modifications: the luminal cells acquire a foamy cytoplasm (because it contains numerous fine lipid vacuoles) and a typical "hobnail" appearance, characterised by vesicular nuclei with prominent nucleoli: the secretion produced by these cells accumulates in the expanded lobules. The so-called "lactation modifications" may also be present outside pregnancy and may alarm

because of the cytological atypic that characterises them: should not be confused with atypical proliferations and carcinoma, in particular with "clinging" ductal carcinoma in situ (CDIS), shown in Figure 0.2.

With advancing age, following the decrease of hormonal stimulation by ER and PgR in the post-menopausal period, the gland undergoes regressive modifications with adipose involution. In more detail, the TDLU become atrophic losing also the intra-stroma specialised lobular and the ducts can become ecstatic. The nipple and areola are covered by a squamous epithelium type multi-layered keratinising that is introduced focal to the superficial outlets of the galactic ducts [43].

1.3.3 Incidence

Breast cancer is the most frequently diagnosed malignancy in the world accounting for 25.5% of all female diagnosed neoplasms in 2020. International Agency for Research on Cancer (IARC) 2020 stated that 2,261 million new cases have been diagnosed worldwide in 2020 and 53,889 in the United Kingdom making it the most common in the world female population. Breast cancer incidence remains higher in developed Countries thanks to a longer life expectancy, industrialisation and screening programmes. This difference is highlighted in the Figure 0.3. In 2020 there were over 70 per 100,000 women in developed countries compared to below 40 per 100,000 women in developing nations diagnosed with breast cancer (International Agency for Research on Cancer (IARC) 2020).

The mechanism can be attributed in part to the change in the prevalence and distribution of different reproductive and hormonal factors, including a tendency to first menstruation in more advanced ages as well as for early births. These changes can partly explain the rapid increases in breast

cancer incidence rates in several countries in Asia (e.g., India, Japan, Thailand and Turkey) and Latin America (e.g., Costa Rica and Ecuador).

By contrast, in countries with high HDI (high development index) like Australia, Canada, the United Kingdom and the United States, incidence rates stabilised after a marked decline in initial incidence in about 2000. This according to some studies is due to the harmful effects of hormone replacement therapies in menopause.

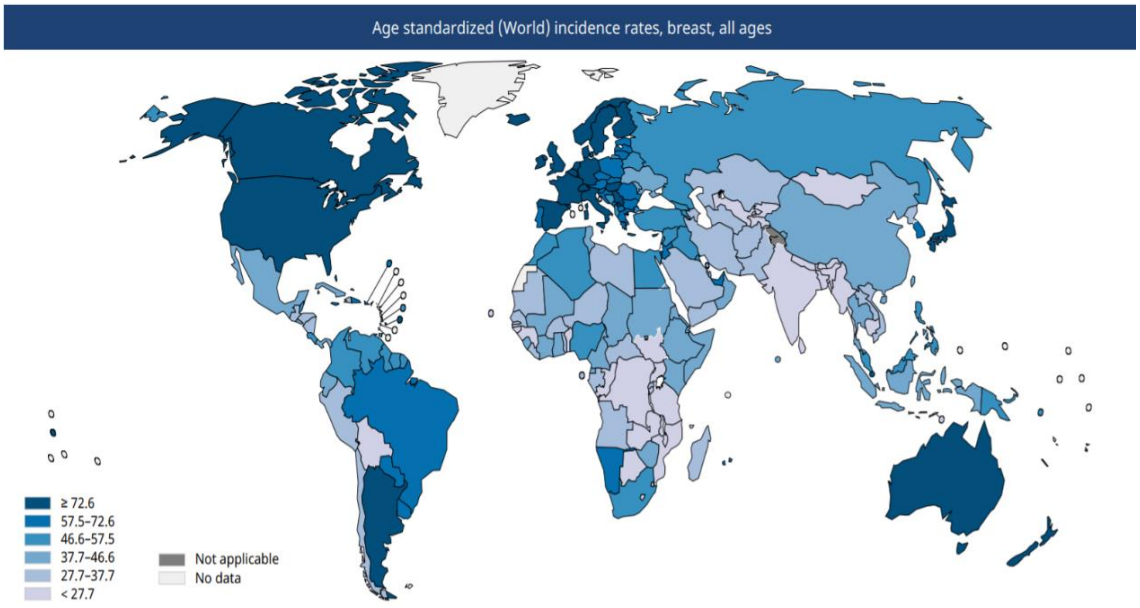

Figure 0.3 Standardised Breast Cancer worldwide incidence in 2020 (IARC).

Dietary factors (including an increasing prevalence of alcohol consumption in women) obesity and physical inactivity cannot be excluded as potential emerging causes in countries with high HDI where there has been an increase in this regard also in women outside the screening age.

1.3.4 Mortality

Breast cancer is the most common cause of death worldwide. Once the cancer is diagnosed, women in the world do not have the same chances of recovery. In high-income countries, mortality rates for premenopausal cancers are around 11% of diagnoses (Figure 0.4).

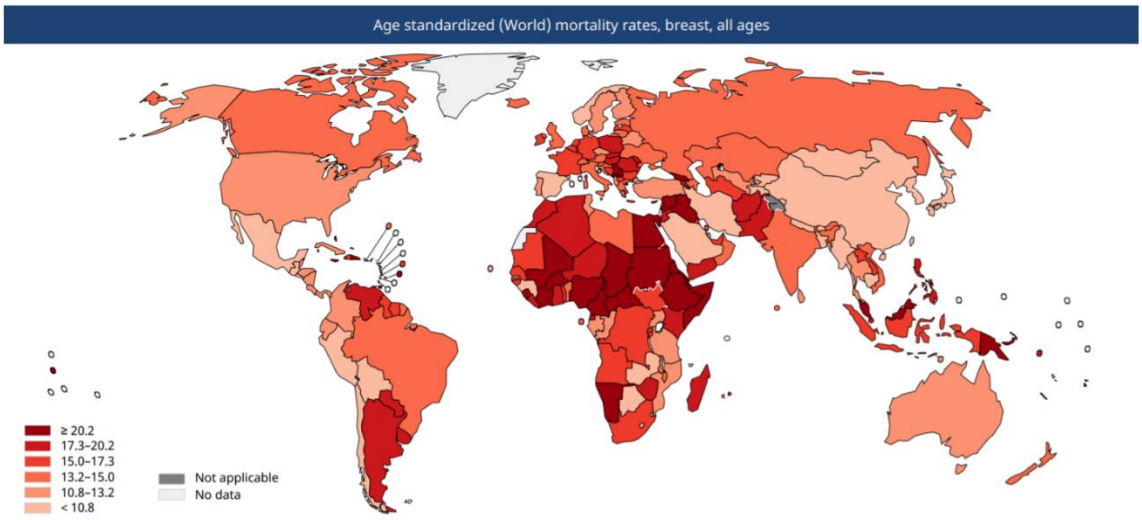

Figure 0.4 Standardised Breast Cancer worldwide deaths in 2020 (IARC).

In low-income countries, like Melanesia and Western Africa the mortality rate reach the 25%. Doubled since too many communities still do not have access to the changes that have improved life expectancy in Europe, such as early detection, screening and effective treatment.

1.3.5 Molecular Classification

Infiltrative ductal carcinoma (IDC), also known as infiltrative carcinoma or invasive breast carcinoma, is a very common type of breast cancer. It

begins proliferating in the milk ducts of mammary tissue and later invades the duct tubes and invades or infiltrates surrounding tissues.

Unlike ductal carcinoma in situ (DCIS) which is a non-invasive tumour, IDC is not a well-contained cancer since it has the potential to invade lymph and blood systems, spreading cancer cells to other parts of your body (metastasis) [46].

IDC is molecularly divided into five main intrinsic subtypes based on the receptors that tare overexpress on the breast cancer cell surface. the receptors considered for the classification are the oestrogen (ER), progesterone receptor (PR), human epidermal growth factor receptor 2 (HER2), and a proliferation marker known as Ki67. The subgroups are the following (Table 0.1):

- *Triple-negative/basal-like breast cancer (TNBC)* is characterised by total absence of oestrogen, progesterone and HER2. It is considered the most aggressive type of breast cancer and it is more common in younger patients and patients with BRCA1 mutations.
- *Luminal A* breast cancer is oestrogen and/or progesterone, HER2 negative, and has low levels of the protein Ki-67. This type grows slowly compared to other types, and luminal A shows good response to anti-oestrogen treatment and good prognosis.
- *Luminal B* breast cancers are oestrogen and/or progesterone, and either HER2 positive or HER2 negative with high levels of Ki-67. Luminal B tend to grow slightly faster than luminal A cancers. Although can respond to hormonal treatments but have a prognosis worse than Luminal A.
- *HER2-enriched* breast cancer is negative to oestrogen and progesterone receptors and HER2 positive. Although these cancers are often successfully treated with targeted therapies (anti-HER2), however, patients with this subtype can have a poorer prognosis [47].

- *Normal-like* breast cancer is similar to luminal A type of breast cancer: it is hormone-receptor positive (ER and/or PR positive), with low levels of Ki-67. Patients with Normal-like breast cancer tend to have a good prognosis. However, the prognosis is worse than luminal A.

Table 0.1 Molecular classification of Breast Cancer subtypes.

BC type	Hormonal status	HER2 status	Ki-67	% of patients
Triple Negative/Basal like (TNBC)	ER- and PR-	-	varies	15-20%
Luminal A	ER+ and/or PR+	-	low level	40-44%
Luminal B	ER+ and/or PR-	+ or -	high level	20-24%
HER2 enriched	ER- and PR-	+	varies	20-24%
Normal-like	ER+ and/or PR+	-	low level	2-4%

1.4 HER2 POSITIVE BREAST CANCER

Approximately 20-25% of invasive breast cancers overexpress the HER2/neu protein and it is considered a particularly aggressive molecular subtype of breast cancer. It is characterised by the hyperexpression of HER2 protein on the surface and it is estimated that the survival rate is only 82.7% after 4 years [48] [49].

Higher expression (20/30% more than usual) of the HER2 gene cluster and the proliferation genes are on the cell surface, while it has a low expression

of genes of the luminal and basal subtype. For this reason, these tumours are most often negative for ER (oestrogen receptor) and PgR (progesterone receptor) and positive for HER2 on immunohistochemical evaluation [50,51].

The HER/ErbB family receptor (Human Epidermal growth factor Receptor) is a group of membrane proteins with tyrosine kinase activity composed of four members: EGFR (ErbB1), HER2 (ErbB2), ErbB3 and ErbB4 (Figure 0.5).

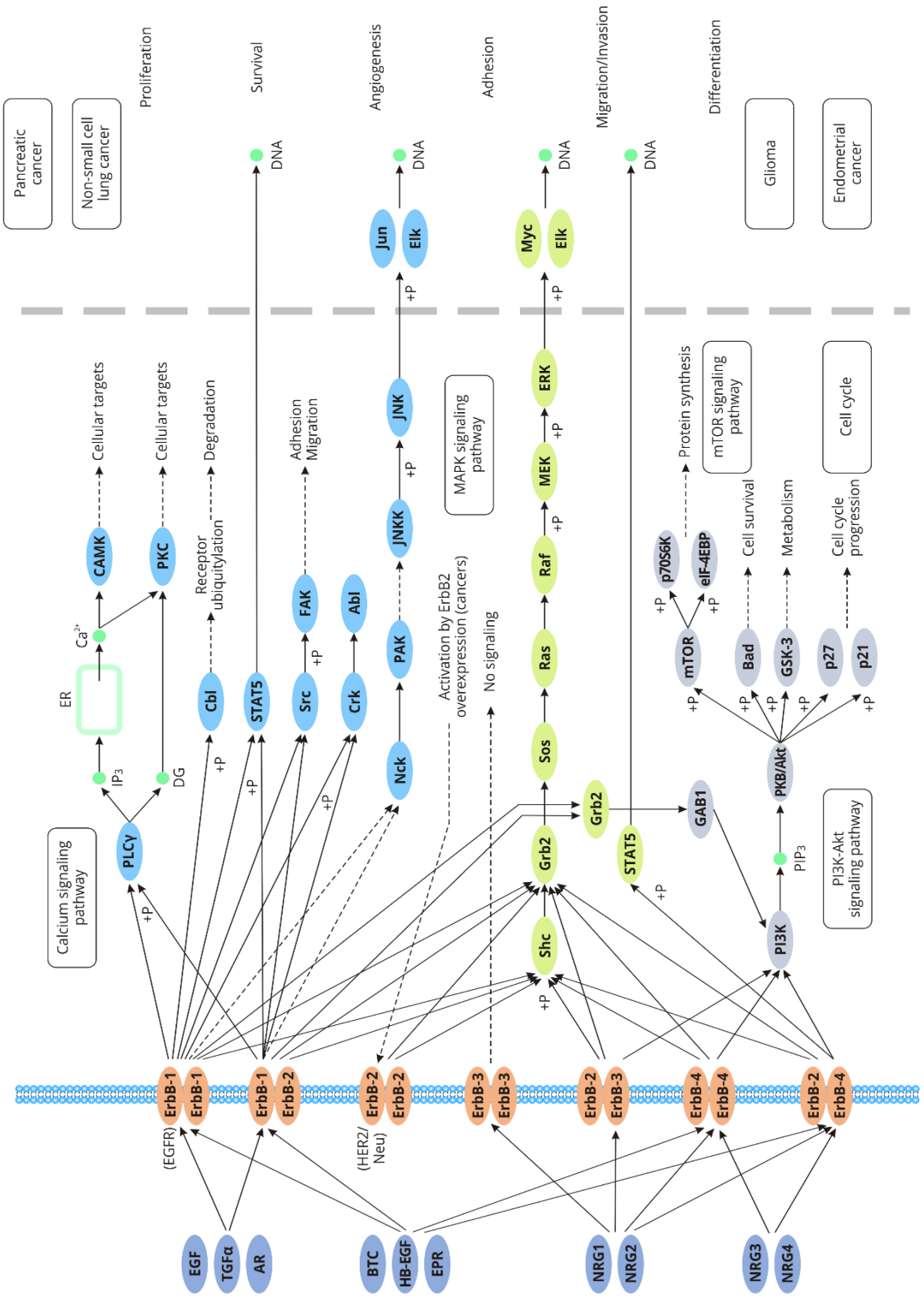

Figure 0.5 ERBB receptors family and their internal pathways.

They are expressed in numerous types of tissues, epithelial, mesenchymal, nervous, where they play a fundamental role in cell proliferation, growth, survival, differentiation and migration, and are involved in the development and progression of numerous types of tumours [52]. ErbB family is a 185-kDa transmembrane tyrosine-Kinase oncoproteins and in each receptor there is an extracellular domain which interacts with a ligand, a hydrophobic trans-membrane portion and an intracellular tyrosine-kinase domain. All these receptors perform an important action of transducing signals between the extra- and intra-cellular environment.

The ErbB1, ErbB3 and ErbB4 activation is ligand-dependent however, ErbB2/HER2 receptor is called "orphan receptor" considering that when overexpressed or mutated it is constitutively activated shape and thus its activation is ligand-independent [53,54].

Combining the receptors with each other can form four homodimers (by coupling two receptors of the same type) or six heterodimers (by coupling two receptors of different types). Following the homo-/hetero-dimerisation of the receptor, many cytoplasmic proteins are activated and include Ras/MAPK, and PI3 kinase/Akt that trigger a series of downstream cascade reactions along the signal transduction pathways.

For example, Ras/MAPK promotes the altered expression of many genes related cell proliferation, differentiation and survival leading to an increased cancer progression. In addition, PI3 Kinase/Atk triggers the activation of many transcription factors that regulate cell metabolism, apoptosis, protein synthesis, epithelial-mesenchymal transition (EMT) and angiogenesis (Figure 0.6).

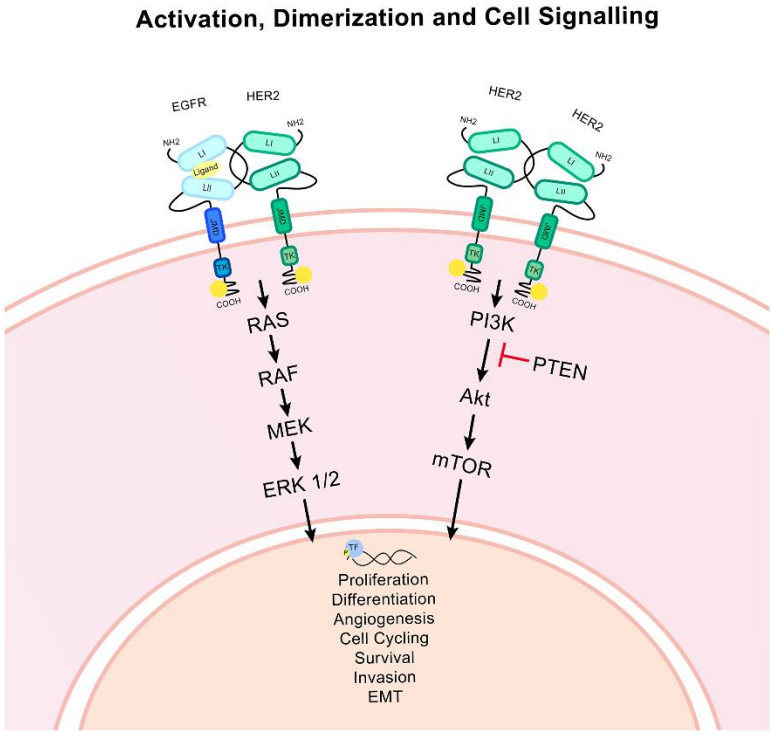

Figure 0.6 Representation of the hetero-dimerisation on the left and its RAS/MAPK pathway activation. on the right, the omo-dimerisation and the phosphorylation of the PI3 Kinase protein and the Akt activation. Both Pathways enhance the cancer progression stimulating genes mutation and transcription factors [53].

1.5 HER2 BREAST CANCER TARGETING TREATMENTS

1.5.1 Introduction

The most successful therapy for the treatment of breast cancer subtypes has been targeted therapy of epitopes expressed on the surface of cancer cells, stressing the importance of molecular classification in addition to histology and the great heterogeneity of the tumour.

1.5.2 Monoclonal Antibody

The main treatment for HER2 is a humanised monoclonal antibody, Trastuzumab (Herceptin®) that presents complementary-determining region amino acids that bind the protein region of the fourth extracellular domain of the HER2 receptor. The Trastuzumab-HER2 complex causes a cytostatic effect due to the arrest of the G1 phase resulting in an upregulation of p27 cyclin inhibitor (CDK). In fact, the drug acts as a block of the intracellular signal of PI3K/Akt [55] that induces an increase of PTEN (homologous tensin phosphatase), a protein fundamental for its activity as onco-suppressor. In addition, the HER2 receptor may undergo a proteolytic cleavage that causes the shedding of the extracellular portion giving rise to a truncated and constitutionally active phosphorylated protein, p95HER2. However, Trastuzumab is able to inhibit the cleavage of HER2 and p95HER2 by blocking the cleavage site of the receptor [56,57].

Moreover, the Fc portion is a potent mediator of the cell-mediated dependent antibody cytotoxicity (ADCC), the effector cells of the immune system such as natural killer cells, monocytes, macrophages, and mast cells then bind to the Fc portion and induce the release of molecules that cause cell lysis.

However, the drug often encounters resistance mechanisms that undermine its effectiveness approximately nine months after the start of treatment [58]. The most common mechanisms are:

- Obstacles preventing binding to the HER2 receptor
- Upregulation of signalling pathways downstream of HER2
- insufficient immune activation that does not lead to cell death
- Alternative routes

An obstacle that reduces affinity with HER2 is the accumulation of the truncated receptor, p95HER2, which has kinase activity but lacks the

binding site of Trastuzumab due to the cleavage of the extracellular domain (Figure 0.7).

The increased activity of the PI3K pathway that makes the protein constitutively active may be due to the loss of function of PTEN, that its activity falls up to 40% in breast cancer [59], or thanks to mutations that activate the catalytic subunit of PI3K [60].

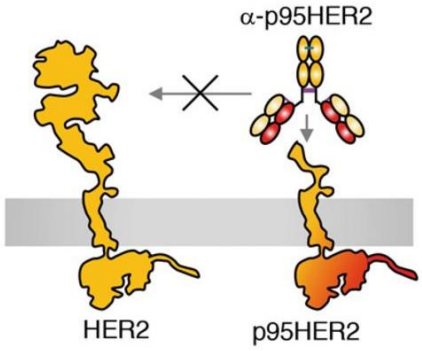

Figure 0.7 HER2 receptor cleavage in p95HER2 to avoid the blockade by Trastuzumab [61].

Other pathways include an increased IGF-1 receptor (IGF-1R) that is amplified in positive HER2 tumours and increase their phosphorylation activity causing activation oh HER2 receptor so the PI3K pathway. Finally, there may be an increase in heterodimers HER2-HER3 that turns out to be the most active heterodimeric complex that induces a powerful downstream signalling. However, the heterodimer HER2-HER3 can be avoided by a new monoclonal body, called Pertuzumab, which is able to bind the second extracellular domain of HER2 by preventing heterodimerisation [62].

1.5.3 TDM-1 Antibody Drug Conjugate

T-DM1 is an antibody-drug conjugate (ADC) studied for use in HER2 positive metastatic breast cancer. It was developed to inhibit the HER2 signalling pathway and deliver DM1 chemotherapy directly within HER2 positive cancer cells. The Trastuzumab antibody binds to positive HER2 cancer cells and blocks uncontrolled signals that contribute to tumour growth, while activating the body's immune system against these cells (Figure 0.8) [63,64].

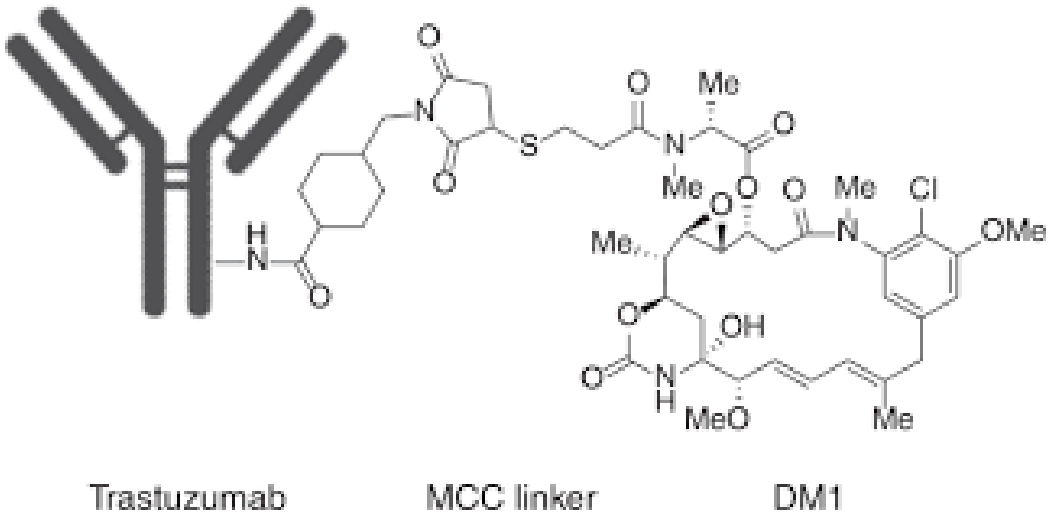

Figure 0.8 Structure of T-DM1. Taken from Hunter et al.

Once inside the cancer cells, T-DM1 leads them to cell death by releasing DM1. T-DM1 combines Trastuzumab and DM1 via a stable linker that keeps the bond intact until the drug is internalised into HER2 positive cancer cells. T-DM1 works as a targeted anticancer therapy because it directly targets HER2-positive breast cancer cells, limiting the rest of the body's exposure to chemotherapy. More specifically, Trastuzumab in T-DM1 binds first to the HER2 protein on the surface of breast cancer cells and DM1 then enters the cells and can cause them to die, preventing tumour growth [65].

1.5.4 HER2 Tyrosine Kinase Inhibitors

Lapatinib is a drug that inhibits the tyrosine kinase activity of the HER2 and HER1 receptor. Unlike monoclonal antibodies, Lapatinib is a small molecule capable of cross the cell membrane and binding the intracellular domain by competing for the ATP binding site (Figure 0.9 [66]).

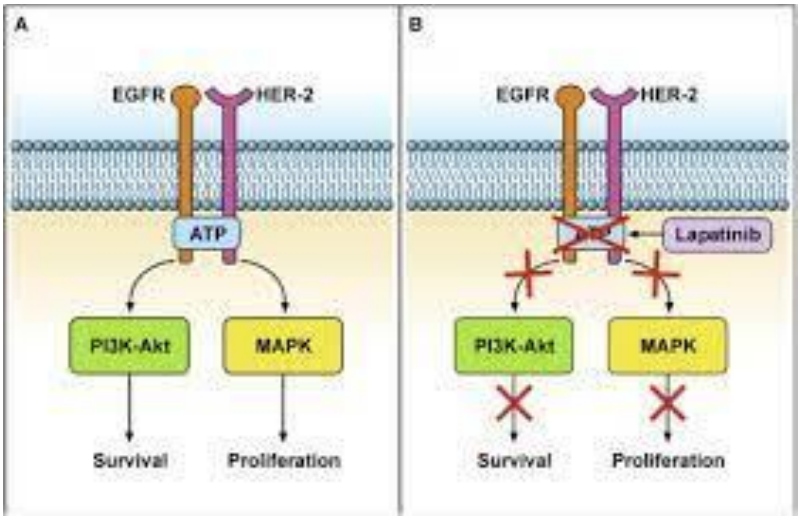

Figure 0.9 Inhibition of proliferation and survival of cells in presence of Lapatinib.

The drug is often used in combination with Trastuzumab since it blocks cell cycle [67].

It is often used in combination with other drugs such as chemotherapy agents (capecitabine and gemcitabine) and agents associated with hormonal therapy (letrozole) when the risk of metastasis is very high and the patient has already shown a poor therapeutic response to Trastuzumab [67].

1.6 CHEMOTHERAPY AND NEW STRATEGIES

In HER2-positive tumours, treatment with combinations of anti-HER2 agents is well established as the first-choice treatment in combination with chemotherapy. Anti-HER2 agents are mainly biological drugs, that is, monoclonal antibodies that bind the HER2 receptor present on the surface of cancer cells, preventing the transduction of the signal inside them. Nonetheless, chemotherapy is often associated with targeted anti-HER2 therapy, and thanks to new molecular discoveries and new drug delivery technologies, even RNA fragments can be used to control acquired mutations in cancer cells.

1.6.1 Paclitaxel

One of the most common chemotherapeutic drugs is Paclitaxel, part of the taxanes class, it is a first-line drug widely used in the pharmaceutical field for different types of cancer including breast cancer. Its mechanism of action promotes the assembly of microtubules and stabilises them, thus reducing the ability to reorganise cells especially in the phases of duplication and cell division.

The hyper-stabilised structure due to the link between Paclitaxel and tubulin, preventing the mobility of cellular organelles, and from recent studies, it seems to interact with the Bcl2 protein, binding it to its chemical structure and zeroing its anti-apoptotic activity [68]. The side effects of Paclitaxel, however, are manifold, such as: the most common side effects are the decrease of red and white blood cells with consequent exhaustion and risk of infection.

Nausea, vomiting, diarrhoea and hair loss are other adverse reactions of the drug. Finally, neuropathy can occur with numbness of hands and feet [69].

However, the use of nanoparticles has been shown to greatly reduce side effects, chemotherapy in combination with albumin nanoparticles allows to increase the concentration of Paclitaxel in the intra-neoplastic region by 33% compared to traditional administration. In addition, smallest percentages of side effects and the higher period of survival and tumour progression [70].

1.6.2 Gene Therapy

Through personalised medicine, traditional drugs currently found in pharmacies can be administered, in suitable dosages for the individual, but also more complex medicines such as nucleic acids that can intervene directly onto the mutated cell and be precisely and safely delivered. These highly personalised therapies are known as gene therapies are intended to:

- Transfer small sequences of genetic material to correct or enhance the clinical condition.
- Cellular targeting (only to specific cells).
- Modify the expression of the therapeutic gene (maintenance of biological activity at high/reduced levels in the desired tissue).
- Be absent of side effects (e.g., immune response)

Since traditional medicine shows obvious limitations such as toxicity, loss of function or many side effects to healthy organs, it is well known that new highly personalised therapies based on the molecular biology of diseased tissues can be of great benefit to the success of selective treatment for the latter. The approaches for the treatment of breast cancer are multiple but can be summarised in four macro-categories:

1. Regulation of onco-suppressor genes
2. Proapoptotic gene therapy
3. Potentiation of immune system
4. Antiangiogenic gene therapy

The disease advancement is often caused by genes mutations that inhibit potential metastatic or invasive effects, or there are indirect mechanisms that interfere with their expression. Through gene therapy it is possible to promote the expression of onco-suppressors and to inhibit the activity of oncogenes, restoring normal cellular activity or inducing programmed death (apoptosis). Also, gene therapy has the potential to stimulate patient's immune system by either administration of tumour antibodies and tumouricidal effector cells to directly kill cancer cells (passive immunotherapy) or activate immune system response to drive the anticancer immunity by tumour vaccines and immune-stimulatory cytokines [71].

The development of the disease is often caused by mutations directed at onco-suppressor genes which controls either the metastatic potential and invasive effects, or there are indirect mechanisms that interfere with their expression. Through gene therapy it is possible to promote the onco-suppressors expression and to inhibit the oncogenes activity, restoring normal cellular activity or inducing programmed death (apoptosis). In addition, gene therapy has the potential to stimulate patient's immune system by either administration of tumour antibodies and tumoricidal effector cells to directly kill cancer cells (passive immunotherapy) or activate immune system response to drive the anticancer immunity through tumour vaccines and immune-stimulatory cytokines.

Finally, it is well established the tumour proliferation is an angiogenesis-dependent process (strengthening of new blood vessels). Therefore, blocking genes that transcribe to proteins that lead to uncontrolled blood vessels growth are a very common target for the cancer tissue treatment [72].

Gene Therapy allows to treat genetic diseases and tumours through the introduction of molecules that completely or partially inhibit the activity of a gene such as: siRNA (Small interference RNA), miRNA (microRNA) or ASOs (inhibitory antisense oligonucleotides); or molecular structures that correct or increase gene expression such as: plasmid DNA, mRNA (messenger RNA), saRNA (small activating RNA) and CRISPR/Cas9 (clustered regularly interspaced short palindromic repeats).

1.6.3 SiRNA

Short interference RNA (siRNA) was discovered by Fire and Mello in 1998 when studying worm *Caenorhabditis elegans* [73]. They understood that when RNA double strand was introduced in worms, they were able to silence some genes essential for worm movement.

RNA interference is a natural protection mechanism from viral RNA or from gene elements which can destabilise cell DNA [74]. This particular defence system can be found in various organisms and all the enzymes necessary for it are highly preserved, in eukaryotic organisms the system is more evolved and it is an important tool to regulate gene expression.

SiRNAs are double stranded RNA of 21-23 non-coding nucleotides (Figure 0.10 [75]). The siRNA precursor is a long double-stranded RNA (dsRNA) that contains 30 over 100 nucleotides and it is cut into a smaller RNA duplex with 3' two-nucleotides overhangs by a ribonuclease (III RNase), called Dicer. Mature double stranded RNA interacts and activates Argonaute proteins (AGO2) to form the multiproteic complex RISC (RNA-induced silencing complex) that possesses endonuclease activity [76] which cleavage the sense strand. Subsequently, the guide strand that is still associated with RISC complex, will bind perfectly the target mRNA causing its degradation or cleavage [77].

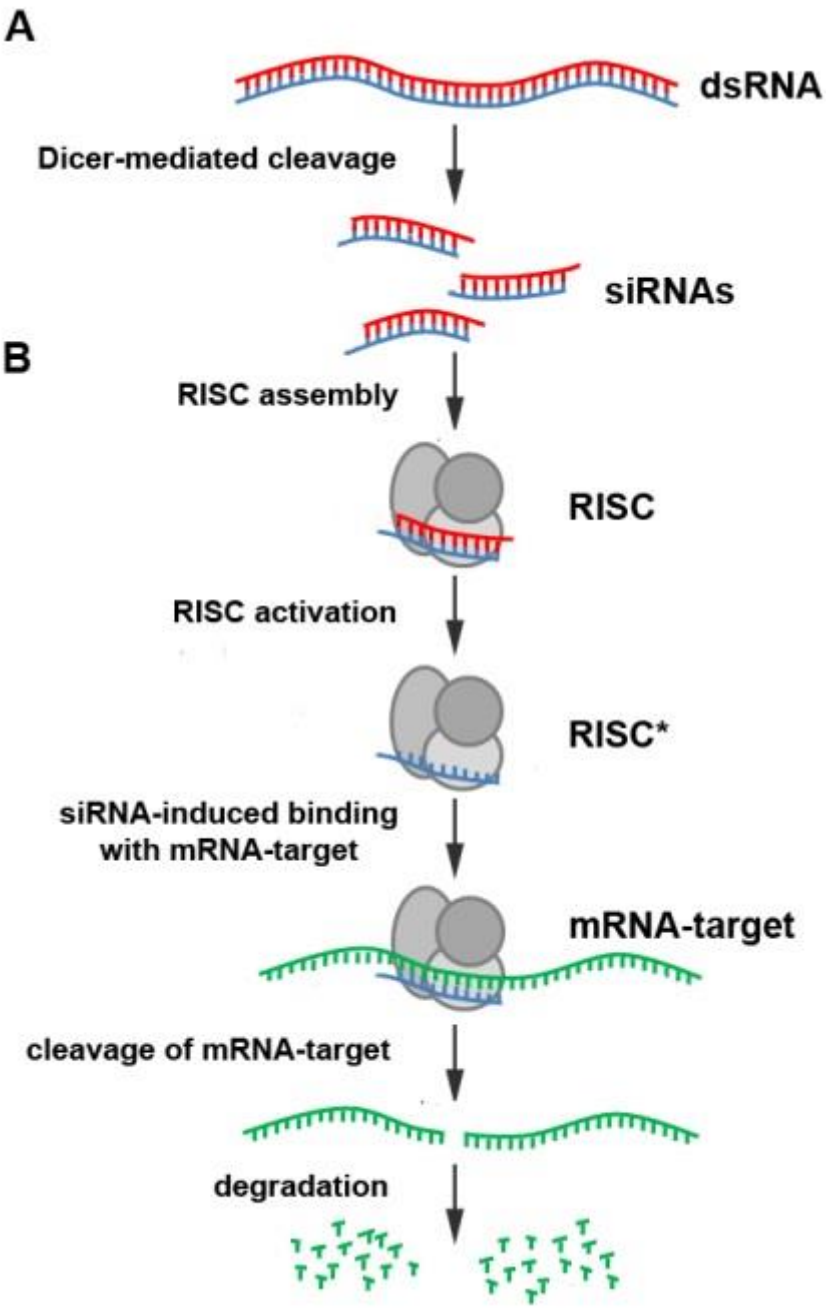

Figure 0.10 SiRNA processing. Firstly, the double strand RNA is it cut by DICER into 21-23 nucleotides. the small RNA recognises and activate the Argonaute protein. Later, the AGO2 protein bind the RISC complex which cleavage one strand of the siRNA, while the guide strand will bind the mRNA causing its degradation (green segments).

Gene silencing is induced by repression of translation or by degradation of target molecules. The choice of the mechanism of action depends on the homology between the SiRNA and the target. In this context, the RISC complex has to degrade the target RNA when its complementarity with SiRNA is total. If complementarity is not perfect, however, the complex represses the translation.

SiRNAs have key roles in regulating numerous processes and a single one is able to control the expression of the target genes. Their involvement in biological processes has led researchers to investigate molecular aspects, in fact whether the mRNA is overexpressed siRNA can reduce or zeroing the concentration of pathological messenger RNA.

1.7 GENE TRANSFER

1.7.1 Introduction

Although this technique is widely recognised as a treatment with a clinical potential, it is applicable only to easily accessible tissues, resulting in poor efficacy because of the rapid degradation of the delivered gene that is caused by serum nucleases as well as by an ineffective cellular internalisation due to the high size of DNA chains and the electrostatic repulsion between negative charged on nucleic acids and cell membrane [71,78]. For this reason, the main objective of gene therapy is the development of methods and vectors that can facilitate the entry of genetic material into the cell, thereby increasing the efficiency of transfection. In particular, there are two main approaches to promoting the transfer of genes to cells: physical methods and chemical vectors (viral or non-viral).

1.7.2 Physical Method

In recent decades, several strategies have been developed for the transfer of genes to target cells, with the aim of modulating their expression for therapeutic purposes. The most intuitive method for transferring genes or fragments is the direct administration of nucleic acids to cells as "naked" DNA or RNA. Physical methods for the administration of genetic material *in vitro* and in vivo exploit physical forces to permeate the cell membrane, accentuating the size of the natural pores of the membrane itself, this makes it easier for the cell to internalise gene material (Figure 0.11 [79]).

Physical methods favour the entry of DNA or RNA fragments by putting them in close contact with the target cells and temporarily damaging the plasma barrier itself.

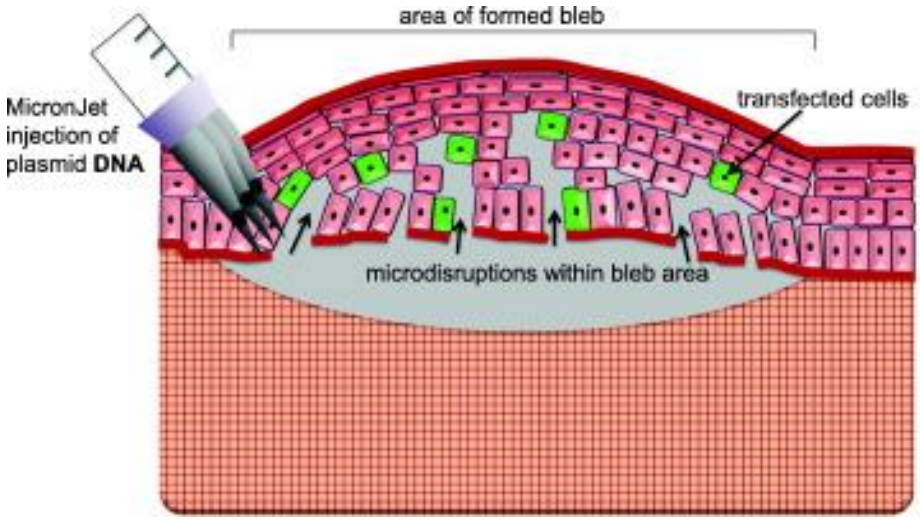

Figure 0.11 Example of physical gene delivery.

An example of a physical method is the electrotransfer, initially used only for *in vitro* cells, today it is used for gene transfer in the skin, muscles and liver, but also for tissues such as heart, retina and lungs [80]. The technique consists in applying electrical impulses to make the membrane permeable and thus allow the passage of large or charged molecules [81].

A similar technique is the sonoporation that uses ultrasound to create micropores in the plasma membrane and promote the internalisation of nucleic acids [82].

Vascular hydrodynamic injection instead exploits a local and transient increase in hydrostatic pressure significantly increasing the efficiency of internalisation of DNA fragments present in the blood [83].

The technique called gene gun exploits the bombardment of cells with microparticles covered with nucleic acid [84,85]. Often gold or tungsten particles are used that have adsorbed a plasmid on the surface, and can cross the cell and nuclear barrier by releasing plasmid directly into the nucleus of the target cell [86].

1.7.3 Viral Vectors and Chemical Method

Given that physical methods can only reach superficial or directly underlying tissues that are easily accessible, chemical methods have also been developed to expand the number of tissues and target cells. Currently, the main challenge of gene therapy in the clinic is to design and master an appropriate vector, capable of effectively delivering nucleic acids within the cell, maintaining biocompatibility without activating the immune system. For instance, research efforts are focusing on the design of carriers able to hide and protect the nucleic acid of interest from degradation by blood and interstitial nucleases, promote the

internalisation of genetic material in target cells and release the gene material, once inside the target cells [87,88].

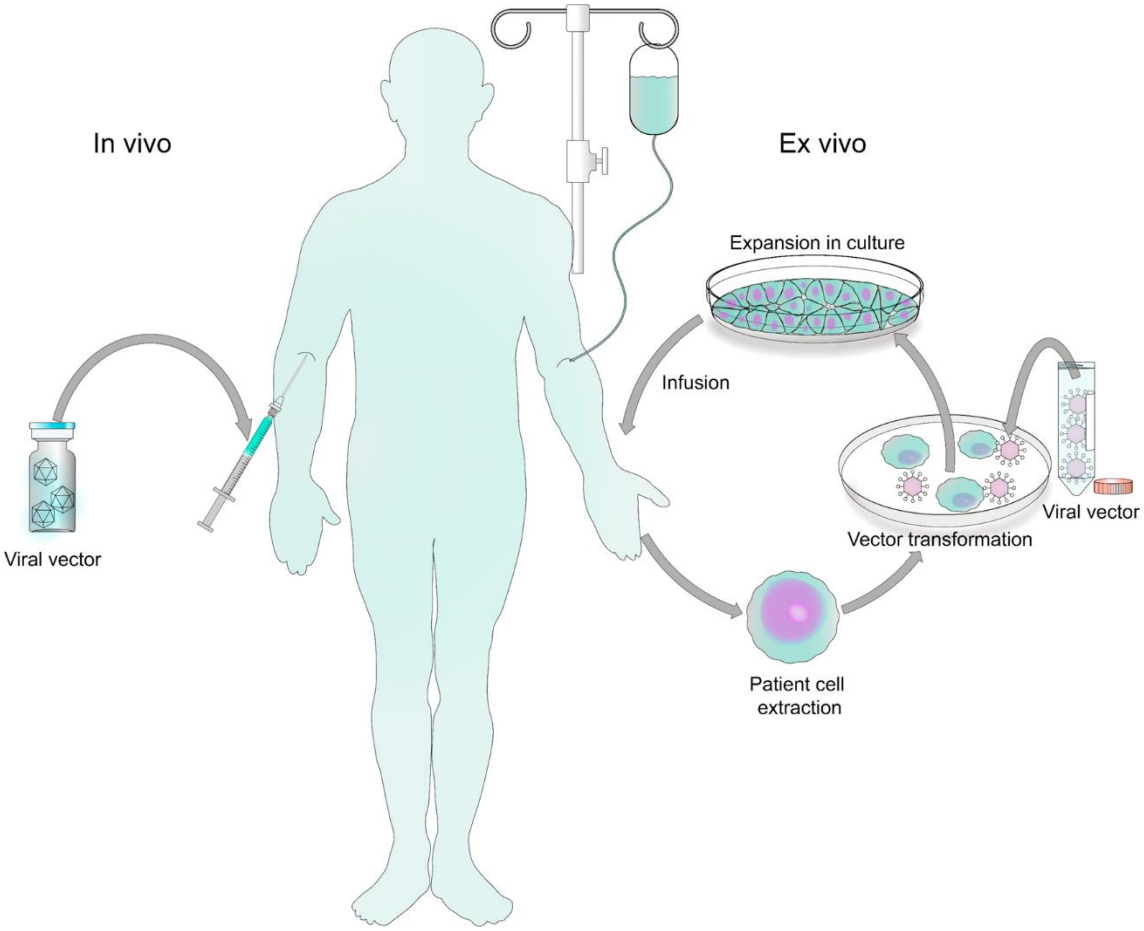

Figure 0.12 Schematic representation of viral gene delivery.

At first, research focused on the use of viral carriers, such as adenovirus, retrovirus, adeno-associated virus and lentivirus, for their ability to carry exogenous DNA/RNA in numerous line cells [89]. When gene therapy uses these organisms as vectors, the transfer of genetic material is called *transduction* (Figure 0.12 [90]). Viruses are biological entities characterised by dimensions in the order of nanometres, since they are obligated

parasites, they exploit all the biochemical and biosynthetic structures necessary for their replication which are present in the host. Some viruses can physically insert their genome into the host's genome so that it is replicated along with it. It is possible to exploit the peculiarities of viral vectors by inserting in their genome the gene of interest and creating a recombinant vector. The viral vectors are therefore deprived of their genes potentially pathogenic to the cell, while those indispensable for the replication of the virus are maintained [91,92]. Despite the advantages offered by viral vectors, among which the high efficiency of transduction, their application *in vivo* is hindered by the reaction of the human immune system, which recognises and removes viruses from the blood circulation, thus reducing the effectiveness of this type of carrier. In addition, these vectors are prone to mutagenesis and recombination.

The delivery of genetic material by non-viral agents is termed *transfection* and the carrier, which is used, is called vectors. The latter can be produced on a large scale, with acceptable costs, high reproducibility, and with relatively stability upon storage. Although they have proved less efficient in gene transfer, they have been studied with great interest as they are less immunogenic, easy to prepare and more versatile [93].

1.8 NANOPARTICLES

1.8.1 Introduction

The advantages of using nanoparticles as a drug delivery system are many:

- Prolonged systemic circulation with improved biodistribution and pharmacokinetic profile.
- Improved chemical stability of drugs;

- Drastic decrease in cytotoxic effects due to the use of biocompatible nanomaterials;
- Use of poorly water-soluble drugs that are encapsulated in nanoparticle systems improving their solubility [94];
- Controlled drug release at specific sites;
- Possibility of simultaneous distribution of several active ingredients for combined synergistic therapy [95,96].

These physical properties-unique chemicals of drug delivery systems with nanoparticles give them the advantage of significantly influencing the therapeutic approaches of various diseases, through their ability to provide a range of therapeutic agents to the desired sites in the body, at a predetermined speed and time [97].

Nanoparticles or NPs are structures ranging in size from 10 to 250 nm and have been extensively studied for drug delivery and diagnostics in recent years.

In the context of drug delivery, nanoparticles are divided into three main classes: inorganic, lipid-based and polymeric (Figure 0.13 [98]).
Inorganic nanoparticles consist of inorganic materials such as gold, iron, and silica that are very often used for different drug delivery and imaging analysis [98].

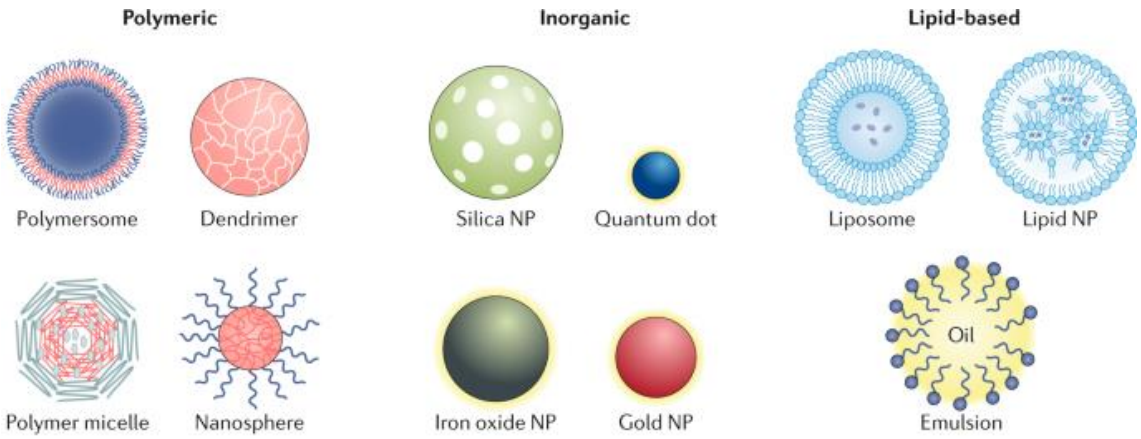

Figure 0.13 classification of Nanoparticles. From Mitchell et all 2021.

Lipid-based nanoparticles are typically spherical structures with one or more double layers of lipid that have an aqueous compartment. These structures have the advantage of being simple, biocompatible, self-assemble, have the ability to carry relatively high payloads and drugs of different physicochemical nature. This class includes liposomes and lipid nanoparticles (LNPs) [99].

Polymer nanoparticles consist of one or several repeated units of natural or synthetic original, due to their variable composition they can carry different actives within their core or can trap the drug between the polymer matrix. Finally, it is possible to chemically bind the active substance to the nanoparticle [100].

Polymer nanoparticles can be divided into two subclasses according to their shape. In fact, they are called nanocapsules if the core is delimited by the matrix or shell, or they are called nanospheres if the matrix is solid and the drug is evenly distributed in it. This class includes polymerosomes, micelles and dendrimers.

1.8.2 Passive And Active Targeting

Ideally, nanovectors should have low toxicity and avoid the removal by immune system and remain in the blood circulation for a prolonged time to ensure the accumulation in the desired tissue.

In fact, it is a peculiarity of nanoparticles to accumulate in specific tissues of the human body, this can happen spontaneously in the case of passive targeting or it can be induced through active targeting. In the first case, passive targeting, takes advantage of the differences between normal and sick tissues to convey the drugs to the requested site. The physiology of sick tissues, in fact, is often altered leading to the EPR effect (enhanced permeability and retention)[101]. This occurs because the vascularisation of the cancer is significantly more developed than in healthy tissues and predominates on the lymphatic system, with increased oedema and accumulation of NPs in tumour tissues rather than in healthy tissues. The EPR effect has also been observed at sites of inflammation and infection due to the presence of bradykinin. The difference between the EPR effect caused by the tumour and that caused by inflammation in normal tissues is duration. In fact, in the first case, the retention time is considerably longer than that found in inflamed tissues due to the collapse of the lymphatic system, an event that does not occur in healthy/inflamed tissue and leads to a resorption of excess fluids after a few days. Active targeting, on the other hand, requires the conjugation of receptor-specific ligands that can promote site-specific targeting [102]. The success of pharmacological targeting depends on a high affinity and specificity of ligands to the receptors of the target cell surface. Active targeting can be achieved through molecular recognition of surface proteins over-expressed at the sick site, either through ligand-receptor, antigen-antibody interactions, or through targeting by aptamers (single-stranded nucleic acids or peptides that specifically bind the target protein). Therefore, the ability to

conjugate different targeting ligands offers excellent opportunities to overcome physiological barriers and promote efficient cellular absorption [103].

1.8.3 Biological Barriers

Physiological factors are important in influencing the fate and distribution of the delivery system. Indeed, when liposomes are injected in blood stream, they are recognised as non-self by immune system and become coated by proteins; a process called "opsonisation" or "*protein corona*". One component of the coating proteins, which is named opsonin, can encourage the clearance by the RES (reticuloendothelial system). Many studies underlined the advantages of the protein corona absorption can reduce the NPs toxic effects and prevent undesired interactions with the immune system (Figure 0.14 [104]). For example, the protein corona can significantly affect the NPs cellular uptake avoiding the interactions with cell membrane; however, whether the binding site of NPs is driven by the protein corona itself, it may increase the targeting capability of the nanocarrier [105].

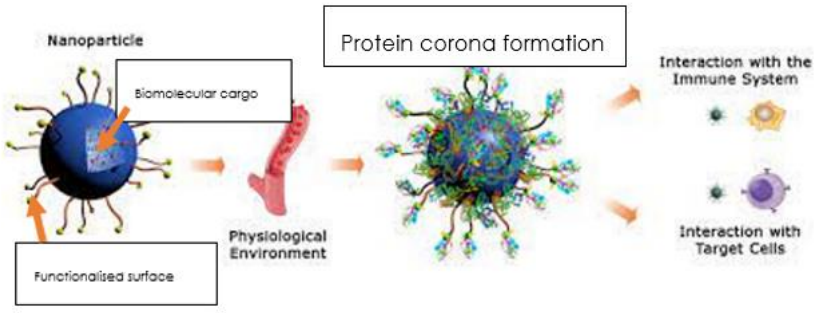

Figure 0.14 Protein Corona recognise the NPs and active the immune system to digest and remove nanoparticles from blood circulation. From DiGiacomo et al, 2020.

It is also important to mention that the protein corona composition is patient-to-patient different like a fingerprint, considering that cancer antibodies start circulating in the plasma of patients and those are specific for each disease and patient. Moreover, protein corona are more attracted by larger NPs (100 nm) than on smaller-sized [106].

Nevertheless, the opsonin proteins are part of the protein corona and have been shown to negatively affect the efficiency of the NPs targeting, due to causing rapid clearance of the nanocarrier by phagocytes immune system cells such as macrophages, monocytes and dendritic cells. One of the key techniques to increase blood circulation is the addition of different groups to the bilayer surface such as polyethylene glycol (PEG), which is one of the most common moieties added. Its long and flexible chain forms a barrier that arguably prevents or reduces opsonin adhesion, making it invisible to phagocytes [107] stabilising the colloid [108,109].

One more obstacle for the NP intake is the reticuloendothelial system (RES), also called mononuclear phagocyte system (MPS) consisting of spleen and liver, which are capable of removing many particles from the blood circulation. In addition to clearance, MPS can induce toxicity by triggering the immune response to release interleukins, interferons and tumour necrosis factors. To reduce the clearance by the phagocyte system it is possible to reduce the interactions coating the NPs with PEG (poly ethylene glycol) or "self"-peptides. In particular, PEGylation is also used in passive targeting approaches to selectively promote the delivery into the diseased tissue rather than healthy tissue through the EPR effect (enhanced permeability and retention), proposed to be at play in solid tumours [110]. Whereas the "self"-peptides mimic cell membranes derived from leukocytes or erythrocytes to enhance the anti-phagocytosis signals.

In addition, one more mechanism to clear the blood circulation from NPs is the renal ultrafiltration that regulates the NP pharmacokinetics.

Blood is constantly filtered by the kidneys' fundamental structures called "nephrons" that selectively remove macro and smaller molecules from blood circulation to secrete them into renal tubules and collecting ducts. Ultimately, whether NPs escape the blood vessels, they will face with another barrier in the extracellular environment space composed of elastic fibres (glycosaminoglycans and other protein), collagen that composes the extracellular matrix (ECM) and is rich of abnormal tumour-associated metabolic and chemical gradients. The ECM, especially in neoplasia, is excessively rigid and the reduced drainage on interstitial fluid leads to a pressure gradient that further inhibits NP internalisation into cancer cells (EPR effect)[98]. In particular, positively charged NPs are hidden by the ECM since they adhere to the anionic proteins of the extracellular environment [98]. Nonetheless, the tumour microenvironment can be exploited to increase the NP penetration, overtaking the higher ECM density and the interstitial pressure. For example, matrix metalloproteinases (MMPS) and other proteases located in the extracellular site can induce the NP deterioration and drug release. Exogenous triggers such as light, magnetic fields and radio frequencies can tightly control from the outside of the body the NPs concentration, sensitive to their impulses, and their drug release [111,112]. In addition another method useful to enhance the NPs tumour penetration is to coat them with collagenase that degrades collagen overcoming the high ECM density or with anti-angiogenesis therapies to normalise the nanoparticles accessibility in the tumour tissue by restoring the blood flow and the regular pressure gradients [113].

1.8.4 Physicochemical Properties of Nanoparticles Affecting Biodistribution

Once the NPs are assimilated, before reaching the targeted tissue at suitable concentrations, they can face many obstacles depending on their physicochemical properties such as size, shape, charge and modification on the surface. As previously mentioned, to minimise the non-specific absorption by RES it is appropriate to coat the NPs surface with PEG which is able to generate a hydrating layer that limit the protein absorption or with zwitterionic ligands like glutathione or cysteine [114]. Otherwise, it is also possible to mask the NP surface with antiphagocytic residues like CD47-SIRPa (signal-regulatory protein alpha) that hide them from the immune system [115]. Not only do the surface modifications affect the nanocarrier stability, but also size is an important factor for its accumulation. It has been shown by Sonavane et al. [116] that the nanocarrier accumulation in the different tissue was size-dependent, i.e. NPs smaller than 15 nm were able to cross the BBB (blood brain barrier) and the renal clearance of the small particles was very quick, while spleen and liver (MPS) instantly accumulate NPs greater than 200 nm [117]. In addition, cytotoxicity is also related to NP dimension, the smaller the size, the greater the toxicity [118].

The charge of the NP is measured by zeta potential (ζ) and they are considered positive when the $\zeta \geq 10$ mV while they are negative when $\zeta \leq -10$ mV and neutral NPs with $+10 \text{ mV} \leq \zeta \leq -10$ mV.

Positively-charged nanocarriers induce the serum protein aggregation and for that reason they tend to accumulate more in the lung tissue due to the electrostatic interactions with blood cells leading to consequent entrapment in the lungs capillaries. Nonetheless, positive charges have shown higher levels of internalisation by the cells rather than negative and

positive NPs, yet they cause more damages to the cell membrane leading to an increased toxicity [119].

Negatively charged NPs are easily removed by RES and penetrate the skin tissue more rapidly than positive NPs [116]. Moreover, NPs with high negative or positive charge, lower than -10 mV and higher than +10 mV, are successfully cleared by Kupffer cells (specialised macrophages localised in the liver).

Neutral NPs surfaces show lower uptake rate by RES and the longer circulation time thanks to the low interactions with blood proteins [120].

1.8.5 Cellular Barriers

Another barrier of NPs is the cellular membrane which encloses the cytoplasm and marks the extracellular environment from the intracellular fluids. The cell membrane (CM) is made of phospholipid ordered into a bilayer, cholesterol and membrane proteins making the membrane extremely elastic, flexible and selective to substance passage.

Cellular membrane permits the substances exchange employing two mechanisms: passive and active transport.

Small molecules such as oxygen, water, carbon dioxide, benzene and hydrophobic molecules diffuse directly through the phospholipid membrane into cell from high to low concentration without involving energy, this kind of transport is defined as passive transport [121].

In contrast, polar and charged biomolecules or molecules that move against the electrochemical gradient need energy provided by adenosine triphosphate (ATP), though active transport [122,123].

Vesicular transport, a type of energy-driven transport specific for big molecules such as protein and nanoparticles, is mediated by endocytosis

that it may be described as an invagination of the membrane encompassing the extracellular material and forming a membrane-bonding vesicle named endosome [124]. Phagocytosis is a type of endocytosis, and it is defined as cells "eating" when specialised cells, such a phagocytes, monocytes, neutrophils and macrophages, internalise large size solute. Phagocytosis happened when opsonin, part of corona proteins, coat the exogenous materials and triggers phagocytosis to remove them from the blood circulation preventing any infections or toxicity.

Once the phagocytes ingest the external materials, it is bordered within the phagosome that will fuse with the lysosome. The new phagolysosomes undergo a process of material digestion thanks to acidification and hydrolytic enzymes present in the lysosomal vesicles [125].

Otherwise, all cells have the ability to internalise small particles, within the range of nanometres, by pinocytosis. Is it known as the "cellular drinking" and can be distinguished by two sub-categories called: clathrin-mediated endocytosis and the caveolae-mediated endocytosis [126].

Clathrin-mediated endocytosis (CME) is receptor-mediated transport that is highly selective due to in the extracellular fluid ligand binding with a specific receptor on the surface membrane forming a ligand-receptor complex. The ligand-receptors complex drives to a specialised zone of thee clathrin enriched. Clathrin molecules are activated and start the formation of a polyhedral lattice on the CM which helps to modify the membrane into a coated pit in Figure 0.15 (2 and 3) [127].

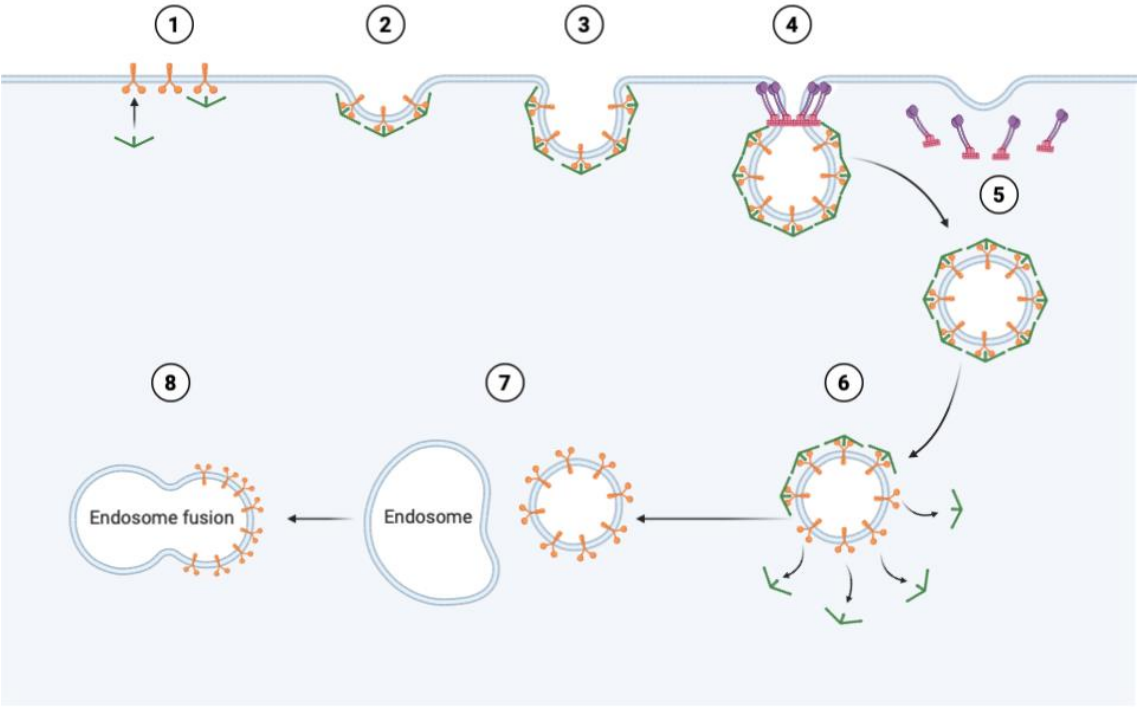

Figure 0.15 Clathrin-mediated endocytosis stages: (1)Target Recognition, (2-4)Clathrin Cage Formation and membrane Invagination, (5) Endocytic Vesicle Formation and scission, (6) Coat Removal and (7-8) fusion with the endosome. From: https://app.biorender.com/biorender-templates/t-5f1a013ed47ad400aa713245-clathrin-mediated-endocytosis .

As the lattice formation progresses, the vesicles lose the clathrin-coat and become "naked vesicle" which fuse with the relatively acid environment of the early endosomes (Figure 0.15, 6 and 7). This new environment causes loss of receptors, that will be recycled as well as the formation of mature endosomes. Late endosomes will fuse with lysosome that, through their lower pH, cause the digestion of the contents of the endosome [128]. Some nanocarriers can take advantage from the acidification from proton pump thus escaping from the endosome and releasing their cargoes into the cytoplasm. For example, the polyethyleneimine are able

to protonate their amine groups consuming the endosomal protons which enhance the chloride anions leading to endosome osmotic swelling.

In the case of some lipids, called "helper", like DOPE, their hexagonal structure and positive charge on the hydrophilic head allows interaction with and subsequently fusion of the liposome with the endosomal membrane thus promoting the release of genetic material [129,130]. Lipid structures can be used in association with other vectors to increase their escaping ability. For example, dendrimeric nanoparticles, made of lysine monomers, bind DNA extremely easily but the amount reaching the cytoplasm is minimal. This is due to the protonation of the lysine side chains and poor buffering capacity under pH 8 that leads to the formation of a very stable peptide:DNA complex that is difficult to dissociate [130,131]

In addition to clathrin, other proteins such as caveolin are able to induce endocytosis. Caveolin is dimeric protein that make small flask-shaped membrane invagination in areas rich in cholesterol and sphingolipid (caveolin coated pits) such as endothelial cells, adipocytes, fibroblasts and muscle cells [132]. The fission of the caveolae vesicle is guided by a GTPase dynamin which recognise the bottleneck of the caveolae generating the caveosome.

In this case, vesicles formed are not combined with endosomes or lysosomes, but there are transported to Golgi or endoplasmic reticulum and therefore the inner material is protected from the hydrolytic enzyme and acidic degradation [133]; hence it is the preferred entry route for viruses and bacteria.

Macropinocytosis is another subtype of endocytosis which internalise via non-specifically manner and is a pathway required to microparticles like to internalise necrotic and apoptotic cells, viruses and bacteria.

1.8.6 Physicochemical Properties of Nanoparticles Affecting Cellular Uptake

Many parameters are involved in non-viral uptake pathways such as size, surface charge of nanocarriers, particles shape and functionalisation, and hydrophobicity/hydrophilicity, all of them are crucial factors for NP internalisation.

Size is one of the key parameters in determining the uptake pathway and the efficiency of cellular intake. Dimensions ranging from few to several hundred nanometres enter predominantly via pinocytosis.

Nanoparticles sized from 120 to 150 nm are internalised via clathrin or caveolin-mediate internalisation. Many studies suggested that the optimum size is 50 nm at which NPs have higher intake and are internalised more efficiently [134].

Moreover, filamentous nanocarriers have been reported to stay in the circulation up to ten times more than spherical counterparts and avoided phagocytosis when came in contact with macrophages. Otherwise, rod-like NPs showed the highest internalisation rates compared to spheres [125].

One more critical factor is the surface charge. It has been highlighted that cationic NPs effortlessly interact with the negative charges on the CM surface and the internalisation rate by clathrin-mediated pathway is higher than neutral and negatively charged nanocarriers. Nevertheless, it may disrupt the cellular membrane enhancing cytotoxicity because of the formation of pores [119].

Finally, the surface modifications are useful to enhance the half-time circulation, stability and internalisation without compromising the membrane integrity. Surface modification comprises predominantly of PEG, -COOH (carboxyl group), -OH (hydroxyl group) and positive amine group as $-NH_2$. The amine group increase the positive charge surface and

so the cellular intake, -COOH functional groups enhance the number of negative surface charges and so the cellular internalisation [135]. In general, the NPs coating lead to a higher efficiency in internalisation which translate into and increased therapeutic effect [119].

1.9 DENDRIMERS AND FAMILY

1.9.1 Introduction

Dendrimer's name is derived from the Greek "dendron" (tree), and "meros" (branch) and refers to their tree-like structure. In fact, they can be defined as highly branched polymers; their growth occurs by the addition of subsequent branch points, each of which increases the "generation" of the dendrimers. The first inspiration for the constitution of a new class of polymers, similar to trees, was by Dr. D. A. Tomalia , but it was Fritz Vögtle in 1978, who carried out the first synthesis of this new class of macromolecules, a synthesis that consists of a "Michael reaction" which promotes the addition of acrylonitrile to primary amino groups [136].

Since their discovery, the dendrimer chemistry has been evolving to present a wide choice of different structures of dendrimers, resulting from different processes of synthesis and functionalisation.

Undefined hyperbranched polymers, Figure 0.16-*a*, resulting from the repetition of a branched unit by polymerisation, characterised by irregular structures and rich in defects.

On the contrary, the so-called *Dendrigrafts* (Figure 0.16-b)[137] have a well-defined structure and develop linear chains (copolymers) along a polymeric linear chain, creating a hyper- branched polymer consisting of a fixed number of combined monomers. Considering that the dendrimers

recall the typical structure of a tree, dendrigrafts can simplistically be described as resembling the structure of palm trees.

Dendrimers (Figure 0.16-d) have an extremely orderly, regular structure and they are relatively easy to synthesise. *Dendrons* (Figure 0.16-c) are defined as fragments of the dendrimer and they are not symmetrical, so they are suitable for the synthesis of the asymmetric compound.

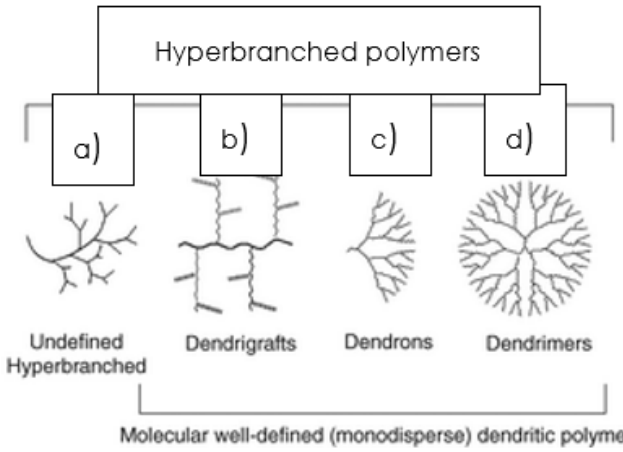

Figure 0.16 Dendrimer Family. a) the undefined hyperbranched polymer, polydispersed and not suitable as drug carrier. b) dendrigraft structures which are based on a central linear structure. c) dendrons are a small, therefore not symmetrical, part of the dendrimer. d) symmetric and well-defined structure.

Thanks to their versatility it is possible to design and synthesise different types of dendrimers, changing their structure according to the needs.

For example, Poly(propylene-imine) (*PPI-dendrimers*) are poly-alkylamines that have as tertiary core tris-propylene amine and terminates with primary amines (surface group). PPIs have a poor transfection ability,

which is why they are often modified to increase the concentration of nucleic acid in cytoplasm [138]. *PEI-dendrimers* [Poly(ethylene imine)] is a derivative of this class that has a nucleus of propane diamine, also modified to reduce the toxicity of positive charges [139].

The most biologically innovative dendrimers and already used for biomedical purposes are the so-called *MAP-dendrimers* (multiple antigen peptide) which consist of a skeleton of poly-lysine; lysine serves as a monomer from which to branch numerous ramifications; they are widely used as vaccines and in imaging techniques [140].

The *Frèchet-dendrimers* are named after the scientist who designed them. The first of this class were characterised by a skeleton of poly-benzyl ether, they develop by condensing several dendrons that can be different from each other, giving rise to dendrimers that can be either symmetric or asymmetric according to the branching generation and the motif of the dendron. The surface of this type of dendrimers is distinguished by -COOH groups that allow to decorate the carrier and to make the hydrophilic compound since the central structure is hydrophobic [137].

PAMAM-dendrimers [Poly(amide amide)] are another class of dendrimers widely studied because they are easy to prepare and thanks to the numerous primary amines can mimic the properties of proteins and therefore useful for biological applications [141].

Finally, *ε-poly-L-lysine* (PLL) is a class of dendrimer peptide characterised by primary amines that act as surface groups easily functionalised and consisting entirely of repeated amines. Because of their structure they have the advantage of being able to host at their molecular core chemotherapeutic drugs, which very often have a lipophilic nature. While on the outside, because of the ionisable amines, can have electrostatic interactions with negative charges, i.e. nucleic acids [142].

1.9.2 Dendrimer characteristics

Dendrimers are molecules that contain a series of ramifications that extend from a central nucleus that generally has several copies of the same monomer. Within a dendrimer there are several distinct parts: a multifunctional nucleus (core), branching units and surface functional groups.

The *nucleus* has a fundamental importance in characterising the final structure, in particular it affects the shape, size and multiplicity of the dendrimer. It can consist of a single atom or a molecule, however multifunctional; it can be homogeneous with the other components or heterogeneous and can accommodate special compounds such as metal atoms fulfilling specific functions [136].

The "*intermediate zone*", called the inner region, is characterised by a symmetrical system of ramifications. This area gives the molecule both specific physical and chemical properties, characterises the flexibility of the entire molecule and influences the presence of free internal volumes available to accommodate other compounds. The typical structure develops radially around the initial 'core' causing an increase in the number of terminal groups and a thickening of branches. The concept of dendritic branching explains how the molecule develops around a reference point, occupying three-dimensional space with its atoms and its repetitive units [143].

The "surface region" consists of terminal units that can be left as such or functionalised with other molecules that enable nanoparticles to target tissues or to protect them from the immune system. In fact, the surface of the dendrimers not only performs the function of protection of the internal groups, but can also react, because of its active sites, with external reagents and solvents [144].

The smaller dimensions of dendrimers, are characterised by a lower density of the surface groups, thus, have a more open structure, with rather spaced chains, which makes the inner part of the dendrimers more accessible to a solvent. On the contrary, dendrimeric later generations are of greater size and spherical shape, highlight a compact external structure with high density of surface groups and rich of internal cavities able to bind sites for the "host" molecules. Such internal niches may have either an essentially hydrophilic character, which allows access to positively charged ions; or low polarity sites that can interact with hydrophobic species. In fact, an important characteristic of these molecules is precisely the possibility of trapping other molecules of various types and sizes in such internal cavities [145,146,147].

1.10 MICROPARTICLES

1.10.1 Introduction

Microparticles (MPs) ranging in size from 1 µm to 1000 µm have become highly functional materials with extensive applications in biomedicine, including drug delivery, tissue engineering, biosensing, and cellular life science. The properties of these microparticles, such as size, structure, composition, and configuration, play a crucial role in determining their application suitability. Therefore, it is essential to develop precise fabrication methods to enhance the pharmaceutical capabilities and reliability of microparticles for biological studies [148].

The importance of controlled drug release systems in the field of therapeutics is well-known and established. The early studies in this area, dating back to the '60s, highlighted the significance of achieving a consistent release of drugs, particularly in anaesthesia [149]. Researchers such as Langer and Folkman were pioneers in demonstrating the

controlled release of anticancer macromolecules and showcasing their advantages in cancer therapy [150]. In the 1980s, there was a rapid expansion of research on microparticulate therapeutic systems for controlled drug release, with a primary focus on developing systems that could facilitate constant zero-order release kinetics. These studies paved the way for the development of therapeutic systems and pharmaceutical products with micrometre-scale dimensions, which gained significant momentum from the 1990s onwards.

The preferred preparation for new medicines or those already on the market is microparticles or MPs as they have had a significant impact on the drug delivery industry and are a good solution in clinical and pharmaceutical fields [151]. MPs are larger than nanoparticles (around 30 to 100 μm in diameter), consisting of an active ingredient embedded by a matrix.

The active ingredient, thanks to the controlled delivery of MPS, can be made more suitable to the final application by the improvement of its physicochemical characteristics, leading to a better solubility and avoiding its aggregation or precipitation in biological fluids. The typical matrices of microparticles are made of polymers, such as PLGA and PLA, alginate and chitosan (approved by FDA); these are polymers of a relatively high molecular weight consisting of simple and repetitive units (monomers). The basic characteristics that polymers must have for the controlled release system are:

- Biocompatibility with fluids and tissues of the receiving organism.
- Biodegradability, which is the tendency to physically erode and is a direct consequence of chemical reactivity to hydrolysis, to the attack of free radicals or by enzymes.
- Lack of immunogenic response [152].

Biodegradability is the tendency to physical erosion in a physiological or biological environment. Physical erodibility is a direct consequence of the chemical reactivity to hydrolysis, to the attack of free radicals, or to the breakdown mediated by enzymes. The term 'Biodegradable' does not always infer biocompatibility: it is when the degradation products are even biocompatible. A material can be defined as biocompatible when the adverse reactions triggered in the organism are reduced to a minimum so that the host organism can adapt to all levels (cell, tissue, organ) [153].

Often, the materials used are referred to as superhydrophobic and have surfaces coated with non-polar materials such as methyl groups (-CH2/CH3) or fluorinated groups (-CF2/CH3). Non-polar surfaces share the ability to not interact with proteins, preventing protein adsorption and subsequent denaturation. However, this approach is temporary due to the inherent nature of proteins. For this reason, researchers are diligently exploring a solution. Superhydrophobic surfaces are also employed to prevent the adsorption of cells and bacteria, reducing interactions, proliferation, and coagulation of red blood cells [154]. As of today, there are no FDA-approved medical devices, but products with superhydrophobic surfaces are marketed for self-cleaning or anti-icing purposes. Moreover, the liberation of carbon dioxide encourages the development of a gel matrix that is more porous and less compact in comparison to matrices generated through external gelation methods. These attributes offer benefits for entrapping cargo that necessitates effective exchange of solutes with the surrounding environment, examples of which include living cells and enzymes employed in tissue engineering or biocatalytic applications [155].

A biodegradable polymer must have functional groups that easily degrade as esters, anhydrides, amines, peptides and glucosides. The

corresponding materials can be divided into natural compounds, such as proteins (albumin, collagen, fibrin, gelatine), polysaccharides (alginate, cellulose, chitosan, dextran, hyaluronic acid and corn), or lipids; or synthetic substances such as polyamide and polyesters (polycaprolactones, polycarbonates, polyglycolides) [156].

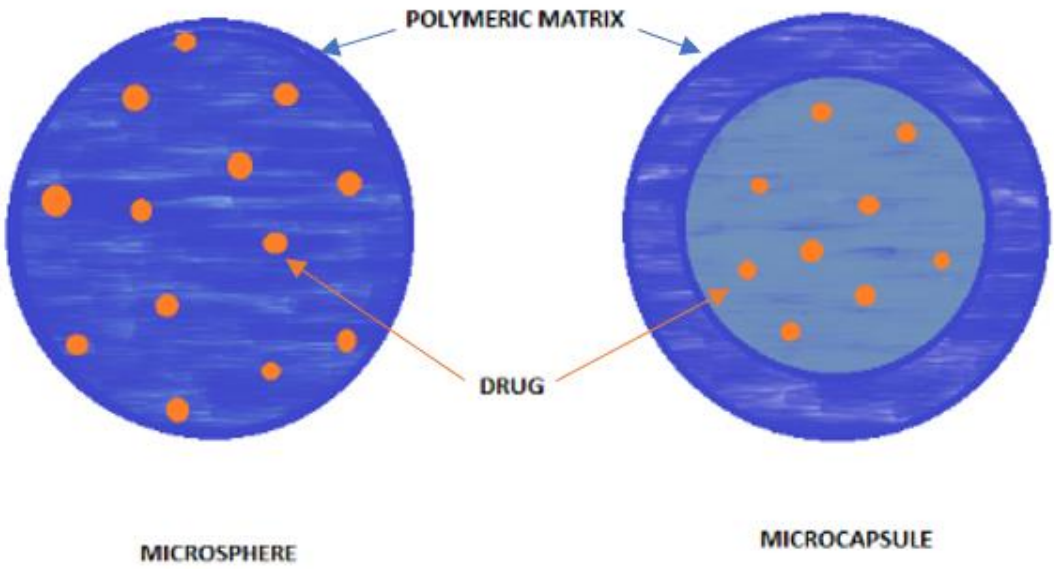

Figure 0.17 On the left there is the representation of microsphere where drug (orange spheres) is absorbed in a matrix (blue). While on the right microcapsule with polymer surrounding drug, respectively in blue and orange.

Through the protection given by the matrix, it is possible to protect drug from *in vivo* degradation or increase its half-life time. For example, nucleic acids have the potential to treat a range of diseases, but their relatively complex structure and susceptibility to enzymatic degradation limit their ability to reach the target tissue at therapeutically efficacious concentrations [157].

In general, depending on the matrix distribution, MPs can be categorised into two large families (Figure 0.17):

- "Microspheres" that are those MPs consisting of an orderly matrix in which the active component is evenly distributed in it, while its release into biological fluids depends on the disintegration and dissolution of the matrix in the fluid [158].
- "Microcapsules" which are a reservoir system in which the matrix delimits the inner core consisting of the drug solution. In this case, it is a prerogative that the matrix is not soluble to the medium used to dissolve the drug, thus avoiding the burst release of the bioactive component. Rather, the drug must permeate the matrix and then dissolve in the biological fluids [159,160].

1.10.2 Controlled release

Controlled release refers to a deliberate and regulated release of a substance, such as a drug or active ingredient, from a carrier system or formulation over a specified period of time. The release is typically designed to achieve a desired therapeutic or functional effect by maintaining appropriate drug concentrations or controlled delivery kinetics. The goal of controlled release systems is to optimise drug efficacy, minimise side effects, and improve patient compliance by providing a sustained and controlled release profile that meets specific therapeutic requirements. This can be achieved through various mechanisms, including diffusion, dissolution, degradation, or a combination of these factors, depending on the specific formulation and desired release characteristics [161].

Controlled release systems that use polymeric substances are classified according to the mechanism that controls the release of the drug. Most

commonly used by the pharmaceutical industry are *diffusional control systems*, in which release rate is determined by the simple diffusion of the active substance, likewise can be distinguished in reservoir systems and matrix systems. As for reservoir systems, the drug is present as a core covered by a diffusional barrier that must be: uniform and of constant thickness over time; made of a polymer material (homogenous or heterogeneous, amorphous or semicrystalline, non-porous, microporous or semi-permeable); and insoluble in aqueous biological fluids. The drug may be present in the reservoir in the form of solid particles suspended in a liquid medium or as a concentrated solution in a solid or liquid dispersing medium. The kinetics are zero, at least for some time [162].

Matrix systems are those in which actives principles are uniformly dispersed in the polymer matrix, such as methyl acrylate-methyl methacrylate insoluble plastics, polyvinyl chloride, polyethylene, and are ceded to the aqueous medium in which it first dissolves and then spreads until the solvent/drug interface moves inwards [163,164]. Since the diffusion distance of the solute does not remain constant over time, but increases continuously following the removal of the active substance, an elution zone is generated whose thickness increases progressively and the release takes place under non-stationary diffusion regime, mathematically described by Fick's second law. Release kinetics, which are influenced by these variables, follow non-zero kinetics [165]. The release of the active substance depends on the type of polymer matrix used, the glass transition temperature of the polymer and its molecular weight. Homogeneous, or granular matrix systems are distinguished in relation to the matrix structure [166].

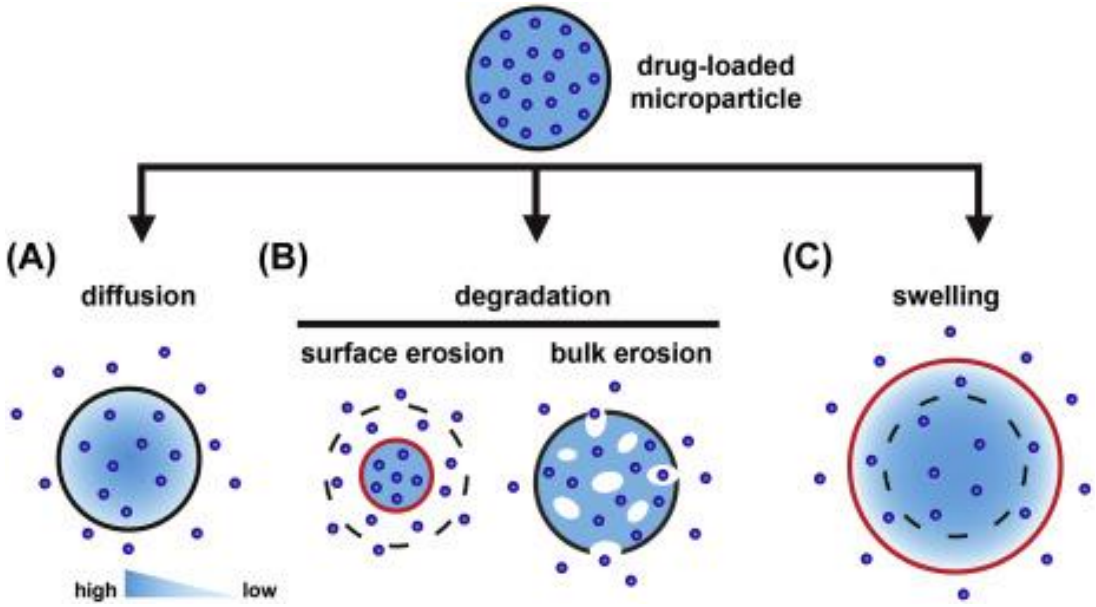

Figure 0.18 Different release of drugs. It can be by Diffusion, Degradation or by Swelling (li et al. 2020).

The first are non-porous polymer systems formed by a continuous phase in which the solute spreads only if it is soluble in it (diffusion mechanism by solubilisation) [167]; the latter consist of porous materials in which the release of the drug takes place by diffusion in the medium that wets the pores. Generally, monolithic systems are simple to prepare and safe, given the impossibility of accidentally releasing the entire dose of medication and equipped with good mechanical strength [168].

These materials, however, have the disadvantage of not being able to release the active substance at a constant rate. A different approach from the previous one is the use of erodible systems, in which the drug is ideally distributed evenly over the entire polymer matrix and its release is generally governed by a combined effect of polymer degradation and diffusion. This results in first-order release kinetics, although more complicated kinetics have frequently been observed, as drug diffusion is affected even by matrix degradation [169].

Systems with controlled swelling or hydrogel, on the other hand, the polymer matrix is affected by complex diffusional processes involving the substances present in the external dissolution medium. The controlled release of drugs by swelling can be achieved by exploiting the glass/amorphous transition of polymers, in presence of swelling agents and macromolecular relaxation associated with this transition. Hydrogels are able to increase their volume even five times and active release is controlled by the swelling produced by the water and the subsequent spread of the drug through the significantly polymer lattice network [170].

Erodible systems have in their constitution a non-toxic erodible polymer matrix that can also be used as implant systems. The release kinetics will rely not only on the diffusion or dissolution phenomena of the active substance in the medium but also on those affecting the matrix (Figure 1.18 B [171]).

1.10.3 Microparticles' material: Alginate

Alginate is a commonly used biomaterial in drug delivery and tissue engineering due to several factors, including its biocompatibility, low toxicity, affordability, and its ability to easily form gels when exposed to divalent cations such as Ca^{2+} and Mg^{2+} [172].

Most commercially available alginates are derived from different types of brown algae: *Laminaria hyperbola, Laminaria Digitata, Laminaria japonica, Ascophyllum nodosum, and Macrocystis pyrifera*. In their natural form, alginates exist as mixed salts containing various cations found in seawater, such as Mg^{2+} and Na^{+} [173].

Alginate has found applications in various fields, including injectable cell delivery, wound dressings, dental impressions, and diabetes treatment [174,175].

However, while alginate gels offer advantages, the native form of alginate may not be the optimal material choice due to its degradation caused by the loss of divalent ions into the surrounding medium. This degradation process is typically unpredictable and uncontrollable. To address this, many approaches involve covalently cross-linking alginate with different molecules to control the swelling and mechanical properties of alginate gels [176].

Another drawback of using alginate is its high molecular weight, which exceeds the kidney's clearance threshold. Nevertheless, extensive efforts have been made over the years to enhance the utilisation of alginate beads for biological and medical applications [177,178].

Alginates are composed of a linear arrangement of consecutive a-l-guluronic (G-blocks) and β-d-mannuronic (M-blocks) acid residues (Figure 1.19) [179].

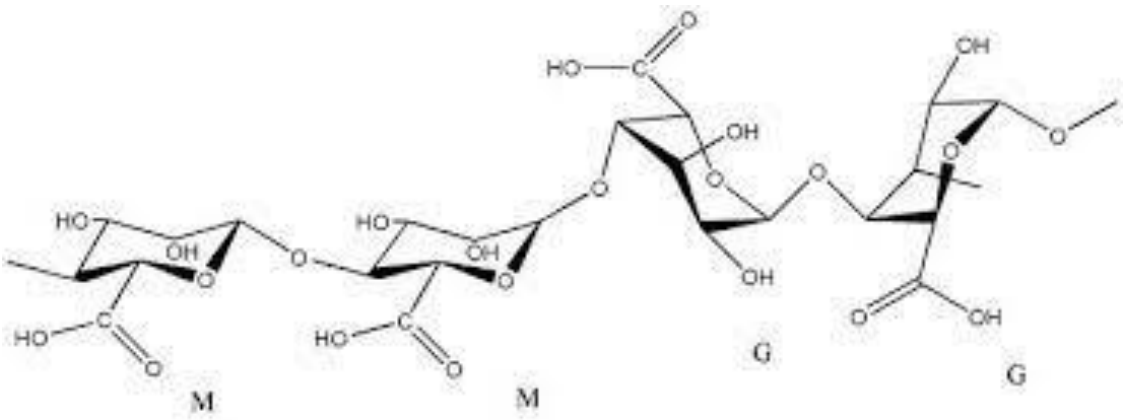

Figure 0.19 Different configuration of Alginate: M-blocks and G-blocks.

The sequence and structure of alginate can vary from one molecule to another, depending on the composition of α and β block regions they contain [180].

Consequently, the physical properties of alginates are influenced by their composition and the length of the sequences [176,181].

1.10.4 Gelation mechanism

The gelation of alginate droplets typically involves cross-linking the alginate polymer chains using divalent cations. These cations bind to the guluronate blocks of the alginate polymer chains, forming a structure known as an "egg-box." Alginate exhibits different affinities for various cations, with the decreasing affinity order: Pb > Cu > Cd > Ba > Sr > Ca > Co, Ni, Zn > Mn [182]. However, calcium (Ca^{2+}) is the most commonly used cation for ionotropic gelation of alginate due to its non-toxic nature compared to other cations.

Calcium chloride ($CaCl_2$) is the frequently employed calcium source for gelation. It readily dissolves in water, allowing the Ca^{2+} ions in solution to instantly cross-link with alginate droplets, resulting in the formation of hydrogel particles. Insoluble calcium salts, such as calcium carbonate ($CaCO_3$), can also be used when gradual or controlled cross-linking is desired [183].

1.10.5 External gelation

External gelation is a widely employed and traditional method of ionotropic gelation for creating alginate hydrogels. This process involves introducing Ca^{2+} ions from an external source into separate alginate droplets, which can be formed using liquid-air or liquid-liquid techniques.

The Ca^{2+} ions diffuse into the spaces between the alginate polymer chains, initiating crosslinking [184]. As an example, an alginate solution containing cargo is extruded and deposited into a gelling bath that contains Ca^{2+} ions. Upon contact, the Ca^{2+} ions begin to crosslink with the alginate polymer chains on the outer edge of the droplet, forming an initial semi-solid membrane that encases the droplet with a liquid centre [185]. The droplets are further immersed in the gelling bath, allowing for the diffusion of Ca^{2+} ions through the membrane via a concentration gradient. This process leads to the solidification of the droplet core [186]. Consequently, an alginate bead is produced, with the cargo randomly entangled within the crosslinked matrix. In the case of capsule formation, the cargo (such as an aqueous or oil core) is co-extruded with the alginate solution and deposited into a gelling bath. The alginate solution surrounding the liquid core undergoes gelation, resulting in a capsule with an insoluble shell [187].

Cross-linking in external gelation starts at the outer edge of the alginate droplet, which leads to the polymer chains being pulled towards the periphery to facilitate the process [188]. As cross-linking progresses, the concentration of alginate chains within the core of the droplet gradually decreases. Once cross-linking is complete, there will be a higher number of Ca-alginate networks formed at the periphery compared to the centre of the bead. This non-uniform gel structure results in a higher elastic modulus for the bead and restricts the penetration of small hydrophilic cargo molecules, thereby enhancing encapsulation efficiency [184].

1.10.6 Internal gelation

In the late 1980s, efforts were made to reduce bead size and increase the efficiency of the industrial process. Researchers explored the emulsification method, where an alginate solution is dispersed into micro-

droplets and then gelled through external gelation by adding a calcium solution to the emulsion. While this method increased bead productivity, it resulted in the coagulation of beads into large masses due to challenges in controlling the gelling conditions in the emulsion. To overcome this issue, the gelation mechanism was modified by controlling the release of calcium ions for gelation [189]. In this technique, an alginate solution containing insoluble calcium carbonate particles was first emulsified into an oil phase. Acetic acid was then added to the emulsion to lower the pH, causing the dissolution of calcium carbonate into Ca^{2+}, carbon dioxide, and water. The released Ca^{2+} ions subsequently cross-linked with the alginate polymer chains internally. Since cross-linking and gelation occurred inside the alginate droplet, this mechanism was termed internal gelation. This gelling mechanism is employed only when the alginate solution is dispersed using an immiscible liquid [190].

In contrast to particles formed via external gelation, the gel structure produced by internal gelation is more homogeneous [191]. The insoluble calcium salt is uniformly dispersed within the alginate droplet, and the dissolution of this salt inside the droplet leads to a more even distribution of polymer across the dispersed droplet when acid is introduced. Consequently, cross-linking between the alginate polymer chains and Ca2+ ions occurs uniformly within the dispersed droplets. Furthermore, the release of carbon dioxide promotes the formation of a more porous and less dense gel matrix compared to those obtained via external gelation. These characteristics are advantageous for encapsulating cargo that requires efficient solute exchange with the external environment, such as living cells and enzymes used in tissue engineering or biocatalytic applications.

1.10.7 Interfacial gelation

A recent study by Leong et al. [192] introduced a novel gelation mechanism known as interfacial gelation. In this process, an oil cargo was emulsified into an aqueous dispersion containing insoluble $CaCO_3$ nanoparticles. These nanoparticles self-assembled at the interface, resulting in an oil in water (O/W) Pickering emulsion. After phase separation, the top layer, enriched with oil droplets, was collected and dispersed into an alginate solution. Subsequently, acetic acid was added to induce the dissolution of the $CaCO_3$ nanoparticles at the O/W interface. As a result, Ca^{2+} ions were released and cross-linked with alginate polymers at the O/W interface, forming a continuous membrane that encapsulated the oil core. Unlike previous gelation mechanisms, the cross-linking of alginate with Ca^{2+} ions occurred in situ at the interface, leading to the term "interfacial gelation."

Interfacial gelation offers notable advantages for the formation of alginate capsules with oil cores compared to other gelation mechanisms. It eliminates the need for a physical nozzle to pre-template the alginate solution into compound drops for capsule formation. Instead, the capsule morphology is achieved through the self-assembly of $CaCO_3$ nanoparticles at the oil-water interface. Any emulsification tool can be employed to create the O/W Pickering emulsion template [193]. The size of the alginate capsules is no longer restricted by the nozzle diameter, as in the co-extrusion method. Instead, capsule size is inversely proportional to the energy input during the emulsification step. Using various emulsification methods, alginate capsules ranging from a few micrometres to several hundred micrometres in diameter can be produced. Additionally, the productivity of the process is not limited by the physical nozzle since oil droplets are not formed on a drop-by-drop basis [194].

1.10.8 Microparticle fabrication

Conventional methods like emulsion polymerisation, dispersion polymerisation, and spray drying have limitations in producing microparticles with desired properties, including high polydispersity, poor reproducibility, limited functionality, and limited control over morphology [195]. To overcome these limitations, researchers have explored various technologies, such as droplet microfluidics, flow lithography microfluidics, electrohydrodynamic co-jetting, photolithography, and soft lithography-based imprinting and micro-moulding, for tailored fabrication of microparticles [196].

Several techniques for the preparation of MPs have been proposed in recent decades. The traditional techniques for the production of microparticles are multiple. Most methods of emulsification are mechanical, based on the principle of extrusion or agitation and they need high energy. In particular, emulsification based on the extrusion process (with the use of microchannels or membranes) provides that the dispersed phase is forced to cross a microfiltration device with a defined size [197]. The formation of emulsions through the use of ultrasound, based on the cavitation mechanism, requires less surfactant and ensures smaller sizes than conventional agitation methods. Also, the spontaneous emulsification process (i.e., a physicochemical process) is classified as a low-energy method. The second stage of particle formation from the emulsion can be achieved by evaporation or solvent extraction [198]. Another physicochemical technique such as coacervation, is characterised by the separation of a polymer solution into two miscible liquid phases, a dense phase and a diluted phase, after the change of certain parameters, such as pH or ion force [199]. Finally, spray-drying in which particles are obtained by drying (under a flow of a gas, usually air) of atomised liquid currents in droplet [200]. Traditional methods are widely

used for the preparation but do not fully meet the parameters for process control or product reproducibility, since it is not possible to achieve perfect mixing conditions resulting in variations in particle characteristics. For this reason, traditional methods are associated with heterogeneous and poorly controlled chemical and mechanical conditions forming vesicles of uneven size; hence MPs have to endure post-processing to obtain homogeneous suspensions [201].

The development of new methods for fabricating microparticles has led to significant advancements in biomedical applications. To overcome traditional method limitations, researchers have explored several innovative techniques for tailored microparticle fabrication.

One such method is droplet microfluidics, which utilises microfluidic devices to precisely generate and manipulate droplets. By controlling the flow rates and parameters, uniform microparticles can be produced with high reproducibility and desired characteristics. This technology enables control over size, composition, and encapsulation of materials within the droplets [202].

Flow lithography microfluidics combines microfluidics with lithographic principles to create microparticles with well-defined shapes and structures. By flowing a pre-polymer solution through microchannels containing patterned moulds or templates, microparticles with controlled features can be fabricated [203].

Electrohydrodynamic co-jetting is another technique that employs an electric field to control microparticle formation. Multiple fluid streams containing different materials are ejected through separate nozzles and subjected to an electric field, resulting in the formation of core-shell or multi-component microparticles [204].

Photolithography relies on photomasks to define patterns on a substrate coated with a photosensitive material. The exposed areas undergo polymerisation, allowing for the precise formation of microparticles with defined geometries. This method is particularly useful for creating microparticles with complex structures or surface patterns [205].

Soft lithography-based imprinting and micro-moulding techniques, such as replica moulding and microcontact printing, enable the replication of patterns from a master mould onto a substrate. These methods can be utilised to fabricate microparticles with specific shapes and surface features [206].

These advanced fabrication technologies offer enhanced control over the size, shape, composition, and functionality of microparticles. They have the potential to significantly improve drug delivery systems, tissue engineering scaffolds, biosensing platforms, and other biomedical applications that require precise control of microparticle properties.

1.11 OBJECTIVES OF THE PROJECT

The present project has the final aim to produce a personalised drug delivery system in a reproducible manner that will be pursued through the following steps:

1. Develop materials, methods and technologies suitable for the nanoparticle production, and determine which amino acids result in a better encapsulation and release of chemotherapeutic drugs and nucleic acids.
2. Determine if the targeting sequence (KCCYSL) achieves targeted drug delivery to HER2 breast cancer cells *in vitro*.
3. Understand the cytotoxicity of the drugs and the NPs

4. Study the physical phenomena behind the production of microparticles and how to achieve monodispersed droplets encapsulating the drug components.
5. Explore the combination of adding small amount of stable chemical compound mixtures in order to expand the possibilities of personalised.
6. Provide a proof of concept *in vitro* of modulated cell response using different dosage of the therapeutic agent. This will be pursued by clinically reflective *in vitro* models.

SYNTHESIS AND CHARACTERISATION OF HYPERBRANCHED PEPTIDES

1.1 INTRODUCTION

HER2 positive breast cancer is recognised to be a very aggressive molecular subtype, characterised by an increase in the expression of the HER2 membrane receptor that is implicated in multiple stages of cell life. It has been hypothesised that lipid-peptides based nanovectors can give numerous benefits for treating this subtype of breast cancer by exploiting the high number of HER2 receptors of cancer cells [207].

In recent years, dendrimers and dendrons have found great interest in the development of new drug delivery systems thanks to their great flexibility and countless potential. Dendrons, consisting of repeated lysine monomeric sequences, have a flexible structure and characteristics similar to biological proteins and so biocompatible, soluble in aqueous solvents and resistant to proteolytic activity [208,209]. The core, the internal and external functionalities give rise to countless molecules with different physio-chemical properties, and easily functionalised for targeted delivery to reduce the toxicity of many cancer drugs [210,211]. Therefore, they can be used as carrier for gene therapy by exploiting the positive charges on the outside of their structure that interact with the negative charges of the phosphate groups present in the nucleic acid chain [212,213]. Nevertheless, they can increase the retention time of many molecules because thanks to the increased solubility in plasma, they increase the passive targeting effect (EPR effect) in solid tumours [214].

Here, the hyperbranched structure of poly-lysine dendrons designed to improve the delivery of nucleic acids and chemotherapy drugs, in

association with a targeting sequence that recognises the HER2 receptor, necessary to concentrate the nanocarriers in the tumoural area and reduce the toxicity of the anticancer drug.

1.1.1 Synthesis of dendrons

Dendrimers can be synthesised through two different approaches: convergent and divergent synthesis. The first begins with what will become the outer part of the molecule. The functional points of the monomers are activated in order to react with each other and form the desired generations (Figure 0.1). At the end of the process the dendritic or dendron segments (Figure 0.1) are reacted together to obtain the dendrimer [215,216]). This type of reaction was devised in the '90s by Hawker and Fréchet for the Fréchet-dendrimers synthesis. The convergent approach allows to obtain dendrimers highly monodispersed. Unlike divergent synthesis, this strategy has limited reactive sites and is more easily controllable, therefore only small excesses of reagents are needed [217].

However the final number of generations will be pre-determined but it is possible to add different types of dendrons depending on the physical-chemical characteristics desired [136].

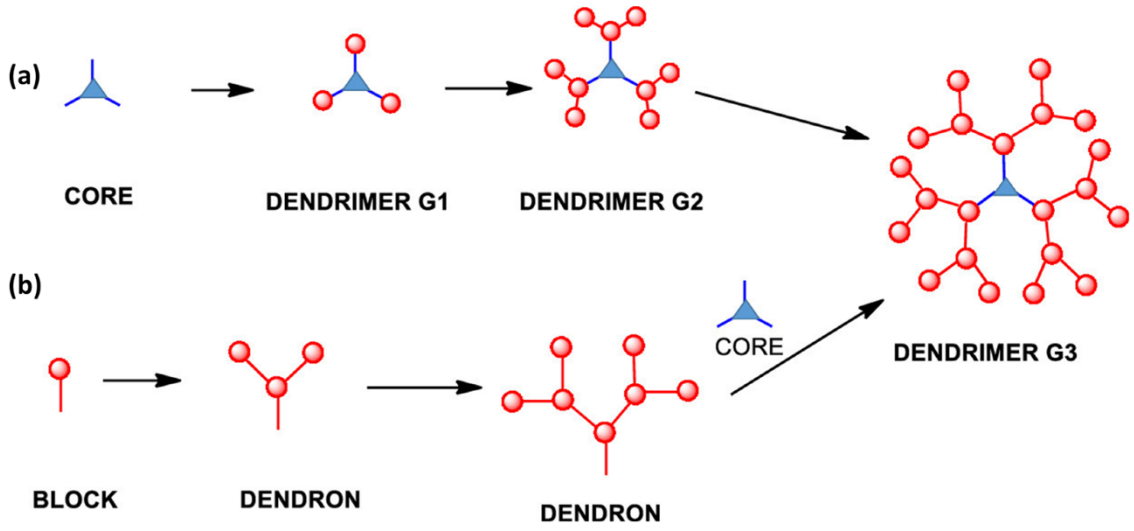

Figure 0.1 a)divergent synthesis and b) convergent synthesis [218].

Another advantage of the convergent methodology is that the difference between the molecular weight of a perfect dendron and an irregular dendron is high enough to allow relatively easy purification of products and thus obtain dendrimers with high purity [217]. The limits of convergent synthesis derive, instead, from the steric encumbrance that is created around the focal point as the dendron grows and might prevents the coupling with the core [219].

Contrariwise, in the divergent synthesis, the reaction starts from the centre and continues outward through the repetition of coupling and activation of the reaction sites. Monomers are designed in such a way that they do not react with each other and, after activation, they react with the substrate or growing core [137]. Repetition of the coupling and activation reaction leads to the formation of subsequent generations. Once the desired generation has been reached, the peripheral groups are properly functionalised according to the desired application of the dendrimers. The divergent methodology is ideal to synthesise large dendrimers that at each step of coupling/ activation double at every generation increment.

However, one of the weaknesses of divergent synthesis is the exponential increase in the number of peripheral sites of reaction when increase in the generation number as well [220]. Due to the high number of reaction sites it is difficult to obtain dendrimers of high generations with a good dendrimeric purity because an imperfect macromolecule cannot be separated from the others because it is too similar in shape, weight and chemical-physical properties (coupling step) [217].

1.1.2 Solid Phase Synthesis

The "solid phase synthesis" (SPPS) it is a variation of the two main synthesising strategies technique, divergent and convergent, is used to obtain an half-dendrimer [216], called dendron consisting of repeated amino-acids sequence (Figure 0.2).

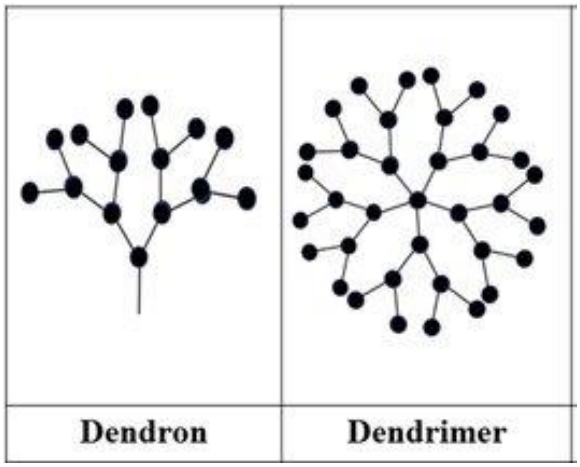

Figure 0.2 On the right a complete dendrimer. On the left a section of a branched dendrimer, called dendron. Modified from "International Journal of Peptide Research and Therapeutics" by N. Hegde et al., 2019.

This synthetic technique is based on the idea of using an insoluble solid support on which to increase the peptide chain from the terminal carboxyl group to the terminal amino group (strategy C→N), contrary to what happens in the biosynthesis of peptides in ribosomes. The synthesis is carried out through a series of steps, cyclically repeated, which involve the coupling of partially protected amino acids and preliminarily activated on the carboxyl groups, and ends with the elimination of the protective groups during the detachment of the peptide from the resin (Cleavage) [221].

Resin used in SPPS shall be insoluble in all solvents used during synthesis, chemically inert and physically stable to mechanical stress. Despite the impossibility of isolating the intermediates, the yield in the coupling of the amino acids is very high thanks to the possibility of using a large excess of reagents. In addition, the sub-group of products that form can be removed by simply washing the resin with a suitable solvent [222]. The resin shall allow the anchoring of the first amino acid by a covalent bond, which is stable enough to remain unchanged during peptide elongation, but which can be easily removed throughout the cleavage. For this purpose linkers are usually exploited and interposed between the solid support and the first amino acid [223].

Peptide synthesis is a very complex operation as the amino acids have several reactive zones that could lead to a very large number of waste products, thus greatly lowering the yield of the process. To overcome this problem, specific protective groups are adopted to temporarily deactivate the functional groups not directly involved in the formation of the amide bond. Many amino acids in fact contain reactive groups in the side chain such as carboxylic acids, alcohols, thiols and amines, which could react with subsequent building blocks [224]. A fundamental characteristic of the protective groups is their orthogonality, that is, the

possibility of being removed in specific reaction conditions and especially independently of each other. There are two main orthogonal protection strategies for solid-phase peptide synthesis: the Boc/Bzl strategy in which the a-amino group is protected as terbutyloxycarbonyl (t-Boc), removable with trifluoroacetic acid (TFA), and Bzl by strong acids. The other is the Fmoc/TBU strategy where the a-amino function is temporarily protected with the Fmoc group, which is easily removed with a 20% piperidine solution in DMF through a β-elimination, while TBU is removed by TFA acidification (Figure 0.3)[225].

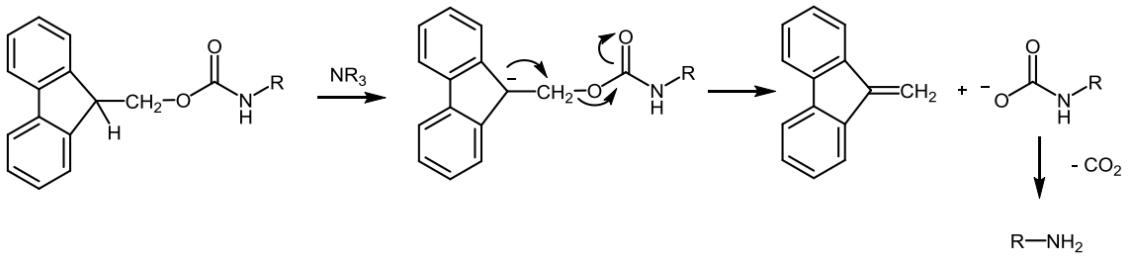

Figure 0.3 Elimination of the protecting group FMOC.

In order for the formation of the peptide bond to occur rapidly and completely, the carboxyl group of the amino acid to be introduced must be activated. To achieve such activation, various methods are available, which are based on the use of different types of "coupling reagents". To facilitate the formation of the amide bond between two amino acids it is necessary to activate the carboxyl group of the incoming amino acid. This procedure is carried out in order to be able to work at room temperature, thus avoiding degradation of the peptide. The activator reacts with the free carboxylic function generating a very reactive ester thanks to the formation of a good outgoing group. The activation reaction is catalysed by uronium salts such as HBTU (O-(1H-benzotriazole-1-yl)-N,N,N0,N0-tetramethyluronium hexafluorophosphate), is able to activate the

carboxyl group and thus react with the free amine of the growing peptide [221].

Peptide cleavage from resin, along with simultaneous deprotection of the side chains of amino acids, is carried out by acidolysis by trifluoroacetic acid (TFA). During this process, highly reactive cationic species are released, which can interact with those amino acid residues that contain functional nucleophilic groups (for example, Trp). To avoid this, TFA is used in the presence of various types of nucleophilic reagents, which act as scavengers against these electrophilic species in association with water and tri-isopropyl silane (95:2.5:2.5 v/v) [226,227,228].

1.1.3 General characterisation

Once the synthesis is complete, the peptides must be analysed to determine if their structure is correct. The instruments used are: infrared, dynamic light scattering, mass spectrometry and column chromatography.

1.1.3.1 Fourier Transform Infrared

Fourier transform Infrared spectroscopy (FTIR) or IR spectroscopy is an absorption spectroscopic technique used in the material characterisation field for the study of chemical bonds. The technique foresees that an infrared photon is absorbed by a molecule, passing from its fundamental vibrational state to an excited vibrational state.

1.1.3.2 Dynamic Light Scattering

Dynamic Light Scattering (DLS) was performed using the Zetasizer Nano series (Malvern Instruments) to measure the size of the peptide or peptide aggregates. In this technique, peptides or particles are illuminated with a

laser and the intensity fluctuations in the scattered light is analysed. The intensity of the fluctuations is then used to calculate the size and the polydispersity of the particles based on their movement in water. Mass spectrometry

1.1.3.3 Mass Spectrometry

is a method that allows the identification and quantitative analysis of a molecule from its mass exploiting two phenomena related to mass and charge:

- the trajectory of an ion or a charged particle in motion can be modified by the action of a magnetic or electric field and at the same charge, particles of lesser mass will suffer greater deviation.
- charged ions or particles that, when accelerated by an electric field, assume different speeds depending on their mass: with the same charge, particles of higher mass assume lower speeds.

1.1.3.4 High Performance Liquid Chromatography

High Performance Liquid Chromatography (HPLC) is an analytical chemistry technique used to separate and purify components in a mixture, to identify each component and to quantify each component. It is based on pumps in which a pressurised liquid solvent containing the sample mixture passes through a column filled with a solid adsorbent material. Each component in the sample interacts differently with the adsorbent material, causing different retention times for the components and leads to separation of the each of them as they flow on the chromatographic column in which they are held.

1.2 AIMS OF THE CHAPTER

In this chapter, the purpose of this chapter is to illustrate the synthesis of various peptide structures through solid-phase synthesis. A range of hyperbranched poly-lysine dendrons have been obtained using solid phase synthesis and characterised to confirm the desired structures shown in Figure 0.4.

The synthesised poly-lysine dendrons were:

- RGen3K
- LSYCCK(Gen3K) also called TGen3K
- CSCLYK(Gen3K) or SGen3K
- K16
- LSYCCK(K16) or TK16

RGen3K was used as control peptide to assess the effectiveness of the polymer structure in the absorption of nanoparticles within the target cell.

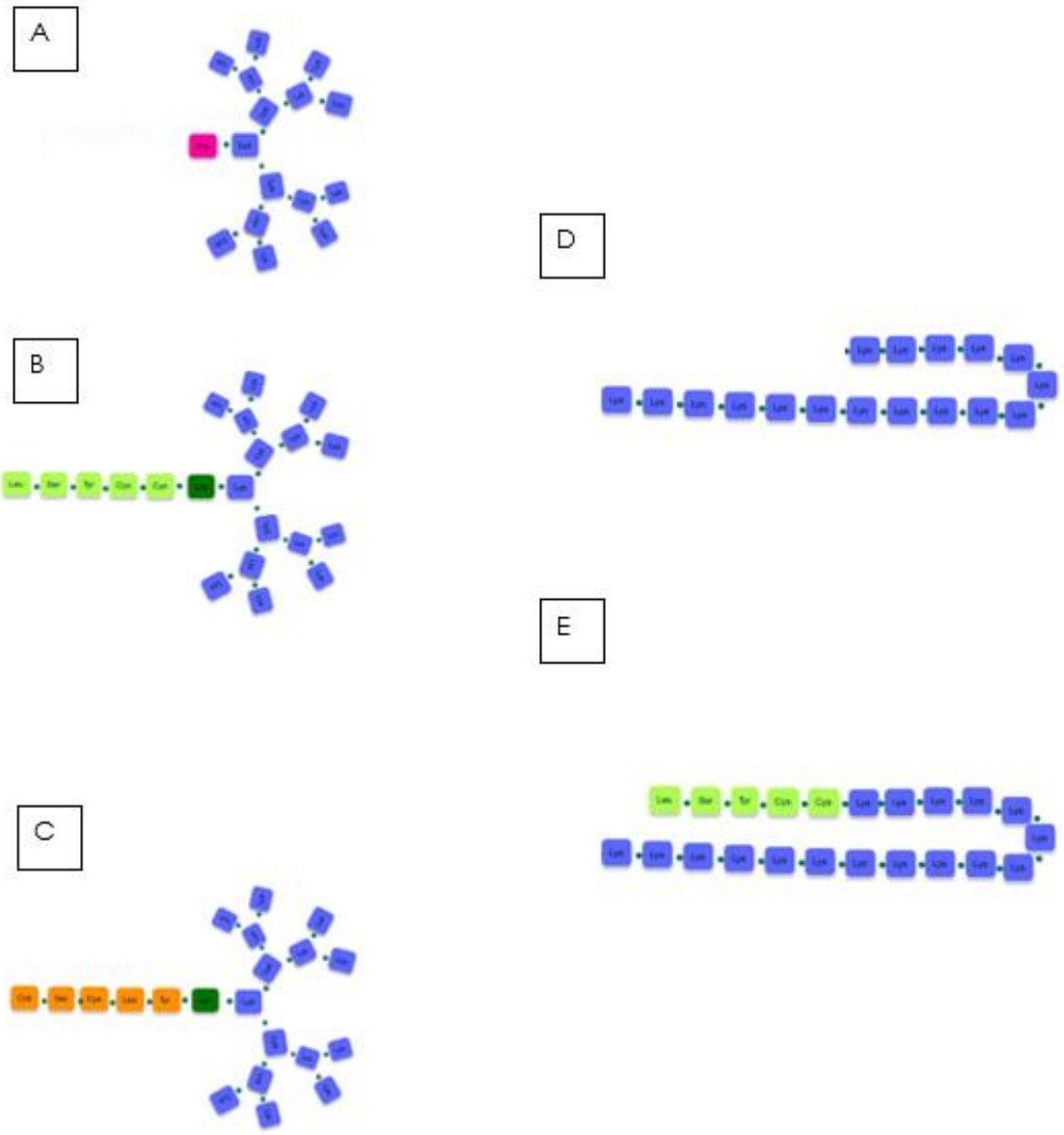

Figure 0.4 a) RGen3K; b) LSYCCK(Gen3K); c) CSCLYK(Gen3K); d) K16; e) LSYCCK(K16).

The more complex structure presents a hexapeptide sequence (LSYCCK) that recognises some sequences of the HER2 receptor and therefore selectively targets the HER2 positive cells. The scrambled, CSCLYK(Gen3K), or SGen3K has the same the same hexapeptides in a different order to define the selectivity of the targeting sequence towards HER2 receptors.

Linear peptides (K16 and TK16) were used as controls to compare the efficiency of the branched structures. Controls also included the relative linear sequences.

The peptide structures were characterised to confirm their chemical structure and subsequent use in *in-vitro* experiments.

1.3 MATERIALS AND METHODS

1.3.1 Solid Phase Peptide Synthesis

The hyperbranched peptide dendrons were synthesised by solid phase peptide synthesis with the manual method. Amino acids: Fmoc-L-Arg(pbf)-OH, Fmoc-Lys(boc)-OH, Cysteine Fmoc-Cys(Trt)-OH, Fmoc-Tyr(tBu)-OH, Fmoc-Leu-OH were purchased from Novabiochem. Amino acid Fmoc-Ser-OH (purity 97%) was purchased from Aldrich and branched Lysine, Fmoc-L-Lys(Fmoc)-OH, was purchased from Iris Biotech GMBH. Organic solvents by Fisher Scientific were HPLC grade. Coupling powder O-(1H-benzotriazol-1-yl)-N,N,N',N'-tetramethyluronium hexafluorophosphate (HBTU) and solvent diisopropylethylamine (DIPEA) were purchased from Alfa Aesar and AGTC Bioproducts.

The structure of the functionalised dendron and the scrambled sequence show a linear hexapeptide linked directly to a three generation (Gen3) branched poly-ε-Lysine (K). Whereas RGen3K root is a molecule of arginine bonded to a three-generation branched poly-ε-Lysine (K). Moreover, K16 an T(K16) are linear peptides composed by sixteen residues of lysine, without and with the targeting sequence, respectively. The solid phase peptide synthesis of both functionalised dendrons (TGen3K and SGen3K), RGen3K and linear peptides (K16 and TK16) started with 0.5 g of Tenta Gel NH_2 resin (Novabiochem and Iris Biotech GmbH) that was swollen in 3 mL of dimethylformamide (DMF) for 15 min in a fritted syringe. DMF was

removed and the resin was washed three times with DMF. The C-terminal 0.4 mmol of Rink Amide Linker (Iris Biotech GMBH) and 0.151 g of HBTU were dissolved in 3 mL of DMF and 0.141 mL of DIPEA. The coupling reaction between Tenta Gel and Rink Amide Linker took 30 minutes at room temperature, then the solvents were removed, and the resin was washed three times with 3 mL of DMF. Fmoc protecting groups were removed to expose the amine group and allow the bond with the new amino acid and the formation of the amide group. Therefore, the resin was blended with 5 mL of piperidine (Sigma-Aldrich Co, Ltd., 99%) for 2 minutes and was washed three times with DMF, the deprotection reaction and the washing was repeated three times. The reactions were repeated until the complete synthesis of the functionalised dendron. Finally, the resin was deprotected again with 3 mL of piperidine for 4 minutes, was washed with DMF three times, still was incubated with 3 mL of piperidine per 30 minutes and was washed with DMF three times.

The resin was washed with 40 mL of dichloromethane (DCM), followed by many washes with 40 mL of methanol and, in the end, with 40 mL of diethyl-ether. The resin was left to dry and weighted. The resin was relocated in a round flask and mixed over three hours with 900 µl of trifluoracetic acid (TFA), 50 µl of water and 50 µl of trisopropyl silane (TIPS). After the cleavage the peptides were precipitated in 5 mL of cooled diethyl ether, centrifuged for 5 minutes at 3500 rpm and resuspended in 10 mL of cooled diethyl ether. The sedimentation step was repeated 6 times in total, and the peptides were characterised by Fourier Transformed Infrared (FTIR), mass spectrometer (MS) and High Performance Liquid Chromatography (HPLC).

1.3.2 Fourier Transform Infrared

The analysis was performed using a Perkin Elmer Spectrum 65 spectrometer. Each sample was analysed using 1 mg of dried peptide compacted onto the diamond probe and measured in the spectrum range 4000-600 cm^{-1} at resolution of 4 cm^{-1} and collected from 16 scans.

1.3.3 Dynamic Light Scattering

Particle size measurement using Zetasizer nano S (Malvern instruments UK), each sample was dissolved in filtered water at a concentration of 10 mg/mL and measured three times at 25° C and the average size calculated. Prior the analysis the sample was vortexed for 10 seconds. The polydispersity index (PDI) indicates the homogeneity of the population which are in the sample. The runs measurement duration is 30, for a total of 10 runs.

1.3.4 Mass Spectrometry

For the mass spectrometry analysis, the sample was dissolved in ethanol at the final concentration of 1 mg/mL, and ionised, the charges were accelerated by entry into an electric field, consequently the separation of ions with different mass takes place; finally, the ions formed were detected and all of them were represented by a range of peaks.

1.3.5 High Performance Liquid Chromatography (HPLC)

For the analysis each sample was dissolved in methanol (6 mg/mL) and filtered prior HPLC the analysis. Two solvents were prepared: Solvent A (0.1% v/v TFA in water) and solvent B (0.1% v/v TFA in acetonitrile). Both solvents were degassed by helium for 5 minutes. HPLC (Agilent

Technologies, 1260 Infinity) was equipped with column Jupiter 5 µ C18 300A 250x4.6 mm (Phenomenex).

The characterisation of the samples was performed on a hydrophobic C18 column (Jupiter® 5 µm C18 300 Å, LC Column 250 x 4.6 mm, Phenomenex, UK) at 25° C. Table 0.1 summarises the conditions used for the reversed phase analysis.

Table 0.1 HPLC conditions for the analysis of samples.

Eluents	Solvent A: deionised water plus 0.1% v /v TFA Solvent B: acetonitrile plus 0.1 % v /v TFA		
Gradient	**Time (min)**	**Solvent A [%]**	**Solvent B [%]**
	0	100	0
	15	50	50
	30	0	100
Flow rate	1 mL/minute		
UV wavelength	230 nm/ 280 nm		
Sample concentration	6 mg/mL		

1.4 RESULTS AND DISCUSSION

Poly-lysine dendrons were synthesised by SPPS technique (solid phase peptides synthesis). This technique allows to obtain hyperbranched peptide with characteristics, at some extent, able to mimic the tertiary structures of proteins (the so-called molecular scaffolds) and therefore non-toxic, biocompatible and soluble in water [226]. The advantage of the solid phase synthesis through the use of the Fmoc Protection Group is, in fact, the ease of purification of the molecule by simple washing of the

resin before cleavage of the product as well as to avoid the use of strong acids thus avoiding an additional neutralisation step before coupling. Moreover, avoiding to expose the carriers to corrosive substances, potential modifications or degradation to the body of the nanovector are minimised [229].

Four dendrons have been analysed: RGen3K as a control; LSYCCK(Gen3K) even called TGen3K the effective molecule for the drug delivery; CSCLSY(Gen3K) or SGen3K as a branched control; K16 and LSYCCK(K16) or TK16 as linear controls.

1.4.1 Fourier Transform Infrared

Figure 0.5 shows the FTIR spectra of the dendrons: RGen3K (blue line), (KCCYSL)Gen3K (red line) and TGen3K (black line) respectively. Between the 600 cm^{-1} and the 1450 cm^{-1} are the fingerprints of the three substances showing very similar peaks as: 721 cm^{-1}, 798 cm^{-1}, 836 cm^{-1},1126 cm^{-1}, 1430 cm^{-1}, e 1461 cm^{-1}.

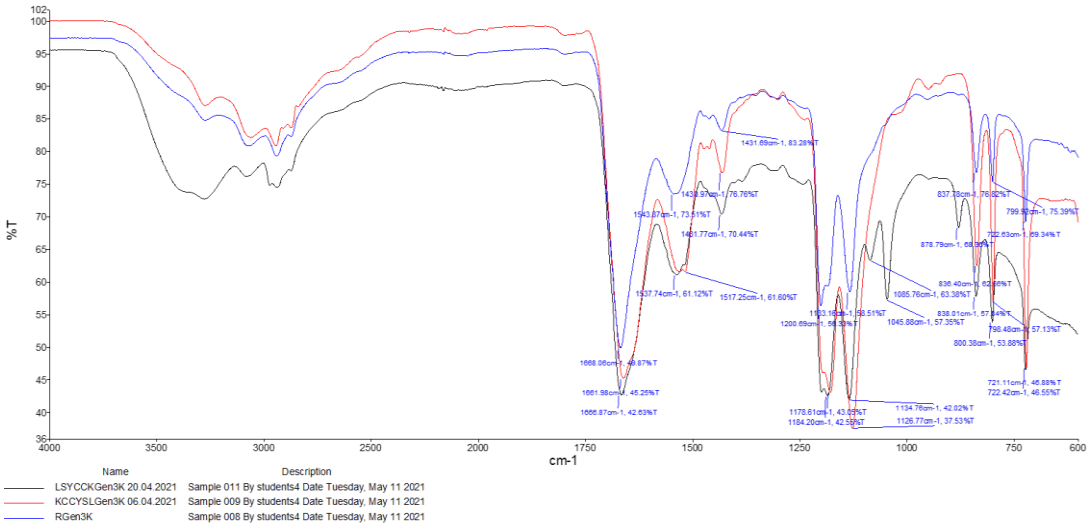

Figure 0.5 FTIR spectrum of RGen3K in blue, KCCYSL(Gen3K) in red and T(Gen3K) in black. One milligram (1 mg) per each dry sample were analysed (n=1).

In common all spectra have: peaks around 3000 cm^{-1} signal of amine groups; a strong peak around 1665 cm^{-1} which is a strong signal of stretching carbonyl group of secondary amide; a second strong peak of 1560 cm^{-1} which is an in plane and out of plane bending vibration of amino group; and a 1200 cm^{-1} signal representing the C-N stretching of ammine groups [230].

TGen3K has three more peaks in the spectra: 878 cm^{-1} C-H bending of Leucine (L) isopropyl group; 1085 cm^{-1} and 1045 cm^{-1} C-O stretching of Tyrosine (Y) phenol group and Serine (S) hydroxyl group respectively; 3400 cm^{-1} broad and strong signal of O-H stretching of Tyrosine and Serine amino acids.

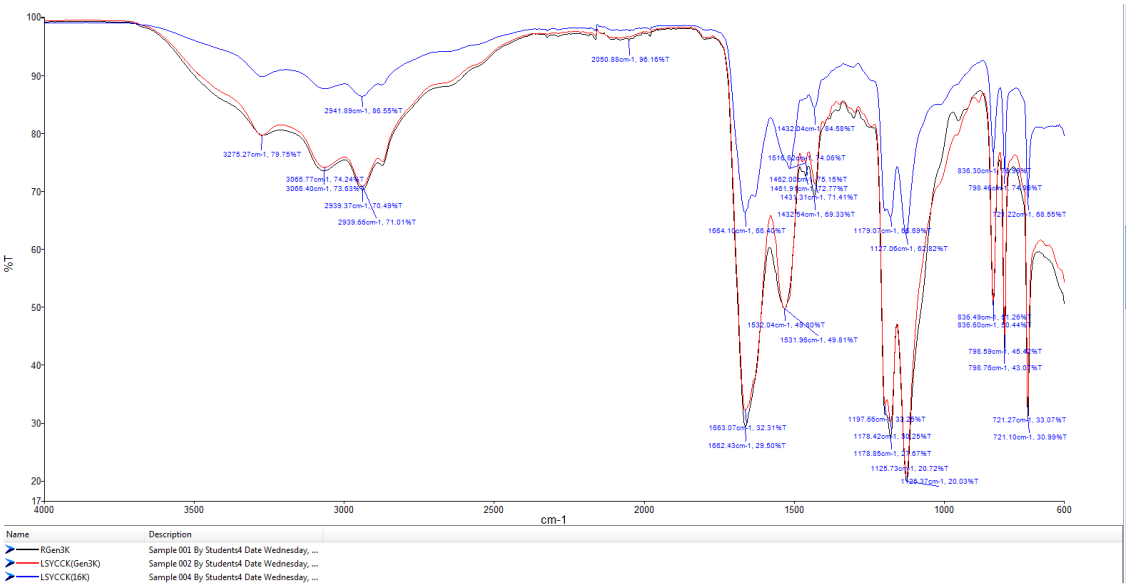

Figure 0.6 FTIR spectrum of RGen3K in black, KCCYSL(Gen3K) in red and T(K16) in blue. One milligram (1 mg) per each dry sample were analysed (n=1).

TK16 in blue (Figure 0.6), was analysed with RGen3K and TGen3K to compare the spectrum. It revealed that the fingerprints at 600 cm^{-1} and the 1450 cm^{-1} are comparable to the other molecules of the three substances showing very similar peaks as: 721 cm^{-1}, 798 cm^{-1}, 836 cm^{-1},1126 cm^{-1} and 1430 cm^{-1}.

In common all spectra have: peaks around 3000 cm^{-1} signal of amine groups; a strong peak around 1665 cm^{-1} which is a strong signal of stretching carbonyl group of secondary amide; a second strong peak of 1540 cm^{-1} which is an in plane and out of plane bending vibration of amino group; and a 1200 cm^{-1} signal representing the C-N stretching of amine groups.

1.4.2 Dynamic Light Scattering

The analysis of dynamic light scattering can be influenced by several factors such as the shape of the nanoparticle and its uniformity of shape and population size. It has also been shown that different sizing methods, solvent type and pH can alter the results.

The average size of RGen3K was 482.5± 51.43 nm, and TGen3K was 146.9± 15.41 nm all the data are an average of three measurements per each sample shown in Figure 0.7.

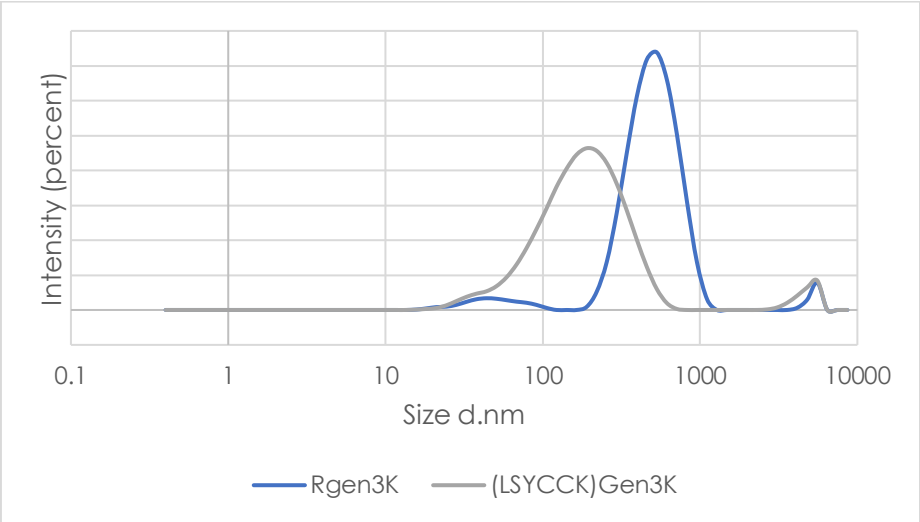

Figure 0.7 Graph showing the average intensity size distribution of the peptides RGen3K (blue), TGen3K (grey) at the concentration of 10 mg/mL in water (n=3 readings). PDI, not shown in the Figure, was 482.5± 51.43 nm, and 146.9± 15.41 nm respectively (n=3).

The measured hydrodynamic size of these macromolecules appears in both cases too large to represent that of a single macromolecule. Indeed, the DLS results suggested that the presence of the targeting sequence reduces particle size, suggesting that they can reduce the aggregation between particles. Likewise, the presence in the HER2 receptor targeting sequence of Leucine (L) and Tyrosine (Y) may favour a high degree of

folding of the dendrimer. In fact, these amino acids present the hydrophobic moieties isopropyl and a phenol group, respectively. This could induce the formation of van der Waals intramolecular bonding forcing the dendrimer in a more compact, and smaller, structure. High polydispersity index (PDI) was found with RGen3K and TGen3K, 0.417 and 0.465 respectively. However, high PDI values can be influenced by several factors, such as the presence of residual impurities formed during synthesis or introduced during the sample preparation. In addition, inadequate sonication of the sample shortly before analysis does not properly dissolve the peptide molecule in the dilution solvent, and therefore large aggregates remain in solution.

Moreover, 10 mg/mL gave a high count rate (>500) at low attenuation (<7) means it is too concentrated and results would not be very accurate due to concentration effects.

1.4.3 Mass Spectrometry

RGen3K, TGen3K, SGen3K and TK16 were analysed. The exact mass of RGen3K is 2095.54 Da, while the synthesised MW (mass weight) appeared in mass spectroscopy as 2097.63 (+1) Da, which confirms the structure assumed during the synthesis. Other peaks reveals either the noise of the instruments or secondary product during the dendron synthesis (Figure 0.8).

The spectra of TGen3K, shown in Figure 0.9, demonstrate that the structure of the molecule is correct after the synthesis. The exact mass of TGen3K was 2636.73 Da and the spectra reveals that the MW was 2637.11 (+1) Da.

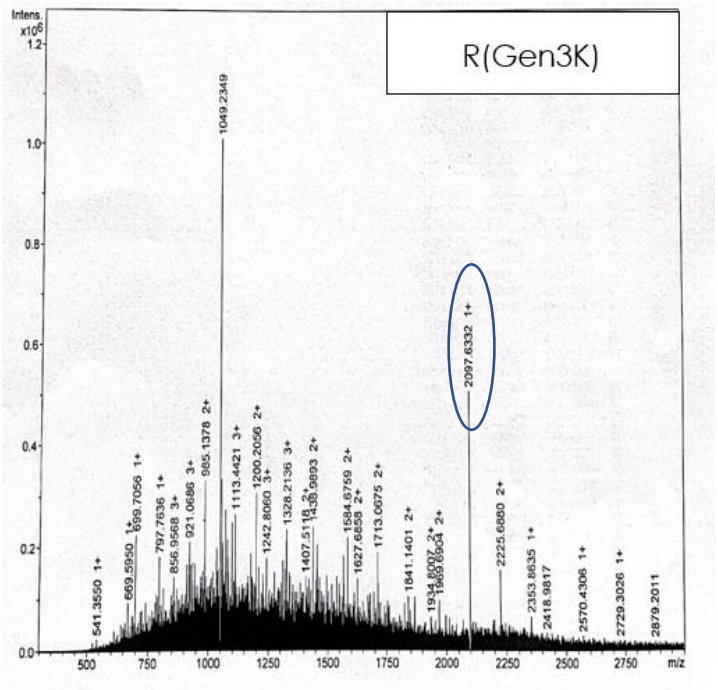

Figure 0.8 RGen3K spectrum. The vector has a concentration of 1 mg/mL dissolved in ethanol. The circle indicates the value of the RGen3K mass which is 2097.63 (+1) Da (n=1).

The dendrimers tethered to the scrambled peptide sequence (SGen3K) have the same mass of the TGen3K, as the targeting sequence consists of the same amino acids, yet arranged in different position. The exact MW was 2636.73 Da and the MW appeared on the spectra was 2639,35 (+1)

as the TGen3K, shown in Figure 0.9. Finally, the targeting linear control (TK16) was analysed, and the calculated MW was 2764.82 Da (Figure 0.11).

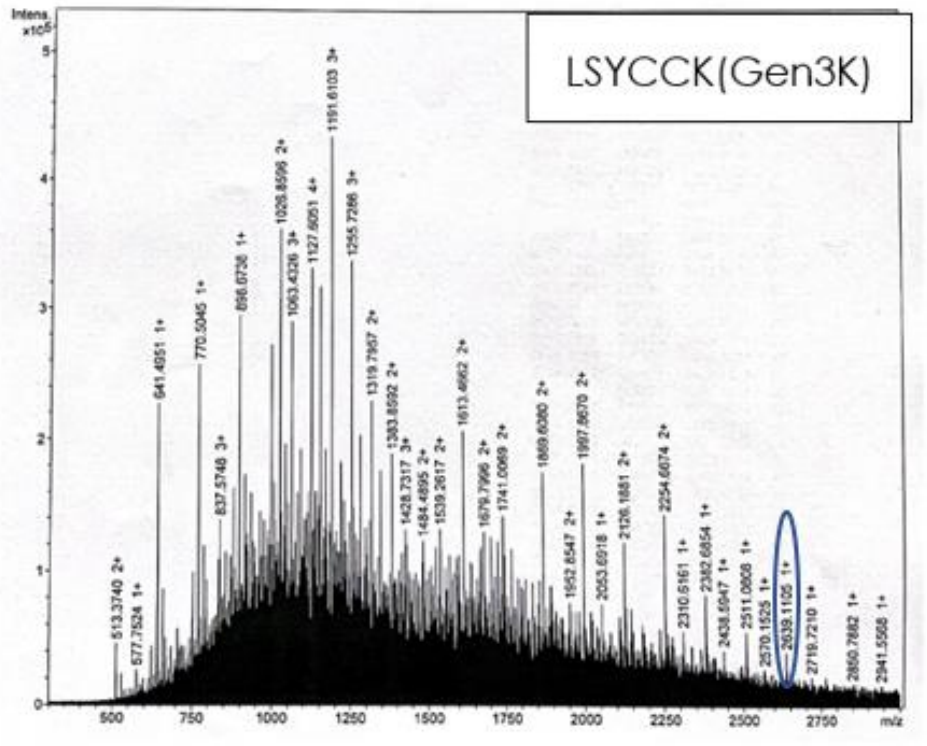

Figure 0.9 LSYCCK(Gen3K), TGen3K, spectrum. The vector has a concentration of 1 mg/mL dissolved in ethanol. The circle indicates the value of the TGen3K mass which is 2639,35 (+1) Da (n=1).

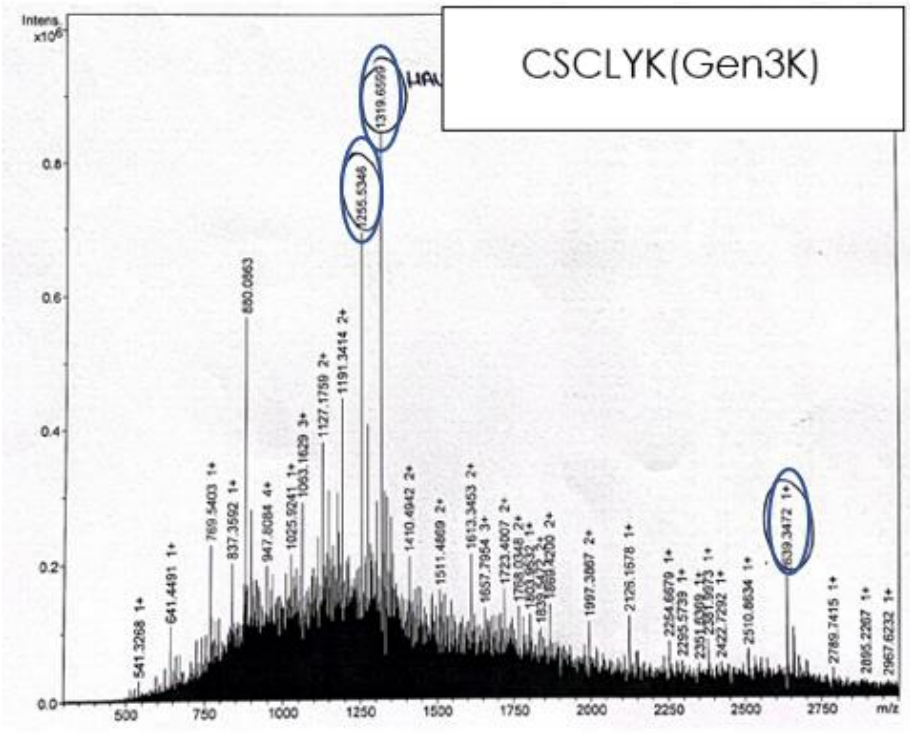

Figure 0.10 CSCLYK(Gen3K), SGen3K, spectrum. The vector has a concentration of 1 mg/mL dissolved in ethanol (n=1).

The total mass value was not detected and was not present on the spectra. However, Table 0.2, shows that smaller fragments of the linear dendron appeared on the spectra.

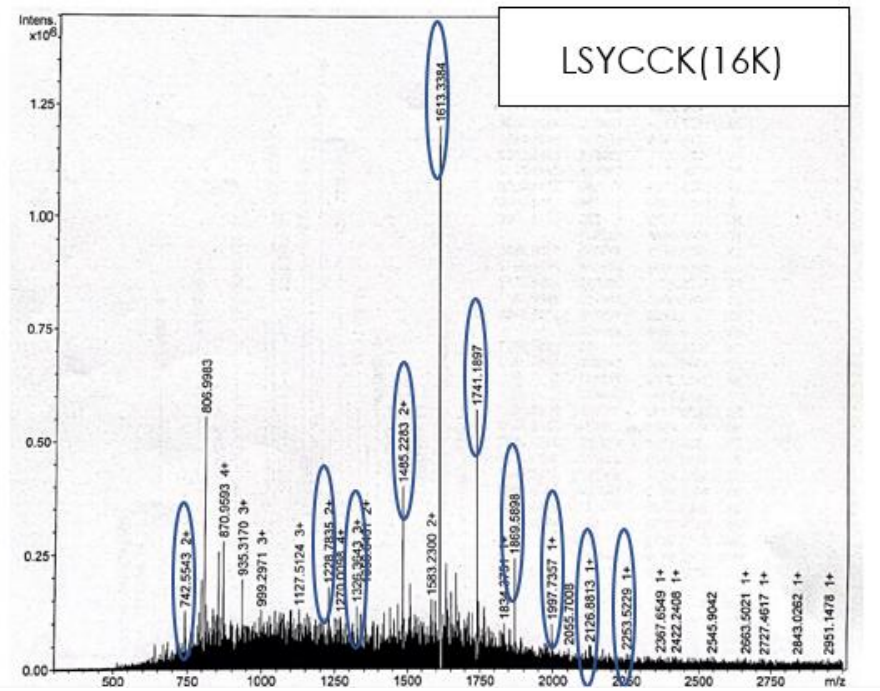

Figure 0.11 T(K16) spectrum. The vector has a concentration of 1 mg/mL dissolved in ethanol. All the circles represent the fragment of TK16 (n=1).

Table 0.2 T(K16) theoretical molecular weight and experimental molecular weight.

	Theoretical Molecular Weight	Experimental Molecular Weight
T(K16)	2764.82	X
T(K15)	2636.73	X
T(K14)	2508.63	X
T(K13)	2380.54	X
T(K12)	2252.44	2253.52
T(K11)	2124.35	2126.88
T(K10)	1996.25	1997.74
T(K9)	1868.16	1869.59
T(K8)	1740.06	1741.19
T(K7)	1611.97	1613.34

T(K6)	1483	1485.23
T(K5)	1325	1326.36
T(K4)	1227.68	1228.78

Fragments containing the linear sequence and the linear lysins are given in Table 0.2. It can be noted that all dendron peaks containing 4 to 12 lysines are present, however the signals above this molecular weight are not detected. This may mean that the total structure is present and that the instrument is not sufficiently sensitive to detect molecules of high molecular weight or the readings are weak and therefore not distinguishable from the background noise of the instrument.

1.4.4 High Performance Liquid Chromatography (HPLC)

RGen3K, T(Gen3K), SGen3K and T(K16) were analysed. The HPLC chromatogram shows in the y-axis the intensity of the peaks, while in the x-axis the retention time and therefore the affinity towards the chromatographic column are determined. HPLC analyses shows peaks with different retention times depending on the structure of the dendron.

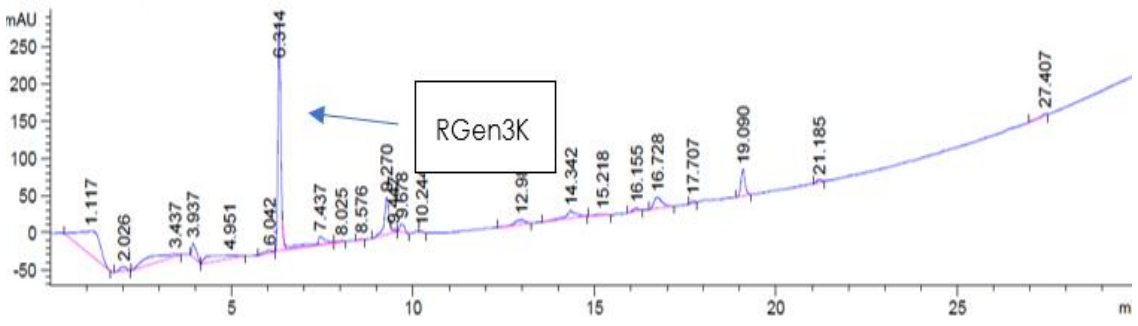

Figure 0.12 RGen3K chromatogram. The vector has a concentration of 6 mg/mL dissolved in ethanol and analysed with UV light at 230 nm (n=1).

The RGen3K dendron, has the smallest size and a retention time of 6.314 minutes with a high intensity of 250 mAU. The chromatogram is shown in Figure 0.12.

In Figure 0.13, the T-Gen3K vector has a relatively higher retention time (7.48 min).

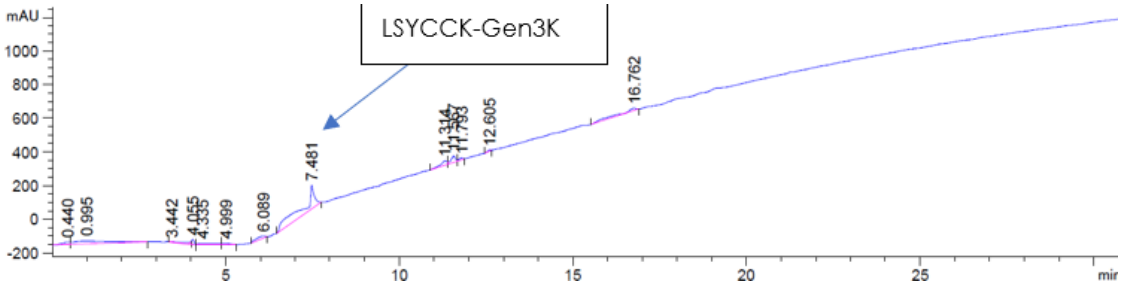

Figure 0.13 TGen3K chromatogram. The vector has a concentration of 6 mg/mL dissolved in ethanol and analysed with UV light at 230 nm (n=1).

Probably the increased size given by the presence of the targeting sequence tends to slow the path of the molecule inside the chromatographic column. Indeed, it has been observed above that the targeting sequence includes hydrophobic amino acids that can establish stronger interactions with the surface of the HPLC column that is meant to separate molecules on the basis of their hydrophobicity. The intensity of the peak, compared to that of the previous Figure (Figure 0.12), seems to be very different, in reality the scale has a different resolution and therefore the peaks have a similar mAU value.

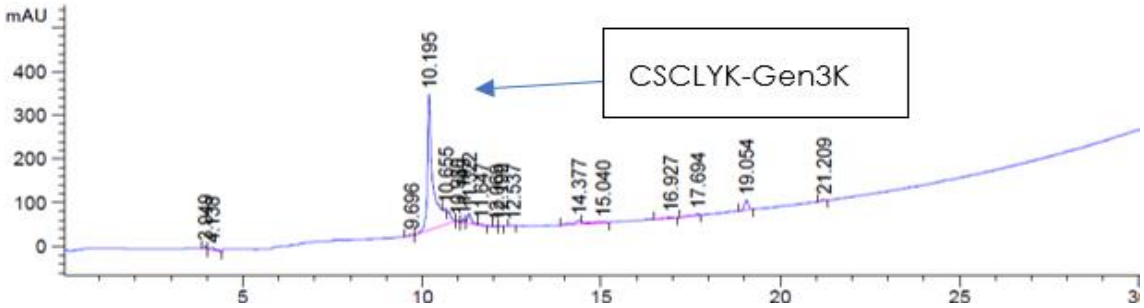

Figure 0.14 CSCLYK(Gen3K), SGen3K, chromatogram. The vector has a concentration of 6 mg/mL dissolved in ethanol and analysed with UV light at 230 nm (n=1).

Finally, SGen3K, shown In Figure 0.14, has a different retention time of 10.195 nm, the shift to the right shows a greater affinity for the hydrophobic chromatographic column. This means that the exa-peptide sequence further increases hydrophobic interactions with the column, delaying its elution from the column to a higher percentage of non-polar mobile phase. The sec-butyl substitution present in leucine and the benzyl presence in tyrosine acquires a conformation able to maximise the interactions of Van der Waals forces with the hydrophobic column, then the path to the detector is further slowed compared to RGen3K and its similar TGen3K.

The linear control, T(K16), shown in Figure 0.15 has a retention time at 9.003 minutes. The shift to the right on the spectra determine the greater affinity for the hydrophobic chromatographic column, like T(Gen3K), influenced by the sec-butyl substitution present in leucine and the benzyl presence in tyrosine. It can be speculated that the more flexible linear structure can expose these hydrophobic moieties to the HPLC solid phase thus enhancing the interactions and extending the retention time.

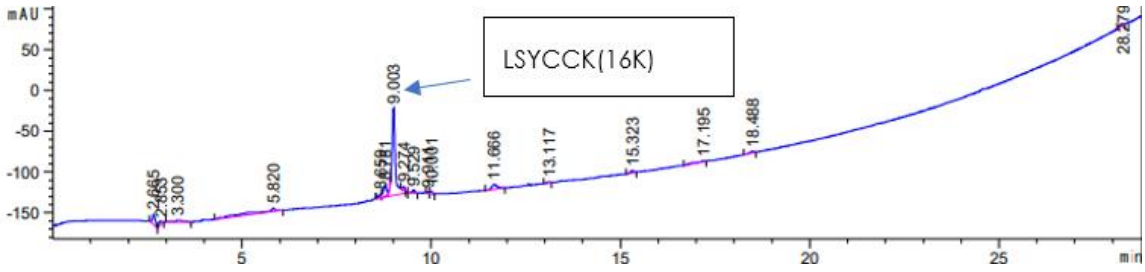

Figure 0.15 T(K16). chromatogram. The vector has a concentration of 6 mg/mL dissolved in ethanol and analysed with UV light at 230 nm (n=1).

In general, all three syntheses yielded very clean chromatogram indicating the ability of solid phase synthesis to give a product with high percentages of purity.

1.5 CONCLUSION

In this chapter it has been shown that the SPPS technique has made it possible to successfully obtain dendrons of interest, this is demonstrated by the characterisation techniques used. In addition, this method allows to synthesise a great variety of good purity dendrons in a relatively short time despite the relative complexity of the structure. Finally, the solid phase synthesis has allowed to obtain products with high percentages of purity, however, from the results of mass spectrometry, it is possible to observe the presence of many secondary structures that could be eliminated through further purification. The high purity of the compounds and the desired structure allow them to be used as nucleic acid vectors in *in vitro* cell tests and thus determine their potential in gene delivery through new molecular designs enabling to increase the cargoes internalisation and release of the cargo within the target cell. These studies are presented in the following chapters.

IN VITRO COMPARISON OF PEPTIDE ACTIVITY AND TRASTUZUMAB

1.1 INTRODUCTION

Breast cancer stands as one of the most frequently detected and fatal cancer forms among women. As indicated by the American Cancer Society, breast cancer accounts for 15% of all cancer-related female fatalities [48]. Thus, approximately 1 out of every 8 women receiving a breast cancer diagnosis at some point in their lives [231,232]. Breast cancers subtypes are determined by the presence or absence of specific receptors. The typical subtypes include breast cancers that express oestrogen receptor (ER) and/or progesterone receptor (PR), those expressing the human epidermal growth factor 2 receptor (HER2), or triple negative breast cancer (TNBC), characterised by the absence of these receptors [231].

In particular, HER2 receptor belongs to the Human Epidermal Growth Factor (ERBB) family and possesses tyrosine kinase activity. This receptor is involved in the regulation of growth, proliferation, and cell migration, and its overexpression in cancer cells is associated to a poor prognosis. HER2 is considered an orphan receptor, meaning it lacks ligands that directly activate it, but it can form homodimers or heterodimers with other receptors from the HER family [233].

In cancer cells, it is estimated that there are between 25 and 100 copies of the HER2 gene, resulting in approximately 2 million receptor proteins on the cell surface [234]. Hence, the elevated expression of this receptor renders it useful both as a diagnostic indicator and as a promising candidate for therapeutic targeting. For patients diagnosed with early-stage HER2-positive breast cancer or following surgical removal of the tumour,

targeted therapy is selected. The monoclonal antibody Trastuzumab (Figure 0.1 [235]) is the preferred treatment for this subtype of tumour as it specifically targets regions of the HER2 receptor, giving protection to healthy cells from anticancer effects and reducing the side effects commonly associated with traditional chemotherapy drugs [62,63,236] .

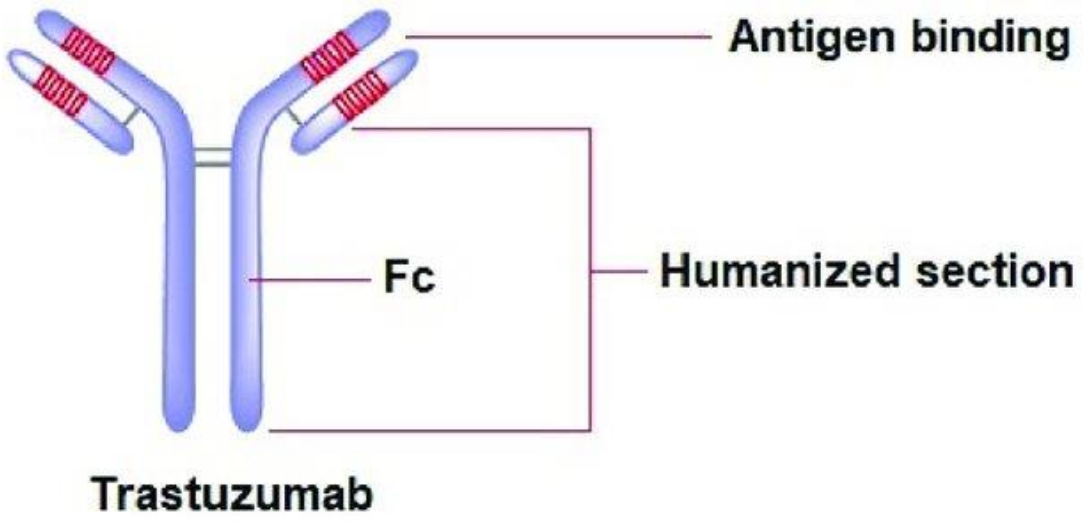

Figure 0.1 Structure of the Humanised monoclonal antibody Trastuzumab.

An antibody has a Y-shaped structure consisting of constant regions and variable regions. The variable regions are responsible for antigen recognition and triggering the necessary inflammatory response to neutralise the pathogen. Unlike polyclonal antibodies, which can recognise multiple antigens, monoclonal antibodies exhibit a high affinity for specific antigens [237]. Trastuzumab is a highly selective monoclonal antibody designed to target the HER2 receptor. It is classified as humanised, primarily derived from human cells except for the variable region [238].

Monoclonal antibodies possess distinct advantages as targeting ligands over small molecules, proteins, and aptamers due to their uniformity,

affinity, and specificity. Nevertheless, despite the considerable success in achieving an anti-tumour effect, immunotherapy employing monoclonal antibodies demands continual administration over a prolonged period, and the half-life of monoclonal antibodies restricts the duration of therapy, resulting in only temporary disease control, particularly once the tumour has metastasised [239–241]. Furthermore, the development of resistance to treatments with monoclonal antibodies [242], immune-related adverse events, hypersensitivity (which may be as a result of the monoclonal antibodies administered doses to ensure their immediate bioavailability and potency) and cardiotoxicity, are some of the monoclonal antibodies' side effects [243–245].

Unlike larger molecules like antibodies, peptides are recognised for their reduced toxicity and improved pharmacokinetic attributes, including higher target-to-background ratios and more rapid blood clearance [246,247]. Various regulatory peptide analogues that bind to receptors found on tumours, such as somatostatin and a-melanocortin-1, are actively being explored in both imaging and therapeutic research [248,249].

One of the extensively researched peptides specifically designed for HER2 is the KCCYSL peptide, or peptides that incorporate the KCCYSL sequence [250,251]. This peptide was identified through screening a random 6-amino acid peptide bacteriophage display library, and it exhibited the highest occurrence in phages that bound to biotinylated extracellular domain ERBB-2 (HER2). Karasseva et al. [250] observed the presence of the KCCYSL sequence in more than 75% of their clones, indicating a robust affinity for HER2. The conjecture is that the oxidised state of the CCY motif within this peptide closely resembles the structural configuration of the EGF-like domain present in common ERBB ligands [250].

The use of peptides as targeting moieties offers a solution to these challenges due to their substantially reduced molecular weight and

diminished immunogenicity. Furthermore, employing peptides as targeting agents presents additional benefits, such as enhanced effectiveness in penetrating tumour masses, stability, and reduced production expenses and extensive adjustability [252].

Poly-L-lysine (PLL) possesses distinct biological attributes, including early indications of limited activity against murine tumours. PLL's cationic nature facilitates the penetration of active compounds through the cell membrane of cancer cells [253]. In HeLa and L1210 murine leukaemia cells, PLL demonstrates cytotoxic effects [254]. As reported by Debnath et al. [255], PLL has been confirmed to inhibit tumour cell growth through the downregulation of the oncogenes Bcl-2 and CD3, leading to increased p53 protein levels and cell-cycle stasis. Additionally, PLL has been demonstrated to reduce peritoneal angiogenesis and micro-vessel density. Apoptosis, or programmed cell death, is a crucial cellular mechanism for rejuvenation, proliferation maintenance, growth inhibition, and death [256]. Apoptosis can be induced intrinsically, via the mitochondrial pathway, or extrinsically, triggered by a protease cascade [257]. Bcl-2 is pivotal in regulating this process [258] and induces mutations in caspase-3 protein expression, an effector of the apoptotic process [259]. Another mechanism that PLL can modulate is angiogenesis. This process is decisive for solid tumour growth by fostering the formation of new blood vessels to supply nutrients to growing tumours [260]. The most potent angiogenic factor influencing angiogenesis is Vascular Endothelial Growth factor (VEGF), which drives tumour progression, invasion, and metastasis [261,262]. Suppressing VEGF expression can halt solid tumour growth [263]. Furthermore, Ki-67, a non-histone nuclear protein, is another factor positively influenced by the presence of PLL. This factor is closely linked to cell proliferation and the cell cycle, expressed during the G1 phase and peaking during the G2 phase, before inhibition during the M

phase. Lastly, *c-Myc*, a transcription regulatory oncoprotein, plays a role in controlling proliferation, apoptosis, and protein synthesis [264,265]. The activation and inactivation of *c-Myc*, as well as tumour suppressor gene alterations, impact DNA repair systems and apoptosis regulation. Modulating *c-Myc* in proliferating cells offers a potential target for cancer therapy [266].

1.2 AIM OF THE CHAPTER

In this chapter, the action of the antibody Trastuzumab is compared with laboratory-synthesised branched poly-lysine peptides (Chapter 2). The branched peptide of interest, TGen3K, is composed of two segments.

Firstly, the hyperbranched peptide structure is composed of lysine molecules that, due to the exposure of amino groups at the uppermost branching generation, easily interact with the negative charges of nucleic acids. Additionally, the small internal molecular core, containing a small aliphatic sequence, can be utilised to protect and deliver small hydrophobic molecules such as many chemotherapeutic drugs.

Secondly, a linear peptide sequence, added at the molecular root of the branched peptide, consists of six amino acids: Leucine (L), Serine (S), Tyrosine (Y), two molecules of Cysteine I, and Lysine (K). As mentioned above this sequence is known for its selectivity towards the HER2 receptor, and it has been demonstrated to accumulate in breast carcinomas with a high concentration of the receptor on the surface, as reported in the study by Kumar et al. [267].

The following experiments allowed the comparative study of the selectivity of the hexapeptide sequence of the dendrimer with the antiproliferative and antimetastatic activity of the monoclonal antibody Trastuzumab as well as with the linear peptide sequence when not

integrated in the branched peptide structure. This selectivity was assessed indirectly by analysing the effect on HER over expressing breast cancer cells.

1.3 MATERIALS AND METHODS

1.3.1 Cell culture

1.3.1.1 Cell culture method

The safety and therapeutic potential of the dendrimers synthesised in Chapter 2 of this thesis were studied by in vitro cell models using two cell types: SKBR3 and MDA-MB-231.

The SKBR3 cell line was isolated from pleural effusion cells of a 43-year old Caucasian female patient. The patient had been treated previously with radiation, steroids and 5-fluorouracil. This cell line is known to over-expresses the HER2 receptor, to grow in grape-like clusters with an invasive phenotype resembling that of the cells *in vivo* [268].

MDA-MB-231 cells are a highly aggressive human breast adenocarcinoma line characterised by lack of expression of ER, PR and HER-2 receptors, over-expression of the EGF receptor (EGFR) and the presence of a mutated form of p53, showing amino acid substitution (G/A) in codon 280 of the corresponding gene. MDA-MB-231 cells have a mesenchymal-like or stromal-like phenotype [269]; in fact, they have many characteristics common to mesenchymal cells: They have a high ability to invade and cross basal membranes and do not express epithelial markers but in contrast show a high level of vimentin.

1.3.1.2 Cell Lines and Culture Conditions

MDA-MB-231 were cultured in 75 cm^2 flasks in the presence of Advanced-DMEM/F12 (Gibco) culture medium, mixed with 10% v/v Foetal Bovine Serum (FBS) and 1% w/v of glutamine. SKBR3 cells grown in McCoy 5 Medium culture medium (Gibco) to which 10% v/v FBS.

1.3.1.3 Routine Cell Culture

The cells were kept in the incubator at a temperature of 37° C with humidified air constituted by 95% of air and 5% of CO_2, while medium was changed every two days. Cells were split when the confluence was around 80%. Before being split, the medium was removed and replaced with sterile PBS to remove any trace of the old media. Subsequently, to detach the cells from the flask surface, 4 mL of Trypsin-EDTA (Gibco) was added and incubated for 5 minutes at 37 C under 5% CO_2. The effect of Trypsin was finally neutralised by the addition of 8 mL of media. Cells were mixed and centrifuged for 5 minutes at 30 G to obtain a pellet that was resuspended in 1 mL of fresh media. An aliquot, selected according to the needs of the experiments, was transferred to a sterile T75 flask where 13 mL of medium were previously transferred.

1.3.1.4 Cell Counting

To determine the seeding density, after the addition of the Trypsin and centrifugation, the pellet of cells was resuspended in 5 mL of fresh media. An aliquot of 100 µl was diluted with 400 µl of fresh medium and 500 µl of Trypan blue (Gibco Life Technologies, UK), a dye that is excluded from viable cells. Only cells with a permeabilised membrane (and therefore dead) will be blue coloured. The final dilution is 1:10 and should be

agitated before taking any volume to maintain a uniform cell concentration.

A drop of the solution was loaded into the haemocytometer and the cells in each of its chambers were counted according to Equation 3.1:

Equation 3.1 Equation used to determine cell concentration. The mean of the cells counted in the four chambers of the blood cytometer are multiplied by 10^4, that is the dilution with the mean and the Trypan blue, and by 104 which determines the final concentration of the cells per millilitre of solution (cell/mL).

$$\frac{\sum_{i=1}^{n} X1}{n} \cdot 10 \cdot 10^4$$

The cells were then diluted according to dilution Equation 3.2:

Equation 3.2 Equation for dilution of solutions. The initial concentrations, C(i), and the initial volumes, V(i), are diluted to obtain the final concentrations, C(f), in determined volume, V(f).

$$C(i) \cdot V(i) = C(f) \cdot V(f)$$

1.3.2 Proliferation assay

Cells that were examined for the proliferation experiment included both SKBR3 cells, which overexpress the HER2 receptor, and MDA-MB-231 cells, which lack hormone receptors and the HER2 receptor.
Both cell types were cultured in 24-well plates at a concentration of 50,000 cells per well in 500 µl of fresh media. After 24 hours, the peptides: RGen3K, TGen3K, and SGen3K were diluted in 100 µl of Opti-Mem in three concentrations: 5 µg/mL, 10 µg/mL, and 15 µg/mL.
The controls used were Trastuzumab (10 µg/mL), from Merck, in Opti-Mem. Among the samples, the hexapeptide sequence (KCCYSL) was tested at three concentrations: 5 µg/mL, 10 µg/mL, and 15 µg/mL .

After sample preparation, and prior adding the samples onto the cells, the medium was removed from the 24-well plates and the cells were washed with 200 μl of sterile phosphate buffered saline pH=7.4 (PBS), followed by the dispensing of additional 400 μl of OptiMem. Finally, the samples, in a total volume of 100 μl, were added into the wells. Cells were incubated for 48 hours at 37° C and 5% CO_2. Afterwards the supernatant was removed and the cells were washed twice with 200 μL sterile PBS and fixed with 100 μL paraformaldehyde (PFA). After 20 minutes, the fixation agent was removed and cells were stored in the fridge and kept hydrated in 100 μL of PBS.

The count of the adhering cells was performed by the ImageJ software. Parameters were set to count single cells by first processing all the microscopy images using the "sharpen" option, followed by "find maxima." Subsequently, the photo under examination was converted to 8-bit, and using the "threshold" option, the best black and white resolution was achieved. Finally, by clicking the "watershed" button, the system was able to separate closely located cells from each other and treat them as separate entities. Ultimately, particle counting was performed.

A typical processing of microscopy images by ImageJ software is shown in the Figure below (Figure 0.2). The experiment was conducted in duplicate and the error bars indicate the standard deviation calculated from two distinct measurements within a single experiment. Data were statistically analysed by a two-tail T Test and data considered significant different at $p<0.05$.

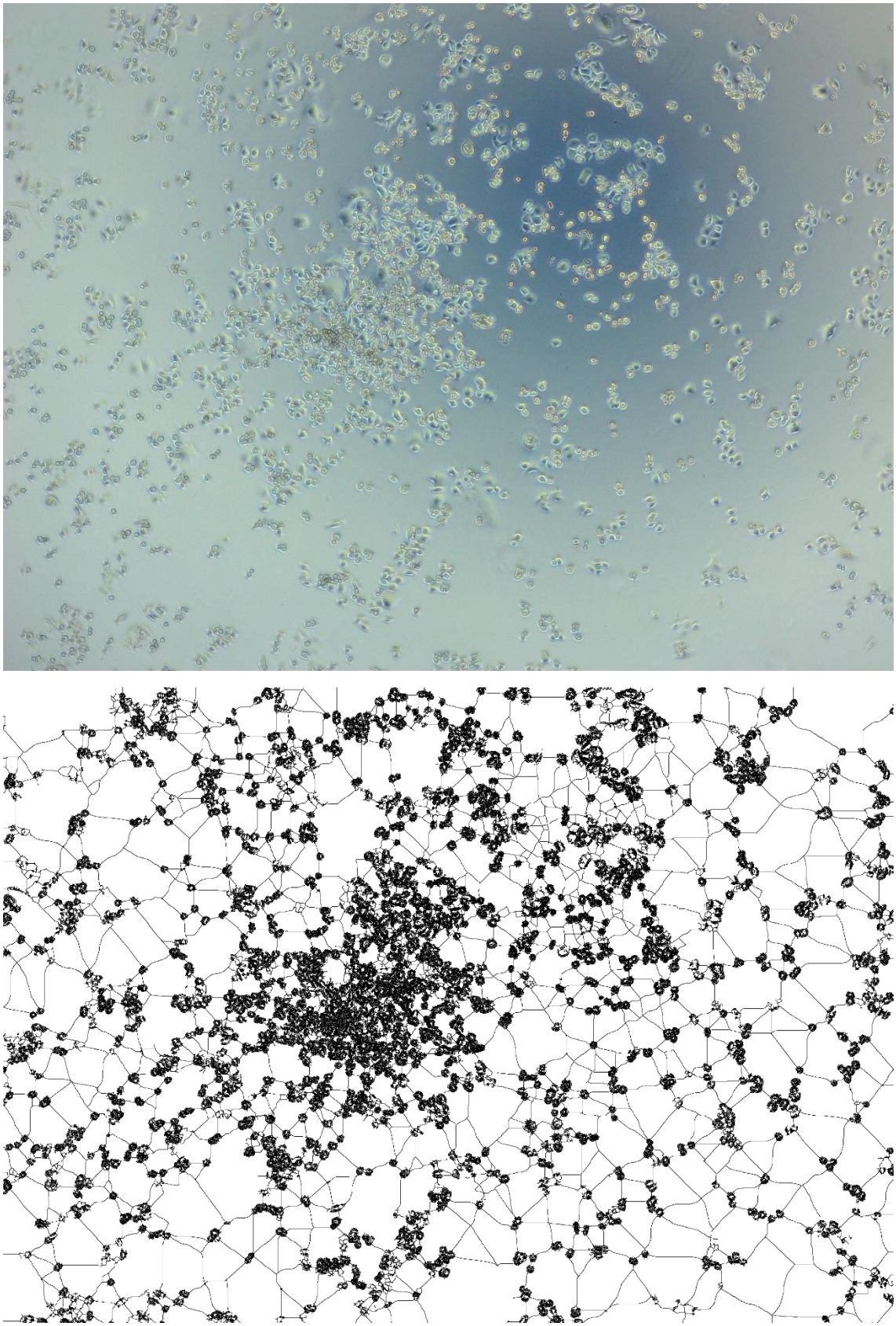

Figure 0.2 Before and after image software rendition using ImageJ.

1.3.3 LDH Cytotoxicity Assay

LDH serves as a commonly employed indicator in studies focusing on cytotoxicity. Lactate dehydrogenase (LDH) represents a stable, soluble cytosolic enzyme found in numerous cell types. and it serves as a well-defined and dependable indicator of cytotoxicity. When the plasma membrane is compromised, LDH is released into the cell culture medium. The LDH present extracellularly in the medium can be quantified through an enzymatic process, wherein LDH facilitates the conversion of lactate to pyruvate by reducing NAD+ to NADH. The oxidation of NADH by diaphorase subsequently reduces a tetrazolium salt (INT), resulting in the production of a red formazan product that can be quantitatively measured via spectrophotometry at 490 nm.

The toxicity test (CyQUANT™ LDH Cytotoxicity Assay, Invitrogen) was applied to the supernatant obtained at specific time intervals after transfection. Some wells were designated for total cell lysis to release all the proteins into the growth medium, serving as positive controls of maximum cytotoxicity. Cell lysis was accomplished by adding 60 µl of a 5X lysis buffer (part of the CyQUANT™ LDH Cytotoxicity Assay, Invitrogen) to the control wells, followed by incubating the well plate for 45 minutes in a CO_2 incubator at 37° C. Subsequently, 50 µL from each well was transferred to a 96-well plate. Next, 50 µl of the Reaction Mixture (prepared by combining 11.40 mL of dH_2O with 600 µL of Assay Buffer Stock) was added, and the samples were allowed to react for 30 minutes at room temperature. Finally, 50 µL of the Stock Solution was added. After 60 minutes, or a maximum of 2 hours, the absorbance at 490 nm and 680 nm was measured to assess LDH activity. The measurements were conducted in duplicate, and the error bars indicate the standard deviation calculated from two distinct measurements within a single experiment.

Data were statistically analysed by a two-tail T Test and data considered significant different at $p<0.05$.

1.4 RESULTS AND DISCUSSION

1.4.1 Proliferation Assay

The experiment was performed to determine the peptides' ability to interfere on cell proliferation and cytotoxic effect either as such or through the HER2 receptor. As previously demonstrated, peptides, due to their multiple positive charges, can be toxic to cells, increasing their toxicity [253]. Furthermore, the chosen target sequence has a structure that enables binding to the overexpressed receptor in HER2+ tumour cells. The sequence LSYCCK shows similarities with the monoclonal antibody Trastuzumab (Herceptin), which is defined as the frontline drug for early HER2+ tumour treatment.

For this experiment, three hyperbranched peptides were analysed: RGen3K, TGen3K, and SGen3K (scrambled hexapeptide sequence of the studied aptamer). The peptides were synthesised following the method described in Chapter 2.3.1 and diluted to three different concentrations: 5 µg/mL, 10 µg/mL, and 15 µg/mL. Along with the peptides, the linear sequence (L) was tested at the same concentrations as the other peptides. The monoclonal antibody Herceptin (H) was used for comparative analysis by testing it at a concentration of 10 µg/mL that is the most commonly used concentration in literature [270–272]. The whole experimental matrix was carried out on both MDA-MB-231 cells (triple negative cells, TNBC) and SKBR3 cells (HER2+).

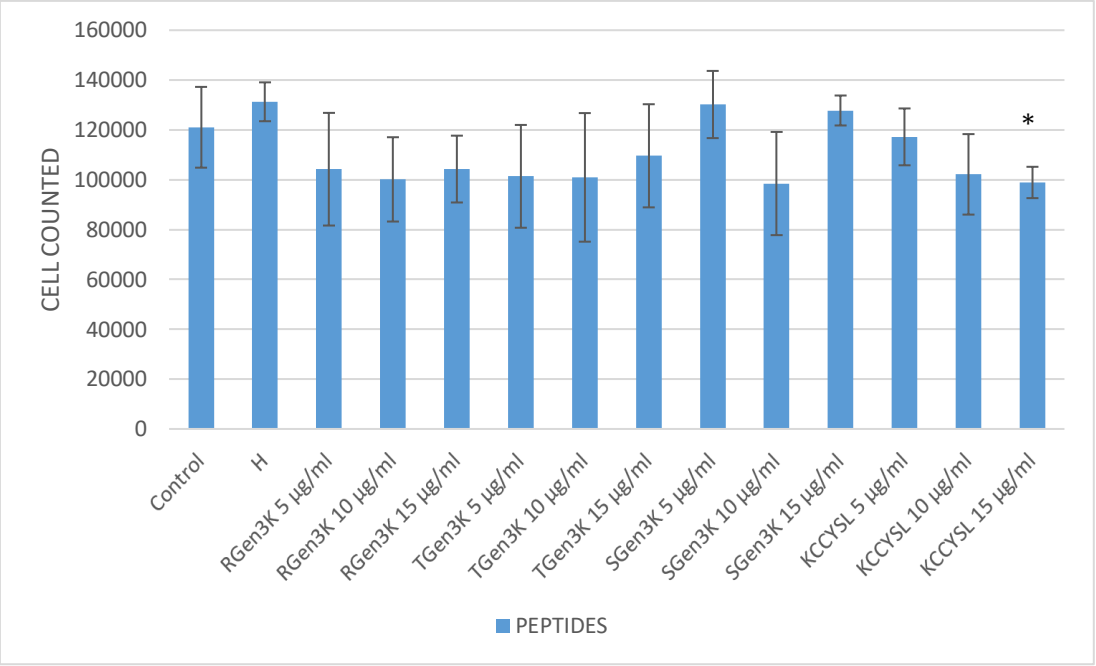

*Figure 0.3 MDA-MB-231 Cells treated with: Herceptin (10 µg/ml); RGen3K, TGen3K and SGen3K at three different concentrations (5 µg/ml, 10 µg/ml and 15 µg/ml); and KCCYSL, the linear hexapeptide at 5 µg/ml, 10 µg/ml and 15 µg/ml. Analysis were performed with ImageJ after 48 H from the seeding. *****P<0.00001, ****P<0.0001, ***P<0.001, **P<0.01, *P<0.05, (n=3).*

Figure 0.3 illustrates the activity of the different peptides on the triple-negative cells (MDA-MB-231). As shown, the proliferation of this cell type did not seem to be affect by hyperbranched structures, to the linear hexapeptide sequence and to Herceptin. Although not statistically significant, most of the branched and linear lysine sequences appear to show reduced cell counts.

As expected, the presence of the HER2 receptor-specific hexapeptide sequence did not have any effect since these cells do not express this receptor. According to the work by Debnath et al. [255], it has been established that poly-L-Lysine peptides alone have a potent antitumour effect on Ehrlich ascites carcinoma (EAC), Sarcoma-180, DAL, HeLa, and Lewis lung carcinoma cells, both *in vitro* and *in vivo*. This activity is attributed to the induction of apoptosis through the modification of

Caspase-3 expression, an essential protein in the cell cycle. Furthermore, PLL (poly-L-Lysine) peptides lead to an *in vivo* deceleration of proliferation. In MDA-MB-231 cells, it seems that other pathways come into play, downregulating VEGF and *c-Myc*, resulting in an antiproliferative and antiangiogenic effect by reducing the concentration of Ki67 and CD34.

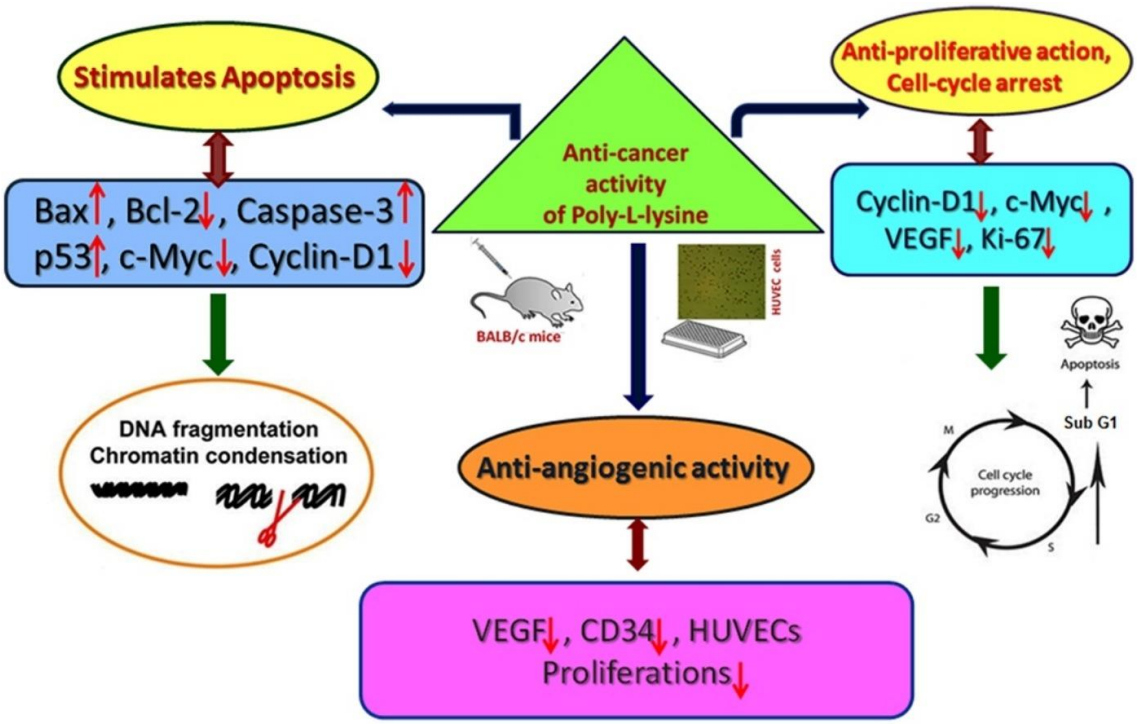

Figure 0.4 Description of the many pathways of poly-L-Lysine. Image taken from Debnath et al.

This effect is dose-dependent and concentrations led to significant decreases in cell number and expression of Caspase-3 (apoptosis regulator) and Ki67 ranged in the range 10 µg/mL to 40 µg/mL. As no statistically significant difference was observed, the results shown in Figure 0.3 only partially reflect the conclusions drawn by Debnath et al. However, some differences such as the number of charges of the PLL and the

concentration could have influenced the final outcomes in the two studies.

Moreover, In the same study published by Debnath et al., it is highlighted that the 3D cell culture of MDA-MB-231 cells, which better mimics the *in vivo* environment, could be another factor favouring the effects of PLL. Peptides seem to have a significant impact on the collagenases present in the tumour's extracellular environment. Therefore, results display in Figure 0.3 might be amplified when replicated i*n vivo*. Figure 0.5 presents cell count values in SKBR3 cells, which overexpress the HER2 receptor. In contrast to the previous results, reductions in the number of treated cells can be observed compared to negative controls cells (Figure 0.5 Control). The positive control (Herceptin) notably affected cell proliferation. The number of cells after 48 hours in contact with the monoclonal antibody is threefold lower than the negative control. Trastuzumab's behaviour stems from its selectivity towards the overexpressed HER2 receptor in HER2+ breast cancer. However, the hexapeptide sequence (LSYCCK) had no effect on cell number, despite being designed to resemble the monoclonal antibody. This behaviour might be attributed to the peptide's reduced length, as reported by Biri-Kovács, B. et al [273]. It's indeed necessary to increase the peptide sequence to achieve better affinity for the HER2 receptor. It seems that the peptide's alpha-helical folding could be crucial for the recognition and binding to the target receptor.

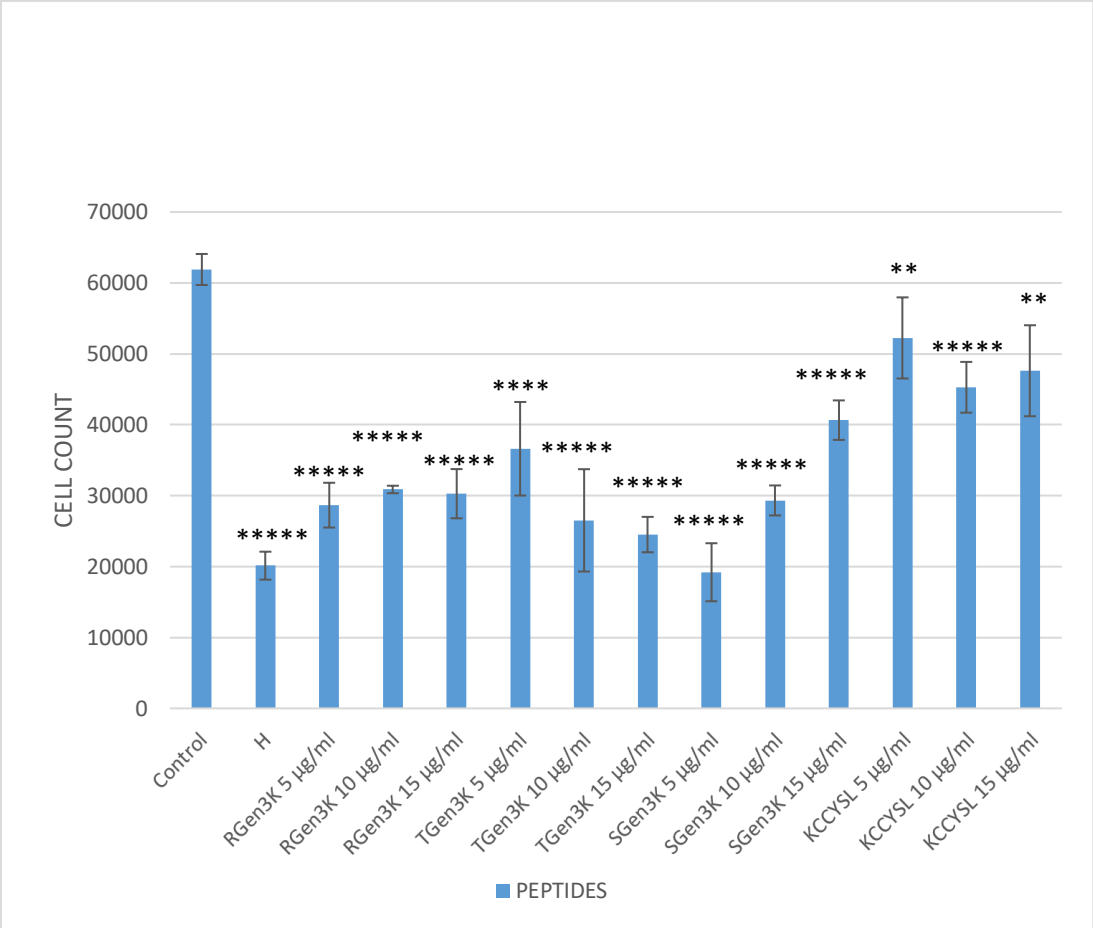

*Figure 0.5 SKBR3 Cells treated with: Herceptin (10 µg/ml); RGen3K, TGen3K and SGen3K in three different concentrations (5 µg/ml, 10 µg/ml and 15 µg/ml); and KCCYSL, the linear hexapeptide at 5 µg/ml, 10 µg/ml and 15 µg/ml. Analysis were performed with ImageJ after 48 H from the seeding. *****P<0.00001, ****P<0.0001, ***P<0.001, **P<0.01, *P<0.05, (n=3).*

RGen3K peptide (the dendrimer not bearing any HER target sequence) reduced the cell count by about half, indicating that the poly-lysine structure has an effect over the proliferative capacity of the cells. However, it does not appear to be dose-dependent, as increasing the concentration of the sample does not lead to a decrease in cell number. In contrast, TGen3K seems to effectively reduce the number of cells in a concentration-dependent manner. Moreover, possibly due to the

presence of the target sequence, at the 15 µg/mL concentration, the cell count approaches a value slightly higher than that achieved with Herceptin (10 µg/mL). These results seem to support the findings of Biri-Kovács et al. [273], where the addition of amino acids to the hexapeptide sequence increases affinity to the receptor, consequently reducing the HER2 receptor-induced cell hyper-proliferation. The ability of the dendrimers to act as molecular scaffolds mimicking the tertiary structure of proteins was here shown to improve the effect of the hexapeptide aptamer to reach an inhibitory effect comparable to that of the monoclonal antibody. Noticeably, when the target sequence was conjugated with the linear polylysine, there was no significant effect on the cells as their counts were not significantly different from the negative control. These findings highlight that the simple addition of amino acid postulated by Biri-Kovacs et al is not sufficient and that the role of the more rigid branching structure of the dendrimer, as molecular scaffold, plays a key role.

Another optimal result was unexpectedly observed at the lowest concentration of the scrambled peptide (SGen3K, 5 µg/mL). However, the antiproliferative capacity diminishes with increasing concentration to return to that observed for the non-functionalised dendrimer, the RGen3K. The positive effect observed at the lowest concentration tested could be due to the structure of the scrambled targeting sequence, which, through the formation of intermolecular disulfide bonding between different dendrimers, might induce the dimerisation of the HER receptors on the cell membrane leading to an inhibition similar to that of the monoclonal antibody and of the highest concentration of TGen3K. At higher concentrations this effect would be loss through steric hindrance that would reduce the binding to the HER2 receptor and decreases the polycation's ability to interfere with *c-Myc*.

In summary, RGen3K and TGen3K show distinct effects on cell proliferation, potentially linked to their structure and concentration. Especially TGen3K demonstrates its selectivity towards the HER2 receptor. Additionally, the presence of the target sequence and the impact of disulfide bonds in the scrambled peptide seem to play significant roles in modulating the interaction with the HER2 receptor and downstream cell signalling pathways.

1.4.2 LDH Cytotoxicity Assay

The cytotoxicity experiment was conducted by collecting supernatant from the wells designated for the previous proliferation experiment (Figure 0.6). Thus, all medium related to the hyperbranched peptides, the linear sequence (L), and Herceptin (H) were tested. The positive control is represented by the total cell lysate from the dedicated wells, indicated as "maximum" in the Figures below. Samples were collected after 24 and 48 hours from adding the samples to the cells. Figure 0.6 and Figure 0.7 show values related to cells not overexpressing the HER2 receptor (MDA-MB-231). In this case, the samples used do not induce toxicity to the cells, as the Absorbance values remain similar to the negative control's value (Control).

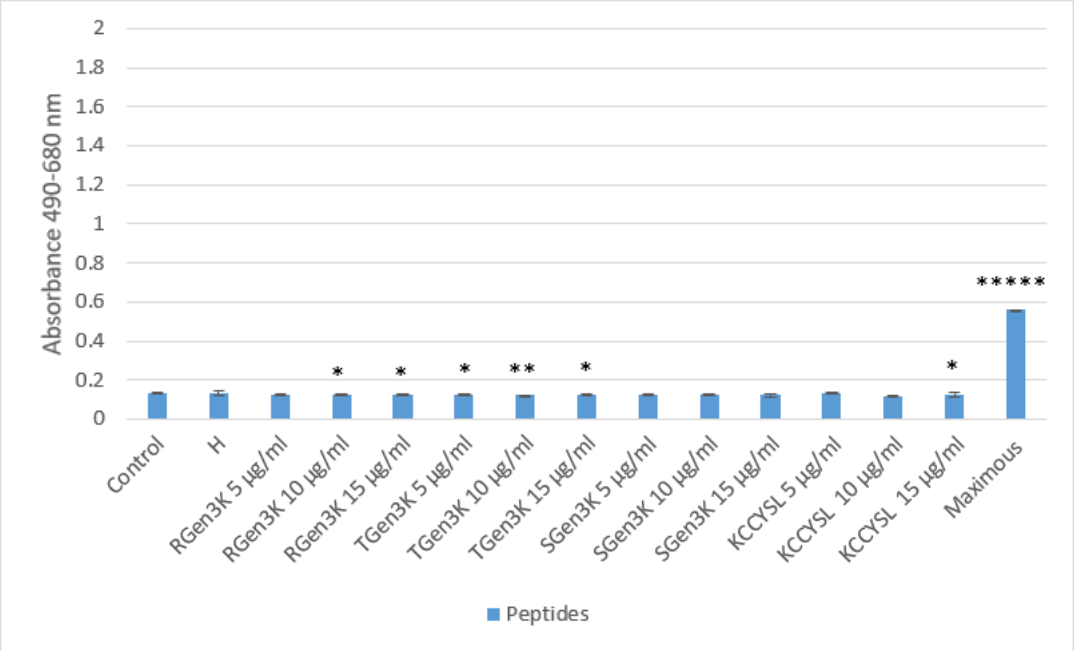

*Figure 0.6 LDH Cytotoxicity Assay on MDA-MB-231 cells after 24 h cells are treated with Herceptin (10 µg/ml); RGen3K, TGen3K and SGen3K at three different concentrations (5 µg/ml, 10 µg/ml and 15 µg/ml); and KCCYSL, the linear hexapeptide at 5 µg/ml, 10 µg/ml and 15 µg/ml. Analysis were performed with ImageJ after 48 H from the seeding. *****P<0.00001, ****P<0.0001, ***P<0.001, **P<0.01, *P<0.05, (n=3).*

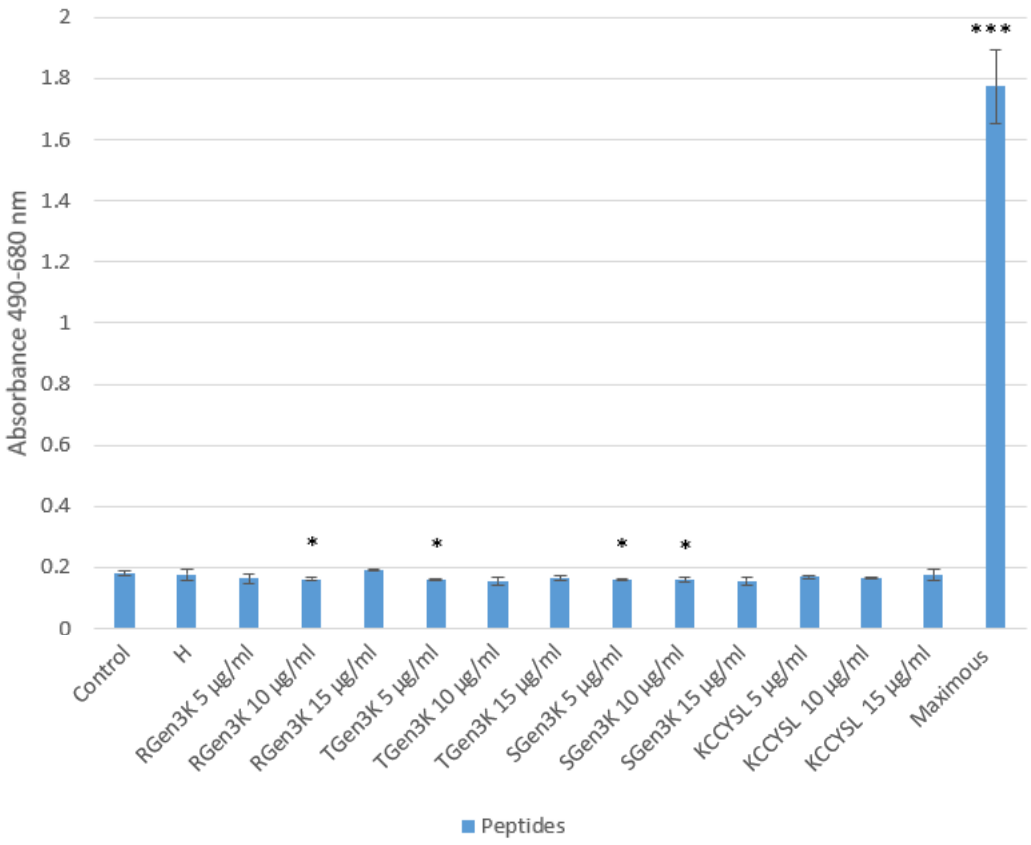

*Figure 0.7 LDH Cytotoxicity Assay on MDA-MB-231 cells after 48 h. are treated with Herceptin (10 µg/ml); RGen3K, TGen3K and SGen3K at three different concentrations (5 µg/ml, 10 µg/ml and 15 µg/ml); and KCCYSL, the linear hexapeptide at 5 µg/ml, 10 µg/ml and 15 µg/ml. Analysis were performed with ImageJ after 48 H from the seeding. *****P<0.00001, ****P<0.0001, ***P<0.001, **P<0.01, *P<0.05, (n=3).*

However, a substantial difference can be observed in the positive control of "maximum" LDH activity when the supernatants deriving from the cells deliberately lysed between 24 hours and 48 hours were analysed. The values refer to the total lysate at the predetermined time points, and its increase over time indicates that the cells continued to duplicate within the 24-hour interval. In relation to the previous experiment (described in Chapter 3.4.1), it can be confirmed that all the synthesised nanocarriers under examination did not induce any significant toxicity in the cells.

Therefore, the data of cell counts in Figures 3.3 and 3.5 suggest a specific effect of the dendrimers on the cell cycle.

In Figure 0.8 and Figure 0.9, values are presented in reference to cells that overexpress the HER2 receptor. In this case as well, the toxicity induced by the peptides was not significantly different from the negative control both after 24 hours and 48 hours.

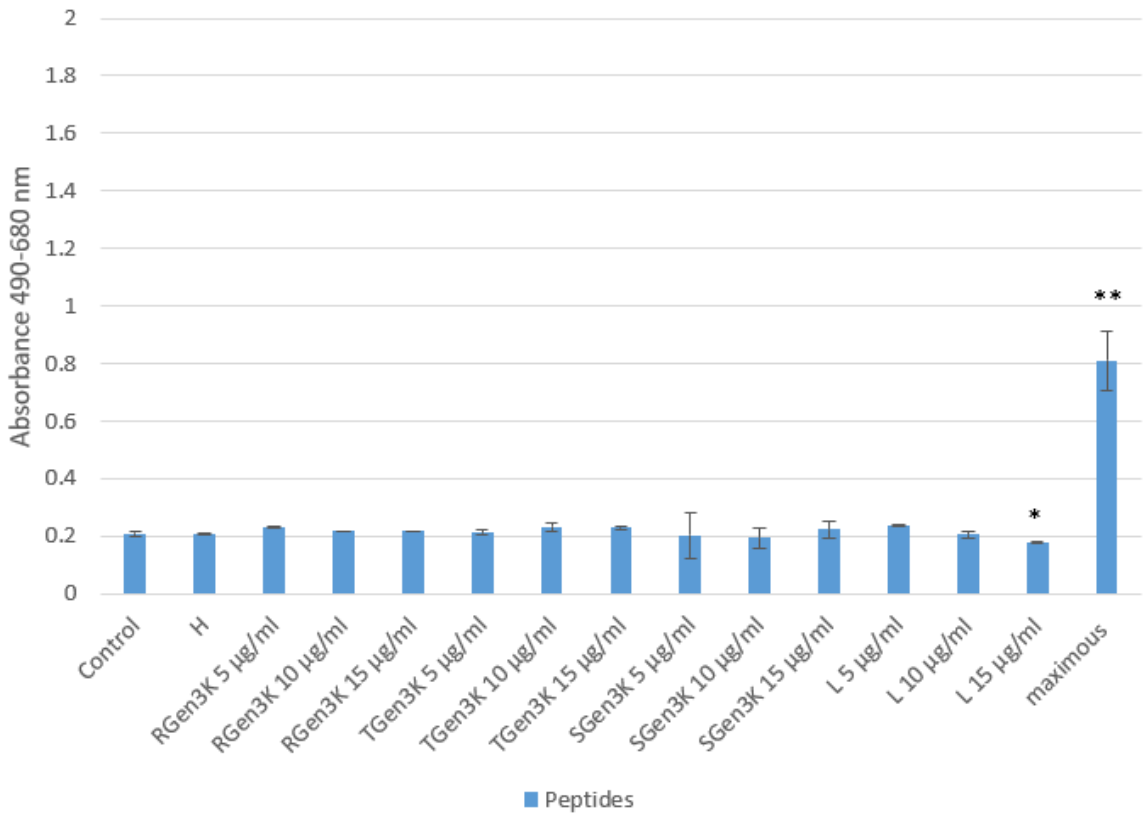

*Figure 0.8 LDH Cytotoxicity Assay on SKBR3 cells after 24 h. Cells are treated with Herceptin (10 µg/mL); RGen3K, TGen3K and SGen3K at three different concentrations (5 µg/mL, 10 µg/mL and 15 µg/mL); and L, the linear hexapeptide at 5 µg/mL, 10 µg/mL and 15 µg/mL. Analysis were performed with ImageJ after 48 H from the seeding. *****P<0.00001, ****P<0.0001, ***P<0.001, **P<0.01, *P<0.05, (n=3).*

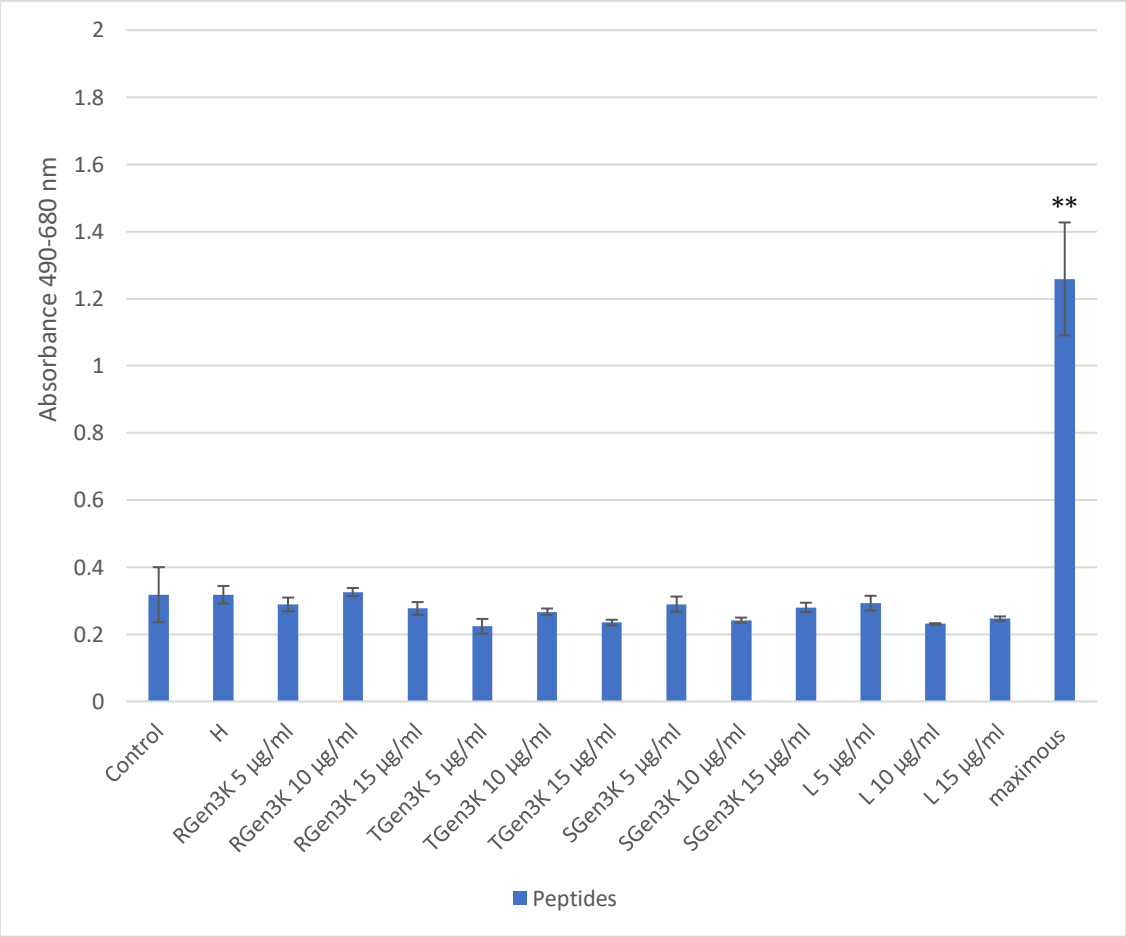

*Figure 0.9 LDH Cytotoxicity Assay on SKBR3 cells after 48 h. Cells are treated with Herceptin (10 µg/mL); RGen3K, TGen3K and SGen3K at three different concentrations (5 µg/mL, 10 µg/mL and 15 µg/mL); and L, the linear hexapeptide at 5 µg/mL, 10 µg/mL and 15 µg/m. Analysis were performed with ImageJ after 48 H from the seeding. *****P<0.00001, ****P<0.0001, ***P<0.001, **P<0.01, *P<0.05, (n=3).*

However, it can be stated that cells have the capacity to proliferate and grow as emphasised by the increasing absorbance between sampling at different time points, albeit at a slower rate compared to MDA-MB-231 cells. Regarding the experiment mentioned in the previous section (Chapter 3.4.1), it can be speculated that samples exhibit a strong anti-proliferative activity rather than a cytotoxic or apoptotic activity. The latter

was not tested by specific kits such as Annexin V or Hoersch Propidium Iodide staining.

As indicated in the research by Debnath et al. [265], PLLs are capable of inducing proliferation arrest, apoptosis, and reducing the formation of new blood vessels to sustain tumour mass. However, in the case of anti-apoptotic activity, there would have been much higher absorbance values, or at least higher than the negative control, which is not the case here. In this instance, the values are around the range of the negative control value.

1.5 CONCLUSION

In conclusion, the experiments performed during this phase of the work have provided insights into the intrinsic activity of hyperbranched peptides on cancer cells when administered into the extracellular environment. The samples have yielded different responses based on their phenotype. The non-overexpressing cells (MDA-MB-231) were not influenced by the presence of peptides in the extracellular environment, and their proliferative capacity remained unchanged. SKBR3 cells exhibited a different reaction to the peptides. As anticipated, Herceptin drastically reduced the proliferative capacity of these cells, as did the TGen3K and SGen3K peptides. In particular, TGen3K influenced proliferation in a dose-dependent manner, while SGen3K was effective only at the lowest concentration tested possibly due to the different arrangement of the hexapeptide sequence, resulting in spatial modifications that interfered with binding to the HER2 receptor.

The proliferative capacity of SKBR3 cells remained intact, as shown in Figure 0.6 and Figure 0.7, and toxicity in the presence of peptides remained very low, if not absent. This, in combination with the proliferation

results (Chapter 3.4.1), highlights the peptide's ability to inhibit cell proliferation without apparently interfering with the apoptosis pathway, which differs from what was reported by Debnath et al. who tested linear PLL [265]. Additionally, it has been possible to demonstrate the targeting sequence's selectivity towards the HER2 receptor and its improved binding to the receptor when non-linear but branched peptides are added to the sequence.

These encouraging results prompted the next phase of research that was to consider the potential of the dendrimer systems to be used as carriers for the delivery of therapeutic agents. This was the focus of Chapter 4 where the potential of the dendrimers, as such or when functionalised with the HER-recognising peptides, to deliver DNA or pDNA. The added negative charges, flexibility, and molecular weight of the nucleic acid could enable the binding to the positively-charged carrier and become and effective delivery system or alter the characteristics of the peptide vector leading to a loss of the inhibitory activity shown in this chapter. This was the aim of the next chapter.

DNA DELIVERY FORMULATION, CHARACTERISATION AND BIOLOGICAL TESTING

1.1 INTRODUCTION

Dendrimers play a crucial role in various fields of science and technology due to their highly branched structure and customisable chemical properties. Their applications range from medicine to nanotechnology, diagnostics, gene therapy, and beyond [274].

A "dendrimer" is a three-dimensional, branched molecule with a highly ordered structure. It's a macromolecule that features a central core from which multiple layers of molecular groups radiate, resembling the branches of a tree (Figure 0.2- Chapter 1.13) . Dendrimers can serve as platforms for transporting and facilitating controlled drug release and thanks to a customisable branching structure, they can encapsulate drug molecules within their branches, offering protection during transport within the body and gradual release at the intended location [275]. Furthermore, they can be tailored with diverse molecules as per requirements, aiming to mitigate toxicity or facilitate vital mechanisms such as internalisation, endosomal escape, and cargo release within the cytoplasmic or nuclear milieu [276,277].

In essence, dendrimers represent a versatile class of materials that are reshaping various sectors, spanning from medicine to nanotechnology, by virtue of their distinctive attributes and the myriad possibilities for customisation, such as: they can be employed in the production of highly sensitive sensors, advanced composite materials, and nanomaterials for electronic applications; they also find applications in nanotechnology for

creating materials and devices at the nanoscale level; they are utilised the efficient delivery of drugs or biological molecules [278].

In the pharmaceutical field, gene therapy holds great promise for treating or preventing diseases by either silencing or expressing specific genes. Some of the most effective delivery agents for this purpose are polycationic dendrimers, which are highly branched structures containing numerous positively charged groups.

Two of the most effective dendrimers in this context are polyethyleneimine (PEI) and poly(amidoamine) (PAMAM), which exhibit high proficiency in overcoming barriers to delivering oligonucleotides. However, due to their high positive charge density, they are associated with significant toxicity [279]. Dendrons made of poly-L-Lysine (PLL) can also be toxic as polycations. However, similar to other dendrimeric structures, their toxicity increases with the number of generations [280]. Therefore, dendrons considered in this study have a lower number of positive charges compared to traditional dendrimeric structures. Additionally, PLL is preferred over PAMAM because, when degraded into L-lysine monomers, it can be recycled by the cell, and the reduced number of positive charges results in a faster release of nucleic acids once they reach the cytoplasm [281].

Dendron-based transfection is a dynamic area of research focused on developing new delivery vectors that enhance DNA internalisation and address associated challenges. Polycationic molecules like PAMAM and PEI are extremely efficient carriers for the delivery of nucleic acids, as they possess tertiary amines in their backbone that can be protonated. As the endosome acidifies, to prevent the buildup of a charge gradient resulting from proton influx, an influx of Cl- ions also takes place. This simultaneous influx of protons and Cl^- ions raises the endosome's osmolarity and triggers water absorption (Figure 0.1 [282]). The combination of polymer swelling and osmotic endosome swelling leads to endosome destabilisation and

content release into the cytoplasm. This mechanism, described by Freeman et al. [283], highlights the "proton sponge" effect induced by certain polycationic molecules, which, however, is lacking in PLL molecules [284]. Nonetheless, recent studies have raised questions about the "proton sponge" effect, and the process of endosomal escape is not yet entirely clear [278].

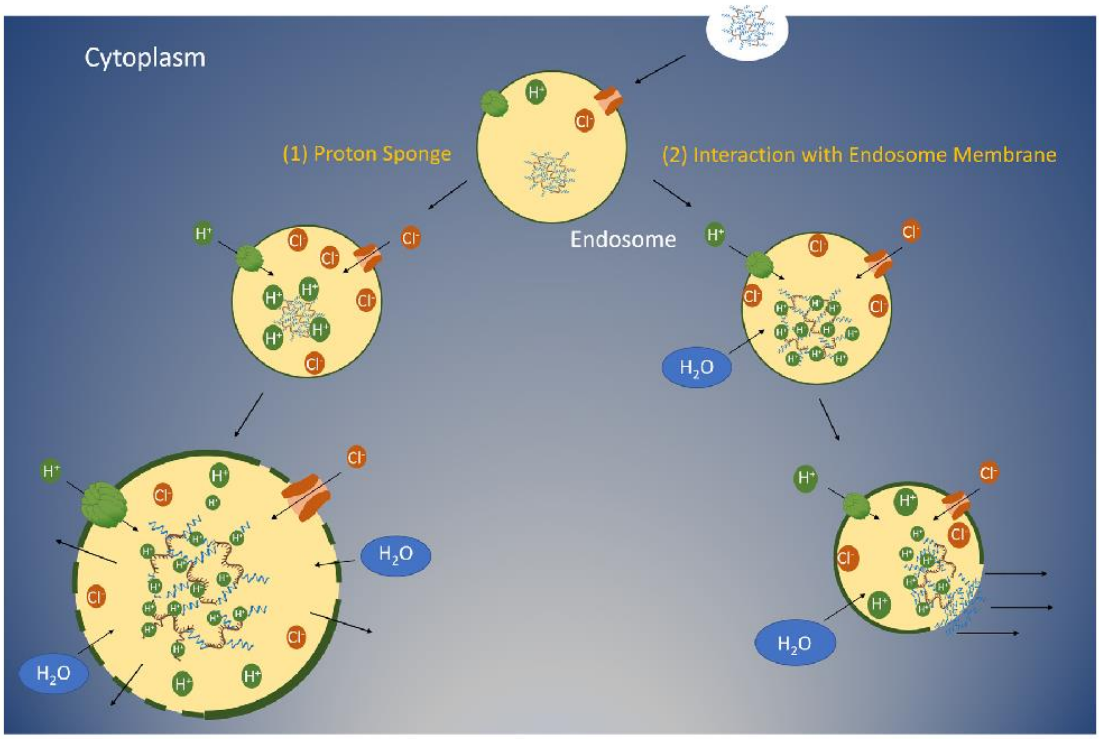

Figure 0.1 Endosomal escape pathway. On the left the endosome goes through the lysis because of the enter of water molecule. while on the right, the endosomal escape of the nanoparticles.

However, PLLs are not capable of releasing the cargo inside the cell due to the absence of tertiary amines and thus the inability to induce the proton sponge effect. Consequently, helper molecules are necessary to

trigger endosome disruption and thereby enhance the release of nucleic acids within the tumour cell [285].

Therefore, it has been demonstrated that the lipid:peptide:DNA complex is necessary. to further enhance cellular uptake and accumulation in the cell cytoplasm [284].

As reported by Kwok et al. [286] it has been shown that the presence of lipids does not increase the toxicity of the complex, but greatly aids in endosome disruption, promoting the amount of DNA that reaches the cell nucleus. Lipid molecules, due to their amphiphilic nature, destabilise the endosomal membrane, leading to the release of peptide nanocarriers into the nucleus and cytoplasm of the cancer cell [287]. The most recognised mechanism of endosomal disruption involves the exchange of individual lipids with the endosomal membrane, a process known as "flip-flop." This mechanism induces membrane destabilisation and subsequent rupture, resulting in the release of materials into the cytoplasm.

One of the most commonly used helper lipids is DOPE (1,2-dioleoyl-sn-glycero-3-phosphoethanolamine), which is a neutral lipid that, as reported by Du et al. [129] The utilisation of the neutral lipid DOPE within cationic lipoplex formulations enhances transfection efficiencies by virtue of the conical nature of this lipid, which stimulates the creation of inverted hexagonal structures. These structures readily merge with the endosomal lipid bilayer in a charge-independent manner, thereby facilitating the liberation of DNA into the cytoplasm. Another lipid frequently associated with DOPE is DOTMA (Figure 0.2 [288]), or N-[1-(2,3-dioleyloxy)propyl]-N,N,N-trimethylammonium chloride. This lipid has given rise to various derivatives such as DOTAP (1,2-dioleoyl-3-trimethylammonium-propane (chloride salt)), DORI (N-(2-hydroxyethyl)-N,N-dimethyl-2,3-bis(oleoyloxy)propan-1-aminium bromide), DORIE (N-(2-hydroxyethyl)-N,N-dimethyl-2,3-bis(((Z)-octadec-9-en-1-yl)oxy)propan-1-aminium bromide), and DMRIE (N-(2-

hydroxyethyl)-N,N-dimethyl-2,3-bis(tetradecyloxy)propan-1-aminium bromide). DOTMA's positively charged portion efficiently complexes with negatively charged DNA, leading to its condensation. The complex formed between cationic lipid and DNA is referred to as a lipoplex. These co-lipids, when incorporated into the cationic lipid-DNA complex, function to facilitate the fusion or destabilisation of cellular membranes, thereby aiding transfection. In fact, the DOTMA/DOPE mixture is one of the commercially successful lipid formulations still widely used for gene transfer into cells. After interacting with the plasma membrane, the lipoplex can be internalised through two different pathways: direct fusion with the membrane followed by the release of DNA into the cytoplasm, or through clathrin-coated vesicle-mediated endocytosis. Most studies indicate that the second process is primarily responsible for DNA internalisation [289–292].

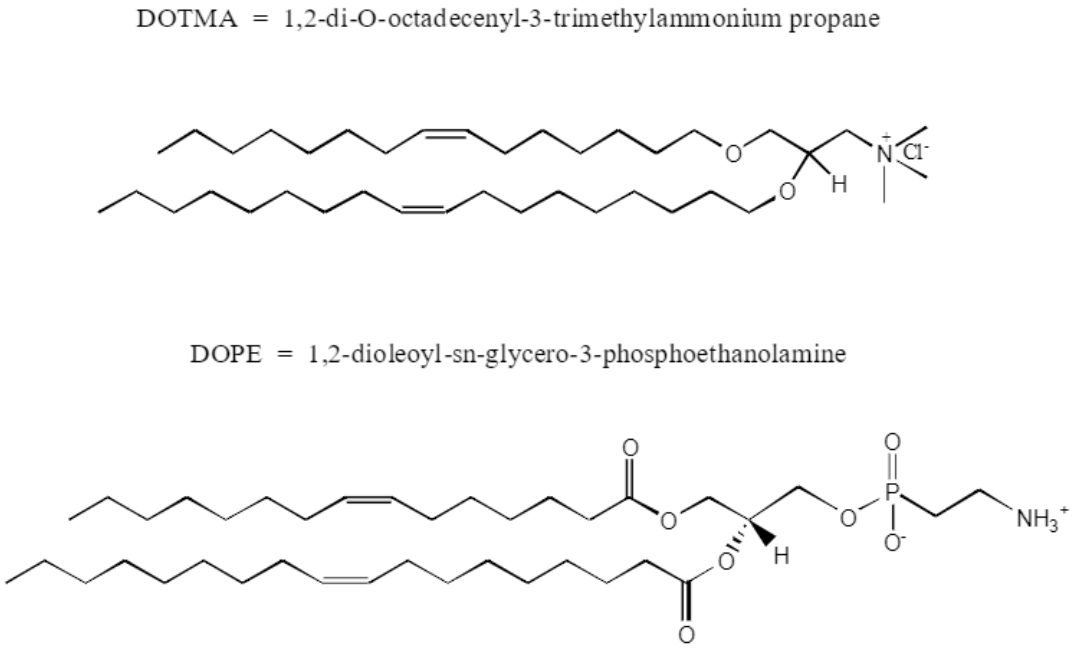

Figure 0.2 DOTMA and DOPE chemical structure.

Although lipoplexes (combinations of polynucleotide molecules with cationic liposomes) are extensively employed for delivering nucleic acids, certain limitations like their considerable size, cytotoxicity at elevated concentrations, and modest transfection efficiency have hindered their effectiveness as gene carriers [293,294]. Meanwhile, polyplexes (combinations of polynucleotide molecules with polycations) have been extensively investigated as nucleic acid delivery tools. Despite their heightened cytotoxicity compared to lipoplexes, polyplexes offer numerous advantageous qualities as gene carriers [295]. A synergistic approach involving these systems has led to the creation of lipopolyplexes, engineered to possess heightened biocompatibility and efficacy. Lipopolyplexes mix the strengths of lipoplexes (notable stability, acceptable cellular uptake, low cytotoxicity) and polyplexes (robust transfection activity and uniform and small particle size). Moreover, Lipopolyplexes exhibit structural merits, including reduced size (nano-scale) and improved nucleic acid condensation when compared to lipoplexes [296,297,298]. In general, dendrons exhibit a pronounced propensity to form highly stable complexes with nucleic acids due to the oppositely charged interactions between the amines of the dendron's backbone and the negative charges on the DNA [299,300]. However, it is crucial to acknowledge that the efficiency and reliability of DNA internalisation depend on several factors, including the design of the peptide, the nature of the DNA, and the characteristics of the target cell [301]. Lastly, the amount of lipid is also an important factor for the formulation. In fact, a small quantity is necessary to facilitate the formation of the lipopolyplex; otherwise, it encourages the formation of only lipoplexes, excluding the peptides from the complex. Often, the appropriate concentration is lower than a 1:1 lipid:DNA charge ratio [302].

1.2 AIM OF THE CHAPTER

The purpose of the chapter is to formulate and aggregate the dendrons synthesised in Chapter 2 with lipids and DNA, and to compare these complexes with the polyplexes (peptide:DNA). Both complexes are characterised by determining:

- their size;
- their ability to bind DNA using gel electrophoresis;
- their ability to pack the DNA using the PicoGreen fluorescence;
- their *in-vitro* transfection efficiency and cellular toxicity was tested in two cell lines expressing and devoid of HER2 receptors.

The peptide:DNA complexes will be compared to those containing lipid:peptide:DNA to ascertain whether the presence of lipid can enhance transfection capacity. Furthermore, the purpose of conducting *in vitro* experiments is to determine if a successful transfection is achieved, identify factors that could enhance it, and assess the selectivity towards target sequences. The underlying hypothesis is that in SKBR3 cells, which overexpress the HER2 receptor, any therapeutic impact of TGen3K on the cells should be significantly greater than that of the control dendron. In this context, it is anticipated that the control dendron will still retain some level of internalisation ability, regardless of any specific bio-recognition process.

Regarding the control cells, MDA-MB-231 cells that lack the HER2 target receptor, it is expected that the internalisation of peptide vectors will occur independently of the presence of a specific hexapeptide target sequence capable of interacting with the receptor in the branched TGen3K structure, as well as its absence in the control vector (RGen3K). In this case, internalisation is likely to be driven by non-selective mechanisms.

1.3 MATERIALS AND METHODS

1.3.1 Lipid vesicles preparation

The lipid component used in lipopolyplex formulation was a mixture of two lipids, DOTMA and DOPE (Avanti Polar), which were formulated into vesicles (also called liposomes). The two lipids were weighed and dissolved in chloroform at 1 mg/mL in a glass vial to facilitate the withdrawal of the appropriate lipid quantity. The two lipids were then mixed in a 1:1 molar ratio, by mixing 1 mg (DOTMA) with 1.1 mg (DOPE). The chloroform was subsequently removed by flowing nitrogen gas over the solution for several minutes until a lipid film was formed. Once the lipid film was completely dry, the correct amount of distilled water was added to achieve a final concentration of 1 mg/mL of DOTMA content. The resulting preparation appeared turbid due to the large size of the vesicles. To reduce the vesicle size, the preparation was sonicated for 3 minutes using a probe sonicator (Vibra Cells, Sonics & Materials) operating at 80% if its maximal capacity.

1.3.2 Polyplexes preparation

The polyplexes (PDs) were complex structures formed by mixing equal volumes of dendrons (synthesised according to the method described in Chapter 2.3.2) and nucleic acid through a self-assembly process. Each sample consisted of DNA diluted in sterile water, prepared in stock according to the number of samples. The dendrons used to prepare the PDs were RGen3K, TGen3K, SGen3K, as well as linear controls without a specific sequence (K16) and with a targeting sequence (TK16) (Figure 0.4). The DNA concentration per sample varies depending on the experiment to be conducted; consequently, the quantity of peptide also varies. Furthermore, peptides are mixed with nucleic acid considering the charge

ratio, so the peptide-DNA complexes were prepared in ratios ranging from 4:1 to 12:1. The charge ratios used were selected based on previous studies by Kudsiova et al., in which polyplex and lipopolyplex formulations containing similar- linear and hyperbranched peptides, were shown to be most effective at 6:1 and 12:1 charge ratios [302]. Intermediate concentrations were also tested to detect any changes in transfection and condensation behaviour of polyplexes prepared using these novel peptides.

The preparation of PRs always followed a specific order of mixing to obtain the optimal physicochemical properties. For each sample, equal volumes of DNA and peptide were mixed and DNA was always added to already diluted peptide solution in water to maintain consistency, as demonstrated by Welser et al. [303].

1.3.3 Lipopolyplexes Preparation

The lipopolyplexes (LPDs) were complex formations obtained via a self-assembly process, involving the lipids DOTMA:DOPE, dendrons, and nucleic acids (DNA either gWIZ-Luc, from Aldevron; or calf thymus, from Invitrogen). Each sample consisted of a constant amount of DNA diluted in sterile water, prepared as a stock solution based on the number of samples. Similarly, the DOTMA:DOPE vesicles also had a constant concentration (prepared according to the method described in Chapter 4.3.1), however the peptide concentration varied to produce charge ratios ranging from 0.5:4:1 to 0.5:12:1 lipid:peptide:DNA. The dendrons used to prepare the LPDs were RGen3K, TGen3K, SGen3K, and the control peptides without a specific sequence (K16) and with the targeting sequence (TK16). As in the case of PDs, the LPDs that have previously been shown to produce the best efficiency were those prepared at 0.5:6:1 and 0.5:12:1, which justifies the range of concentrations chosen in this study [302].

Similarly to PDs, the preparation of the LPDs followed a specific method and order to achieve optimal activity, since previous studies by Kudsiova et al showed that the order of mixing, particularly in the LPDs affected both the structure of the complexes formed, their physicochemical properties and consequently their biological activity. LPDs were therefore prepared by mixing the lipid and peptide first at equal volumes. Followed by addition of the DNA at an equal volume to the PD mixture [303].

1.3.4 Dynamic Light Scattering

LPD complexes were generated using RGen3K, and TGen3K, K16 and TK16, varying charge ratios, specifically, 0.5:4:1, 0.5:6:1, 0.5:8:1, 0.5:10:1, and 0.5:12:1, respectively. Each sample was prepared with a final volume of 50 µL with 0.75 µg of calf thymus DNA. The LPDs were prepared as previously described in Section 4.3.3, resulting in a total sample volume of 50 µL, composed of 12.5 µL of lipid stock solution, 12.5 µL of the total peptide solution, and 25 µL of DNA stock solution. Each sample was measured three times at 25° C and the average size calculated. The polydispersity index (PDI) indicates the homogeneity of the population which are in the sample. The experiments was repeated twice. Data were statistically analysed by a two-tail T Test and data considered significant different at $p<0.05$ and considering only the charge ratio x=10.

1.3.5 Gel Electrophoresis

Electrophoresis was conducted in 1% w/v agarose gel prepared by dissolving 0.7 g of agarose in 70 mL of Tris-Acetate-EDTA, TAE buffer, (Fisher Scientific). The agarose gel was heated until the agarose was completely dissolved, then, 2 µL of gel red nucleic acid stain (Merck Life Science) was

added and left to cool at room temperature. The solidified gel was then immersed in TAE buffer (1X) in the electrophoresis tray.

The analysed samples included polyplexes and lipopolyplexes containing RGen3K, TGen3K, SGen3K, and the linear controls K16 and T(K16). The polyplexes were prepared as described in the Section 4.3.2, by preparing 10 µL samples containing equal volume of calf thymus DNA and peptides necessary to achieve charge ratios of 4:1, 6:1, 8:1, 10:1, and 12:1. In all samples, including the DNA controls, the DNA content was 0.25 µl/well. For example, to achieve a total volume of 10 µl, 5 µl containing 0.25 µg of DNA was mixed with 5 µl of the adjusted concentration of peptide. Table 0.1 shows the volumes of peptide and water used in each sample.

Table 0.1 Calculation of branched and linear peptides and their dilution in water to reach a final volume of 5 µl, mixed later with 5 µl diluted DNA. The ratio 0.5:x:1 equals the charge ratio, with the lipid and DNA amount fixed.

BRANCHED PEPTIDES		
RGen3K		
Charge ratio (0.5: x : 1)	amount of peptides (µl)	Sterile water Volume (µl)
4	0.40	4.60
6	0.60	4.40
8	0.81	4.19
10	1.01	3.99
12	1.21	3.79
TGen3K		
Charge ratio (0.5: x : 1)	amount of peptides (µl)	Sterile water Volume (µl)
4	0.51	4.49
6	0.76	4.24
8	1.01	3.99
10	1.27	3.73
12	1.52	3.48
SGen3K		
Charge ratio (0.5: x : 1)	amount of peptides (µl)	Sterile water Volume (µl)
4	0.51	4.49
6	0.76	4.24
8	1.01	3.99
10	1.27	3.73
12	1.52	3.48

LINEAR PEPTIDES		
K16		
Charge ratio (0.5: x : 1)	amount of peptides (µl)	Sterile water Volume (µl)
4	0.40	4.60
6	0.60	4.40
8	0.80	4.20
10	1.00	4.01
12	1.19	3.81
TK16		
Charge ratio (0.5: x : 1)	amount of peptides (µl)	Sterile water Volume (µl)
4	0.50	4.50
6	0.75	4.25
8	1.00	4.00
10	1.25	3.75
12	1.50	3.50

Table 0.2 Amount of peptide per well considering the charge ratio with DNA. The ratio 0.5:x:1 equals the charge ratio, with the lipid and DNA amount fixed.

BRANCHED PEPTIDES		
RGen3K		
Charge ratio (0.5: x : 1)	amount of peptides (µl)	Sterile water Volume (µl)
4	0.40	2.10
6	0.60	1.90
8	0.81	1.69
10	1.01	1.49
12	1.21	1.29
TGen3K		
Charge ratio (0.5: x : 1)	amount of peptides (µl)	Sterile water Volume (µl)
4	0.51	1.99
6	0.76	1.74
8	1.01	1.49
10	1.27	1.23
12	1.52	0.98
SGen3K		
Charge ratio (0.5: x : 1)	amount of peptides (µl)	Sterile water Volume (µl)
4	0.51	1.99
6	0.76	1.74
8	1.01	1.49
10	1.27	1.23
12	1.52	0.98

LINEAR PEPTIDES		
K16		
Charge ratio (0.5: x : 1)	amount of peptides (µl)	Sterile water Volume (µl)
4	0.40	2.10
6	0.60	1.90
8	0.81	1.69
10	1.01	1.49
12	1.21	1.29
TK16		
Charge ratio (0.5: x : 1)	amount of peptides (µl)	Sterile water Volume (µl)
4	0.50	2.00
6	0.75	1.75
8	1.00	1.50
10	1.25	1.25
12	1.50	1.00

Similarly, the lipopolyplexes were prepared at a final DNA concentration of 0.25 µg per 10 µL per well, and at lipid:peptides:DNA ratios of 0.5:4:1, 0.5:6:1, 0.5:8:1, 0.5:10:1, and 0.5:12:1.

For each ratio, the lipids (DOTMA:DOPE 1 mg/mL stock) and DNA values were kept constant, in contrast, the amount of peptides increased. Therefore, for a total volume of 10 µL, 2.5 µL of peptide was added to an equal volume of lipid suspension. To these, 5 µL of diluted DNA (0.25 µg in a total of 5 µl of sterile water) were then added. Table 0.2 reports the dilutions performed to achieve the precise peptide concentrations.

The PDs and LPDs were prepared in two ways: some samples were loaded onto the agarose gel without the addition of loading buffer; while others were prepared by adding 2 µL of loading buffer (composed of bromophenol blue and sucrose 4% in water) to each sample. The purpose of removing the loading buffer was to determine whether the loading buffer interferes with the DNA binding within the formulation, as the loading buffer molecule, being negatively charged, could act as a competitor in the complex formation, thereby potentially reducing the amount of DNA bound to the lipid-peptide complex.

Since loading the complexes into the gel wells was challenging due to their colourlessness (Bromophenol blue, on the other hand, ensured the physical visualisation of product loading), it is not possible to ensure that all DNA/RNA was effectively loaded onto the agarose gel. To achieve the best possible outcome, few precautions were followed:

1. Ensuring precise placement of the pipette within the well.
2. Allowing a few seconds after releasing the sample.
3. Conducting duplicate experiments, which produced highly similar gel results.

4. Additionally, there are faintly illuminated wells when the complex does not migrate.

After loading the samples onto the gel, electrophoresis was performed in 1x TAE buffer (Tris Acetate EDTA) at 80 V, 400 A for 30 minutes using a Biorad Powerpac 300 power supply and analysed with BioDoc-it2 Gel Imaging System at 302 nm. The measurements were conducted in triplicate per each sample and the experiments was repeated twice.

1.3.6 Picogreen Assay

The Picogreen analysis was conducted by preparing the polyplexes and lipopolyplexes complexes in a 96-well plate. For the polyplexes, 50 µL of nucleic acid was added to 50 µL of peptides, while for the lipopolyplexes, 25 µL of peptides was added to an equal volume of lipids, followed by the addition of 50 µL of DNA calf thymus, resulting in a total volume of 100 µL. The concentrations of DNA (0.25 µg/well) and (DOTMA:DOPE 1 mg/mL stock) were kept constant, while the amount of peptides increased. The peptides used were RGen3K, TGen3K, SGen3K, as well as the linear controls K16 and TK16. For both preparations, dendrons charge ratios of 4, 6, 8, 10, and 12 were used as reported in Table 0.3. The experiment was also repeated in the absence of lipids, and in this case, the peptides were diluted in 50 µL of the appropriate buffer or solvent.

Table 0.3 Calculation of branched and linear peptides and their dilution in water to reach a final volume of 5 µl, mixed later with 5 µl diluted DNA. The ratio 0.5:x:1 equals the charge ratio, with the lipid and DNA amount fixed.

BRANCHED PEPTIDES		
RGen3K		
Charge ratio (0.5: x : 1)	amount of peptides (µl)	Sterile water Volume (µl)
4	0.40	24.60
6	0.60	24.40
8	0.81	24.19
10	1.01	23.99
12	1.21	23.79
TGen3K		
Charge ratio (0.5: x : 1)	amount of peptides (µl)	Sterile water Volume (µl)
4	0.51	24.49
6	0.76	24.24
8	1.01	23.99
10	1.27	23.73
12	1.52	23.48
SGen3K		
Charge ratio (0.5: x : 1)	amount of peptides (µl)	Sterile water Volume (µl)
4	0.51	24.49
6	0.76	24.24
8	1.01	23.99
10	1.27	23.73
12	1.52	23.48

LINEAR PEPTIDES		
K16		
Charge ratio (0.5: x : 1)	amount of peptides (µl)	Sterile water Volume (µl)
4	0.40	24.60
6	0.60	24.40
8	0.80	24.20
10	1.00	24.01
12	1.19	23.81
TK16		
Charge ratio (0.5: x : 1)	amount of peptides (µl)	Sterile water Volume (µl)
4	0.50	24.50
6	0.75	24.25
8	1.00	24.00
10	1.25	23.75
12	1.50	23.50

Subsequently, 50 µL of Picogreen reagent, diluted 1:150 v/v in Tris-EDTA (TE buffer), was added to each sample. The fluorescence emitted by the Picogreen reagent was analysed using a Biotek fluorescent plate spectrophotometer, with fluorescence measured at λex/λem = 480/520 nm.

All obtained values were normalised by comparing them with the analysis of naked DNA, which reacted with only the Picogreen reagent in the absence of peptides. The measurements were conducted in triplicate, and the error bars indicate the standard deviation calculated from three distinct measurements within a single experiment. The experiments was repeated in duplicate. Data were statistically analysed by a two-tail T Test and data considered significant different at $p<0.05$ and considering only the charge ratio x=10.

1.3.7 DNA Transfection Assay

Cells were passaged, counted and plated into 24 well plates at a concentration of $8 \cdot 10^4$ cell/mL per well. The cells were then incubated overnight at 37° C, and 5% CO_2. After 24 hours and sample preparation, the medium in the 24-well plates was removed and the cells washed with 200 µl of sterile PBS, followed by the addition of 200 µl of Opti-MEM. Finally, samples containing either polyplexes (peptide:DNA) or lipopolyplexes (lipid:peptide:DNA) were tested.

For the polyplex or PDs samples (peptide:DNA) each well one charge ratio was calculated with a fixed amount of DNA (6:1) Chosen based on the previous study by Kudsiova et al. [302]. Accordingly, 100 µL of diluted peptide, to which 0.75 µg of DNA diluted in 100 µL of OptiMEM (serum-free media) was added. Then, the total amount of PDs (200 µl) in Opti-MEM added to 200 µL OptimMEM that was previously added in the well. The

peptides tested were: RGen3K, TGen3K and the linear controls K16 and T(K16).

For LPDs samples (lipid:peptides:DNA) were first added 50 µL diluted lipid, then 50 µL of diluted peptide, to which 100 µL of DNA gWIZ-Luc was added. For each ratio the lipids (DOTMA:DOPE 1 mg/mL stock) and DNA values were kept constant (0.75 µg per well), in contrast, the amount of peptides increased. Then, the total amount of LPDs (200 µl) in Opti-MEM (serum-free media) added to 200 µL OptimMEM that will already be in the well.

Table 0.4 Example of peptides calculations. The ratio 0.5:x:1 equals the charge ratio, with the lipid and DNA amount fixed.

DNA per well	volume optiMEM per well
0.75	99.25

LIPID per well	volume optiMEM per well
0.75	49.25

BRANCHED PEPTIDES		
RGen3K		
(0.5: x : 1)	amount of peptides (µl)	Sterile water Volume (µl)
4	1.209	48.79
6	1.8135	48.19
8	2.418	47.58
10	3.0225	46.98
12	3.627	46.37
TGen3K		
(0.5: x : 1)	amount of peptides (µl)	Sterile water Volume (µl)
4	1.521	48.48
6	2.282	47.72
8	3.042	46.96
10	3.803	46.20
12	4.563	45.44
SGen3K		
(0.5: x : 1)	amount of peptides (µl)	Sterile water Volume (µl)
4	1.521	48.48
6	2.282	47.72
8	3.042	46.96
10	3.803	46.20
12	4.563	45.44

LINEAR PEPTIDES		
K16		
(0.5: x : 1)	amount of peptides (µl)	Sterile water Volume (µl)
4	1.194	48.81
6	1.791	48.21
8	2.388	47.61
10	2.985	47.02
12	3.582	46.42
TK16		
(0.5: x : 1)	amount of peptides (µl)	Sterile water Volume (µl)
4	1.5	48.50
6	2.25	47.75
8	3	47.00
10	3.75	46.25
12	4.5	45.50

The analysed samples were: RGen3K, TGen3K and linear controls K16 and T(K16) and lipid:peptides:DNA ratios prepared were: 0.5:4:1, 0.5:6:1, 0.5:8:1, 0.5:10:1, and 0.5:12:1. Calculations are reported in Table 0.4.

After 4 hours of incubation, the samples were removed, and the medium replaced with 1 mL of growth media. Cells were incubated for 48 hours at 37°C and 5% CO_2. Afterwards the medium was removed and the cells

were washed once with 200 µL sterile PBS. Immediately after aspirating the PBS, 200 µL of 1x strength lysis buffer (supplied with the luciferase assay kit, Promega) was added to each well. The 24-well plate was then placed in a -80° C freezer, until the cells were completely frozen to help the lysis process. Cells were then placed in an orbital incubator at ~38º C to thaw. 50 µL from each well of the lysed cells were transferred into a white, opaque disposable ninety-six well plate. The luminescence was then measured using a FLUOstar OPTIMA microplate reader (B MG LabTech). The injector channel was cleaned with ultrapure water to remove any kind of residue and dust, then purged by the Luciferase assay solution, which was prepared by mixing the Luciferase assay buffer with the Luciferase assay substrate (provided in the luciferase assay kit, Promega). Once the microplate reader was set, results were displayed in by MARS data program. The final transfection was then calculated by dividing the luminescence (relative light units (RLU) by mg of protein measured by the protein assay as reported below. Luciferase activity was quantified in terms of relative light units (RLU) per milligram of protein (RLU/mg protein). The measurements were conducted in quadruplicate, and the error bars show the standard deviation calculated from four distinct measurements within a single experiment. Data were statistically analysed by a two-tail T Test and data considered significant different at $p<0.05$ and considering only the charge ratio x=10.

1.3.8 Protein Assay

Firstly, a calibration graph was prepared for the protein assay, using a series of dilutions of bovine serum albumin 2 mg/mL (BSA) from the BCA Protein Assay Kit (ThermoFisher). The volumes used are shown in Table 0.5.

Table 0.5 Dilutions for the standard protein assay calibration graph. From the BCA kit were mixed BSA with sterile water.

BSA Concentration (mg/mL)	*Quantity of BSA 2 mg/mL (µL)*	*Quantity of Purified Water (µL)*
0	0	100
0.125	6.25	93.75
0.25	12.5	87.5
0.5	25	75
0.75	37.5	62.5
1	50	50
1.5	75	25

Twenty microlitres of each BSA concentration samples were pipetted in quadruplicate into a clear, disposable ninety-six well plate. Subsequently, 20 µL of the lysed cells were pipetted into a clear ninety-six well plate in the same layout they were configured in the twenty-four well plate. Into each well having the calibration graphs and cells samples, 200 µL of the reagent from BCA Protein assay was then added. The reagent was made up by mixing Reagent A with Reagent B (at 1:50 ratio). The plates were incubated at 37° C for 30 minutes and then the absorbance in each well was read using a Synergy HT Plate Reader (Biotek Instruments) set at a wavelength of 562 nm. The measurements were conducted in triplicate, and the error bars show the standard deviation calculated from three distinct measurements within a single experiment. Experiments was repeated twice. Data were statistically analysed by a two-tail T Test and data considered significant different at $p<0.05$ and considering only the charge ratio x=10.

1.4 RESULTS AND DISCUSSION

1.4.1 Dynamic Light Scattering

The size of lipid-peptide-DNA complexes was measured. Specifically, the analysed peptides were RGen3K, TGen3K, K16, and TK16 at charge ratios of 4:1, 6:1, 8:1, 10:1, and 12:1, using the plasmid DNA gWIZ-Luc. The results are reported in the following paragraph.

All LPDs have sizes ranging from 50 to 150 nm, except for RGen3K, which exhibits peaks reaching up to 200 nm. It is noticeable that linear peptides have the ability to form complexes with smaller sizes at each charge ratio (except for the 0.5:8:1 ratio). This can be explained by a higher availability of positive charges, which increases DNA binding sites, consequently allowing for the reduction in complex size, Figure 0.3. A second hypothesis is that with dendrons, DNA is forced to fold, and the smaller the

generations, the more apparent the DNA distortion, making it less prone to complex formation [304].

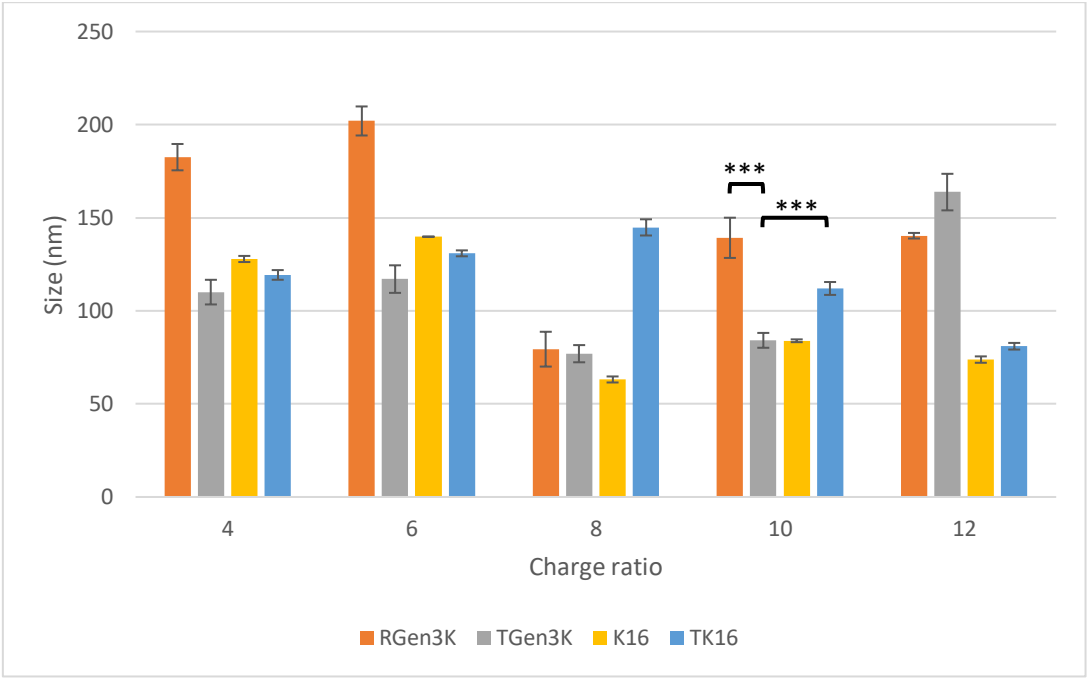

*Figure 0.3 Graph showing the average intensity size distribution of the of the lipid:peptide:DNA complexes. Peptides involved were: RGen3K, TGen3K and the linear K16 and TK16. The numbers on the X axis represent the lipid:peptide:DNA as 0.5:X:1 charge ratio. *****P<0.00001, ****P<0.0001, ***P<0.001, **P<0.01, *P<0.05 considering only the charge ratio x=10.*

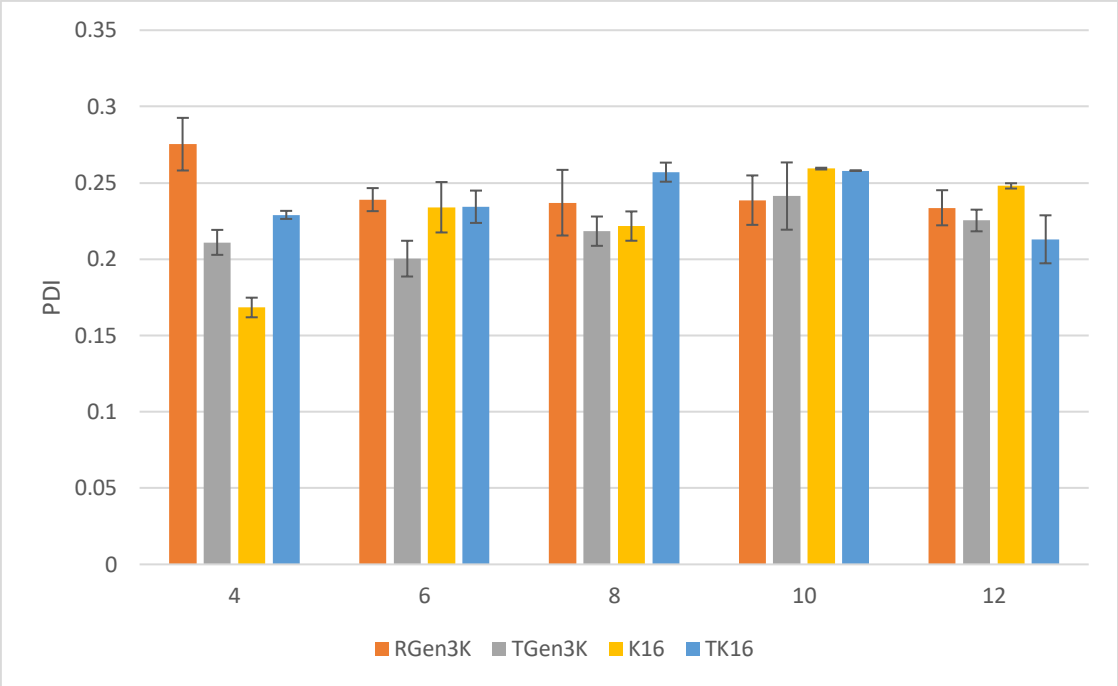

*Figure 0.4 Graph showing the polydispersity index of the of the lipid:peptide:DNA complexes. Peptides involved were: RGen3K, TGen3K and the linear K16 and TK16. The numbers on the X axis represent the lipid:peptide:DNA as 0.5:X:1 charge ratio. *****P<0.00001, ****P<0.0001, ***P<0.001, **P<0.01, *P<0.05 considering only the charge ratio x=10.*

While the sizes of the complexes vary between low and high values, the PDI (poly-dispersity index) remains consistently between 0.2 and 0.25. This indicates a high degree of uniformity within the population, Figure 0.4.

1.4.2 Gel Electrophoresis

Electrophoresis is a technique that allows the separation of biological molecules according to their molecular weight and charge, and to determine the vector's ability to complex nucleic acid [305]. Gel electrophoresis exploits the net charge, positive or negative, that biological molecules have once placed in a particular buffer solution. If subjected to the passage of electric current the molecules will tend to

migrate towards the electrode with an opposite charge than their own, separating according to their molecular weight: the larger the molecules the slower the migration down the gel. Furthermore, if the nucleic acid is complexed, it would not bind the nucleic acid stain or migrate down the gel, making it impossible to see the band. Due to the difference in charge within the electrophoresis chamber, nucleic acid rich in groups of negatively charged groups, whether complexed or free, will tend to migrate to the positively charged anode. Presence of bands indicates that DNA is still free and not fully condensed inside the nanoparticles. Absence of bands means that the lipopolyplexes have fully complexed the DNA And the formed complex is too large to migrate through the agarose gel, so it remains trapped in the well where it was loaded.

Polyplexes (PDs) and lipopolyplexes (LPDs) are compared. For polyplexes preparation the charge ratios were 4:1, 6:1, 8:1, 10:1, and 12:1, using plasmid DNA gWIZ-Luc. The peptides tested were: RGen3K, TGen3K, SGen3K and the linear controls K16 and TK16. For lipopolyplexes the concentrations used were 0.5:4:1, 0.5:6:1, 0.5:8:1, 0.5:10:1, and 0.5:12:1. The peptides evaluated were: RGen3K, TGen3K, SGen3K and the linear controls K16 and T(K16). The gel was then analysed to evaluate the interaction of lipids and peptides with DNA at different ratios and determine the most effective charge ratio for DNA binding and migration during electrophoresis. Figure 0.5-a top row shows gel electrophoresis of polyplexes prepared using the branched control (RGen3K), branching peptide with the targeting sequence (TGen3K) and the scrambles branched peptide (SGen3K). Figure 0.5-b also shows gel electrophoresis of lipopolyplexes prepared using the linear control with and without the targeting sequence, TK16 and K16.

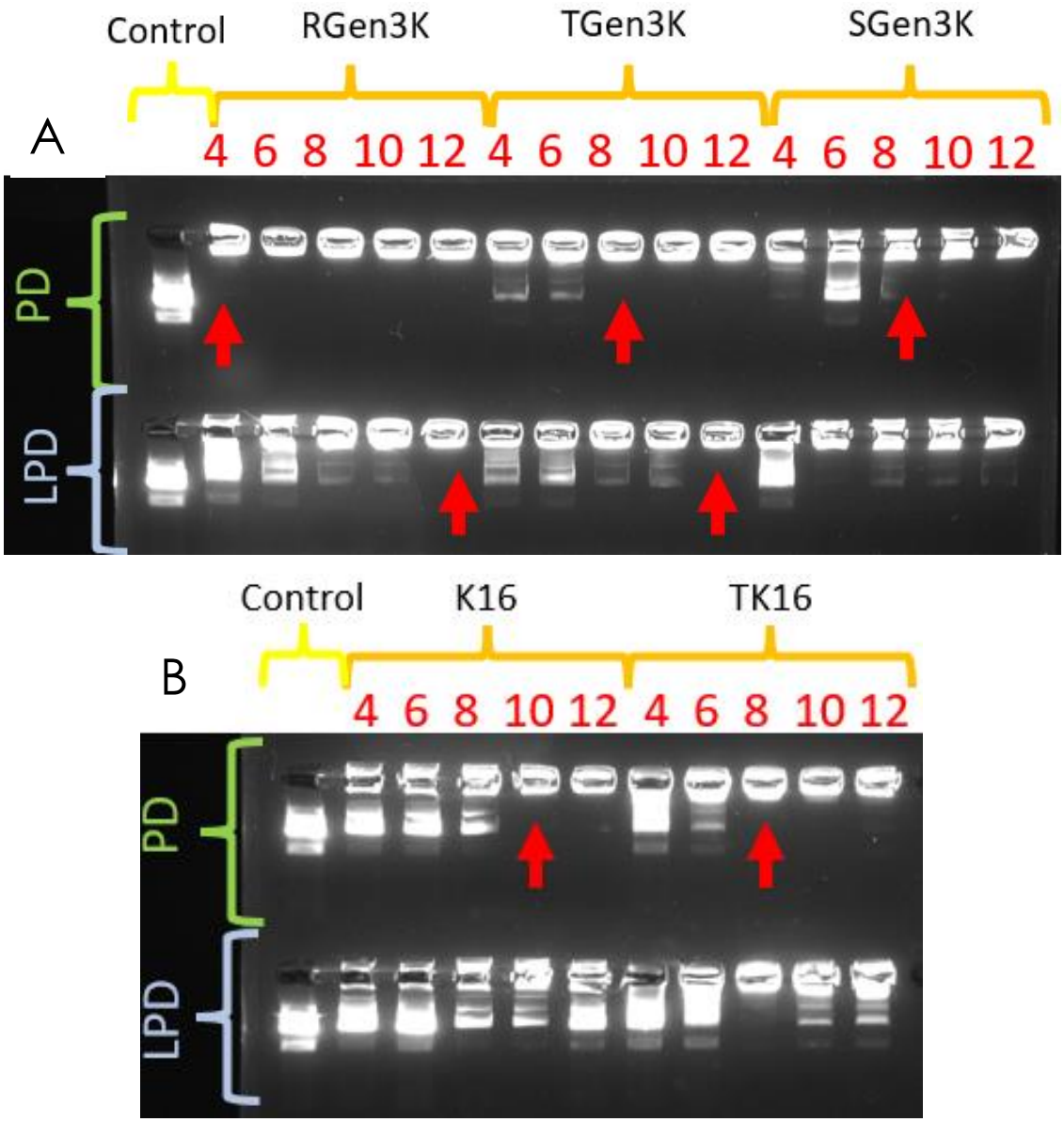

Figure 0.5 A) Polyplexes containing RGen3K and the targeting version TGen3K and SGen3K. On the second row same peptides complexed with lipids and DNA (LPDs). The lipopolyplex charge ratios used were 0.5:x:1 lipid:peptide:DNA with x being the ratio number displayed above to each peptide ratio. Red arrows indicate the smallest ratio at which there is complete DNA condensation. B) Gel Electrophoresis of polyplexes (PDs) prepared using the linear peptide with and without the targeting sequence (respectively K16 and TK16) on the top row. Below, lipopolyplexes (LPDs), thus linear peptides complexed with DNA.

In Figure 0.5-b, on the top row, the linear peptides without and with the targeting sequence, K16 and TK16, mixed with the nucleic acid (PDs) are shown. The results highlight that higher concentrations or ratios of linear peptides are needed to fully complex the DNA, while hyperbranched peptides (Figure 0.5-a, top row) are more efficient at condensing DNA (8-12 positive charges of linear peptides per negative charge of DNA were needed to fully condense the DNA as opposed to 4-8 charges of the branched peptides). Furthermore, the presence of a targeting sequence seemed to hinder DNA condensation (by 2 charge units) since higher ratios of branched targeting peptides were needed to fully condense the DNA. Moreover, RGen3K exhibits the most stable formation at any concentration. No migrated band can be observed. It is argued that the additional positive charge of arginine (R) may have a stabilising effect on the polyplex complex.

Linear peptides are unable to complex with DNA at any concentration in presence of lipids (Figure 0.5-b, second row). However, hyperbranched peptides RGen3K and TGen3K (Figure 0.5-a, second row) can form complexes at high concentrations. On the other hand, the peptide bearing the scrambled peptide (SGen3K) does not show any ability to retain the total amount of DNA, as indicated by the presence of faint bands at all ratios. However, it is important to note that the intensity of the bands differs between linear and hyperbranched peptides. Linear peptides exhibit very intense bands, while hyperbranched peptides show a much less intense signal of migrating bands. This implies that linear peptides are less effective at binding DNA, whereas hyperbranched peptides exhibit a more efficient complexation with the nucleic acid. This complexation could be advantageous for the *in vitro* release of DNA. It is crucial that DNA is bound to the peptide, but the formed bond should not be too strong to allow for its release into the cytoplasm.

In general, the difference in behaviour between linear peptides and hyperbranched ones is thought to lie in the flexibility of the vectors. In the case of dendritic structures, due to the proximity of the amino groups and the branching itself, the molecule is more rigid [284,]. On the other hand, linear peptides are more unconstrained and with reduced steric hindrance, thus more flexible. Branched molecules, with a more regular structure, can bind the negative charges of pDNA in a more efficient and consistent manner compared to linear ones. The multiple primary amine groups on the hyperbranched structure provide better opportunities for electrostatic interactions and complex formation with DNA, leading to enhanced binding capability compared to the linear structure [285].

In addition, when comparing LPDs (lipopolyplex delivery systems) and PDs (polyplex delivery systems) formulations, it is easy to notice a significant difference that can be attributed to the presence of lipids. Preparations where lipids are present (LPDs) show more bands compared to PDs. The helper lipid DOPE (Figure 0.6) is a zwitterionic molecule, meaning it has both a positive and a negative charge, resulting in a neutral net charge. However, despite its overall neutral charge, the presence of opposing charges can create a solvation shell around the molecule. The solvation shell can impact the formation of complexes between DOPE lipid and other molecules such as nucleic acids or peptides [308]. Interactions within the solvation shell can make it more difficult to form stable complexes or influence their dynamics.

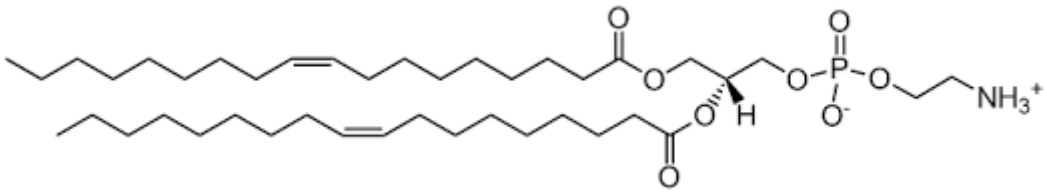

Figure 0.6 DOPE structure form Avanti Polar.

It appears that lipids weaken the binding between the vector and the nucleic acid, but this can be advantageous following the internalisation of the complex into the cell. The presence of lipids in LPDs may enhance the cellular uptake of the complex due to their ability to interact with cell membranes. While the weakened binding between the vector and nucleic acid can reduce the stability of the complex, thus facilitating the release of the nucleic acid payload within the intracellular environment. This is deemed to be beneficial as it allows for the efficient delivery of the genetic material to its target site and promotes gene expression. Therefore, the presence of lipids in LPDs can have both advantages and disadvantages, with the overall goal of achieving effective intracellular delivery of the nucleic acid payload.

The same experiment was also conducted without the loading buffer. The loading buffer is a substance used to facilitate the loading of the preparations into the wells and to visually track the migration of the bands, preventing sample loss [309].

In the absence of the loading buffer, loading the samples into the wells consistently and accurately is more challenging. However, in this work the loading of the samples in the wells without the loading buffer, was considered to provide information about the stability of the DNA/carrier

complexes that can be affected by the presence of anionic molecules in the loading buffer acting as potential competitors with the binding of the DNA. The potential drawback in performing the electrophoresis without the loading buffer is that its absence can make the final analysis of data more difficult to interpret.

Indeed, the loading buffer, composed of bromophenol blue and 4% sucrose in water, serves a specific purpose. The presence of the second molecule is particularly necessary to increase the density of the sample, thereby aiding its deposition into the well of the gel. Both bromophenol blue and sucrose are molecules containing hydroxyl and carboxyl groups. In solution, these molecules can acquire negative charges. The negative charges present in the loading buffer can potentially interfere with the interaction between nucleic acids and peptides, as they can compete for binding to the positive charges on the peptides, affecting the stability and efficiency of complex formation. Therefore, when analysing the interactions between nucleic acids and peptides, it is important to consider the presence of the loading buffer and its potential influence on the binding interactions.

In Figure 0.7, the results of the gel electrophoresis without the use of loading buffer are presented.

Similarly, the first lane the PDs, with RGen3K, TGen3K, and SGen3K peptides in the upper section. On the second line, LPDs with branched peptides. The charge ratios used for the PDs were 4:1, 6:1, 8:1, 10:1, and 12:1, with plasmid DNA. In Figure 0.7-b PDs linear peptides are shown, while linear LPDs on the second row LPDs. Ratios tested are the same as the branched peptides.

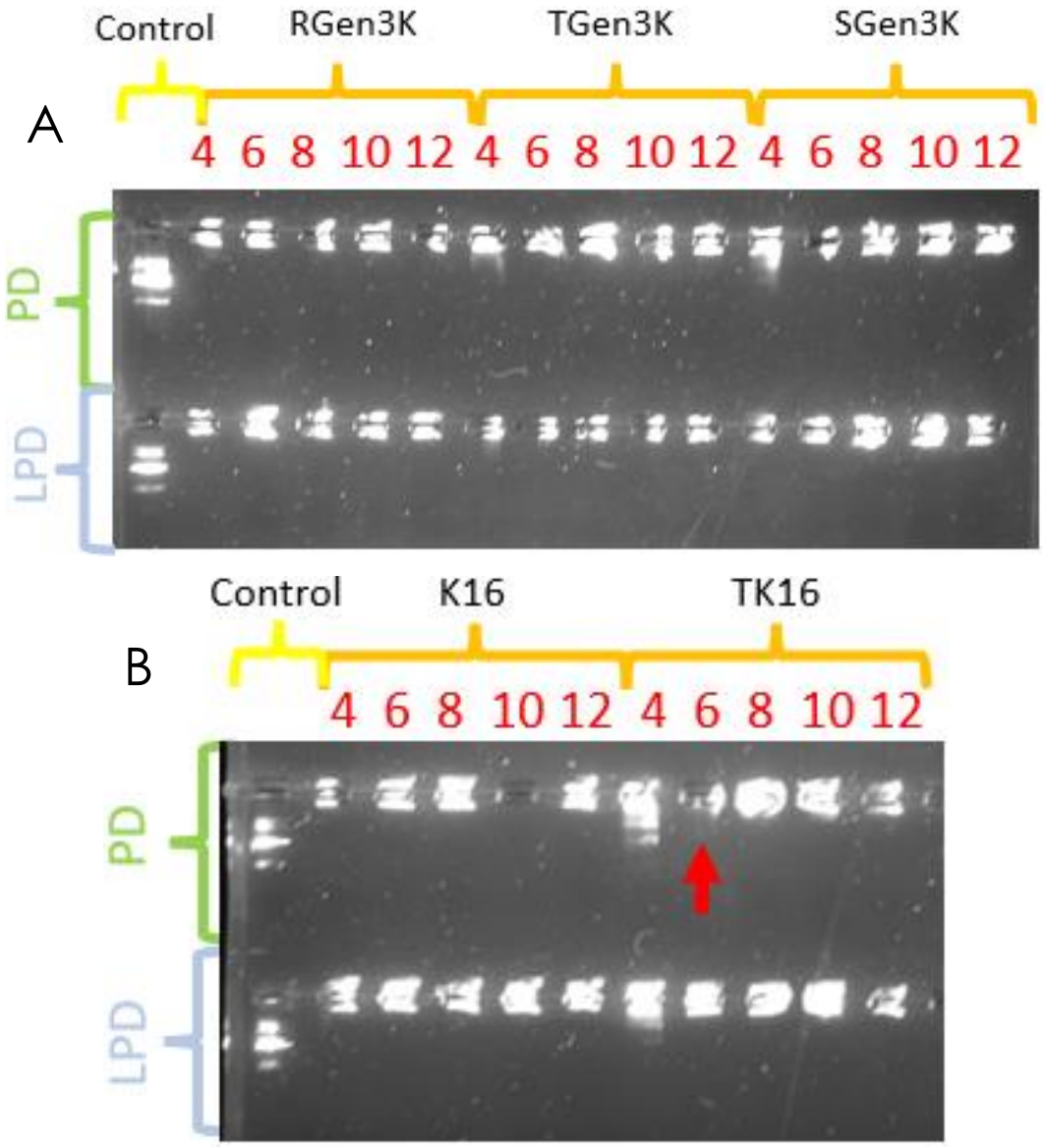

Figure 0.7 A) Gel electrophoresis of polyplexes (PDs) containing RGen3K and the targeting version TGen3K and SGen3K. On the second row same peptides complexed with lipids and DNA (LPDs). The lipopolyplex charge ratios used were 0.5:x:1 lipid:peptide:DNA with x being the ratio number displayed next to each peptide ratio. B) Gel Electrophoresis of polyplexes (PDs) prepared using the linear peptide with and without the targeting sequence (respectively K16 and TK16) on the top row. Below, lipopolyplexes (LPDs), thus linear peptides complexed with DNA. Red arrows indicate the smallest ratio at which there is complete DNA condensation.

From the agarose gel without the loading buffer, it is evident that it is significantly different from the gel shown in Figure 0.7, on the top lane, where lipid-free formulations (PDs) were considered, there are only a few bands present, indicating an increased binding affinity of the peptides to the nucleic acid. Similarly, the lipid-containing formulations show an increased binding strength to DNA, almost eliminating all bands and enhancing the stability of the complexes. However, the interference of the targeting sequence remains evident. As seen in the image, the sequence induces an increase of two units for complete complexation of the nucleic acid, both for linear peptides and hyperbranched peptides, with or without lipids. This implies that the loading buffer acts as a competitor for binding between the peptide and nucleic acid.

1.4.3 PicoGreen Assay

In this experiment, PicoGreen dye was used to conduct a fluorescent test to evaluate the complexation of LPDs and PDs complexes. PicoGreen is a fluorescent dye that binds to the base pairs of DNA molecules, emitting fluorescent light in the process. However, when cationic peptides are present, the PicoGreen reagent fails to attach to the DNA, leading to a decrease in the amount of fluorescent light emitted by the complex.

This technique provides valuable information about the efficiency and stability of the peptide:DNA complexes, which is crucial for the development of effective gene delivery systems and gene therapy applications.

Figure 0.8 shows the PicoGreen results that provide information about the complex formation without the possible artifacts created by the loading buffer and the electric current applied during the electrophoresis

experiments. The peptides tested were: RGen3K, TGen3K, SGen3K and the linear controls K16 and TK16. charge ratios were 4:1, 6:1, 8:1, 10:1, and 12:1, using calf thymus DNA. The experiment was also repeated with the lipopolyplex formulation . The same peptides were complexed with the lipid component and DNA, Figure 0.9, at the following charge ratios: 0.5:4:1, 0.5:6:1, 0.5:8:1, 0.5:10:1, and 0.5:12:1. As highlighted by both graphs (Figure 0.8 and Figure 0.9), a gradual decrease in fluorescence is noticeable both in the presence and absence of lipids. The displacement of PicoGreen by the cationic peptides indicates the condensation of nucleic acid within the LPD complexes.

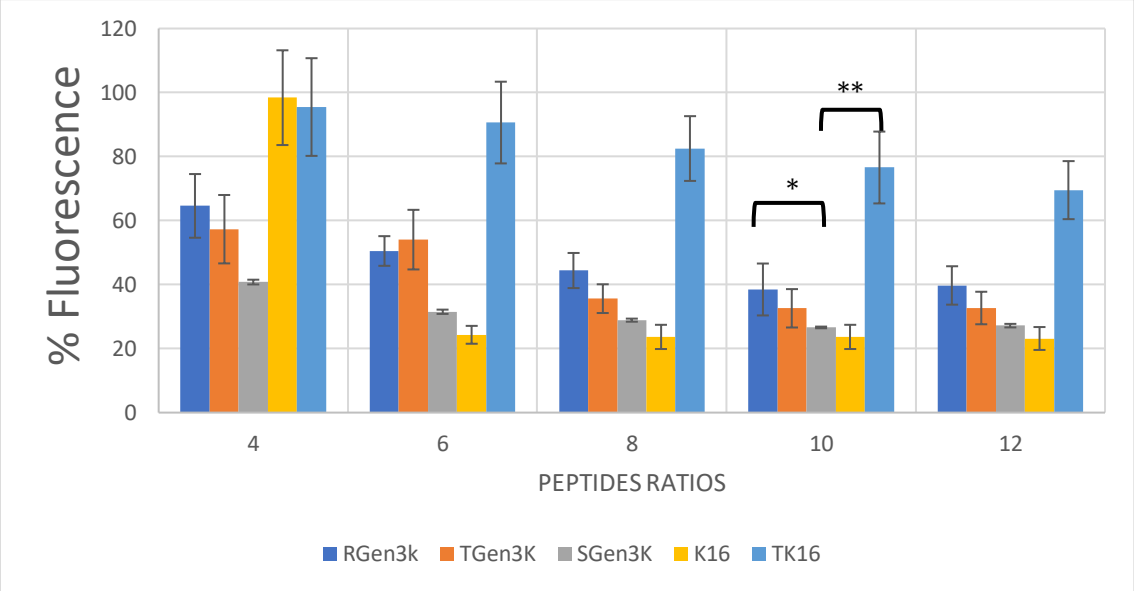

*Figure 0.8 PicoGreen analysis and fluorescence percentage of the peptide:DNA complexes. Peptides involved were: RGen3K, TGen3K, SGen3K and the linear K16 and TK16. The numbers on the X axis represent the lipid:peptide:DNA as 0.5:X:1 charge ratios. *****P<0.00001, ****P<0.0001, ***P<0.001, **P<0.01, *P<0.05 considering only the charge*

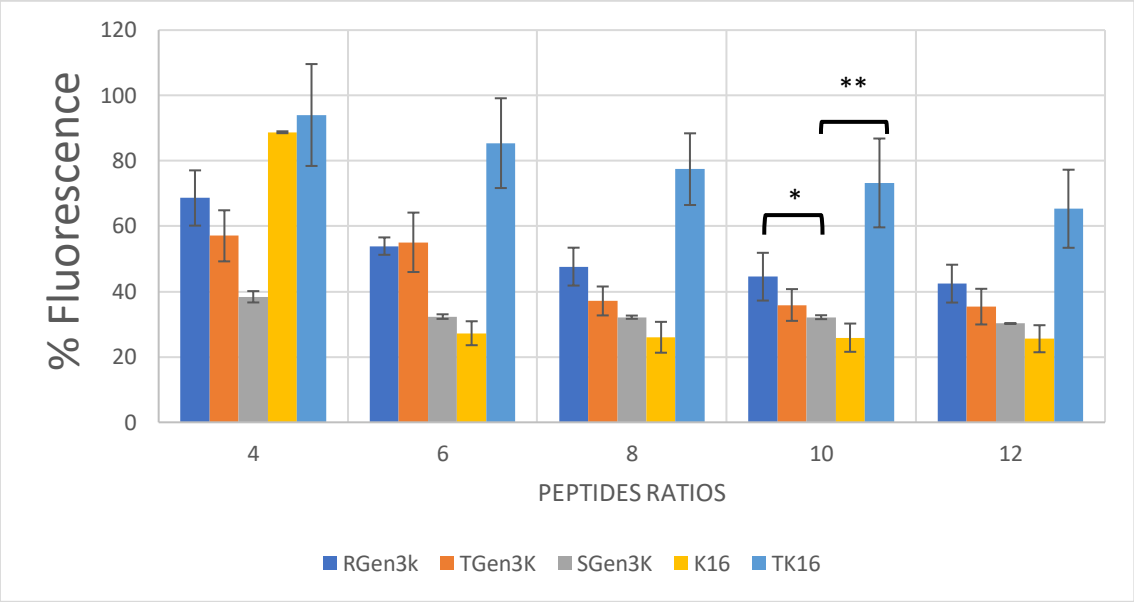

*Figure 0.9 PicoGreen analysis and fluorescence percentage of the lipid:peptides:DNA complexes. Peptides involved were: RGen3K, TGen3K, SGen3K and the linear K16 and TK16. The numbers on the X axis represent the lipid:peptide:DNA as 0.5:X:1 charge ratios. *****P<0.00001, ****P<0.0001, ***P<0.001, **P<0.01, *P<0.05 considering only the charge ratio x=10.*

As the charge ratio of the peptides increases, there is a reduction in emitted fluorescence until it reaches a plateau at 10:1 when the maximum complexation of nucleic acid with the vectors.

LPD complexes efficiently condense DNA as the charge ratio increases. However, beyond a certain point, further increasing the charge ratio of the cationic peptide does not significantly impact the packaging of DNA. This observation suggests that all the negative DNA molecules were already combined with the cationic peptide through electrostatic interactions at higher charge ratios, reaching a saturation point in the complexation process.

In both cases, with PDs and LPDs, the best condensation profile is observed with the linear peptide without the targeting sequence. This is evident as it exhibits the lowest percentage of fluorescence, indicating a higher level of complexation and tighter binding with the nucleic acid. Overall, the results of the PicoGreen experiments seem to confirm those of the gel electrophoresis when performed without loading buffer. The combination of the electrophoresis and PicoGreen experiments may also suggest that at relatively low ratios, not all the nucleic acid is complexed with the peptide, this being particularly true in the linear sequence bearing the targeting peptide sequence. This effect generated by the targeting sequence is somehow lost when the targeting sequence is integrated in a branched structure.

1.4.4 DNA Transfection Assay

Figure 4.8 shows the PicoGreen results that provide information about the complex formation without the possible artifacts created by the loading buffer and the electric current applied during the electrophoresis experiments. The peptides tested were: RGen3K, TGen3K, SGen3K and the linear controls K16 and TK16. charge ratios were 4:1, 6:1, 8:1, 10:1, and 12:1, using gWIZ-Luc plasmid DNA. The experiment was also repeated with the lipopolyplex formulation . The same peptides were complexed with the lipid component and DNA, Figure 0.10, at the following charge ratios: 0.5:4:1, 0.5:6:1, 0.5:8:1, 0.5:10:1, and 0.5:12:1.

However, since transfection or luminescence intensity is dependent on cell concentration, any toxicity induced by the vector would also affect the absolute luminescence reading, which is why the luminescence has to be normalised by the protein content, which is determined by a protein assay.

Peptides involved in the transfection test were the linear peptides with and without the targeting sequence (TK16 and K16) and the branched dendron (TGen3K) and the control (RGen3K). The first experiment was conducted on HER2 negative cells (MDA-MB-231) to compare the transfection efficiency of polyplexes (peptide:DNA complexes), prepared at 6:1 charge ratio with lipopolyplexes (containing the lipid DOTMA:DOPE 1 mg/mL, peptide and gWIZ-Luc plasmid DNA prepared at 0.5:6:1 charge ratio) together with comparison to a commercial vector lipofectamine 2000 (L2K).

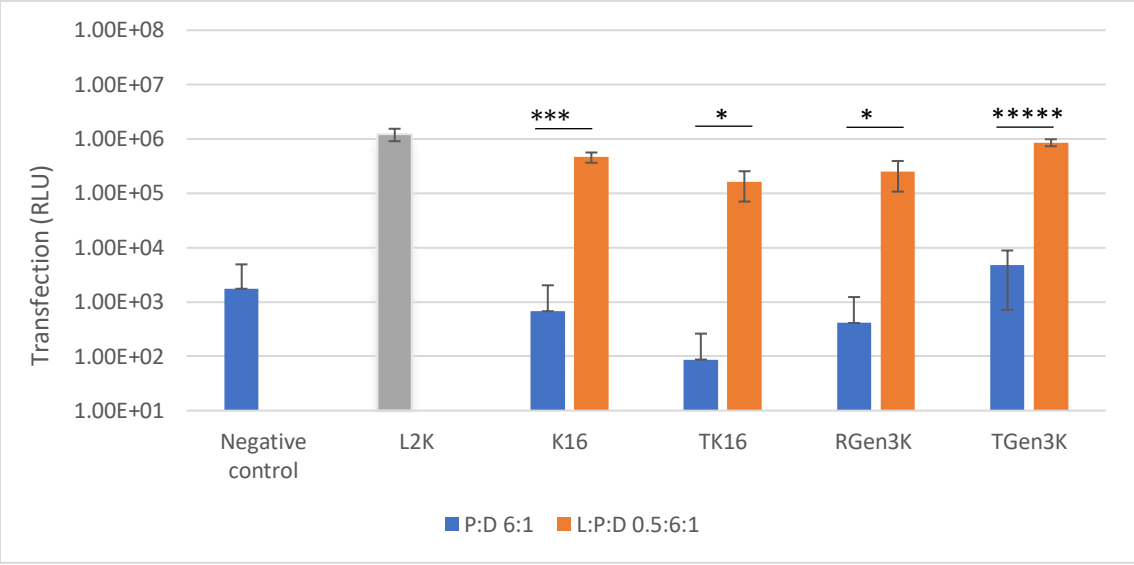

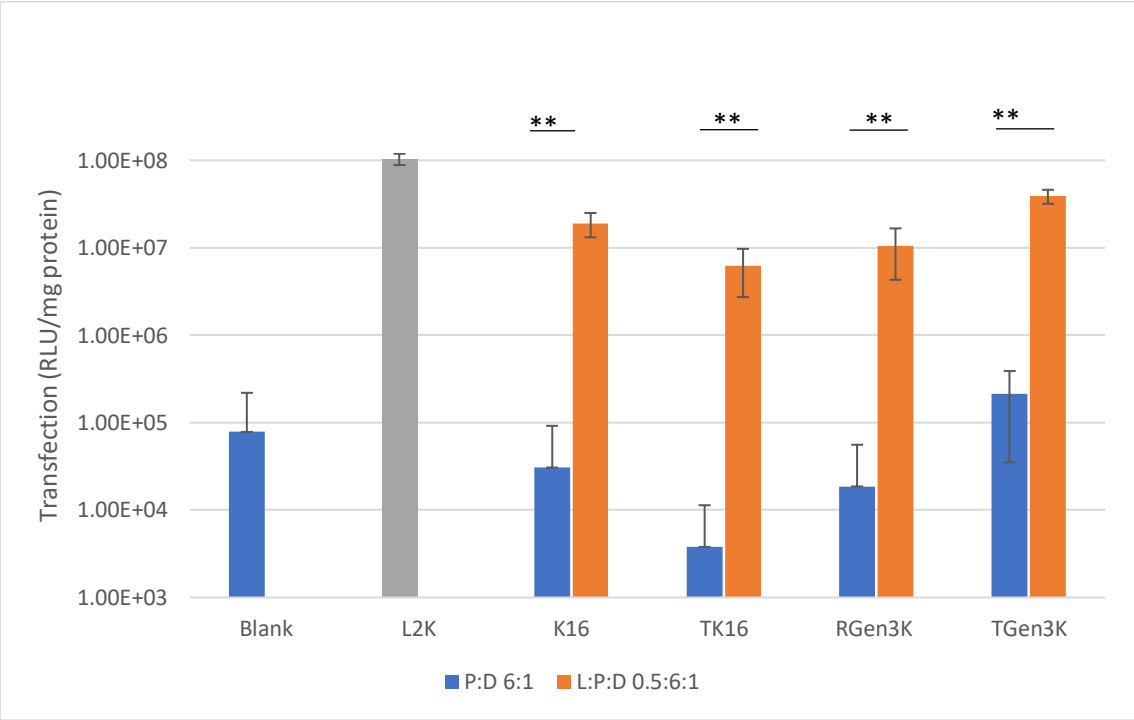

*Figure 0.10 Transfection of polyplexes (peptide:DNA complexes) at 6:1 charge ratio (blue bars) compared to lipopolyplexes (lipid:peptide:DNA) at 0.5:6:1 charge ratio (red bars) in MDA-MB-231 cells. Each sample was an average of n=4 repeats +/- SD. On top, the results before the normalisation. Below, the normalised results statistically analysed: *****P<0.00001, ****P<0.0001, ***P<0.001, **P<0.01, *P<0.05 considering only the charge ratio x=10.*

Figure 0.10 shows the transfection efficiency of polyplexes and the lipopolyplexes. It's obvious that in the absence of the lipid component the peptide:DNA complexes show comparable or even less than the negative control so effectively it is no transfection (~1000-fold lower than lipopolyplexes, as the Y-axis is a log scale), possibly due to lack of endosomal release which is usually facilitated by the lipid component in the lipopolyplex.

Poor transfection of polyplex is likely due to strong interaction and stability of the complex that is formed when the DNA is complexed by dendrons alone [310]. In addition, as suggested by studies of Mahesh et al. [311] peptide:DNA complexes are unable to buffer acidification and escape the hostile endosomal environment efficiently over time to avoid enzymatic degradation of lysosomes [126]. The poor ability of endosomal escape is due to the absence of amino acids with a pKa ~5-7 that weakens the effect "Proton sponge" therefore the endosome is not subject to the heavy variation of pH that causes the lysis. Intracellular studies by Kudsiova et al. [287] state that complexes composed of both lipid and peptide facilitate the release of DNA within the nucleus. It has been dismissed that lipids help DNA release from endosome as the lipid fraction is likely to remain bound to the endosomal membrane, while the peptide then facilitates nuclear import as it is detected with the DNA in the nucleus [312].

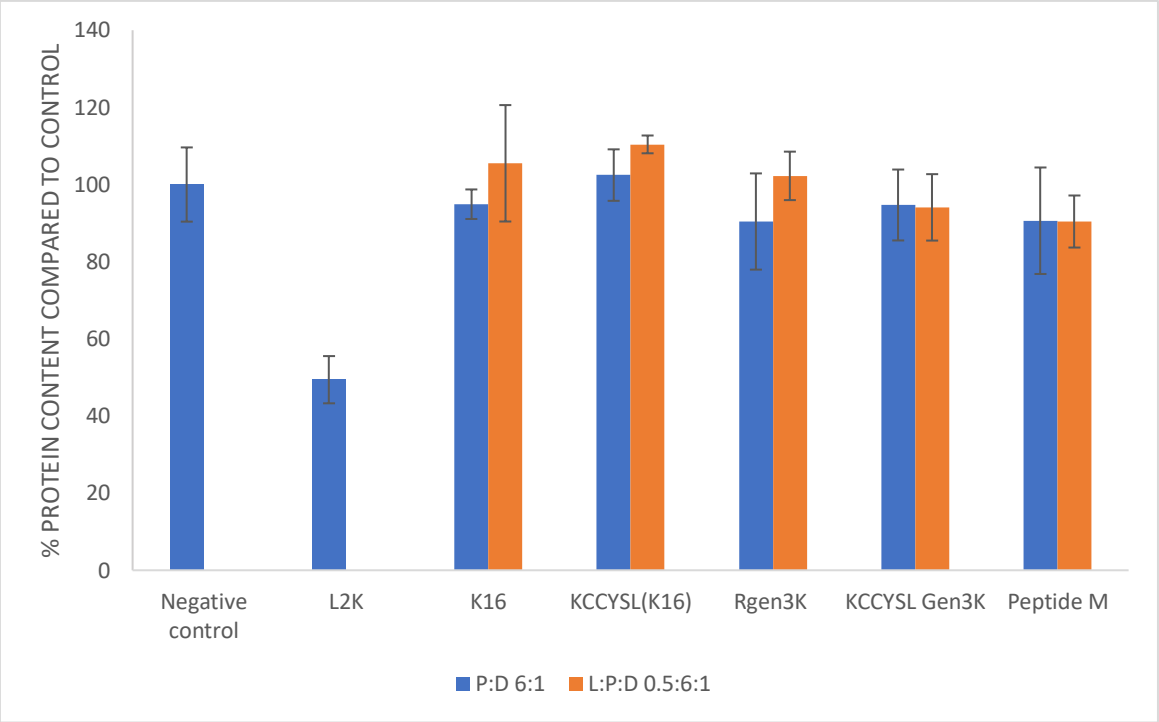

*Figure 0.11 Protein content of polyplexes (peptide:DNA complexes) at 6:1 charge ratio (green bars) compared to lipopolyplexes (lipid:peptide:DNA) at 0.5:6:1 charge ratio (blue bars) in MDA-MB-231 cells. Each sample was an average of n=4 repeats +/- SD. *****P<0.0001, ****P<0.0001, ***P<0.001, **P<0.01, *P<0.05.*

DOPE (dioleoylphosphatidylethanolamine) is often included in cationic lipid mixtures as a so-called "lipid helper", since, in almost all systems formed by cationic lipids, DOPE inclusion has been shown to increase *in vitro* transfection efficiency [313]. The neutral lipid DOPE at approximately pH 9.0 is negatively charged and adopts a lamellar phase but, at pH close to neutrality or acidic pH [314], which is generated during endosomal maturation, the lipid becomes a zwitterion and undergoes a transition from the lamellar phase to the inverse hexagonal phase (not lamellar). This phase, in essence, destabilises the bilayer. The adoption of this phase appears to be an important step in the mechanism by which the genetic material, after the internalisation of the lipid complex exits the endocytic

vesicles and passes into the cytosol for subsequent internalisation into the cell nucleus [315,316].

The protein content shown in Figure 0.11, suggests that the cell viability is high since all the samples, with the exception of the L2K showed protein content which was higher than 90%, which highlights the safety of the peptides used in relation to the commercially available reagent L2K which showed significant toxicity. As expected from cells not expressing the receptors, there was no difference between the control dendrimer and the ones presenting the peptide sequence able to recognise the receptor HER2.

Afterwards, lipopolyplexes containing the non-targeting peptide RGen3K, the targeting TGen3K and SGen3K were tested and compared with the linear controls (K16 and TK16) at increasing peptide ratios in both cells lines: MDA-MB-231 which are HER2 negative breast cancer cells; and SKBR3 that are HER2 positive cells and overexpress the receptor on the surface.

Figure 0.12 represents the transfection in MDA-MB-231 cells, which shows that there is a gradual increase in transfection with increasing the peptide ratio within the lipopolyplex particularly between 0.5:4:1 and 0.5:10:1 lipid:peptide:DNA charge ratios.

Interestingly, it is observed a difference between the non-targeting hyperbranched peptide and the targeting dendrons since the MDA-MB-231 cell line lacks HER2 receptors.

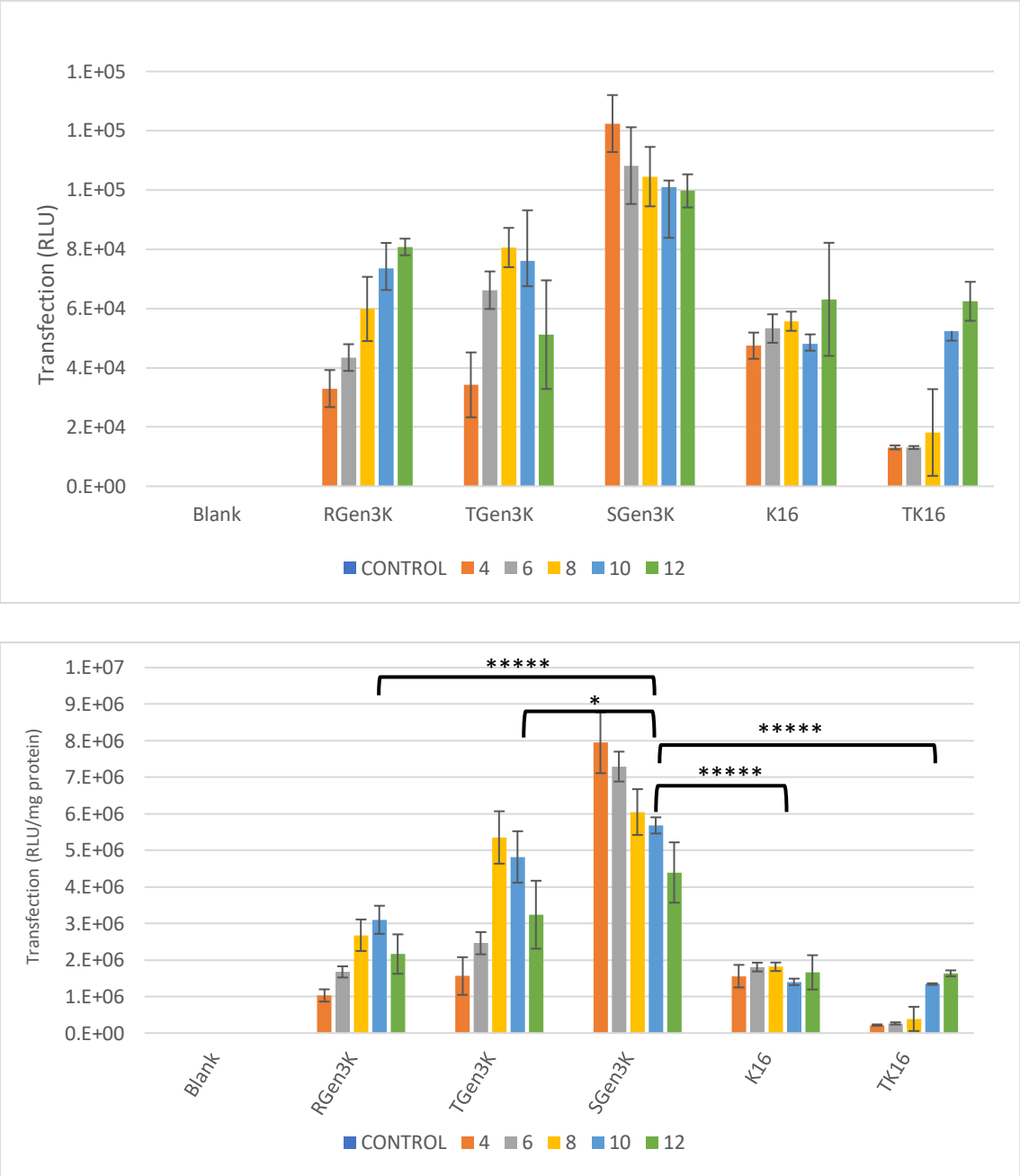

*Figure 0.12 Transfection of RGen3K, TGen3K, SGen3K, K16 and TK16 lipopolyplexes (peptide:DNA complexes) at 0.5:X:1 charge ratio (4,6,8,10 and 12) in MDA-MB-231 cells. On the top the non-normalised results, on the bottom the normalised results with the mg protein. Each sample was an average of n=4 repeats +/- SD. Each sample was an average of n=4 repeats +/- SD. Normalised results were statistically analysed *****P<0.00001, ****P<0.0001, ***P<0.001, **P<0.01, *P<0.05 considering only the charge ratio x=10.*

It can be noticed that the non-targeting peptide has lower transfection capability compared to TGen3K and SGen3K. However, the scrambled peptide allows for high DNA internalisation, especially at very low charge ratios. In general, hyperbranched peptides are much more efficient in internalisation compared to linear peptides. This is also evident in the agarose gel electrophoresis (Figure 0.5) where linear peptides demonstrated limited ability to form stable complexes, resulting in DNA release and migration along the agarose gel. The difference can be explained by the number of protonated primary amines present on the surfaces and by the flexibility of the molecule. As a result, the disorder of the more flexible linear molecules can lead to inefficient shielding of positive charges, thus it becomes more challenging to form stable complexes with the large nucleic acid molecules [317].

Therefore, the best configuration that hyperbranched peptides assume positively conditions DNA internalisation. SGen3K seems to induce the optimal conformation of the complex by maximising the positive charges that form an electrochemical bond with the pDNA molecule. Meanwhile, linear peptides, due to their non-regular conformation caused by flexibility, lack a sufficient number of charges bound to pDNA. This is further accentuated by the presence of the lipid solvation shell. Consequently, they do not provide adequate transfection, as also justified by the electrophoresis gel in Figure 0.5 a-b.

Transfection experiments in SKBR3 cells, Figure 0.12, which are HER2 positive, show that high transfection is observed in lipopolyplexes containing the targeting peptide TGen3K at all ratios tested (even the lowest 0.5:4:1 ratio), while lipopolyplexes containing the non-targeting peptide RGen3K show a gradual increase in transfection with increasing peptide ratios, a similar behaviour observed in the MDA-MB-231 cells (Figure 0.13).

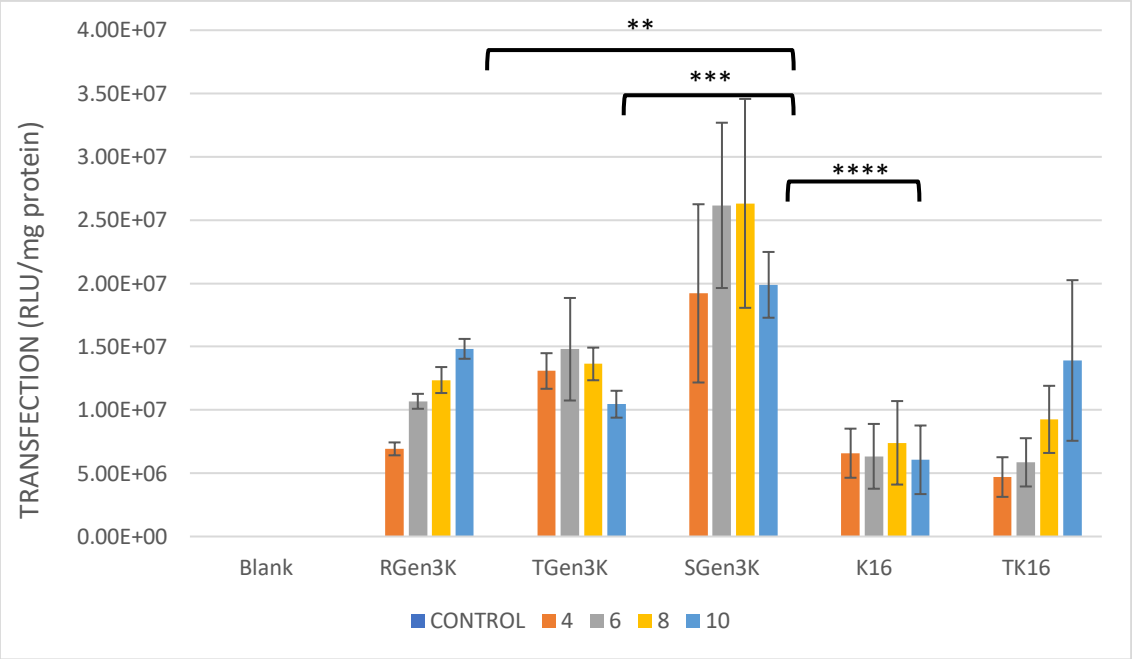

*Figure 0.13 Transfection of RGen3K, TGen3K, SGen3K, K16 and TK16 lipopolyplexes (peptide:DNA complexes) at 0.5:X:1 charge ratio (4,6,8 and 10) in SKBR3 cells. Results are normalised with the mg protein and statistically analysed *****P<00001, ****P<0.0001, ***P<0.001, **P<0.01, *P<0.05 considering only the charge ratio x=10.*

This indicates that, although non-targeted internalisation is being exploited due to the good activity of the non-targeting peptides as well, the targeting sequence does improve transfection efficiency, by interacting with the HER2 receptors, allowing for lower concentrations to work as effectively as higher ones, and, as a consequence, it is possible to reduce the concentration of the peptides within the lipopolyplex, which would presumably cause less toxicity and side effects. The unexpected selectivity of the scramble sequence is probably due to the "CCY" (Cys-Cys-Tyr) residues in the oxidised state are able to mimic the structure of ErbB ligands with an EGF-like domain [318]. In addition, RGen3K reach a similar transfection rate to the TGen3K increasing the concentration of lipid:peptide:DNA. As Rewatkar PV et al. [319] stated that peptides use caveola-mediated endocytosis as their entry mechanism and are dose

dependent. Caveolae-mediated endocytosis allows the internalisation of material through invaginations of the plasma membrane, in areas rich in cholesterol and sphingolipids, shaped like little caves called caveolae. In fact, the caveolae are coated with caveolin, a dimeric protein that binds cholesterol thereby inserting itself into the plasma membrane. Then, endocytosis is mediated by dynamin and by actinic microfilaments. Once formed, the caveolae pour the material contained in them into the caveosome, which differ from endosomes in both pH and enzymatic content. From the caveosome the endocytosed material is then sorted, through transport vesicles, or to the Golgi or the wrinkled endoplasmic reticulum, where it is modified by the enzymes contained in them [320].

However, the presence of lipids within the carrier may interfere with the secondary internalisation mechanism. According to Friend et al. [321], lipoplexes (lipid:DNA) have a preferential internalisation route through the clathrin-mediated endocytosis. The ligand binding receptor induces the activation of clathrin molecules that distort the cell membrane forming a curved structure to form a vesicle that is then released into the cytoplasm. Here, the clathrin molecules are disassembled and recycled, while the vesicle will be degraded by lysosomes.

Nevertheless, the secondary internalisation mechanism for lipopolyplexes with both lipid and peptide components is still unclear.

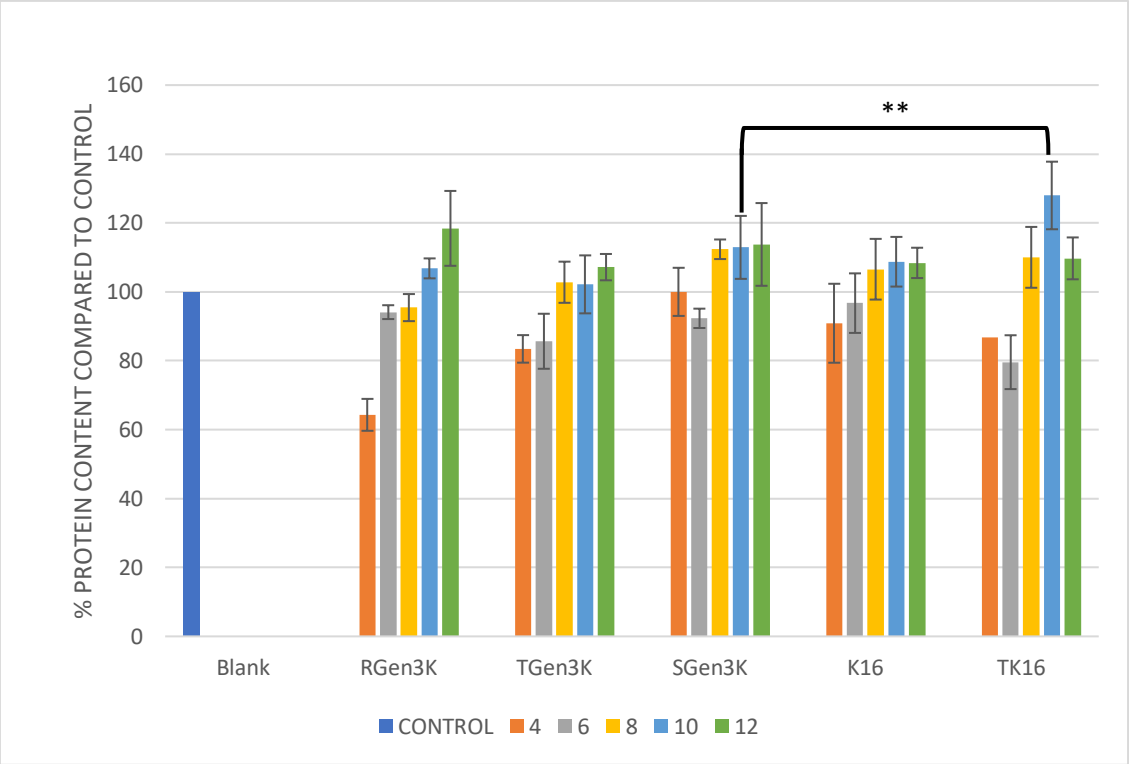

*Figure 0.14 Protein content of RGen3K, TGen3K, SGen3K, K16 and TK16 lipopolyplexes (peptide:DNA complexes) at 0.5:X:1 charge ratio where X is: 4, 6, 8, 10 and 12 in MDA-MB-231 cells. Each sample was an average of n=4 repeats +/- SD. Each sample was an average o f n=4 repeats +/- SD. *****P<0.00001, ****P<0.0001, ***P<0.001, **P<0.01, *P<0.05 considering only the charge ratio x=10.*

The peptide TGen3K demonstrated the highest internalisation rate at charge levels of 8 and 10, which was also predicted by the PicoGreen results, where the lowest fluorescence value was observed at a charge level of 8. However, despite the TGen3K peptide having a specific target sequence for the HER2 receptor, it did not exhibit the highest efficiency in cell transfection. This result was surpassed by the dendrimers bearing the scrambled peptide which showed significantly higher values compared to all the other tested peptides. Even the SGen3K peptide reached its peak transfection efficiency at charge levels of 6 and 8, and it already

displayed the lowest internalisation percentage at a charge level of 6 in the PicoGreen test.

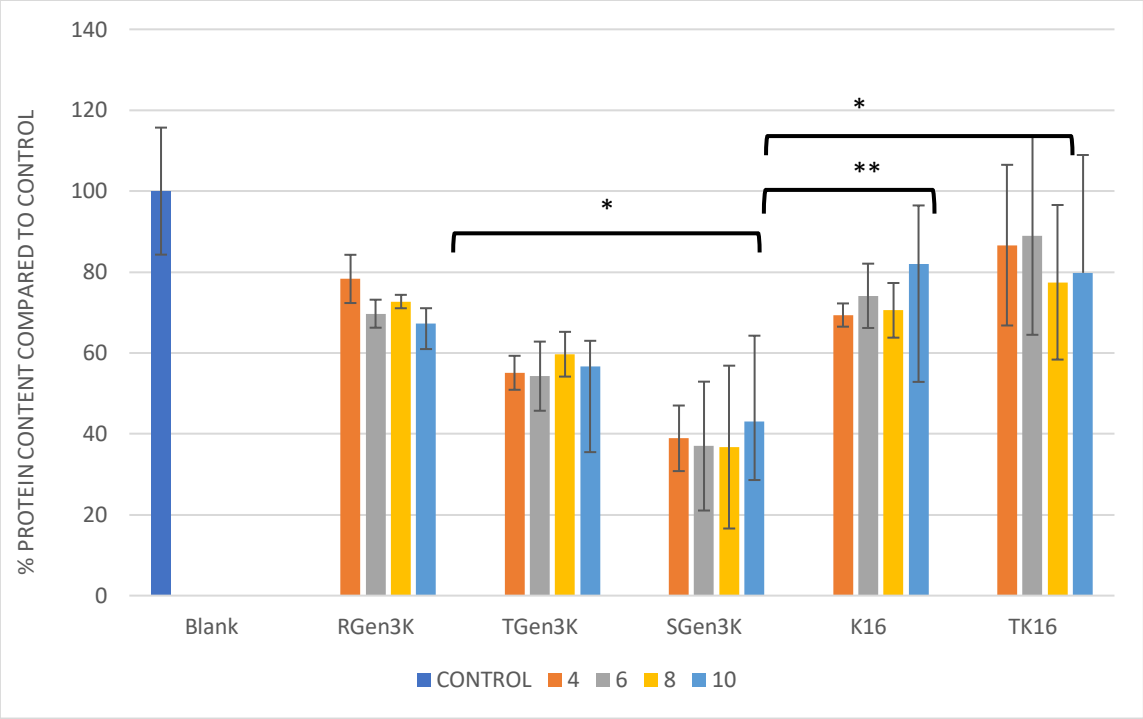

*Figure 0.15 Protein content of RGen3K, TGen3K, SGen3K, K16 and TK16 lipopolyplexes (peptide:DNA complexes) at 0.5:X:1 charge ratio where X is: 4, 6, 8, 10 and 12 in SKBR3 cells. Each sample was an average of n=4 repeats +/- SD. Each sample was an average of n=4 repeats +/- SD. *****P<0.00001, ****P<0.0001, ***P<0.001, **P<0.01, *P<0.05 considering only the charge ratio x=10.*

It is possible that the spatial arrangement of SGen3K is more favourable for binding with DNA and confers a better packaging of the nucleic acid molecule compared to the sequence of TGen3K.

Figure 0.14 and Figure 0.15 show that the lipopolyplexes at all the ratios tested (from 0.5:4:1 to 0.5:12:1) have high protein content (above 60% in all samples) which suggests good viability and limited toxicity in both cell lines tested.

1.5 CONCLUSION

In this chapter, results from the characterisation analysis of LPD complexes were reported. It was crucial to determine the interaction occurring between the peptide molecules and the DNA. From the dimensional results, it became evident that linear peptides form smaller complexes compared to their branched counterparts. However, regardless of the peptide chosen, the uniformity remains quite similar.

The analyses of the binding strength with DNA revealed that the peptide concentration is critical for the formation of stable complexes. Moreover, branched peptides were found to be more effective even at lower concentrations compared to linear peptides. As in the case of size analyses, the structure and, most importantly, the flexibility of both the peptides and DNA appear to be crucial factors.

Lastly, the presence of lipids can significantly influence the stability of the formed complex, which, in turn, reflects on transfection efficiency. In fact, the analysis on cells revealed valuable information about the biological activity of dendrons. The DNA delivery vectors need a small amount of DOTMA:DOPE lipid to ensure a good transfection efficiency, thought to be facilitated by the enhanced escape of DNA from endosomes which is essential for good transfection efficiency.

Moreover, the targeting sequence was shown to recognise the HER2 receptors. It is believed that the structure -CCY- when oxidised is similar to the Trastuzumab scaffold able to bind the HER2 protein. This implies that hyperbranched vectors with the targeting sequence are more selective towards HER2 positive cells and lower concentration of peptide within the lipopolyplex are needed to result in the same transfection efficiency.

In addition, the improved transfection activity of the scramble sequence (SGen3K) compared to all other peptides highlights how similar sequences

can influence the DNA binding ability, packaging, and release within the cell. Even minor differences in the arrangement of the six amino acids can be crucial for nucleic acid delivery.

As can be observed, the scramble sequence CSCYSK- appears to exhibit greater selectivity towards the HER2 receptor compared to the hexapeptide sequence linked to the hyperbranched structure LSYCCK-. This difference is likely attributed to the spatial arrangement of amino acids, favouring the scramble sequence in terms of DNA packaging and transfection efficiency.

The ability of a peptide to efficiently deliver nucleic acids into cells is of significant importance in various fields of research and biotechnology. Different sequences of peptides can have varying affinities for nucleic acids and other cellular components, affecting their overall efficiency in delivering genetic material. Minor changes in the amino acid composition or spatial arrangement can significantly impact the interaction of the peptide with DNA and its ability to facilitate cellular uptake and intracellular release. Understanding these nuances in peptide-DNA interactions is crucial for developing effective gene delivery systems for gene therapy, genetic engineering, and other applications in biomedicine.

However, despite DNA and RNA being remarkably similar molecules, they can exhibit significantly different behaviour when conjugated to lipid-peptide-based nanoparticles. As described by et al. [322], nucleic acids can respond differently based on their number of charges and their size, which can influence their flexibility and packaging within the complex formation. Moreover, in comparison to traditional pharmaceuticals directed at proteins and those based on DNA, RNA-based therapies hold promise because of their unique physicochemical and physiological attributes. RNA plays a crucial role among the three fundamental biological

macromolecules: DNA, RNA, and proteins. RNA molecules like ASOs, small interfering RNA (siRNAs), and microRNAs (miRNAs) possess the ability to recognise mRNAs and noncoding RNAs (ncRNAs) through Watson–Crick base-pairing [323]. Consequently, RNA has the theoretical capacity to target any gene of interest by binding the correct nucleotide sequence on the target RNA [324].

siRNA Delivery Formulation, Characterisation And Biological Testing

1.1 INTRODUCTION

According to the FDA "Human gene therapy seeks to modify or manipulate the expression of a gene or to alter the biological properties of living cells for therapeutic use". Small fragments of nucleic acids such as siRNA (small interfering RNA) are promising molecules that can correct mutations accumulated in the genome [325]. Indeed, the activity of siRNAs involves binding to the target mRNA through precise base pairing and subsequently inducing the degradation of the overexpressed molecule. In contrast to other drugs, the advantage of siRNAs lies in the ability to pair Watson-Crick bases with mRNA, whereas biological molecules such as monoclonal antibodies, which bind proteins, must recognise a complex and often difficult to identify spatial combination [325]. siRNAs are molecules that, thanks to their biological mechanism, are used by the cell to protect its genetic code from external invasions. Nowadays, they are studied for their therapeutic potential in controlling gene expression; increasing it, in the case of onco-suppressors, or decreasing it to correct the activity of oncogenes. Hence, due to its extremely high selectivity resulting from the perfect base pairing between siRNA and mRNA, it could be a straightforward solution for the treatment of many diseases that lack an easily identifiable target or for pharmaceutical molecules that struggle to reach the target. Despite siRNA silencing being considered a promising therapeutic approach, it has limitations that hinder its full exploitation.

Unmodified (naked) siRNAs suffer from poor stability in extracellular environments due to the presence of the host's endonucleases or exonucleases that degrade nucleic acids, reducing its concentration at

the target tissue. Additionally, due to its small size, it is easily eliminated through the renal pathway. Moreover, its substantial negative charge prevents it from efficiently passing through the phospholipidic double layer of the cellular barrier [326]. For this reason, encapsulating siRNA within gene delivery vectors, which can vary in nature, becomes a necessity. New and improved formulations are being studied to achieve the best results in terms of gene silencing while minimising the toxicity induced by these formulations. [327].

So far, FDA has approved four siRNA-containing products: Patisiran, Givosiran, Lumasiran, and Inclisiran. Patisiran was the first nucleic acid to be approved by the FDA in 2018. It is indicated for hereditary transthyretin amyloidosis-related polyneuropathy and aims to reduce the transcription of the mRNA encoding for transthyretin. [328,329].

Givosiran, approved in 2019, is recommended for adults with acute hepatic porphyria. It induces the degradation of amino levulinate synthase 1 (ALAS1) mRNA, leading to a subsequent reduction in aminolaevulinic acid and porphobilinogen (PGB) [330,331].

The third siRNA in chronological order is Lumasiran, which targets hydroxy acid oxidase 1 (HAO1) mRNA. It is indicated for the paediatric treatment of primary hyperoxaluria type 1 (PH1) [165].

Finally, Inclisiran, through the degradation of PCSK9, increases the uptake of LDL-C and thus has a protective effect in patients with familial hypercholesterolemia or atherosclerotic cardiovascular diseases [332] (Clinical Atherosclerotic Cardiovascular Disease, ASCVD). Another eight siRNA-containing therapies are awaiting approval, and of these, five are being tested for cancer treatment. As mentioned earlier, siRNA requires protection to reach the cytoplasm and form a complex with mRNA for

subsequent degradation. Even in the case of commercially available siRNAs, two different solutions have been employed.

The first and most widely used solution is the combination of the nucleic acid with GalNAc (N-acetylgalactosamine), which selectively binds to the Asialoglycoprotein receptor (ASGPR) in the liver, facilitating clathrin-mediated endocytosis of the complex [333]. When the pH within the endosome drops, ASGPR is recycled by the cell and brought back to the cell surface, while GalNAc is cleaved from the siRNA. The siRNA itself remains mostly trapped in the endosomal vesicle lumen. The mechanism allowing the siRNA to escape endosomal degradation is still unknown. The process of endosomal escape is not yet fully understood, but it enables achieving a high concentration of siRNA in the cytoplasm [334].

The second method of delivery involves using LNPs (Lipid Nanoparticles) composed of DLin-MC3-DMA and PEG2000-C-D MG, DSPC, and Cholesterol. DLin-MC3-DMA is a lipid referred to as "fusogenic," meaning it can destabilise the endosomal membrane when the pH becomes acidic, thus releasing the ribonucleic material into the cytoplasm. Meanwhile, DSPC and cholesterol stabilise the lipid structure [335].

These solutions are just the beginning of future ribonucleic acid-based drugs, but there are several studies also highlighting peptide-based structures for siRNA delivery [299,336]. PLL (Poly-L-lysine) are molecules primarily composed of lysine residues, an amino acid that can be recycled within the cell. Lysine has an amino group in the alpha position to the carboxyl group and a second amino group in the epsilon position in the side chain. However, modifications to the structure or amino acids are common. The amino acid residues most commonly added to the basic lysine structure are arginine and histidine. Both amino acids have an aliphatic structure with amino groups that can be protonated, enhancing nucleic acid internalisation and promoting endosomal escape. Additionally, the

guanidine group of arginine seems to have a high affinity for the phosphate groups of nucleic acids, allowing for more efficient siRNA or DNA complexation [337]. Meanwhile, the imidazoline group of histidine can increase the number of positive charges and also facilitate the release of the nucleotide molecule depending on pH variations. This is due to the imidazole group, which can carry either a neutral or a positive charge depending on the surrounding environment's pH [209]. Not always, however, these modifications can bring benefit to intracellular delivery. Firstly, the increase in positive charges induced by the presence of arginine or histidine leads to a consequent permeabilisation of the cell membrane, hence an increase in toxicity. Secondly, the addition of arginine residues to the internal structure can reduce peptide flexibility and thus affect siRNA condensation, a molecule equally rigid [338]. Variations in transfection results are not solely due to the vector, but the choice of nucleic acid can be equally important for the final outcome. In fact, as reported by Gorzkiewicz et al. [209] and Ali Alazzo et al. [338], PLLs exhibit different behaviours when interacting with plasmid DNA or siRNA. The rigidity of the system increases as the size of the nucleotide chain decreases and delivering DNA with up to 2000 bp or siRNA with 19-23 bp is extremely different. Consequently, achieving proper siRNA packaging becomes more challenging. It is therefore important to design the transfection vector by considering various factors, including the chosen nucleic acid for gene editing.

1.2 AIM OF THE CHAPTER

In this chapter, the investigation focused on formulating the hyperbranched dendrons into polyplexes and lipopolyplexes with siRNA and testing their ability to bind siRNA. Since, as reported in other studies as well, there are substantial differences between the delivery of DNA and

siRNA, the behaviour of hyperbranched and linear peptides has been compared in the presence of siRNA. Gel electrophoresis was employed to study their binding capacity, and *in vitro* transfection efficiency and cellular toxicity were tested in the two cell lines studied in Chapter 4: one expressing HER2 receptors (SKBR3) and another devoid of them (MDA-MB-231). Additionally, the aim of the *in vitro* experiments was to assess the selectivity of target sequences. The hypothesis suggested that in MDA-MB-231 cells, the internalisation of peptide vectors would be similar for both the branched structure with the hexapeptide (TGen3K) and the control vector (RGen3K). Conversely, in SKBR3 cells that overexpress the HER2 receptor, the activity of TGen3K would be significantly higher than that of the control dendron due to the presence of the target sequence. The effectiveness of vector internalisation will result in a decrease in cell migration capacity.

The siRNA used in this study was TRPM8 that interfere with the synthesis of an ion channel that regulates calcium homeostasis within the cell thus leading to the inhibition of both tumoral cell proliferation and migration, two fundamental processes in the increase of the tumoral mass and liberation of metastases. Indeed, the effects of the various carriers and of the siRNA linked to it were assessed in terms of the reported ability of these two type of cells to either proliferate or aggregate [339].

1.3 MATERIALS AND METHODS

1.3.1 Sample Preparation

LPR complexes were generated using RGen3K, and TGen3K, K16 and TK16, varying charge ratios, specifically, 0.5:4:1, 0.5:6:1, 0.5:8:1, 0.5:10:1, and 0.5:12:1, respectively. Each sample was prepared with a final volume of 50 µL and contained 0.1 µg of TRPM8 siRNA (ThermoFisher). The LPRs were

prepared as previously described in Chapter 4.3.3, resulting in a total sample volume of 50 µL, composed of 12.5 µL of lipid stock solution, 12.5 µL of the total peptide solution, and 25 µL of RNA stock solution. Analysis were conducted as reported in Section 4.3.4.

1.3.2 Gel Electrophoresis

The electrophoresis gel was prepared as reported in Section 4.3.5 and placed in the electrophoresis tray. The samples analysed consisted of RGen3K, TGen3K, SGen3K, and the linear controls K16 and T(K16), synthesised according to the method described in Section 2.3.1. Polyplexes were prepared with a consistent RNA concentration per well (0.1 µg) and charge ratios of 4:1, 6:1, 8:1, 10:1, and 12:1.

The lipopolyplex samples were prepared by mixing equal volumes of lipid and peptide, followed by the addition of an equal volume of siRNA to the lipid-peptide mixture. The final siRNA concentration in each well was 0.1 µg in a volume of 10 µL. The lipid:peptide:siRNA ratios tested were 0.5:4:1, 0.5:6:1, 0.5:8:1, 0.5:10:1, and 0.5:12:1, with the lipids (DOTMA:DOPE 1 mg/mL stock) and siRNA proportion kept constant while varying the amount of peptides. The detailed preparations can be found in the Section 4.3.3.

The PRs and LPRs were prepared in two ways: some samples were loaded onto the agarose gel without the addition of loading buffer as reported in Section 4.3.5. To ensure that all siRNA was effectively loaded onto the agarose gel and achieve the best possible outcome, few precautions were followed:

1. Ensuring precise placement of the pipette within the well.
2. Allowing a few seconds after releasing the sample.

3. Conducting duplicate experiments, which produced highly similar gel results.
4. Additionally, there are faintly illuminated wells when the complex does not migrate.

1.3.3 Picogreen assay

The Picogreen analysis was conducted by preparing the polyplexes and lipopolyplexes complexes in a 96-well plate. For the PRs, 0.1 µg in 50 µL of nucleic acid was added to 50 µL of peptides. For the LPRs, 25 µL of peptides was added to an equal volume of lipids, followed by the addition of 50 µL of RNA, resulting in a total volume of 100 µL. The method is detailed in Section 4.3.3. The measurements were conducted in triplicate, and the error bars indicate the standard deviation calculated from three distinct measurements within a single experiment. The experiments was repeated in duplicate. Data were statistically analysed by a two-tail T Test and data considered significant different at $p<0.05$ and considering only the charge ratio x=10.

1.3.4 siRNA Transfection Assay

Both cell types were cultured in 24-well plates at a concentration of 50,000 cells per well in 500 µl of fresh media. After 24 hours, polyplexes and lipopolyplexes peptides with RGen3K, TGen3K, and SGen3K were diluted in 100 µl of Opti-Mem (Gibco) in a single charge ratio (10:1) like reported in Section 4.3.1, 4.3.2 and 4.3.3. The final concentration of siRNA (ThermoFisher) (siRNA +) and the scrambled siRNA (ThermoFisher) was 50 nM per well. The same procedure was repeated for LPRs. In this case, only TGen3K at a ratio of 0.5:10:1 was tested. Trastuzumab (MedChemTronica, at 10 µg/mL) and Lipofectamine 3000 (ThermoFisher, charge ratio 4:1) in 100 µl of Opti-Mem were used as controls. Following sample preparation,

the medium in the 24-well plates was removed, and the cells were washed with 200 µl of sterile PBS. Subsequently, 400 µl of fresh medium was added, and the samples (in a total volume of 100 µl) were introduced into the wells. The cells were then incubated for 48 hours at 37° C and 5% CO_2.

After the incubation period, the supernatant was removed, and the cells were washed twice with 200 µL of sterile PBS. They were then fixed with 100 µL of paraformaldehyde (ThermoScientific) for 20 minutes. Following the fixation, the cells were washed twice with 200 µL of sterile PBS and then stored in the fridge hydrated in 100 µL of PBS. Subsequently, 100 µL of 3% v/v BSA (Sigma Aldrich) were added. After the removal of 3% v/v BSA, the primary antibody was diluted to 1:100 in 3% v/v BSA and it was added and incubated for 2 hours at room temperature. The primary antibody used was mouse monoclonal to N-Cadherin (Abcam, UK) that is a marker of cell migration.

The cells were then washed two more times with 200 µL of sterile PBS, and the secondary anti-mouse AlexaFluor 488 antibody (Goat Anti-Mouse IgG, Abcam) was added at a dilution of 1:100 in 3% v/v BSA. This was incubated for at least 4 hours at room temperature. Cellular nuclei were stained with DAPI or 4',6-Diamidino-2-Phenylindole (Vector Laboratories, UK) and imaged with a laser scanning confocal microscopy (Leica RM2135, Technologic Ltd, UK).

1.4 RESULTS AND DISCUSSION

1.4.1 Dynamic Lyght Scattering

The size of complexes containing lipids, peptides, and siRNA was measured. Specifically, the analysed peptides were RGen3K, TGen3K,

K16, and TK16 at charge ratios of 4:1, 6:1, 8:1, 10:1, and 14:1, using TRPM8 siRNA. The results are presented Figure 0.1.

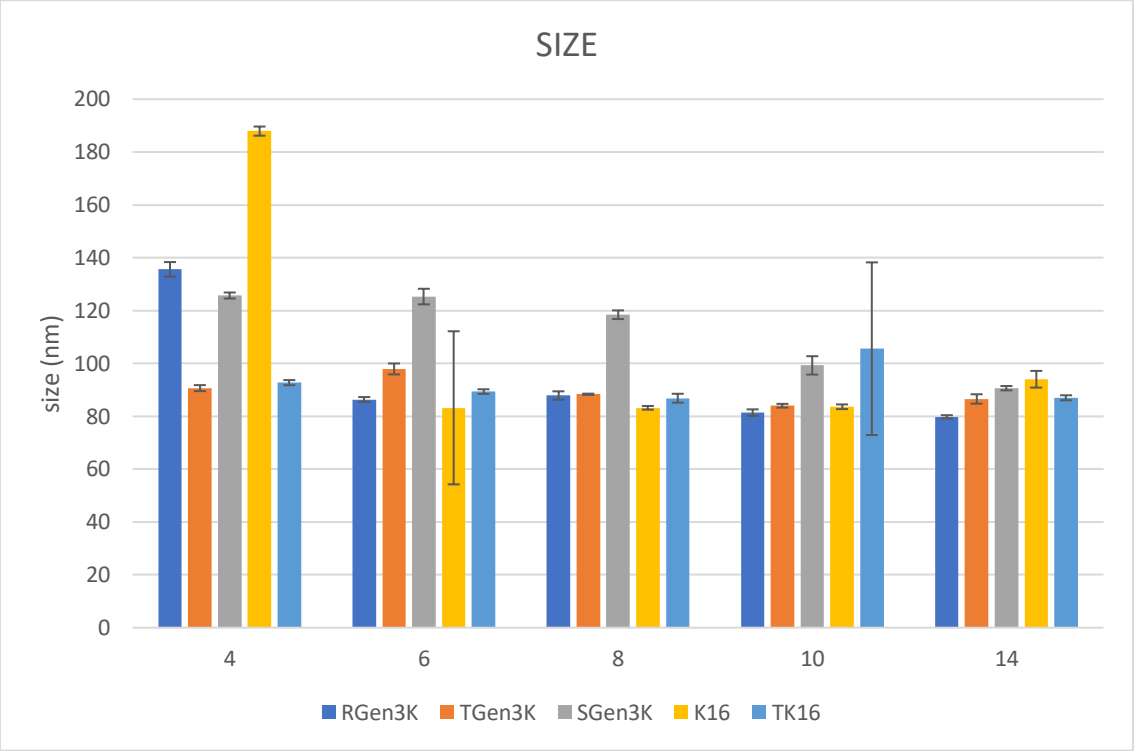

Figure 0.1 Graph showing the average intensity size distribution of the of the lipid:peptide:SIRNA complexes. Peptides involved were: RGen3K, TGen3K and the linear K16 and TK16. The numbers on the X axis represent the lipid:peptide:SIRNA as 0.5:X:1 charge ratio.

As it can be seen from the results, starting from the charge ratio of x=6, the sizes of the complexes become very similar and stable. Only the carrier SGen3K appeared to maintain a relatively higher size that then consistently reduces to a size comparable to the other carriers at x=14. Additionally, there were no significant differences observed between linear or branched peptides, and the target sequence does not appear to interfere with the size of the LPRs.

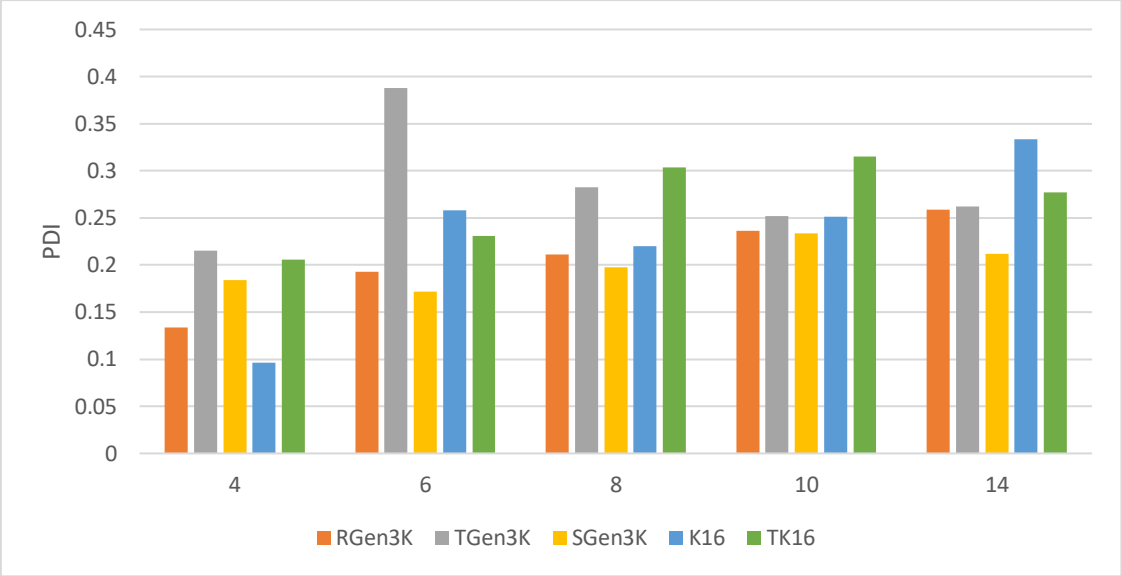

Figure 0.2 Graph showing the polydispersity index of the of the lipid:peptide:SIRNA complexes. Peptides involved were: RGen3K, TGen3K and the linear K16 and TK16. The numbers on the X axis represent the lipid:peptide:SIRNA as 0.5:X:1 charge ratio.

On the other hand, the PDI of the complexes increases with the increase in peptide concentration, in contrast to the complexes with DNA (Section 4.4.1), where uniformity remained constant as the quantity of peptides increased. The statistical analysis has not been conducted because there are not enough values to perform the T-test analysis.

1.4.2 Gel Electrophoresis

Figure 0.1-a shows the results of gel electrophoresis on siRNA/branched carrier complexes without (PRs) and with lipid components (LPRs) at different ratios and in presence of loading buffer, respectively on the top and bottom rows. On Figure 0.3-b are represented the linear peptides. The top row represent the complexes composed solely of PRs (peptide:RNA

complexes), while the second row feature complexes with the addition of lipids DOTMA:DOPE (LPRs).

For polyplexes preparation, the charge ratios used were 4:1, 6:1, 8:1, 10:1, and 12:1, as chosen in the experiments of transfection using the plasmid DNA (Chapter 4). These different charge ratios were used to vary the ratio of cationic peptides to DNA and siRNA in the complexes and study their transfection/therapeutic potential. The gel electrophoresis allowed visualising the migration patterns of the complexes, indicating their degree of condensation and stability. The peptides tested were: RGen3K, TGen3K, SGen3K and the linear controls K16 and TK16. For lipopolyplexes the concentrations used were 0.5:4:1, 0.5:6:1, 0.5:8:1, 0.5:10:1, and 0.5:12:1. The peptides tested were: RGen3K, TGen3K, SGen3K and the linear controls K16 and TK16.

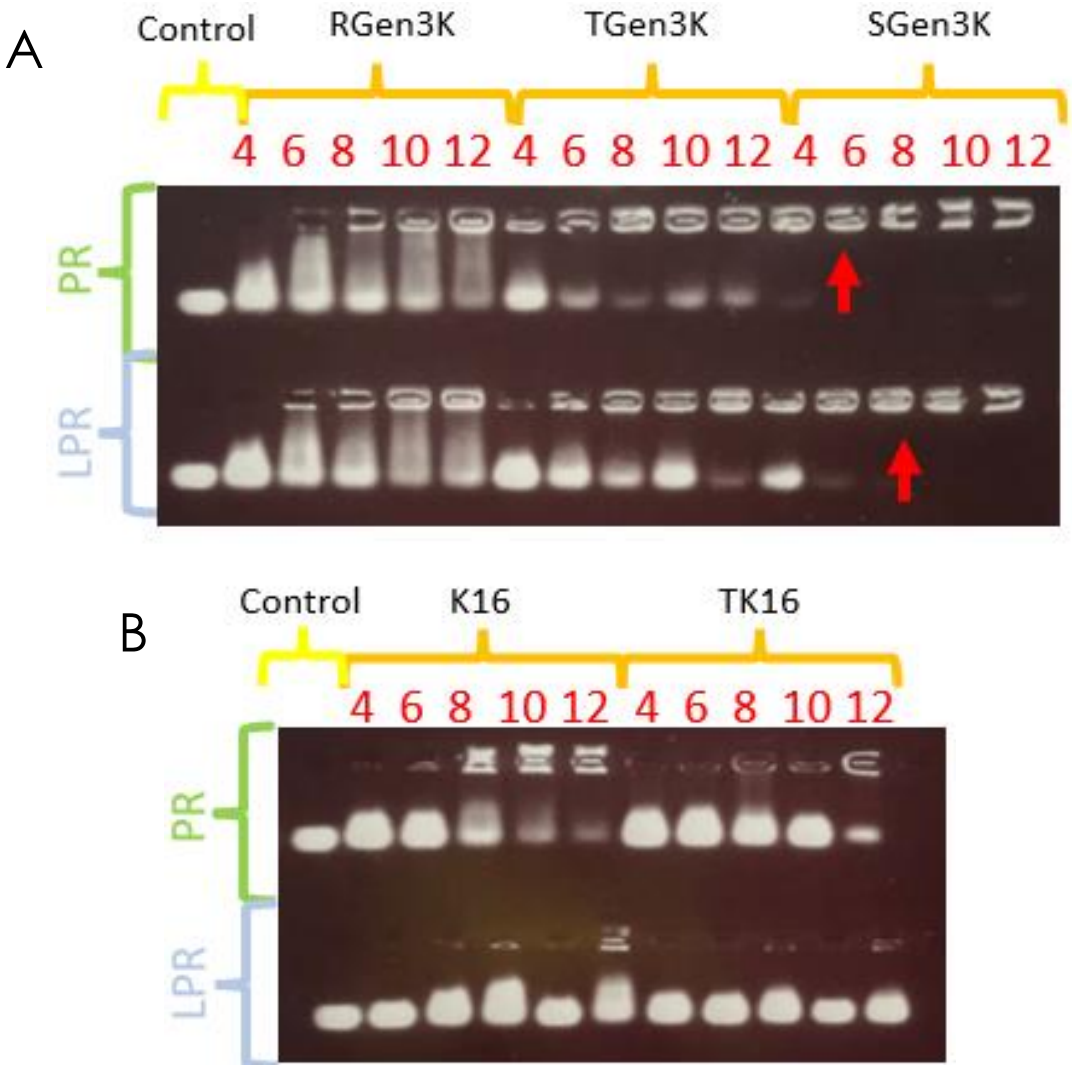

Figure 0.3 A) Polyplexes containing RGen3K and the targeting version TGen3K and SGen3K. On the second row same peptides complexed with lipids and RNA (LPRs). The lipopolyplex charge ratios used were 0.5:x:1 lipid:peptide:RNA with x being the ratio number displayed next to each peptide ratio. Red arrows indicate the smallest ratio at which there is complete RNA condensation. B) Gel Electrophoresis of polyplexes (PRs) prepared using the linear.

Based on the results of PRs (peptide:siRNA complexes), it is evident that linear peptides are not as efficient in condensing the small nucleic acid. Between the two linear controls, it seems that K16 only partially complexes with siRNA, as indicated by the reduced intensity observed as the charge

ratio increases. On the other hand, this is not observed for TK16, which might be due to a partial steric hindrance allegedly caused by the targeting sequence. In contrast, the hyperbranched peptides appear to be more effective in siRNA packaging. In particular, RGen3K shows band smears suggesting some complex dragging, with part of it remaining trapped in the starting well. TGen3K seems to have a lower percentage of the complex capable of migrating, suggesting that most of the PR is unable to move within the gel thus indicating the formation of a stronger complex. Meanwhile, SGen3K demonstrated to induce the strongest siRNA packaging capabilities as no migration of bands was detected and the uploaded complexes remained in the loading well at all ratios tested. The spatial arrangement of amino acids in the targeting sequence is likely to generate a better interaction with the nucleic acid's charges. Furthermore, the targeting sequence seems to play a crucial role in enhancing the siRNA packaging efficiency of TGen3K and SGen3K peptides.

The LPR complexes, bottom row in Figure 0.3 (a and b), show to form less stable complexes when compared to the results obtained with PRs as they show a more marked release of free siRNA, a behaviours similar to that observed when complexes with DNA were analysed (Chapter 4, Section 4.4.2). However, when compared to the results of Figure 0.5, it appears that the binding of siRNA to peptides in absence of lipid is less stable than that observed with DNA. In the presence of lipid, the data of Section 4.4.2 show that the complexes with DNA were much less stable as indicated by the higher number of bands compared to the complexes without lipids. Here, the lipid led to a higher release of free siRNA, while the peptides in absence of lipid show less amounts of free nucleic acid.

The distinct behaviour of the lipid complexes with siRNA and DNA may be attributed to the specific interactions between the cationic peptides and

the nucleic acids, along with the different properties of siRNA and DNA molecules; e.g. the significantly different molecular weight that is likely to change the number of carriers per nucleic acid and/or the folding of the nucleic acid around the carriers or the different ratio in the number of carrier molecules versus nucleic acid molecules. The results emphasise the importance of carefully studying and understanding the interaction between different components in gene delivery systems to design efficient and stable gene delivery vehicles for therapeutic applications.

The same experiment was also conducted without using the loading buffer as performed with the DNA in Chapter 4.

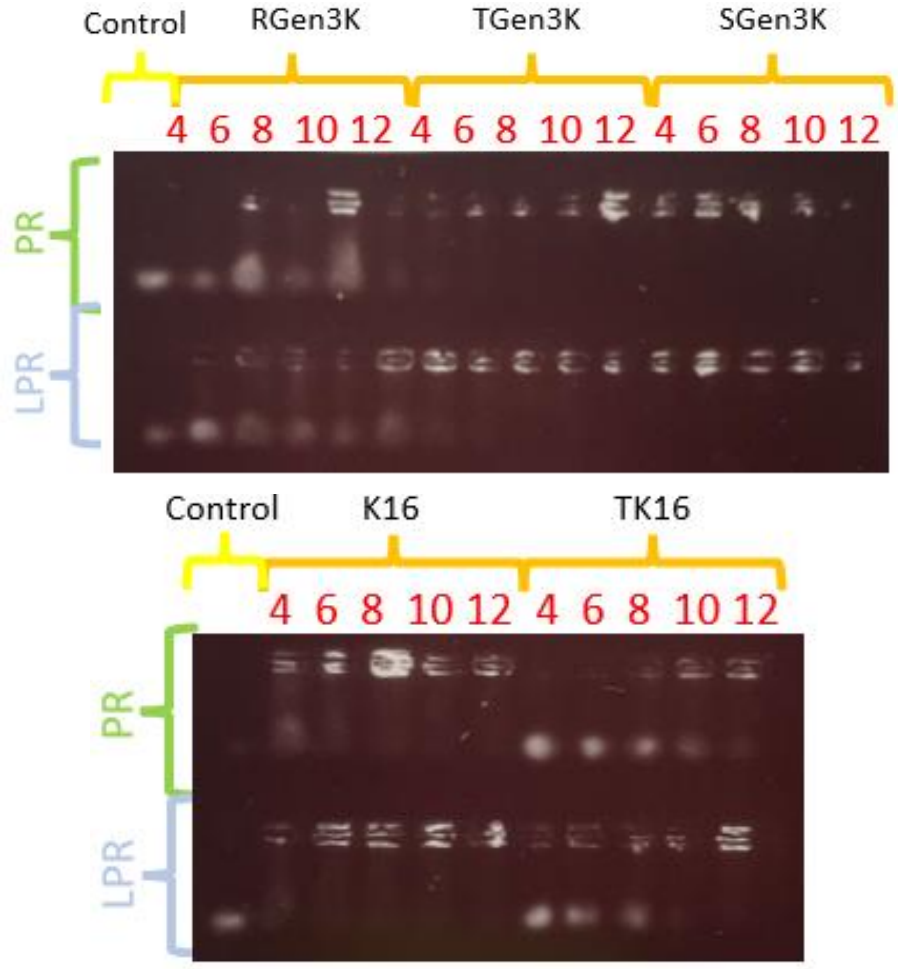

Figure 0.4 A) Gel electrophoresis of polyplexes (PRs) containing RGen3K and the targeting version TGen3K and SGen3K. On the second row same peptides complexed with lipids and RNA (LPRs). The lipopolyplex charge ratios used were 0.5:x:1 lipid:peptide:DNA with x being the ratio number displayed next to each peptide ratio. B) Gel Electrophoresis of polyplexes (PRs) prepared using the linear peptide with and without the targeting sequence (respectively K16 and TK16) on the top row. Below, lipopolyplexes (LPRs), thus linear peptides complexed with RNA. Red arrows indicate the smallest ratio at which there is complete RNA condensation.

In Figure 0.4 a and b, the results of the gel electrophoresis conducted without the use of loading buffer are presented. In particular, Figure 0.4 top row represents the PRs (Peptide:SIRNA complexes), with RGen3K, TGen3K, and SGen3K peptides located in the upper section. On the bottom are shown the LPRs with the branched peptides. Figure 0.4-b

displays the linear peptides. PRs on the top and LPRs on the second row. Furthermore, in the third lane, the linear peptides are depicted. The charge ratios used for the PRs were the same of those used for the plasmid DNA; i.e. 4:1, 6:1, 8:1, 10:1, and 12:1. For lipopolyplexes, the concentrations used were 0.5:4:1, 0.5:6:1, 0.5:8:1, 0.5:10:1, and 0.5:12:1, also as tested in the case of the plasmid DNA. The peptides tested in this context included RGen3K, TGen3K, SGen3K, as well as the linear controls K16 and TK16.

As per the electrophoresis results obtained with loading buffer, In this case as well there were no substantial differences when the loading buffer was absent, which is in stark contrast to the behaviour observed with DNA complexes (Figure 0.7). Figure 0.7, the gel electrophoresis appearance was significantly different when the bromophenol blue loading buffer was added. This suggests that the binding strength between siRNA molecules and nanoparticles is much stronger compared to DNA complexes.

Additionally, siRNA complexes appeared to be less susceptible to variations caused by competitors such as the loading buffer and lipids, indicating greater stability. This stronger and more stable binding between siRNA and nanoparticles is likely due to the specific interaction and condensation capabilities of the cationic peptides with the negatively charged and relatively small siRNA molecules, resulting in the formation of stable and robust complexes [340].

1.4.3 PicoGreen

As Section 4.3.6 PicoGreen dye was utilised to perform a fluorescent test, aiming to assess the complexation of LPRs (lipid:peptide:RNA complexes) and PRs (peptide:RNA complexes).

Figure 0.5 shows the PR results obtained from the PicoGreen assay. The peptides tested were RGen3K, TGen3K, SGen3K, and the linear controls

K16 and TK16. The charge ratios utilised were 4:1, 6:1, 8:1, 10:1, and 12:1. Furthermore, the experiment was replicated in the presence of the same peptides complexed with the lipid component and siRNA using the following charge ratios: 0.5:4:1, 0.5:6:1, 0.5:8:1, 0.5:10:1, and 0.5:12:1 (Figure 0.5). These experiments enable a comprehensive evaluation of the complexation properties of both the LPRs and PRs complexes, shedding light on their potential applicability in gene delivery and therapeutic interventions.

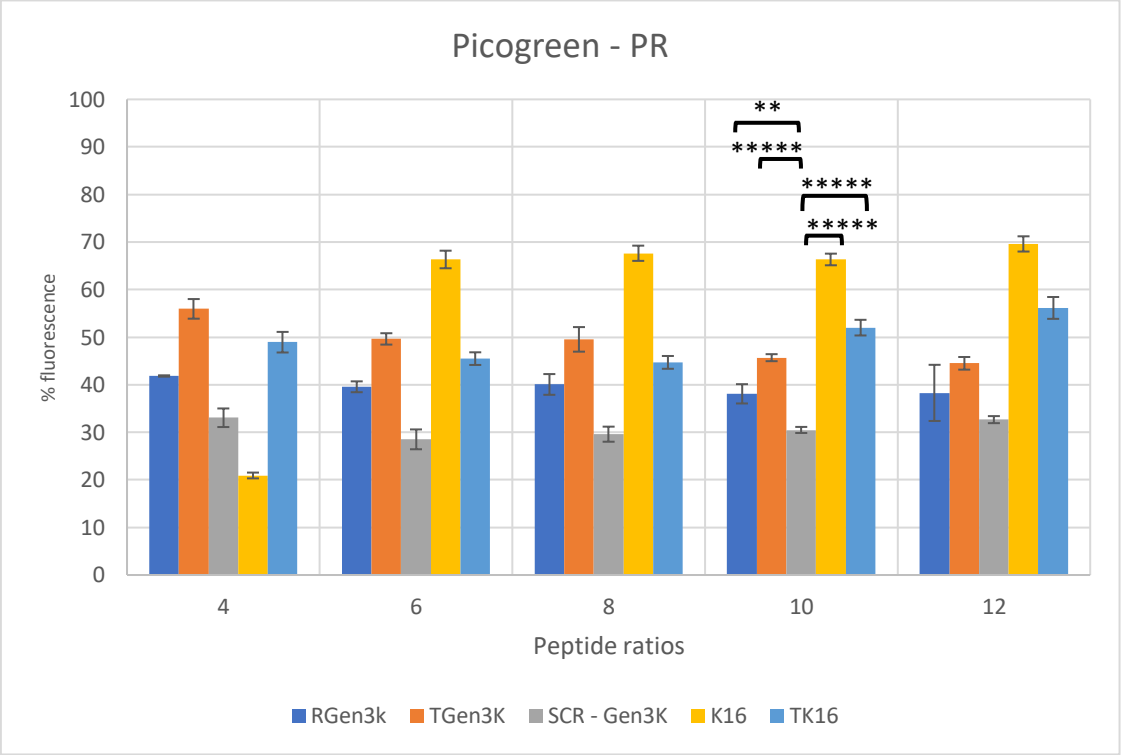

*Figure 0.5 PicoGreen analysis and fluorescence percentage of the peptide:DNA complexes. Peptides involved were: RGen3K, TGen3K, SGen3K (SCR-Gen3K) and the linear K16 and TK16 and 5 different charge ratios ranging from 4 to 12. The numbers on the X axis represent the lipid:peptide:DNA as 0.5:X:1 charge ratios. *****P<0.00001, ****P<0.0001, ***P<0.001, **P<0.01, *P<0.05 considering only the charge ratio x=10.*

The PR values show predominantly linear and stable values that fall within the range between 20% and 70%. All peptides, when complexed with RNA, form highly stable complexes even at very low charge ratios, except for K16. The latter, perhaps due to its large flexible structure that fail to complex with the small structure of the nucleic acid. Consequently, it reaches the highest PR value already at a charge ratio of 6:1.

On the other hand, considering the hyperbranched structure, the lowest PR values are achieved when using ten peptide charges ratio 10:1. In particular, all dendrimers show a plateau-like profile, with all starting values below 60% of fluorescence and the scrambled peptide (SGen3K) showing to be able to capture higher levels of siRNA (value of ca 30%) at all ratios. This result seems to be confirmed by the gel electrophoresis in Figure 0.4, where stable complexes are present at all charge ratios.

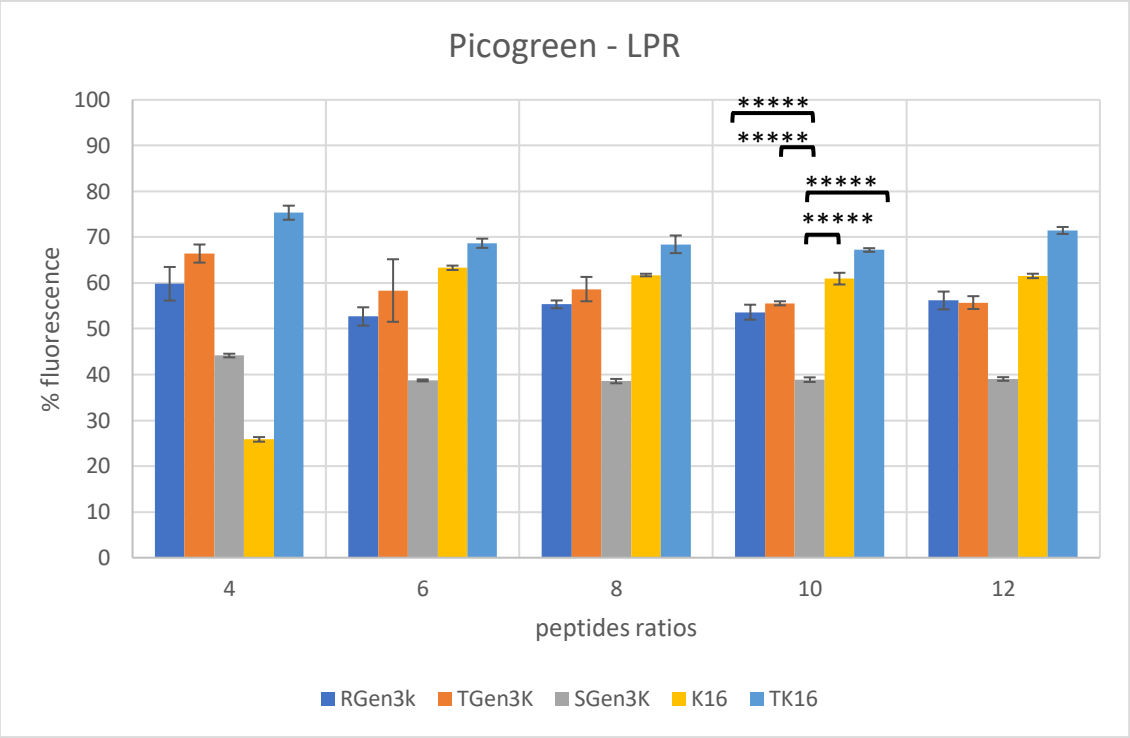

*Figure 0.6 PicoGreen analysis and fluorescence percentage of the lipid:peptides:DNA complexes. Peptides involved were: RGen3K, TGen3K, SGen3K and the linear K16 and TK16 and 5 different charge ratios ranging from 4 to 12. The numbers on the X axis represent the lipid:peptide:DNA as 0.5:X:1 charge ratios. *****P<0.00001, ****P<0.0001, ***P<0.001, **P<0.01, *P<0.05.*

In Figure 0.6, the values of peptide-RNA complexation in the presence of DOTMA:DOPE lipids are presented. The trend of the graph is very similar to that depicted in Figure 0.5, where the values are flattened and show minimal variations. Only K16, between the charge ratios of 4:1 and 6:1, reaches a plateau. Hyperbranched peptides, on the other hand, exhibit the best binding values as they have fluorescence values lower than the linear peptides. Compared to the results obtained in PRs, the percentages are higher, and the ranges transition from 30-60% to 40-70% (excluding the lowest ratio of 4). This implies that lipids still influence the strength of the binding between the complexes and the nucleic acid. The binding

becomes weaker, making it easier for the competitor (PicoGreen reagent) to displace the complex from the nucleic acid structure, resulting in increased fluorescence emission.

A second difference lies in the standard deviations. Both PRs and LPRs in siRNA-laden complexes have very smaller error bars compared to PDs (Peptide:DNA complexes) and LPDs (Lipid:Peptide:DNA complexes), indicating less variability in the obtained fluorescence values and, therefore, better stability and reproducibility compared to the presence of DNA. The large structure of the nucleic acid likely renders the complex more unstable and prone to variations.

1.4.4 SiRNA Transfection Assay

The selected siRNA is TRPM8, which is a nucleic acid that induces changes in the concentration of calcium channels [341]. Given that TRPM8 siRNA is capable of reducing cellular proliferation, it was hypothesised, and also reported in the study by Ochoa et al. [339], that the activity of N-Cadherin might be influenced. Indeed, N-Cadherin is a marker of cell migration. During tumor progression, carcinoma cells, especially those found at the invasive front of the primary tumor, often exhibit a downregulation of epithelial phenotype markers and a loss of intercellular junctions. This results in the loss of the typical polarity seen in epithelial cells and reduced intercellular adhesion. This is frequently accompanied by increased cellular motility and the expression of mesenchymal markers such as vimentin, an intermediate filament protein, and N-cadherin. The upregulation of these proteins can facilitate the formation of pseudopodia and cytoskeletal remodelling [342,343].

For the transfection experiment, polyplexes containing the non-targeting peptide RGen3K, the targeting TGen3K, and SGen3K were prepared and

tested at a single charge ratio (10:1) in both cell lines: MDA-MB-231, which are HER2-negative breast cancer cells, and SKBR3, which are HER2-positive cells that overexpress the receptor on their surface. The final concentration of TRPM8 siRNA (siRNA +) was 50 nM, as it was for the negative control, scrambled sequence siRNA (siRNA -). Following transfection, cells were treated with an antibody to visualise the presence of N-Cadherin on the cell surface and with DAPI to visualise their nuclei.

Significant differences were introduced regarding the charge ratios, the tested complexes, and the positive controls used. Firstly, the experiment was conducted at a single charge ratio, as both PRs and LPRs yielded the best results following the PicoGreen experiment outlined in Section 5.4.3. Furthermore, the tests conducted in the presence of DOTMA:DOPE lipids were reduced, and only the LPRs complexed with the branched targeting peptide (TGen3K) at a single charge ratio of 0.5:10:1 were evaluated.

Similarly, due to the inefficient retention of siRNA by linear peptides, as demonstrated by TK16 in the electrophoresis gel and both linear peptides in the PicoGreen test (charge ratio from 6 to 12), they were not included in the experimental matrix. Instead, the linear controls were replaced with Lipofectamine 3000, a lipid-based material recommended as an optimal carrier for cell transfection (Section 4.3.6 and 4.4.3). The other control used was Herceptin (H) at a concentration of 10 µg/mL. These concentrations were determined based on the monoclonal antibody's quantity, as the commonly employed concentration in the literature is 10 µg/mL. [270–272].

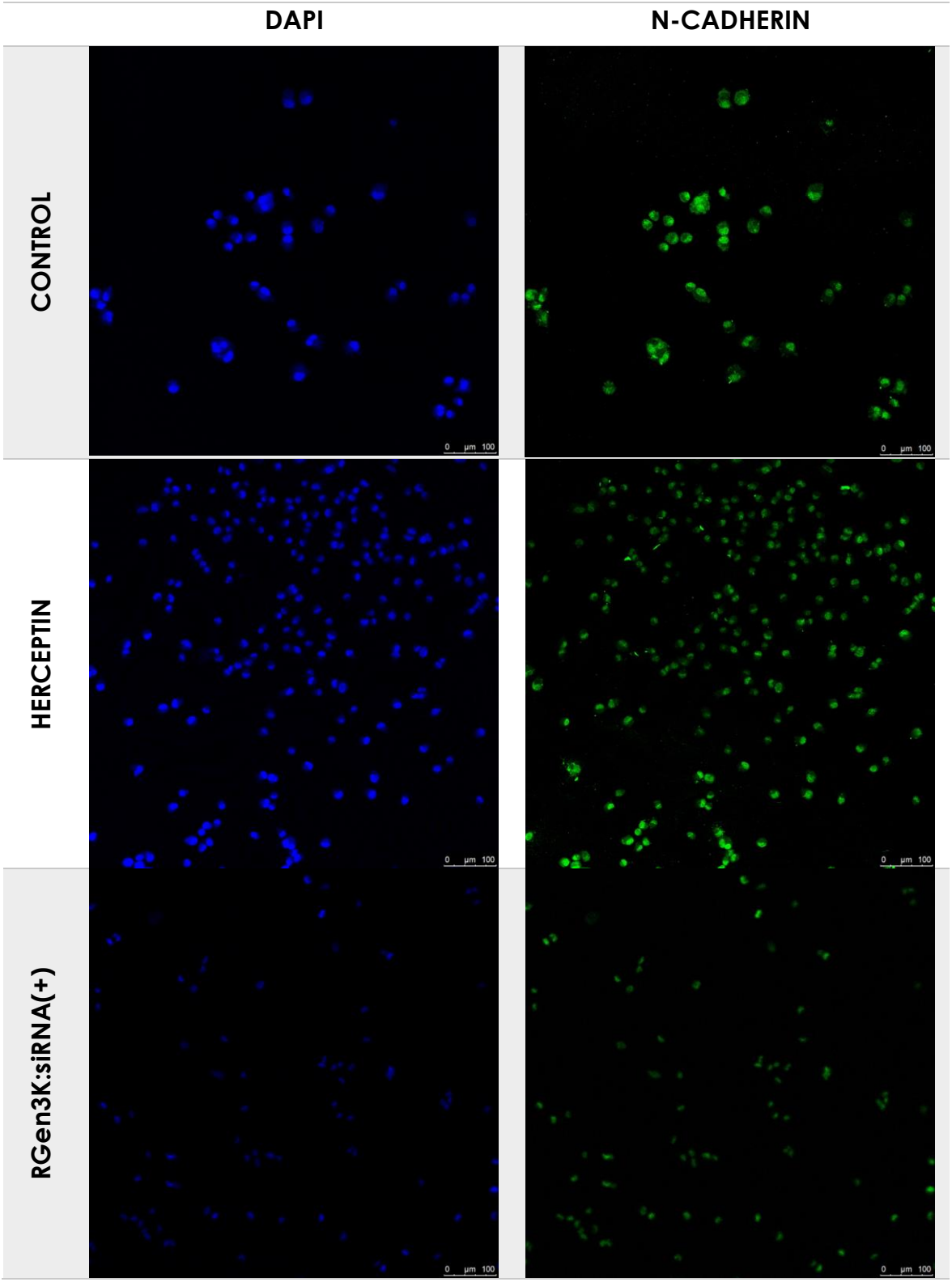
DAPI
N-CADHERIN
CONTROL
HERCEPTIN
RGen3K:siRNA(+)
0 µm 100

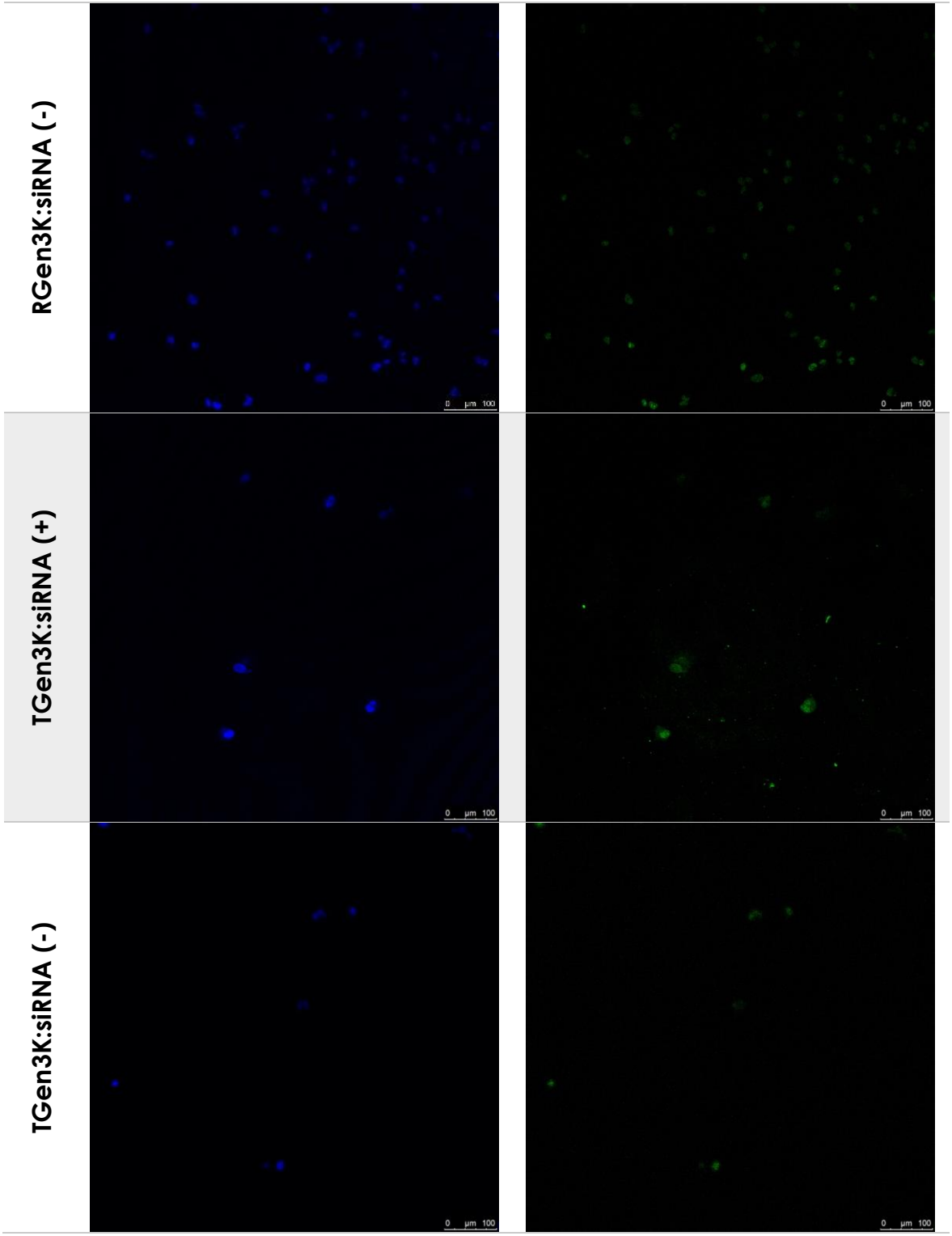
RGen3K:siRNA (-)
TGen3K:siRNA (+)
TGen3K:siRNA (-)
0 µm 100

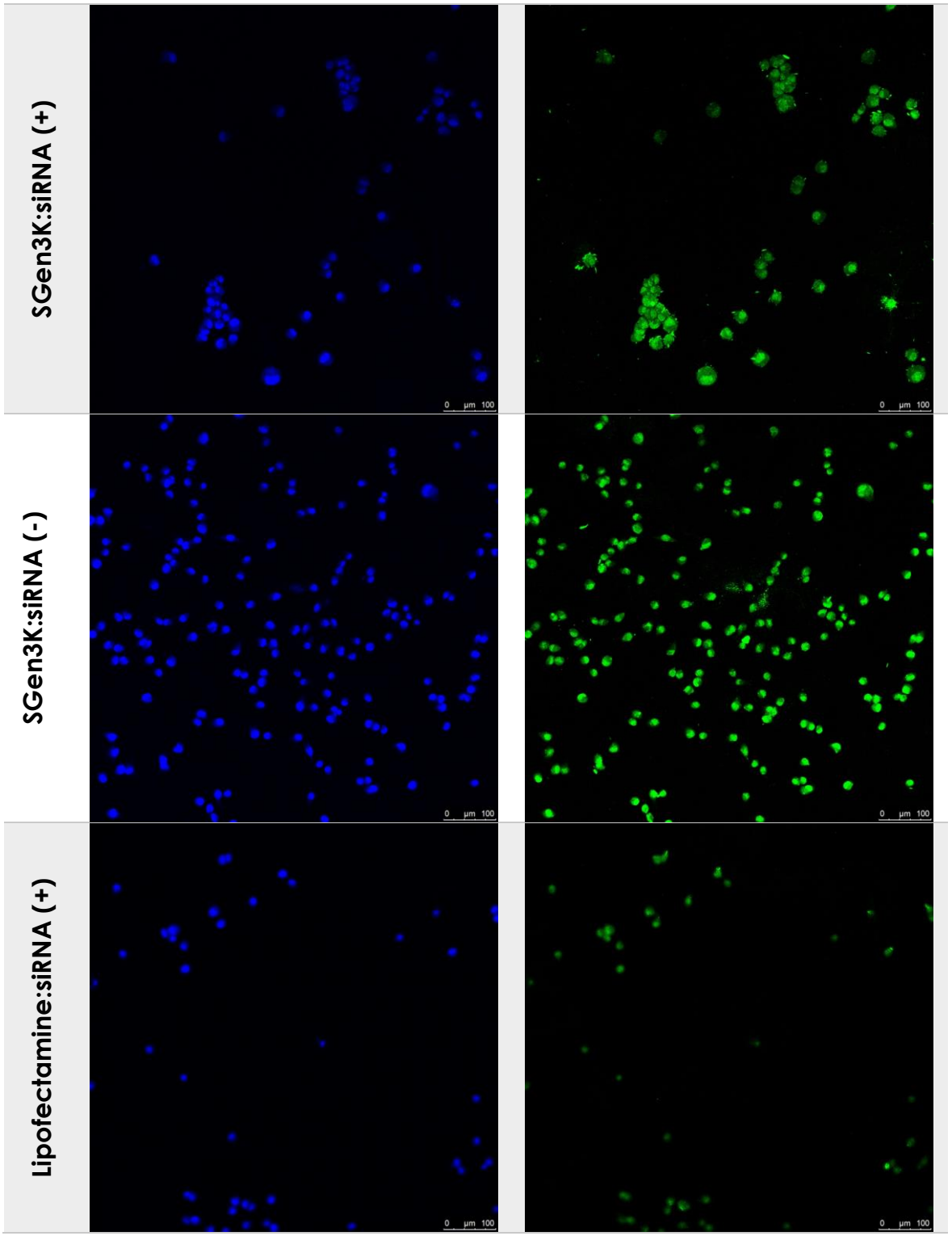
SGen3K:siRNA (+)
SGen3K:siRNA (-)
Lipofectamine:siRNA (+)
0 µm 100
0 µm 100
0 µm 100
0 µm 100
0 µm 100
0 µm 100

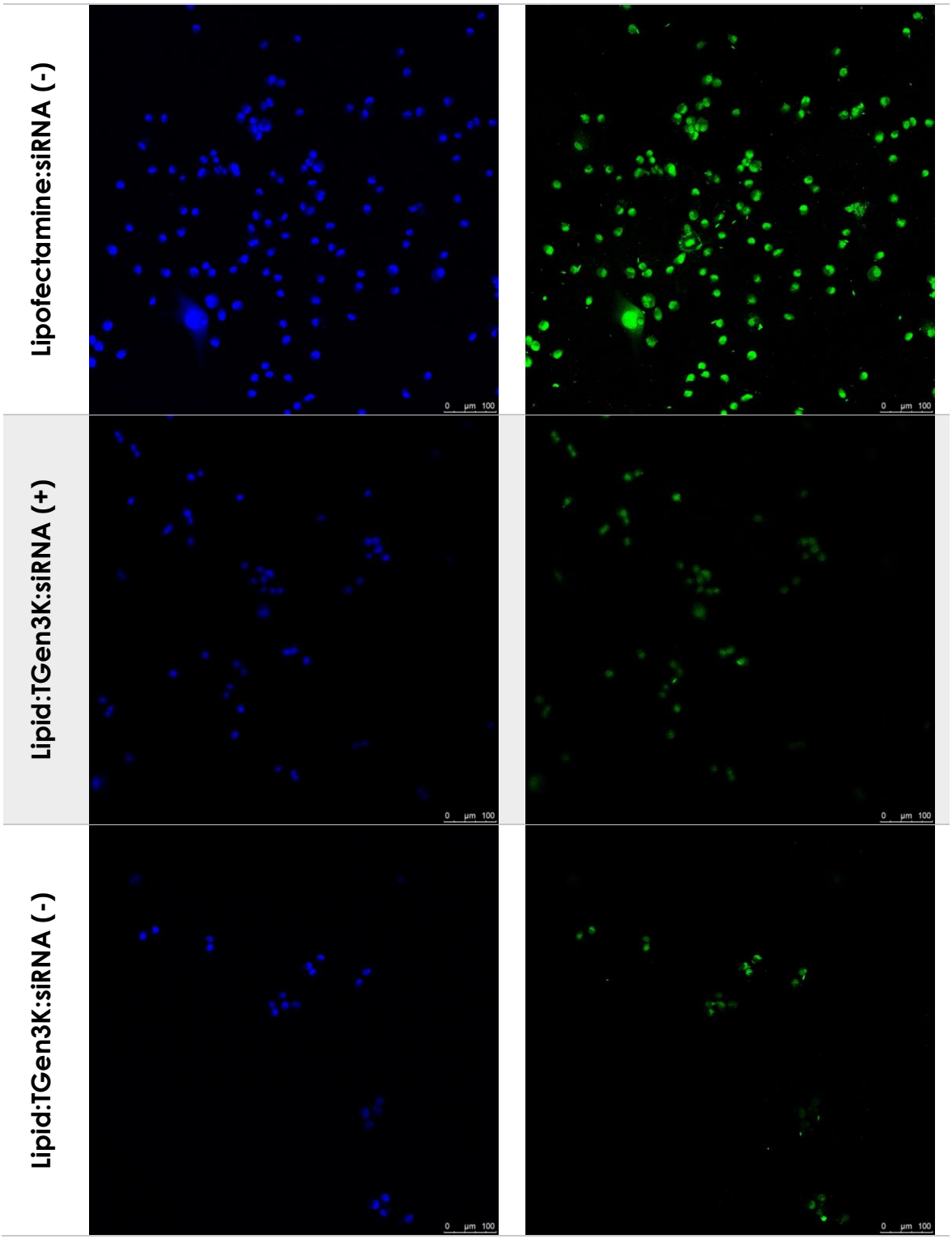

Figure 0.7 Images of MDA-MB-231 cells taken with the confocal microscope. Were transfected Herceptin, RGen3K, TGen3K and SGen3K (charge ratio 10), Lipofectamine 3000 and the lipopolyplex lipid:TGen3K:siRNA. On the left side of the nuclei, on the right the N-Cadherin.

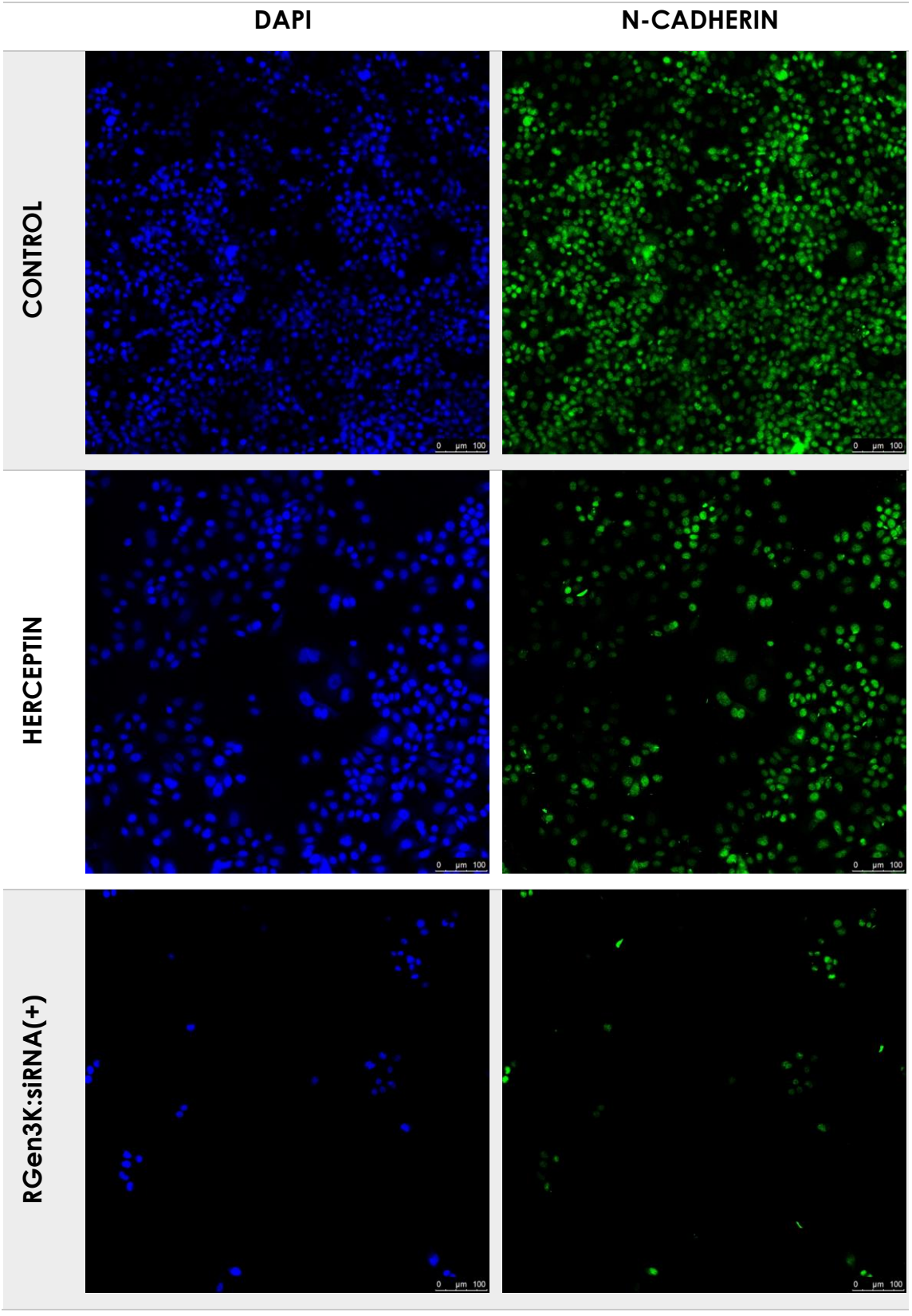
DAPI
N-CADHERIN
CONTROL
HERCEPTIN
RGen3K:siRNA(+)
0 µm 100

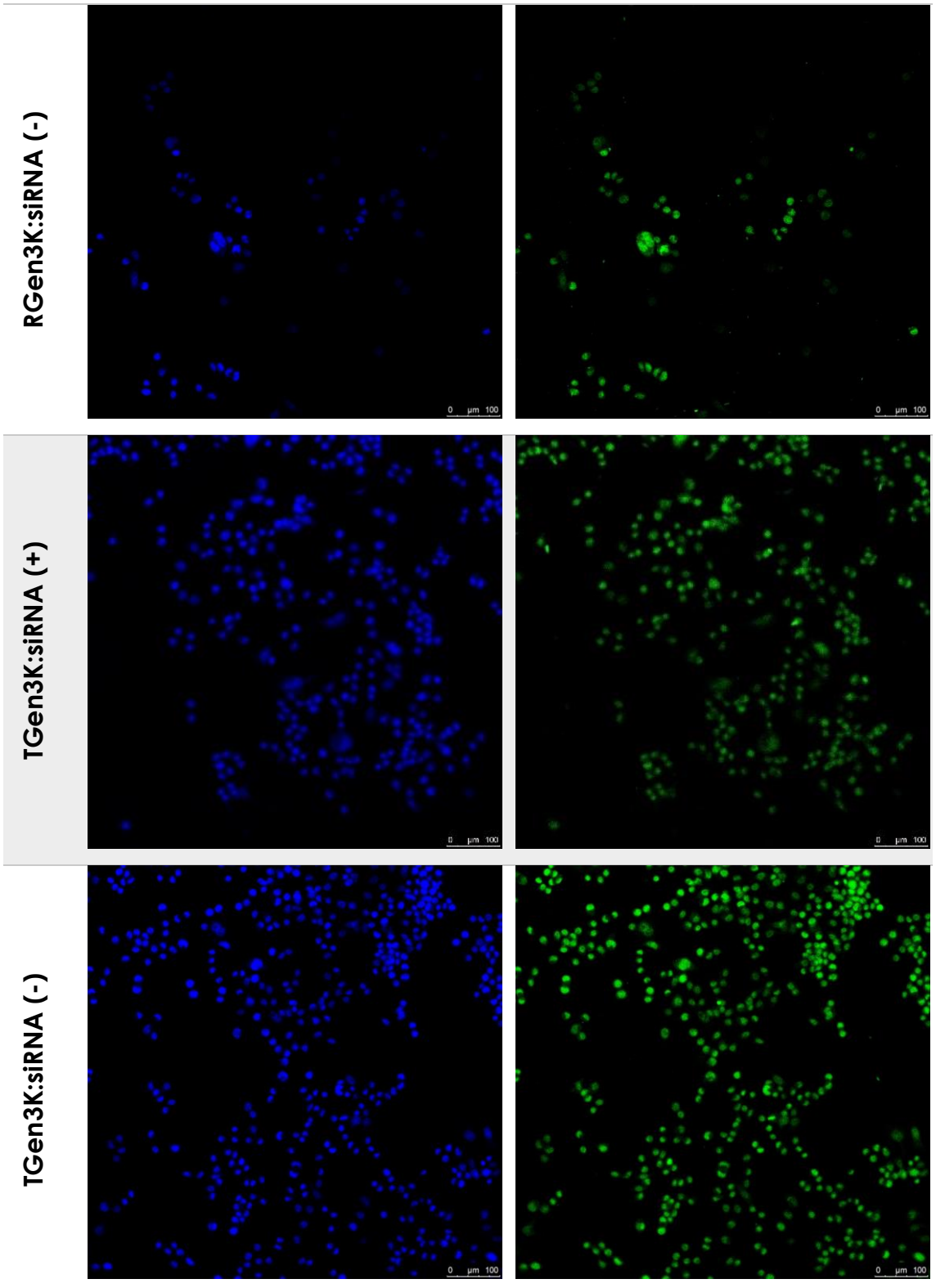
RGen3K:siRNA (-)
TGen3K:siRNA (+)
TGen3K:siRNA (-)

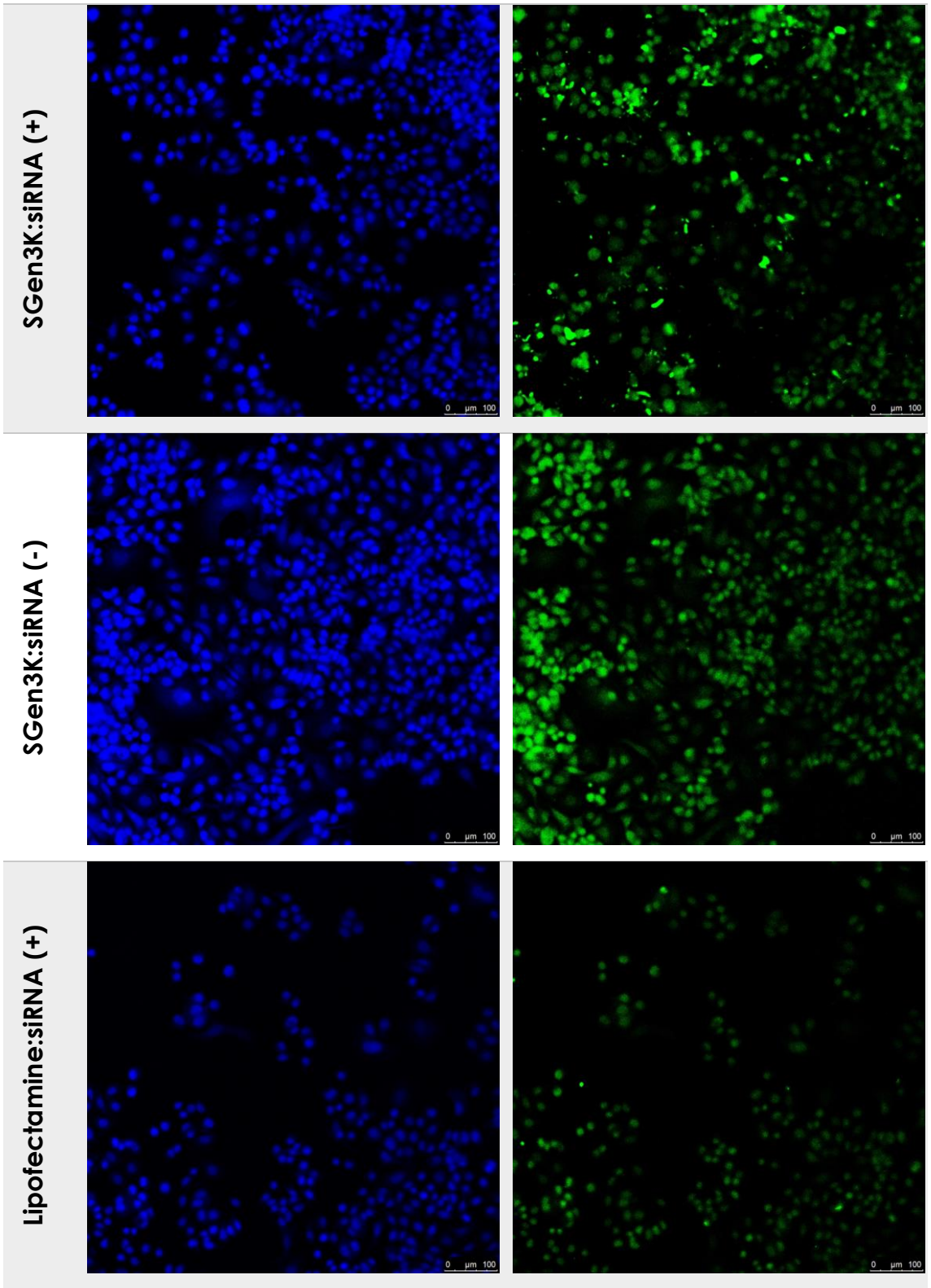
SGen3K:siRNA (+)
SGen3K:siRNA (-)
Lipofectamine:siRNA (+)
0 µm 100

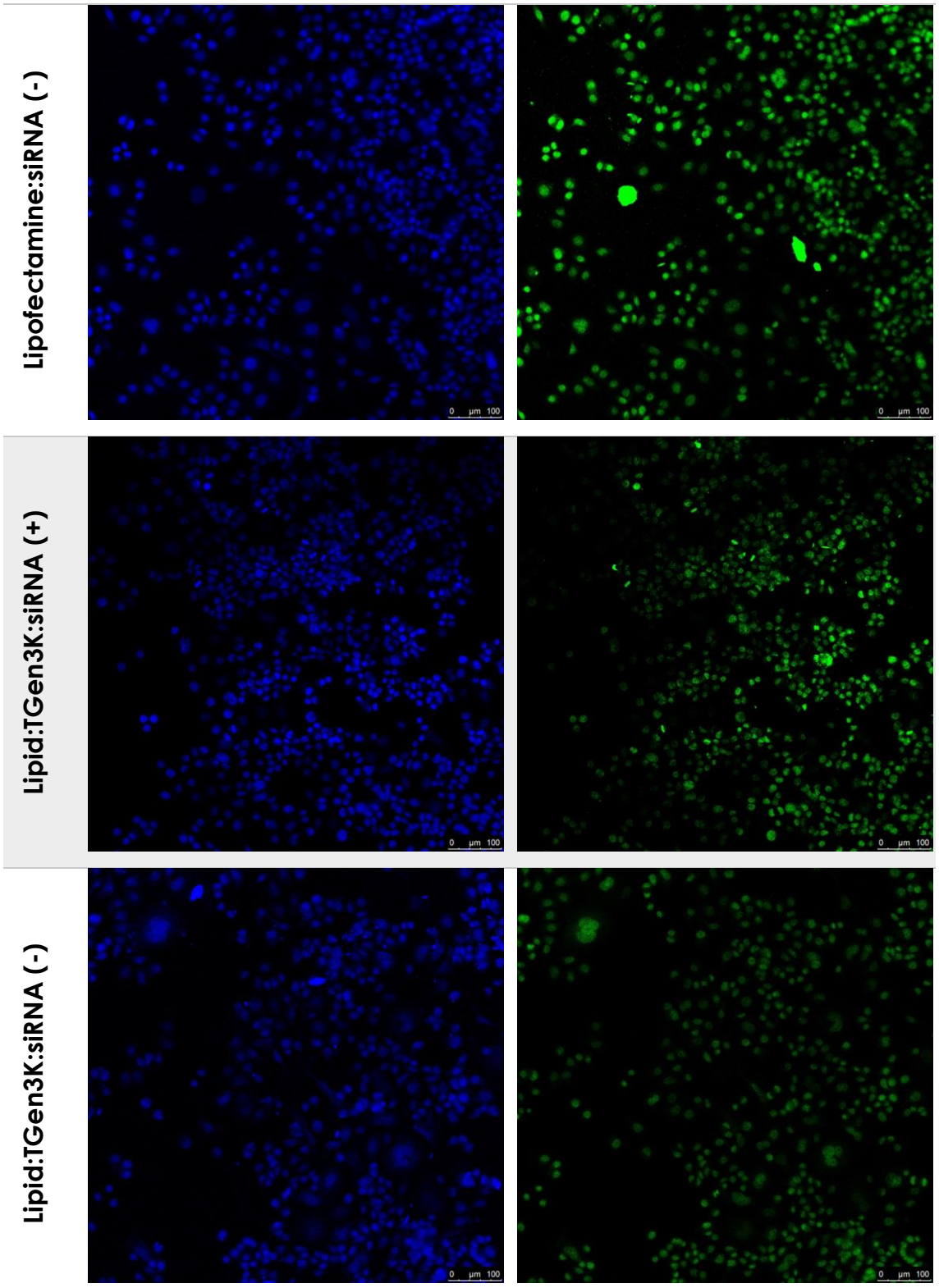

Figure 0.8 Images of SKBR3 cells taken with the confocal microscope. Were transfected Herceptin, RGen3K, TGen3K and SGen3K (charge ratio 10), Lipofectamine 3000 and the lipopolyplex lipid:TGen3K:siRNA. On the left side of the nuclei, on the right the N-Cadherin.

Figure 0.7 and Figure 0.8 show a panel of all the images obtained by confocal microscopy at high magnification. In the left column, all cell nuclei are coloured in blue (DAPI); in the right, N-Cadherin is highlighted in green.

As can be observed from both Figure 0.7 and Figure 0.8 panels, it is evident that in both cell types (MDA-MB-231 and SKBR3), there are no variations in the expression of N-Cadherin. However, the positive control consisting of Lipofectamine 3000 does not induce any difference when complexed with control siRNA (-), but in the presence of TRPM8 siRNA (+), its effect becomes apparent. Lipofectamine is commonly used in the pharmaceutical industry due to its high transfection capacity, and in this experiment, it not only confirms its effectiveness but also highlights the ability of siRNA to reduce proliferation.

Nevertheless, a clear effect on cell count can be observed. In fact, both RGen3K and TGen3K peptides have an impact on the cell count, both in the presence of TRPM8 siRNA and control siRNA. This highlights the impact of the hyperbranched structure. As reported in Chapter 3, there was a visible result of the hyperbranched structure on the number of SKBR3 cells. In the cases of all the complexes tested, the number of adhering cells was comparable to that of the control. However, RGen3K showed a significant reduction of cell number suggesting the potential synergistic effect that the presence of arginine at the root of the molecular tree may have on the cell cycle inducing breast cancer cell apoptosis [344].

At some extent, these data are supported by the cell proliferation data obtained in Chapter 3 where the hyperbranched carriers (in particular RGen3K), tested as such, showed to inhibit the proliferation of both cell types, more markedly in the case of the SKBR3 cells and with a trend not statistically different in the MDA-MB-231 cells. Such a significant reduction of cell numbers makes difficult to assess in a definitive manner, the effect

of the siRNA on N-Cadherin expression. The more limited effect of Herceptin and the TGen3K on the SKBR3 cells may be ascribed to the interference on different cellular pathways. Indeed, Herceptin and the hyperbranched carrier bearing is analogue sequence (TGen3K) would affect the cell cycle by interacting with the HER2 receptor at the surface of the cell membrane. Hence, the carrier bearing the antibody analogue sequence is not necessarily suitable to increase the internalisation of the complex, but mainly favouring the targeting of this specific cell type. Whereas, the RGen3K can be internalised by the cells independently from cell surface receptor and interfere on the cell cycle through both its intrinsic properties and the release of siRNA.

This interpretation may be substantiated also by the analysis of the effect of the TGen3K on the two types of cells is analysed. This dendrimer showed to inhibit cell proliferation more markedly in the case of the MDA-MB-231 cells than SKBR3 as in the latter the interaction with the receptor may well reduce or completely inhibit the complex internalisation. There are still inconclusive results regarding the SGen3K as, while showing to compact the complex in a smaller size, it does not seem to have consistent data across tests.

It is important to note that the presence of lipids does not seem to be essential either. In this case, a minor reduction in N-Cadherin is not distinctly visible upon TRPM8 siRNA internalisation. However, as anticipated by Gel Electrophoresis and PicoGreen results, the outcomes do not deviate significantly from the peptide:siRNA complex. These findings stand in stark contrast to DNA transfection, where DOTMA:DOPE lipids were necessary to achieve adequate levels of internalisation and luciferase translation. This emphasises how DNA and siRNA, despite being composed of the same nucleic acid units, can exhibit different behaviours when complexed with small amino acid molecules.

1.5 CONCLUSION

In conclusion, it can be affirmed that peptide:siRNA complexes behave differently from DNA complexes. The dimensional analyses of the LPRs have already provided different information compared to LPD complexes (Section 4.4.1). Here, the data indeed show a much narrower range, while the PDI increases with the rise in peptide concentration.

Electrophoresis experiments have highlighted that the peptide:RNA bond is much less stable compared to DNA, Section 4.4.2. This phenomenon can be attributed to the rigidity of nucleic acids, which influences the binding strength and the number of peptides that bind to the molecule. Larger size, as in the case of DNA, increases structural flexibility, making it easier to package compared to the smaller and more rigid siRNA. Additionally, electrophoresis gel, as well as the PicoGreen test, has shown that the presence of lipid (DOTMA:DOPE) is ineffective for complex formation. This is significantly different from results obtained in the same experiments with DNA (Section 4.4.1 and 4.4.2). In this case, the size of siRNA is crucial; it can vary between 19 and 23 nucleotides, and the reduced sequence may facilitate complexation, despite the rigidity of the two counterparts (branched peptide and siRNA), making the lipid unnecessary.

This pattern can also be recognised in transfection. The presence of the lipid (LPRs) does not show any improvement in nucleic acid internalisation. Moreover no reductions in N-Cadherin are observed in SKBR3 and MDA-MB-231 cells.

The results indicate that peptides, particularly RGen3K and TGen3K, have an effect on the number of cells. As can be observed, the cell count is significantly lower compared to other cells (e.g., Herceptin). Therefore, since the variation in cell count occurs both in the presence of TRPM8 siRNA and control siRNA, the effect can be attributed to the structure of

the peptide itself. This behaviour could be associated with the Caspase 3 pathway, as described in Chapter 3.3.2. The same effect is observed even in the presence of a small amount of lipid (DOTMA:DOPE).

On the contrary, the peptide carrying the scrambled sequence has no effect on the cell count, which is in contrast to what was observed in pDNA transfection (Section 4.4.4).

Although there isn't a significant effect of siRNA on proliferation, it may still be necessary to determine the release capacity of the PRs complex when encapsulated in microparticles, which could alter its stability or potentially trap it, nullifying its protective effect.

Microparticles can serve as an initial vector to protect molecules that are easily degraded due to their size or susceptible to protease activity due to their structures. Alginate microparticles can protect PRs and release them into the extracellular environment, maximising the quantity of released product, and subsequently overcoming further cell barriers. The next chapter will study various methods for microparticle preparation and their PRs release rate.

PREPARATION OF MICROVECTORS

1.1 INTRODUCTION

In recent years, there has been a significant revolution in the field of microfluidics, resulting in advancements in the manipulation, analysis, and control of small fluid volumes. This progress has been made possible by the development of new materials, manufacturing techniques, and microfluidic systems, enabling precise and accurate activities in various fields such as chemistry, biology, physics, and engineering [345].

Particularly in the pharmaceutical industry, microfluidics has seen incredible growth, benefiting various aspects. One example is the development and screening of new drugs. Thanks to this technology, the effectiveness and toxicity of new molecules can be rapidly and accurately tested, effectively screening potential pharmaceutical candidates [346]. Additionally, microfluidics can be used for the preparation of new drug formulations and delivery systems that protect "delicate" drugs such as proteins and nucleic acids. It can also be employed for the customisation of medicines tailored to individual patients, addressing genetic diseases or cancer treatment. Finally, in the diagnostic field, it can quickly analyse biomarkers and select the appropriate treatment for a patient's condition [347].

The field of microfluidics was born due to a gradual miniaturisation of systems and the need for greater control over very small volumes. On the one hand, microelectronics development was vital for the birth of microfluidics. In fact, in the 1950s Werner Jacobi, a German engineer, and a few years later Geoffrey Dummer, a British scientist, developed the Integrated Circuits (CI) commonly called Chips. These were part of semiconductors made up of Germanium but were later replaced with

silicone, thus becoming the basis for modern technology. Moreover, in the early 1950s in the United States the evolution of microelectronics was possible thanks to the invention of photolithography, which allowed the miniaturisation and integration of thousands of transistors on semiconductor wafers, mainly silicon wafers, producing smaller and smaller semiconductors and chips still used in the medical field [348].

On the other hand, the origins of microfluidics are also found in microanalysis methods such as: gas chromatography, HPLC (high pressure liquid chromatography) and capillary electrophoresis that arose around the 1950s and 1960s. These systems made it possible to separate, detect and identify the concentration of molecules effectively and accurately with reduced time and cost [349]. Understanding the enormous potential, an immediate effort was made to produce increasingly efficient and compact systems. This was possible during the 1980s thanks to the production of the first device containing mechanical microelements integrated into a silicon wafer. The new types of devices called MEMS (Micro Electro Mechanical Systems) were engaged in biology, chemistry and biomedical in the 1990s. These applications had to control the movement of liquids in micro-channels and contributed significantly to the development of microfluidics [350].

Today microfluidic devices have microchannels with a very small and precise internal structure, they can be made up of different materials, and allow to obtain extremely repeatable and controllable conditions for the preparation of microparticles.

1.1.1 Microfluidics Advantages

Microfluidic progressing gives life to new perspectives for gene therapy and gene delivery, offering a tool focused on the automation of the experiments and centred on the efficiency of results (Figure 0.1).

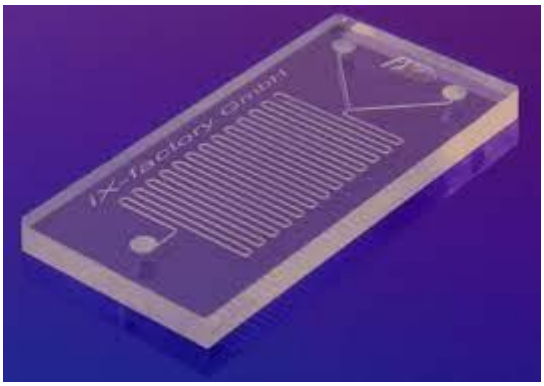

Figure 0.1 Microfluidic chip. https://www.nsmedicaldevices.com/analysis/microfluidics.

Microfluidics, an innovative and still developing field, involves systems that process and manipulate small quantities of fluid using channels of micrometric size. This is precisely the peculiarity that differentiates it from conventional fluid dynamics theory. The validity of the continuity approximation, even on a microscopic scale, allows to exploit the principles of classical fluid mechanics for the study of microfluidic devices. This approximation is very important from the computational point of view, as it allows to analyse only the average values of the parameters that characterise the motion of a fluid, thus neglecting the more complex interactions between the molecules of the fluid itself, present in the formulation of Navier Stokes [351]. In detail, the limited dimensions of the channels involve a dynamic fluid determined by laminar motion, described as a regular, predictable and swirls free flow system. In other

words, thanks to microfluidics it is possible to finely control the concentration and transport of molecules in space and time. This enables the control of very small amounts of samples and reagents (so also reducing manufacturing costs, waste and reduced analysis time) [352].

1.1.2 Droplet-based microfluidics

Droplet-based microfluidics is a technique used to manipulate fluids in microscale channels. It involves mixing immiscible or partially miscible fluids in junctions within the channels to generate microdroplets [353]. This approach offers advantages such as precise control over experimental conditions, resulting in monodisperse and repeatable droplets. The droplets created in this technique can act as microreactors for various physical, chemical, or biological reactions. Due to their small volume (nanolitres to microlitres), they require minimal amounts of reactants.

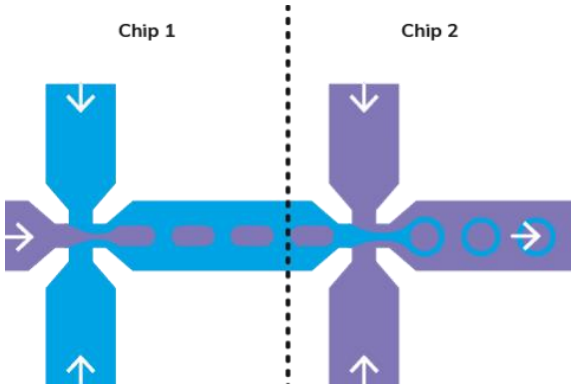

Figure 0.2 Chip 1 on the left where simple emulsion is formed. In the second chip droplets are covered by another phase for the preparation of a double emulsion. From https://www.dolomite-microfluidics.com/applications/double-emulsions/.

Additionally, the ability to generate identical droplets enables multiple experiments to be performed, allowing for reliable statistical analysis of the data [353,354].

In droplet-based microfluidics, a continuous fluid and a dispersed fluid are injected separately and mixed at a junction (Figure 0.2) [355]. The properties of the fluids, including density, dynamic viscosity, and surface tension between the two fluids, along with the flow velocities and channel dimensions, influence droplet formation. Fluid dynamics in this context can be characterised as follows:

1. The Reynolds number (Re) Re values expresses the ratio between inertial forces and viscous forces. Depending on the value of the Reynolds number, a distinction is made between laminar and turbulent regimes.

$$Re = \frac{(vD\rho)}{\mu}$$

*v=flow speed [m/s]
*D=diameter [m]
*ρ=density [kg/m^3]
* μ=viscosity [Pa·s]

   At a macro scale, Reynolds numbers higher than 2000 indicate turbulent flow. In microfluidic systems, the flow is entirely laminar, and there is no mixing between neighbouring flows flowing side by side within the same hollow channel.

2. The capillary number (Ca) compares shear stress to interfacial energy.

$$Ca=(\mu_C v_C)/\gamma_{CD}$$

It is calculated using the continuous fluid's viscosity (μ_C), flow velocity (v_C), and the interfacial energy (γ_{CD}) at the interface between the continuous and dispersed fluids.

By understanding and controlling these fluid dynamics parameters, droplet-based microfluidics can effectively generate and manipulate droplets for various applications [356–358].

A significant boost for microfluidics occurred during the COVID-19 pandemic in 2020. Notably, companies like Moderna and Pfizer chose microfluidic preparation for encapsulating the mRNA used in vaccines. Nucleic acids such as mRNA, siRNA, and DNA are utilised in gene therapy and as therapeutic agents in vaccine development. Messenger RNA-based vaccines gained importance due to their ease of production and better immunogenic response. However, negatively charged mRNA molecules require carriers for delivery and protection from enzymatic activity during transportation. Various carriers like nanoparticles, liposomes, polymer complexes, micelles, and cationic peptides have been developed for mRNA vaccine delivery.

Pfizer's mRNA vaccines are lipid nanoparticles (NPs) with encapsulated mRNA. Lipid NPs (LNPs) serve as delivery vehicles and protect mRNA from degradation. The production process involves using an impingement jet mixer (IJM), Figure 0.3, to mix lipid solvent solution with mRNA solution under high pressure (Figure 0.4).

Figure 0.3 Impingement Jets Mixing for the production of Lipid Nanoparticles (LNP). https://www.dksh.com/th-en/products/ins/knauer-impingement-jets-mixing-skids .

Pfizer scaled up production by replicating quarter-sized mixers and achieving parallelisation of 100 static mixers, allowing the synthesis of 100 million vaccine doses per month. Automation ensures precise control over flow rates and pressure. The scalability of the IJM design is crucial for pharmaceutical manufacturing during pandemics like COVID-19.

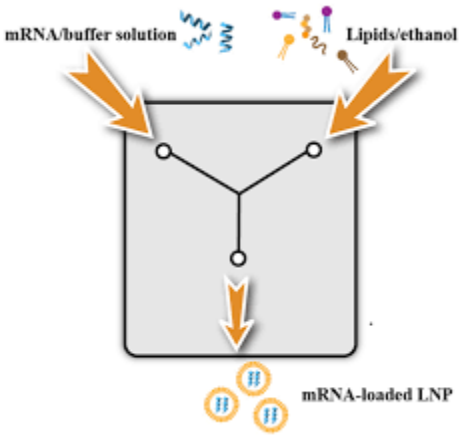

Figure 0.4 Refiguration of microfluidics chip for the preparation of LNP, where lipids and the cargo (nucleic acid) are mixed together to have LNP as results [359].

The success of Pfizer's mRNA vaccine represents a milestone for mRNA vaccines, microfluidics, and nanomedicines, demonstrating the feasibility and versatility of microfluidics in producing nanomaterials for drug delivery.

In summary, microfluidics offers numerous advantages in the pharmaceutical industry, including accuracy, cost reduction, and the handling of extremely small volumes. This allows for simultaneous screening of multiple molecules, enhancing accuracy. Controlled small volumes reduce susceptibility to result variability, leading to reduced material usage, less toxic solvents, and waste reduction. Microfluidics is becoming an integral part of drug screening and development, not only in small laboratories but also on a large scale within the pharmaceutical industry.

1.2 AIM OF THE CHAPTER

This chapter focuses on the preparation of alginate microparticles, comparing two different techniques: the bulk method and microfluidics.

As discussed previously, microparticles are structures that can be utilised to protect nanocarriers or nucleic acids from the extracellular environment, which can compromise their therapeutic efficacy. Consequently, efforts have been made to improve the preparation of these microstructures, which is not yet optimised. Bulk techniques, in particular, lack control over the formation of microparticles [360].

In this chapter, the bulk technique, previously developed at York University, Toronto (Canada), is compared with the microfluidics technique developed at the University of Brighton (United Kingdom).

For the bulk technique, significant changes were made to enhance the preparation process. These changes included:

- Formulation optimisation to confer biocompatibility to the microparticles.
- Covalent modification of alginate with the peptide RGen3K to introduce positive charges that interact with the negative charges of the polymer, to avoid the gelation by the cation (Ca^{2+}).
- Investigation of various calcium concentrations, which are necessary for alginate polymer gelation but can be toxic to the patient. Lower concentrations below 2% w/v may be favourable for administration and tolerance.

Subsequently, the microfluidics technique was explored. Thanks to the small dimensions of microfluidic chips, better control over microparticle formation is achievable. The first method was chosen to complement the bulk technique. However, various modifications have been made to

increase control, not only over the formation of W/O droplets but also over the subsequent gelation, which can occur both outside the microfluidic chip and inside it.

The optimised technique was then used to assess the release of nanocarriers combined with siRNA (TGen3K:siRNA). It was crucial to determine the release of the nanocarrier during emulsion handling and subsequently during storage in an environment mimicking the bodily conditions.

1.3 MATERIALS AND METHODS

1.3.1 Bulk method developed at *York University*

1.3.1.1 Microparticles preparation

Microbeads of alginate were prepared using Phenol Red (Sigma Aldrich) at a concentration of 3 mg/mL dissolved in a 60% v/v ethanol solution. The Phenol Red solution was mixed with 5 g of AmberChrom resin (Sigma-Aldrich), which had been pre-washed three times with deionised water and then with ethanol. The mixture was then centrifuged at 1500 rpm for 1 minute. After allowing the resin to absorb the dye, the water/ethanol solution was removed, and the mixture was added to a 4% w/v sodium alginate solution (ThermoScientific). The entire mixture was stirred for 30 minutes under magnetic agitation. The compound was transferred into a syringe, and the droplets were extruded using an 18 G needle, onto a bath of 2% w/v calcium chloride solution maintained under constant magnetic agitation during the extrusion process. MPs were subsequently analysed using ImageJ software, where three measurements were taken for each granule using a ruler.

1.3.1.2 Alginate Functionalisation

The alginate was functionalised with the peptide RGen3K. To achieve this, a 0.1 M MES buffer at pH 6.5 was prepared, in which the alginate was dissolved to a final concentration of 1 mg/mL. Similarly, the dendron was dissolved in the MES buffer with a concentration of 1 mg/mL. The dendron solution was stirred on a magnetic stirrer for 15 minutes, and then EDC (N-(3-Dimethylaminopropyl)-N'Ethycarbodiimide hydrochloride) 4 mM and NHS (N-Hydroxysuccinimide) 10 mM were added and stirred for 30 minutes.

After the addition of β-Mercaptoethanol to neutralise the excess EDC, the dendron-containing solution was added to the alginate solution in a 1:1 volume ratio. The final solution was stirred for at least 3 hours at room temperature. At the end of the process, Hydroxylamine-HCl (5/10 mM) was added to the solution, purified through an ultrafiltration spin column (MWCO 100,000), lyophilised, and stored at -20° C.

1.3.2 Microfluidics technique

1.3.2.1 Out-of-chip Gelation

The microbeads prepared using microfluidics were obtained from a mixture of 0.3 mg/mL Phenol Red and 2% w/v Na-Alginate, which was kept under magnetic agitation overnight to ensure complete polymer dissolution. Subsequently, the mixture was filtered using a 0.2 µm filter to prevent chip clogging during microfluidic processing. The oil phase, necessary for droplet formation within the chip, consisted of mineral oil.

The microfluidic chip (DG-DM-35, Droplet Genomics, Figure 0.5) used for the preparation of water-in-oil (W/O) emulsions had a T-junction structure, where the central channel was designated for the alginate (aqueous phase), while the two lateral arms carried the oil phase. The pressures used

were 200 mBar for the aqueous phase and 700 mBar for the oil phase (Figure 0.6). The flow controller was OB1 and the software to control the pressure was ElveFLow Smart Interface from ElveFlow System. Picture were taken thanks to the high speed camera from Photron FastCam Viewer 4 (frame rate: 2000 fps; shutter speed: 1/frame second), connected to the Nikon TE2000-U microscope.

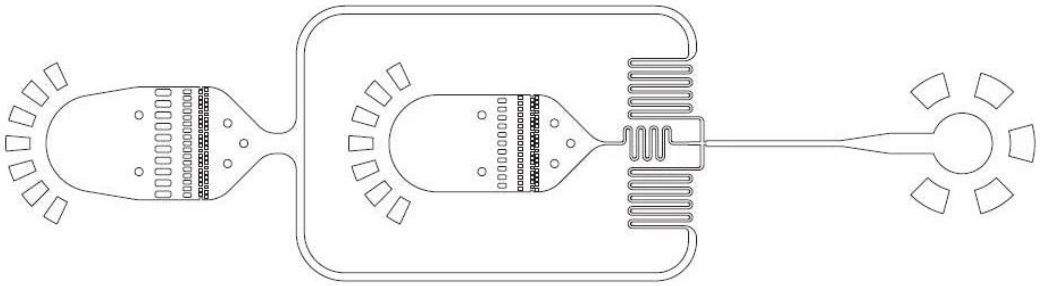

Figure 0.5 DG-DM-35 microfluidic chip from Droplet Genomics.

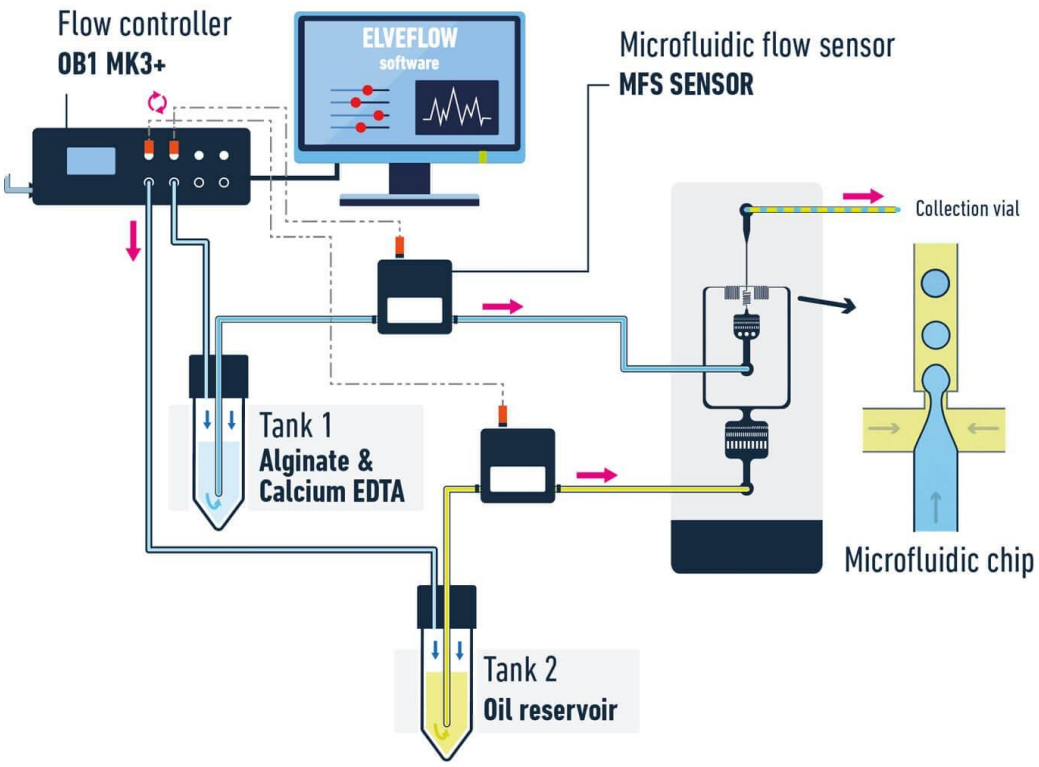

Figure 0.6 instrument set up for the OFF- chip microfluidics gelation. From ElveFLow.com

The gelation of the droplets occurred outside the chip, where they were dropped into a 2% w/v calcium chloride solution. This external gelation process facilitated the crosslinking of the alginate, resulting in the formation of solid microbeads. Microparticles size was then analysed with Mastersizer 3000.

1.3.2.2 In-chip Gelation

Microbeads obtained through microfluidics were prepared from a mixture of 0.3 mg/mL Phenol Red, 2% w/v Na-Alginate, and 0.05 M Ca-EDTA (Sigma Aldrich). The mixture was kept under magnetic agitation overnight

to ensure complete polymer dissolution and then filtered using a 0.2 µm filter to prevent chip clogging during microfluidic processing.

The first oil phase consisted of mineral oil and 5% v/v Span 80 (Sigma), while the second oil phase had the same composition enriched with 0.05% v/v CH_3COOH (acetic acid).

The microfluidic chip used for the preparation of water-in-oil (W/O) emulsions was a custom chip from Droplet Genomics (Figure 0.7), made of PDMS. It featured a double junction structure designed and studied by Håti et al. [361].

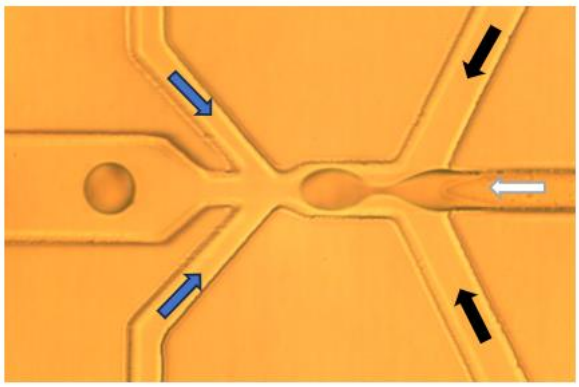

Figure 0.7 Second chip design. The white arrow shows the alginate flow. Black arrows highlight the first oil phase (mineral oil and span 80). The blue ones refer to the secondary oil phase enriched with acetic acid.

The central channel was designated for the aqueous phase, while the lateral arms carried the oil phase. The pressure used was 200 mBar for the polymer phase, 600 mBar for the first aqueous phase, and 100 mBar for the second oil phase. The flow controller was OB1 and the software to control the pressure was ElveFLow Smart Interface from ElveFlow System. Picture were taken thanks to the high speed camera from Photron FastCam

Viewer 4 (frame rate: 2000 fps; shutter speed: 1/frame second), connected to the Nikon TE2000-U microscope.

1.3.2.3 Oil Removal

To remove the oil phase, the microbeads were centrifuged at 3000 rpm for 5 minutes to achieve an initial phase separation. Subsequently, the top layer of oil (above the aqueous phase) was removed, and 1 mL of isopropyl alcohol was added to facilitate the complete removal of mineral oil. The process was repeated twice. Finally, 1 mL of dH_20 was added twice to wash microparticles and remove the alcohol as well. At the end of the process, it was possible to completely remove the aqueous solution and leave the microbeads to dry.

1.3.2.4 Microparticles Characterisation: Mastersizer

Following the removal of the oily phase, the instruments were cleaned with ethanol and then with water a couple of times. Each sample was dissolved in deionised water and measured five times at 25° C, and the average size was calculated. The polydispersity index (PDI) indicates the homogeneity of the population present in the sample.

1.3.2.5 SiRNA Encapsulation

6.3.2.5.1 Calibration Curve

A calibration curve was generated. Complexes of siRNA and TGen3K (charge ratio 1:10) were prepared at a final concentration of 1.6 µg/ µl in 1000 µl. The sample was then analysed using a spectrophotometer to obtain the spectrum. Subsequently, diluted samples were prepared to achieve five different concentrations as shown in Table 0.1. A diluted

sample was then analysed using a spectrophotometer at a fixed wavelength to determine their absorbance values. Then all the concentration are analysed at λ=252 nm.

Table 0.1 Dilutions for the calibration curve of siRNA complex. Final volume 1000 µL

siRNA (µL)	**Quantity of purified water (µL)**	**TGen3K (µL)**	**Quantity of Purified Water (µL)**	**+ 900 µL of purified water**
Total volume 50 µL		Total volume 50 µL		
1.6	48.40	8.11	41.89	
1.28	48.72	6.49	43.51	
0.96	49.04	4.87	45.13	
0.64	49.36	3.24	46.76	
0.32	49.68	1.62	48.38	
0	50	0	50	

6.3.2.5.2 Microparticles Preparation Encapsulating The Nucleic Acid

Microfluidics was employed to fabricate microbeads using a mixture composed of 2% w/v Na-Alginate, and 0.05 M Ca-EDTA. To ensure complete dissolution of the polymer, the mixture was subjected to overnight magnetic agitation and subsequently filtered through a 0.2 µm filter to prevent chip clogging during microfluidic processing. The siRNA was then complexed with TGen3K at a final concentration of 1.6 µg/mL, with a charge ratio of 1:10 and added to the alginate solution.

Two oil phases were: the first containing mineral oil and 5% v/v Span 80, and the second enriched with 0.05% v/v acetic acid (CH_3COOH).

The microfluidic chip used for generating water-in-oil (W/O) emulsions was a custom PDMS chip from Droplet Genomics. It featured a double junction structure, as previously described and studied by Håti et al. [361]. The central channel was dedicated to the aqueous phase, while the oil phase was carried in the lateral arms. The pressure applied during the process was 200 mbar for the polymer phase, 600 mbar for the first aqueous phase, and 100 mbar for the second oil phase. Finally, during and at the end of the oil phase removal process, 100 µl samples are collected and diluted in 900 µl, then analysed using a spectrophotometer (λ=252 nm) to determine the amount of nucleic acid released from the microparticles.

6.3.2.5.3 Sirna

After that, dendron complexed with siRNA was mixed with the alginate, thus, droplets are formed and gellified inside the chip, described in Chapter 6.3.2.2. Thus, PRs solubilised in alginate are initially shaped into droplets and then gellified through the presence of acetic acid. Then were collected at the end of the outlet channel. The final compound consists of two phases: the aqueous phase containing the beads and the oily phase that needs to be completely removed to avoid inducing toxicity in the patient. After each centrifugation step following the addition of water to wash the cells, 100 µl of the supernatant containing the microbeads are collected. The withdrawal happened after 2 hours and 24 hours from the end of the microparticles washing step. Then, the 100 µl samples were diluted in 900 µl of dH_2O to obtain a final volume of 1 mL, and the sample is analysed using a spectrophotometer at a wavelength of 252 nm.

1.4 RESULTS AND DISCUSSION

1.4.1 Bulk Method

The bulk method of extrusion is a technique used for the production of microparticles or microbeads. In this method, a polymer solution or suspension containing the desired drug or active ingredient is extruded through a small orifice or nozzle. Generally, the technique involves the preparation of the biocompatible polymer solution or suspension by its dissolution or dispersion in an aqueous medium. Polymer solution or suspension is loaded into a syringe or extruder system and forced through a small orifice or nozzle under controlled pressure, resulting in the formation of droplets. Finally, as droplets exit the nozzle, come into contact with a crosslinking agent or a coagulation bath which triggers the solidification or gelation process, leading to the formation of solid microbeads.

Microparticles were enriched of an ionic resin to enhance the retention of negatively-charged molecules within the alginate beads over an extended period. Specifically, red phenol dye, a negatively-charged molecule, was utilised for monitoring the controlled release of similarly charged small molecules from microcarriers and to determine the pH by its changing in colour.

Preliminary results in the presence of resin and high concentrations of Phenol Red (3 mg/mL) and Na-Alginate (4% w/v) led to the formation of beads with a cylindrical shape rather than the spherical shape depicted in Figure 0.8 and Figure 0.9. This distortion of the beads was caused by the high viscosity of the suspension, resulting from the high concentration of the alginate polymer. Additionally, the presence of the ion exchange resin may have contributed to increased resistance to movement. For this reason, it was necessary to use a needle with a large diameter (18 G).

Figure 0.8 Extruded microbeads with high concentration of Alginate (4% w/v) in presence of the ionic exchange resin. In the centre, the microparticles took on a blue/purple colour because they were wetted by a basic solution. Yellow circle indicates the beads treated at different pHs and showing different intensity of red.

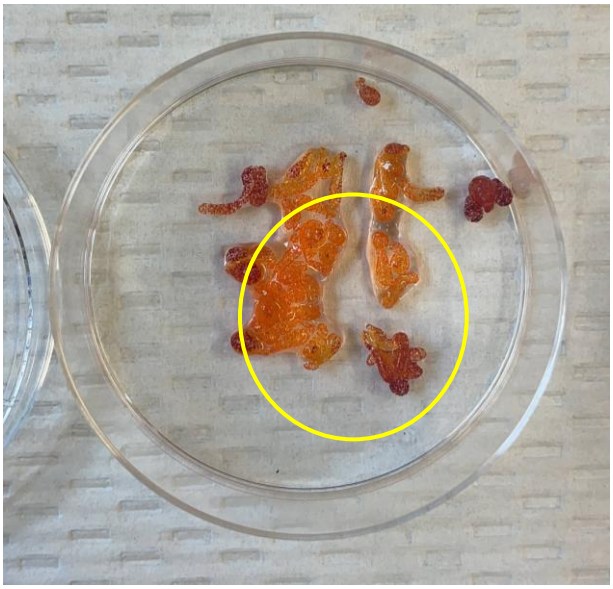

Figure 0.9 Extruded microbeads with high concentration of Alginate (4% w/v) in presence of the ionic exchange resin. Microparticles took on a red/orange colour because they were wetted by acid solution. Yellow circle indicates the beads treated at different pHs and showing different intensity of red.

In Figure 0.8 and Figure 0.9, it is also possible to observe the reactivity of the dye (Phenol Red) at different pH levels. In an acidic environment, the resin, which absorbed the Phenol Red and is seen as small crystals, takes on red/orange colours. On the other hand, in a basic environment with a pH higher than 8, the crystals assume colours that tend towards purple. This indicates the tendency of the gellified polymer to absorb water from the outside while simultaneously preventing the release of the dye. As seen in the Figure 0.8, the dye forms small crystal aggregates (bound to the resin) that remain trapped within the cross-linked structure of the Alginate. Firstly, the protocol was modified to prepare microbeads suitable for local injection for the treatment of HER2 breast cancer, thus biocompatible. Secondly, the goal was to reduce the size of the microbeads. To overcome the difficulties in microparticle formation and in an attempt to reduce their size, some modifications were made to the original protocol established at the York University, Toronto, Canada.

First of all, it was necessary to avoid the use of ethanol to prevent the presence of alcohol molecules in the final preparation. Therefore, the concentration of Phenol Red in the preparation had to be reduced. Its maximum concentration in an aqueous solvent is 3 mg/mL, and a 60% v/v alcoholic preparation was necessary for the complete dissolution of the dye. The chosen concentration for optimal dissolution without ethanol was 0.3 mg/mL. Additionally, since the viscosity of the preparation was primarily due to the alginate polymer, two reduced concentrations of 1% and 2% w/v were selected.

Furthermore, for reasons related to the preparation of biodegradable and bio-erodible microbeads, it was necessary to eliminate the presence of the ion exchange resin. On Table 0.2 is outlined all the experiments conducted to determine the optimal concentration of Phenol Red and to

highlight the difference between preparations with and without ion exchange resin (Figure 0.10).

Table 0.2 Below is an outline of the experiments conducted to determine the optimal concentration of Phenol Red and to highlight the difference between preparations with and without ion exchange resin.

	1	2	3	4	5
Phenol Red Dilutions	1:10	1:100	1:10	1:10	1:100
Resin	-	-	1:10	1:100	1:100
Alginate 2%	+	+	+	+	+

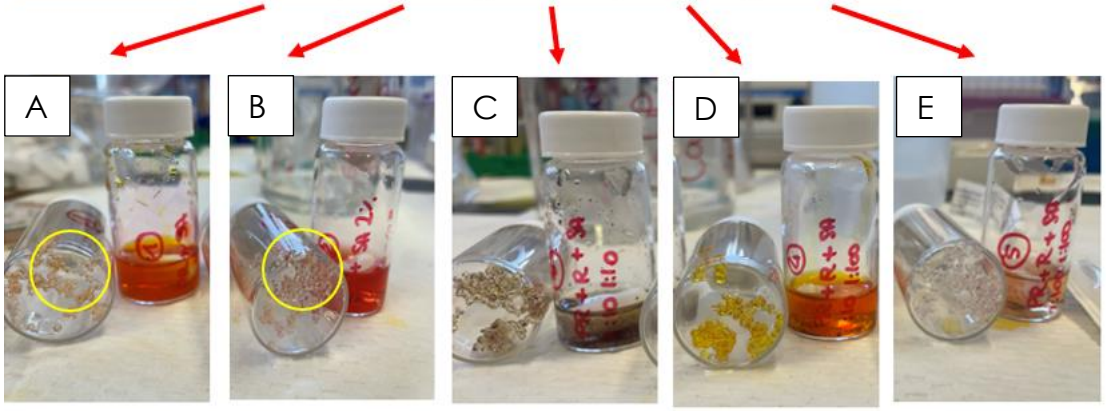

Figure 0.10 Different composition of the preparation of Alginate Microparticles. Yellow circles highlight the retention of Phenol Red because of the resin absence.

As depicted in Figure 0.11 and Figure 0.12, the microbeads, prepared without resin and with a reduced quantity (1:100) of phenol red (Table 0.2-2) exhibit a significantly different appearance compared to the initial preparations. Firstly, reducing the concentration of the dye did not lead to substantial differences in the ability of the particles to change colour in acidic or basic environments.

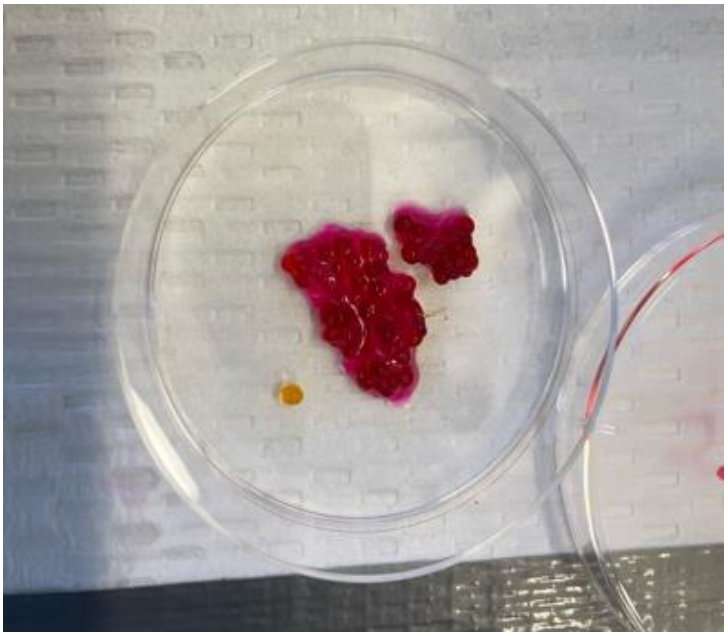

Figure 0.11 Extruded microbeads with high concentration of Alginate 2% w/v in absence of the ionic exchange resin. Microparticles took on a red/orange colour because they were wetted by basic solution.

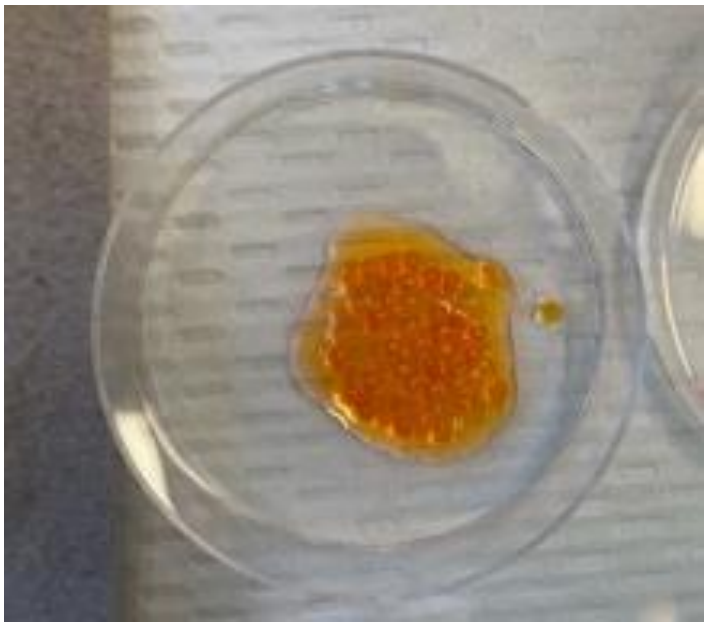

Figure 0.12 Extruded microbeads with high concentration of Alginate 2% w/v in absence of the ionic exchange resin. Microparticles took on a red/orange colour because they were wetted by acid solution.

This implies that the microbeads' capacity to absorb water from the surrounding environment remains unchanged. However, as evident comparing Figure 0.8 and Figure 0.11 or Figure 0.9 and Figure 0.12(a and b) the ability to retain the dye within the alginate matrix is reduced compared to the initial method. Nevertheless, this is not considered a disadvantage of the new microparticles, In fact, they need to maintain the ability to release cargo in order to facilitate their internalisation into tumour cells.

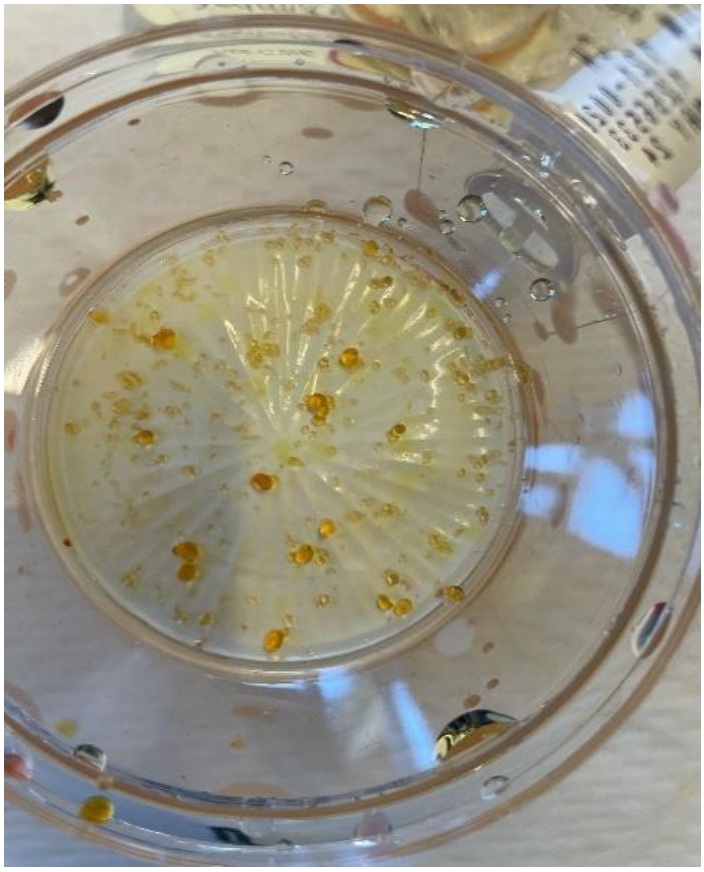

Figure 0.13 Preparation of microparticles without the resin with Phenol Red 0.3 mg/mL and alginate 1% w/v.

Figure 0.14 Preparation of microparticles without the resin with Phenol Red 0.3 mg/mL and alginate 2% w/v.

The morphological aspect has also improved due to the reduced viscosity, allowing for the use of a smaller diameter needle (27 G) and obtaining spherical microparticles (Figure 0.14), although their size is approximately 1 mm. In this case, the size, which is at the limit of the definition of microparticles, can be considered an advantage. Recent studies have suggested that hypoxia in tumor tissue can lead to a lack of essential materials such as oxygen and nutrients from the bloodstream, thus can induce apoptosis [362]. Therefore, microparticles with a diameter

similar to the blood vessels irrigating the tumour, formed due to the formation of new blood vessels (neoangiogenesis), can be used for blocking blood flow [18]. However, this theory has been contradicted as many papers demonstrate that the absence of oxygen leads to the formation of neoangiogenesis, lead the tumour tissue to continue growing, escaping the lack of oxygen [363–365]. It is important to note that the suitable shape of the microbeads is only achieved when the alginate concentration is 2% w/v. When the polymer is not present in sufficient quantities (1% w/v), the microparticles do not maintain their structure and tend to dissolve after 10 minutes from preparation (Figure 0.13 and Figure 0.14).

Once the appropriate percentage of alginate was determined, modified alginate with RGen3K was used. Due to the positive charges carried by the hyperbranched peptide structure, it could gel in the absence of calcium ions. The purpose was to replace the cross-linker with the peptide to reduce traces of calcium in the final formulation, which could induce toxicity in the patient. Therefore, the alginate and Phenol Red droplets were allowed to drip into a bath of physiological solution, required to induce a positive charge on the peptide's surface, facilitating its interaction with the carboxyl group of the alginate chain. As a result, the peptide is capable of substituting calcium ions in the formation of the polymer network.

The pH is a measure of the acidity or alkalinity of a solution and ranges from 0 to 14. A pH of 7 is considered neutral, values below indicate acidity, and values above indicate alkalinity. The physiological pH of the human body is around 7.4. Lysine is a type of amino acid that can have a positive charge when the pH is below their pKa value, which for lysine is around 10.53. When the pH is higher than the pKa value, lysine exists in a neutral form.

The isoelectric point (pI) of an amino acid or molecule is the pH at which the molecule is electrically neutral, meaning it has no charge. In the case of lysine, their pI is 9.74. This means that at a pH lower than 9.74, lysine tends to have a positive charge, while at higher pH values, they are neutral or may have a negative charge.

Alginate only loses a proton (positive charge) when the pH is below 3.5. This means that at physiological pH (pH 7.4), alginate maintains its negative charge.

If an attempt is made to form a network using alginate in a physiological solution (pH 7.4), the negative charges of the alginate may repel each other due to the repulsion of like charges. As a result, it may not be possible to form the network and microparticles.

The formation of the network and microparticles, is probably avoided by the repulsion of negative charges could be one of the factors preventing the formation of the network. The benefits of conjugating poly-lysine and alginate molecules have been recognised in many studies [366].

The process enables the conversion of alginate droplets into completely spherical gel beads and incorporating poly-lysine is essential for creating a semi-permeable membrane with controlled porosity, as well as enhancing the strength and stability of the microcapsule [367]. Furthermore, thanks to the work of Strand et al., it has been demonstrated that the presence of lysine leads to a reduction in the diameter of the microparticles [367]. It is important to highlight that in all studies, alginate is complexed with calcium to form the hydrogel, and only afterwards are the microparticles functionalised on the surface with poly-lysine.

Since the formation of microparticles did not occur, despite the pH being able to activate the surface charges of the peptide, the presence of

calcium in the bath where the droplets are dropped was deemed necessary for gelation.

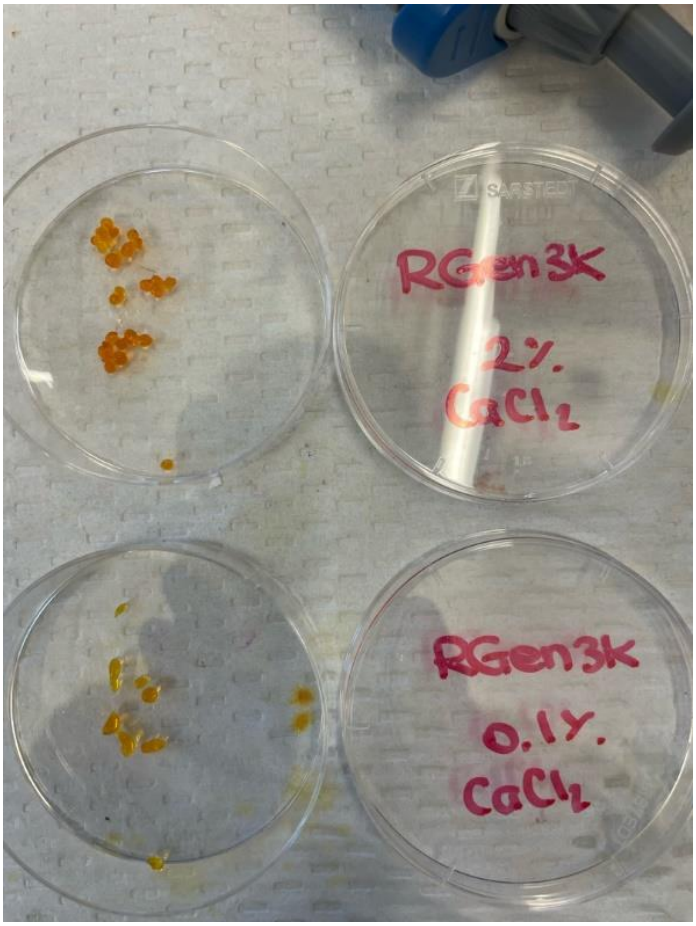

Figure 0.15 On the top left, the functionalised microparticles hardened in Calcium bath 2% w/v. On the bottom left, the functionalised microparticles gellified in 0.1% w/v $CaCl_2$ bath.

As seen in the Figure 0.15, microbeads achieve an optimal shape only when an appropriate concentration of calcium is reached. Furthermore, it can be observed from the darker coloration that with a higher concentration of calcium chloride, it allows for better retention of phenol red.

1.4.2 Microfluidics

Microfluidics was chosen because there was a need to reduce the size of the microparticles. As previously explained (Section 6.4.1), microparticles with a diameter similar to that of blood vessels would allow for the obstruction of nutrient flow to the tumor mass, thereby halting its growth and proliferation. As demonstrated, the diameter of tumor blood vessels ranges from 50 µm to 80 µm [368], and consequently, the sizes obtained through bulk techniques are inadequate for this purpose.

1.4.2.1 Out-of-chip gelation

Out-of-chip gelation refers to a process in which the formation of microdroplets occurs within a chip, while the solidification of the external structure (shell) takes place outside the chip in a bath of calcium chloride [369]. As shown in Figure 0.16, the internal structure of the chip is referred to as flow focusing, and the droplet formation happens when the force of the oil phase disrupts the flow of the aqueous phase.

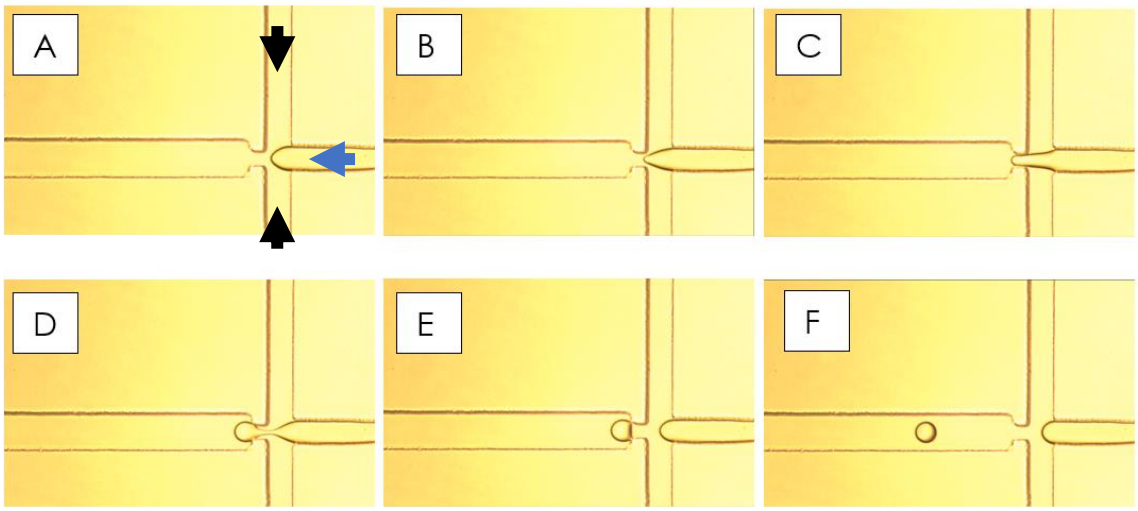

Figure 0.16 Flow focusing chip and alginate microparticle formation (out-of-chip gelation). Microfluidic chip DG-DM-35, Droplet Genomics.

In this case, the aqueous phase, consisting of 2% w/v Na-alginate and 0.3 mg/mL Phenol Red (indicated by the blue arrow in Figure 0.16, is in the centre, while the oil phase, initially composed of mineral oil, is in the two lateral arms (black arrows).

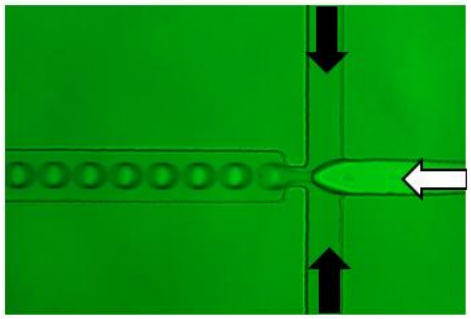

Figure 0.17 Internal structure of the microfluidics chip (out-of-chip gelation). The white arrow shows the alginate flow (inner phase), in black the oil phase (continuous phase).

As can be observed in Figure 0.17, the formation of microdroplets is successful, with minimal variation in terms of diameter and shape. However, towards the outlet channel (Figure 0.18), it is noticeable that the droplets tend to aggregate, forming larger aqueous droplets. Surface tension refers to the inherent property of a liquid that causes it to minimise its surface area and form spherical droplets. Emulsions are unstable colloidal systems that tend to separate through the formation of larger-sized particles.

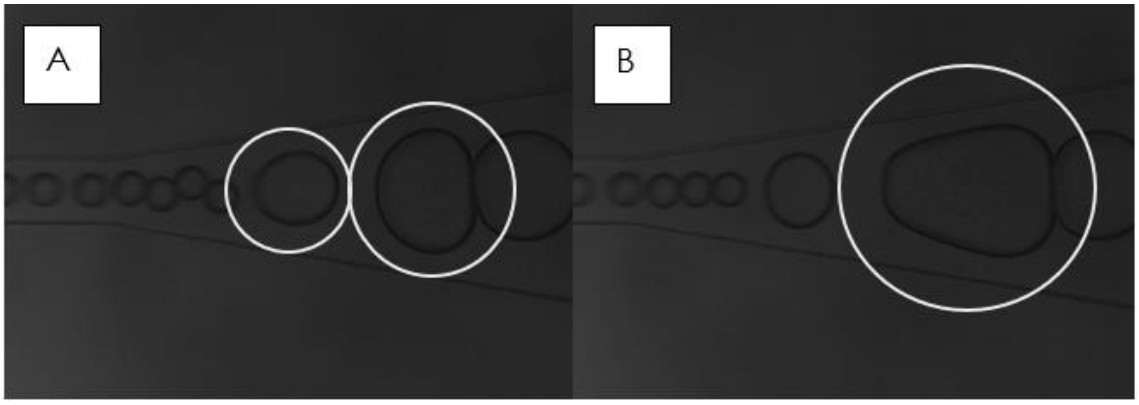

Figure 0.18 Exit chamber of the microfluidics chip (out-of-chip gelation). The white circles (A) show how two droplets fuse together (B) because of the high surface tension.

As mentioned by Chen et al. 2020 "Interfacial tension can be defined as the force per unit length or the excess energy per unit area at a fluid−fluid interface, and it arises from unbalanced cohesive forces between molecules in the two bulk phases. In general, systems with high interfacial tensions tend to separate out or coalesce more easily since higher interfacial energy drives a reduction in the interfacial area" [370].

Thus, high surface energy can lead to the aggregation or coalescence of droplets, as observed in the formation of larger aqueous droplets towards the outlet channel.

To overcome this issue, the addition of a surfactant (Span 80) was required. A surfactant, also known as a surface-active agent, is a compound that reduces the surface tension between two liquids, between a liquid and a solid, or between a liquid and a gas. Surfactants contain both hydrophobic (water-repellent) and hydrophilic (water-attracting) regions in their molecular structure, which allows them to interact with different phases and reduce the interfacial tension between them.

Surfactants are commonly used in various applications, including detergents, emulsions, foams, and pharmaceutical formulations. In the context of microfluidics and droplet formation, surfactants can be added to the fluid to stabilise the droplets and prevent coalescence or aggregation. They work by reducing the surface tension at the interface of the droplets, allowing for the formation of smaller and more stable droplets.

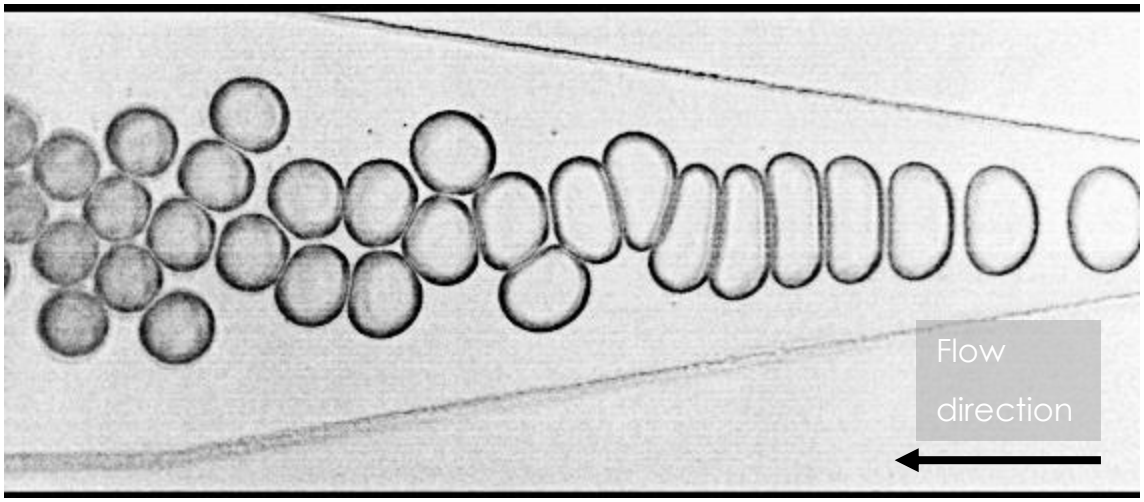

Figure 0.19 Exit chamber (out-of-chip gelation). Microparticles in presence of the surfactant do not collapse together. They deform their shape as the gellification happen outside the chip.

As stated by Oveysi et al. [371] the diminutive droplets were acquired when employing the greatest concentration of Span 80, leading to the generation of smaller hydrogels characterised by a more heterogeneous size distribution. As seen in Figure 0.19, the presence of the surfactant reduced high surface tension and promoted the formation of more stable and uniform droplets. The surfactant interacted with the interface between the aqueous phase and the oil phase, reducing the cohesive forces between water molecules and facilitating droplet dispersion.

However, within the same study, (Oveysi et al.) it is also asserted that the surfactant Tween 80 produces more uniform microparticles. Therefore, it would be interesting to replicate the experiments using Tween 80 instead of Span 80.

1.4.2.2 In-chip gelation

In-chip gelation is the process in which the formation of droplets and their solidification occur simultaneously within the microfluidic chip. The first attempt was to gel alginate with calcium chloride. Therefore, a chip with a first Y junction was used in which alginate and calcium chloride were mixed, a second junction (flow focusing) in which microparticles were formed thanks to the oil phase. However, calcium chloride (2% w/v) gave an instantaneous reaction with alginate, causing a swift jellification and therefore chip blockage.

Later, the aqueous phase consisted of Na-Alginate and Ca-EDTA. Since calcium ions are sequestered by EDTA, they cannot directly interact with alginate and induce polymer hardening. Therefore, an activator is required to release calcium from the chelating agent and allow it to form a coordination bond with the biodegradable polymer. As described by Håti et al. [361], pH variation can be exploited for this purpose. Thus, CH_3COOH (acetic acid) was used to trigger the release of calcium from the chelator and promote the formation of the shell on the surface of the microparticles towards the chip's outlet channel.

It is important to have an appropriate concentration of Ca-EDTA and CH_3COOH. A high amount of acid and Ca-EDTA can lead to rapid gelation of alginate, potentially causing blockages within the chip. The concentration of 0.5% v/v acetic acid and Ca-EDTA 0.5 M were found to

be too high, where the formation of microbeads is difficult, and the chip becomes blocked shortly after.

To address this issue, the concentration of acetic acid and chelated Calcium was reduced by a factor of 10. As depicted in Figure 0.20, a concentration of 0.05 M is already sufficient to initiate the formation of the shell within the microfluidic chip's outlet channel.

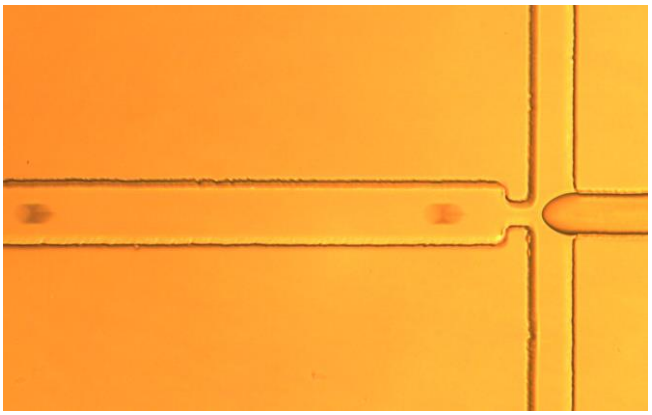

Figure 0.20 Flow focusing chip (out-of-chip gelation). in the central channel: alginate 2% and Ca-EDTA 0.05 M. The oil phase, made by Mineral oil and Span 80, it is enriched with acetic acid 0.05% v/v.

However, despite the modifications to the formulation, the preparation of microparticles is still not optimal. As can be seen in Figure 0.21, at cyclical

intervals, there is the formation of this large microparticles, a process that can increases their polydispersity index.

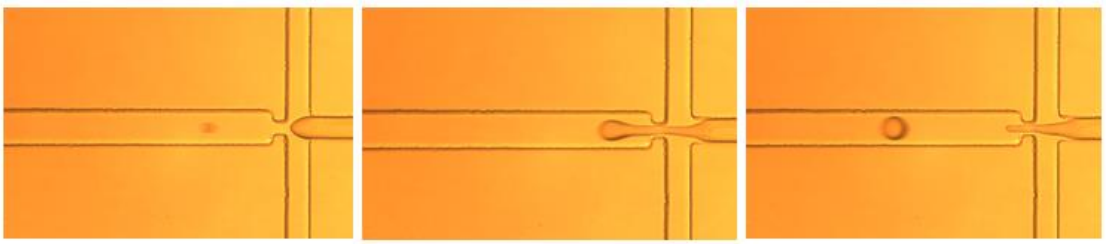

Figure 0.21 No-optimal preparation (out-of-chip gelation). Droplets are formed after the elongation of the neck.

It is known that the microfluidics chip design, can also affect the formation of microparticles. The first configuration (Figure 0.21) featured only three inlet channels: one central channel for the aqueous phase (Alginate and Ca-EDTA) and two channels for the oil phase (Mineral Oil, Span 80, and CH_3COOH). Therefore, a second configuration (Figure 0.22) was chosen presenting five inlet channels: the main channel for the aqueous polymer phase (white arrow), two channels for the oil phase (Mineral Oil and Span 80, black arrows), and two additional channels for a second oil phase that includes acetic acid (Blue arrows).

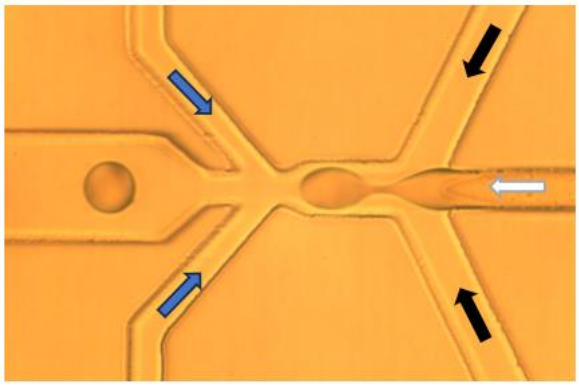

Figure 0.22 Second chip design (in-chip gelation). the white arrow shows the alginate flow. Black arrows highlight the first oil phase (mineral oil and span 80). The blue ones refer to the secondary oil phase enriched with acetic acid.

The second configuration was found to be optimal for microparticle formation (Section 6.3.2.2). This setup likely allowed for the solidification of the microparticles to occur only after the droplets were formed within the mixing chamber.

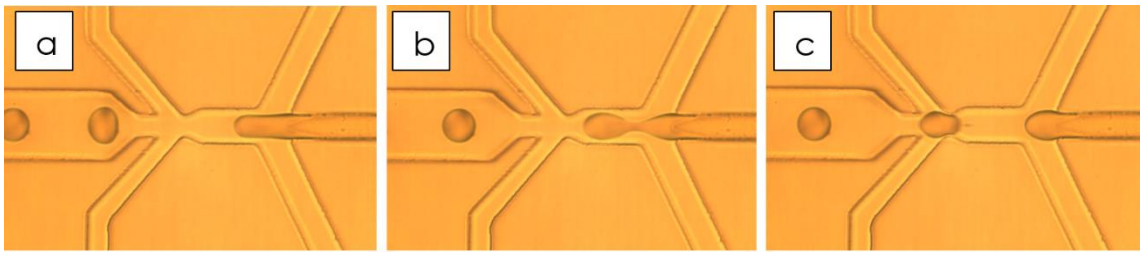

Figure 0.23 Microparticles formation in the second chip design (in-chip gelation).

The simplicity of the first configuration, Figure 0.21, led to a rapid pH change despite the already reduced concentration of acetic acid. As a result, the formation of microparticles was challenging and often caused blockages in the microfluidic chip. The more complex chip, Figure 0.23, let to the formation of the micrometric droplet occurs first, and then it starts to gellify due to the pH change induced by the presence of acetic acid.

The geometry proves to be optimal for the formation and subsequent gelation within the microfluidic chip, thus it can be affirmed that geometry may constitute an essential factor for in-chip gelation.

1.4.3 Oil removal

An important phase for completing the preparation of the microparticles is the removal of oil from the formulation to avoid toxicity at the injection site in the patient.

This method, similar to the one described by Yasmin et al. [372], allowed for the complete removal of oil. However, some difficulties were encountered in maintaining the spherical shape and small size of the microparticles. In both formulations, out-of-chip and in-chip gelation, the samples are collected in Eppendorf tubes, where a first phase separation occurs with water settling at the bottom and oil floating on the surface. Most of the microparticles, despite being aqueous in nature, remain in the oil phase due to the presence of the surfactant that stabilises them. However, in the case of the out-of-chip preparation, microparticles are not solidified, and after the initial centrifugation, they undergo a rapid precipitation in the aqueous phase, which is composed of a 2% w/v calcium chloride solution. As a result, the microparticles often form large aggregates (Figure 0.24).

Figure 0.24 In the yellow circle the clog made after the centrifugation because of the droplets instability.

On the other hand, the in-chip formulation, since the microparticles are already solidified, is not affected by centrifugation, making it much easier to remove the oil phase and wash the microparticles with deionised water.

1.4.4 Characterisation

Size analysis was conducted using ImageJ for the microparticles obtained through extrusion, while the microparticles generated through microfluidics were analysed using the Mastersizer 3000.

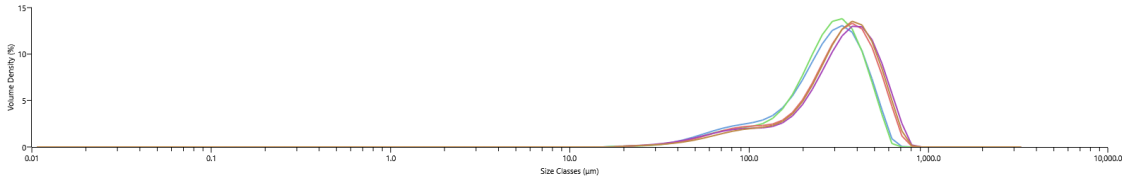

Figure 0.25 Mastersizer 3000 analysis of microparticles prepared with microfluidics chip and hardened outside the chip. Analysis have been repeated five times.

As depicted in Figure 0.25 below, noticeable differences in diameter can be observed for each formulation. In the case of needle-extruded beads, the size exceeded 1 mm (1.09 mm ± 0.05).

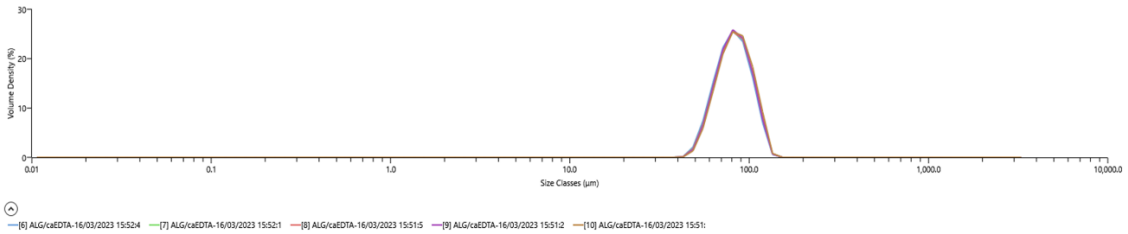

Figure 0.26 Mastersizer 3000 analysis of microparticles prepared with microfluidics flows and hardened within the chip. Analysis have been repeated five times.

However, the size of the microparticles significantly decreased when the alginate was fragmented into droplets using microfluidic flows and subsequently solidified in an external calcium bath. It should be noted that the removal of oil proved to be a complex process, leading to the formation of large alginate clumps. Prior to DLS analysis, filtration was employed to eliminate larger aggregates. Despite this filtration step, the presence of two peaks and thus two populations within the sample preparation can be identified. The obtained sizes averaged at 307±29.1 µm (mean of 5 replicates, Figure 0.25) and PDI is 0.395.

With the preparation of the microparticles and subsequent hardening within the chip, there is a further reduction in size (Figure 0.26). The diameter measures at 82.2 µm, and reproducibility has improved, as evidenced by the lower standard deviation is ± 0.83 and as shown in the graph below.

As can be observed, the graph exhibits a single and uniform population (PDI 0.17). It is important to note that in this case, the removal of oil is much easier, and there was no need to filter the beads to remove clumps as they were not present.

1.4.5 SiRNA Release

First, different concentrations of the dendron:siRNA complex were prepared. One of these concentrations was analysed using a spectrophotometer to determine the compound's spectrum and the peak of maximum absorbance, which was found to be at 252 nm. Subsequently, was measured the absorbance of all the concentrations reported in Figure 0.27

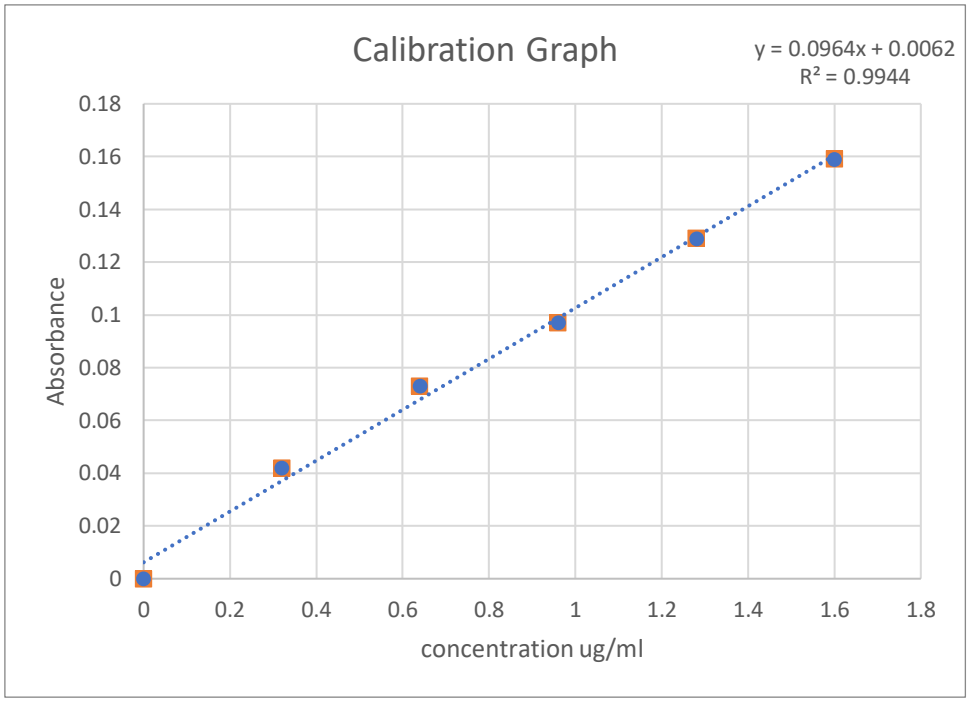

Figure 0.27 Calibration graph of five concentrations of TGen3K:siRNA.

In Figure 0.28, it can be seen the release profile of the TGen3K:siRNA complex following the initial centrifugation steps with water to remove all traces of oil and isopropyl alcohol during the manufacturing phase.

As well as the 2-hour and 24-hour time points after completing the microbeads washing process, shows a simulation of the release of the TGen3K:siRNA complex in a patient.

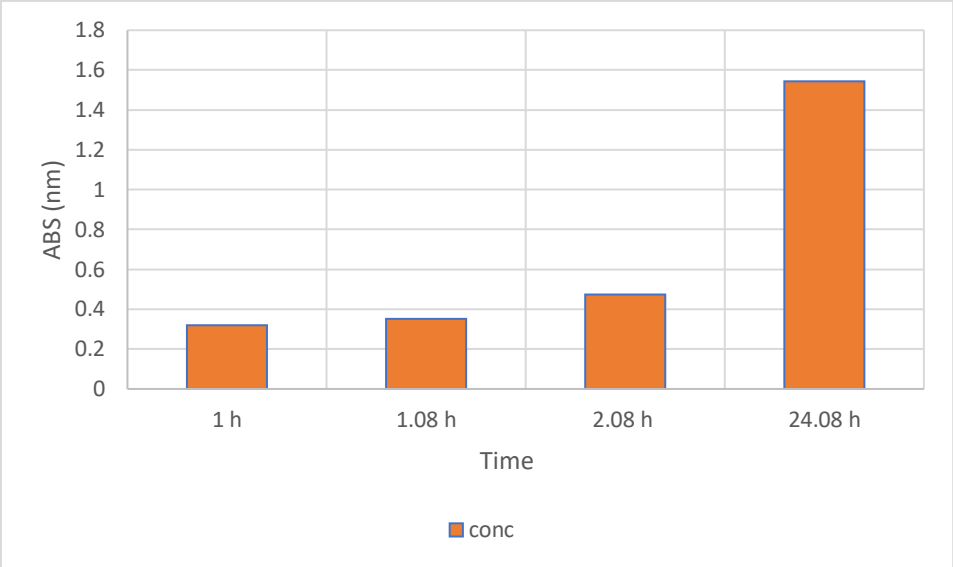

Figure 0.28 TGen3K:siRNA release at different time detected at the spectrophotometer during the manufacturing process

The initial two absorbance readings show a very low value, indicating that despite the washing of the beads, they are stable enough to retain the dendron:siRNA complex. This can be advantageous when considering large-scale preparation in the pharmaceutical field for the development of alginate microparticles that incorporate pharmaceutical molecules. Even at the 2-hour time point after completing the bead washing process, the absorbance value remains low. The highest ABS value, therefore, the highest release of the complex, corresponding to almost the entire complex, occur after 24 hours.

It would be advisable to investigate the release profile of the complex by increasing the number of total sampling points. Additionally, factors such as temperature, pH, and formulation should be considered to evaluate how to modify the release of the complex. These factors can significantly impact the release kinetics and provide insights into optimising the release behaviour of the complex.

1.5 CONCLUSION

In conclusion, in this chapter, three different methods for the preparation of alginate microparticles were compared. The bulk method, after several optimisations, proved to be the least suitable for microbead preparation. On the other hand, microfluidics demonstrated itself as a cutting-edge technology for producing small and uniform beads. However, there is room for further improvement in the technique. As demonstrated, the in-chip preparation yielded significantly better results than the out-of-chip method. These results can be very useful for preparing microparticles with a diameter similar to that of blood vessels, which is crucial for blocking the supply of essential nutrients to the tumor. These microparticles with a diameter of 82 µm could leverage their size to obstruct blood flow to the tumor while simultaneously releasing therapeutic material, creating a synergistic effect in the fight against cancer.

The in-chip gelation technique was then employed for the encapsulation of the vector: siRNA (TGen3K:siRNA) selective for HER2+ breast cancer. The experiments showed that the microparticles are capable of protecting the cargo during emulsion manipulation but tend to release it into the external environment within 24 hours.

GENERAL CONCLUSIONS AND FURTHER WORK

1.1 INTRODUCTION

The overexpression of HER2 usually leads to the malignant transformation of cells and accounts for approximately 25% of all breast cancer cases. It is consistently associated with more aggressive tumor phenotypes, a higher likelihood of lymph node involvement, and increased resistance to hormone therapy [373,374].

While the overall mortality rate for breast cancer has decreased in recent years due to a greater emphasis on early diagnosis, mortality rates for women with aggressive tumors remain high. This is primarily due to the overall complexity of the disease and the lack of safe and effective therapies for these malignant tumors [375]. A key player in breast cancer malignancy is the human epidermal growth factor receptor 2 (HER2). HER2 belongs to the epidermal growth factor receptor (EGFR) family, which includes four major proteins: EGFR (also known as HER1 or ErbB1), HER2 (p185 neu/ErbB2), HER3 (ErbB3), and HER4 (ErbB4) [376]. HER2-positive breast cancers tend to be more aggressive and are more likely to develop resistance to therapy than cancers that do not express HER2. The elevated expression of HER2 on the extracellular membrane of cancer cells, along with its overexpression in both primary tumors and metastatic sites, makes HER2 an ideal candidate for targeted therapies. Therefore, targeted inhibition of HER2 represents one of the most validated therapeutic modalities for treating various human cancers, including ovarian, gastric, bladder, salivary, and lung carcinoma [377].

Trastuzumab (Herceptin®) is a recombinant humanised monoclonal antibody (mAb) directed against the extracellular domain of the HER-2 protein [378]. Although the mechanism of action is not fully understood,

several molecular and cellular effects have been observed in *in vivo* and *in vitro* experiments. Trastuzumab prevents the cleavage of the extracellular domain and the dimerisation of HER-2 by binding to this domain, inhibiting receptor activation and subsequent signal transmission through intracellular pathways such as the phosphatidylinositol 3,4,5-trisphosphate kinase (PI3K) and mitogen-activated protein kinase (MAPK) pathways [379]. This reduction in signalling can lead to receptor internalisation and subsequent degradation. Furthermore, Trastuzumab, in addition to these cytostatic mechanisms, also induces antibody-dependent-cell-mediated cytotoxicity.

The most common adverse effects after the infusion of Trastuzumab (> 10%) include abdominal pain, asthenia, chest pain, fever, headache, diarrhoea, nausea, vomiting, arthralgia/myalgia, and skin rashes. Less frequently (approximately 1-3%), but potentially dangerous, is cardiotoxicity with a reduction in ventricular ejection fraction, especially when the antibody is administered in combination with other chemotherapy drugs [380].

To avoid these adverse effects, new technologies are being developed for the treatment of HER2-positive breast cancer. In this context, nanomedicine studies have been conducted to formulate nanoscale delivery systems capable of carrying drugs and/or diagnostic agents inside tumor cells. The small size of these nanoparticles gives them unique physicochemical and pharmacokinetic properties, such as an extended circulation time in the blood, as they are generally not captured by the reticuloendothelial system. Furthermore, the ability to modify the surface of these nanoparticles, for example, by inserting specific ligands, makes them selective for certain tumor targets, enabling targeted and effective therapies, as well as early diagnosis.

1.2 GENERAL CONCLUSION

1.2.1 Peptide synthesis

In the described project, branched peptides were used for the selective delivery of drugs against HER2-positive breast cancer, while linear peptides were used for the selective recognition of the HER2 receptor. They were synthesised using the solid-phase peptide synthesis (SPPS) technique, as reported in Section 2.3.1. The solid-phase peptide synthesis technique is based on polymer growth starting from a solid support called resin. Thanks to this technique, peptides with few impurities were obtained, as confirmed by high-performance liquid chromatography (HPLC) tests. The successful and complete synthesis was confirmed by Fourier-transform infrared (FTIR) and Mass Spectrometry tests.

1.2.2 Peptides' activity

The peptides were then tested *in vitro* at different concentrations as they have the intrinsic ability to reduce cell proliferation and, as reported by others [381, 382], induce apoptosis, as reported in Section 3.3.2 and 3.4.1. Peptides were tested on two types of cells: control cells defined as triple negative, meaning they do not express oestrogen, progestin, or HER2 receptors (MDA-MB-231); and target cells, which are tumor cells that overexpress the HER2 receptor (SKBR3).

In the case of MDA-MB-231 cells, the tested peptides did not show any significant antiproliferative activity, as reported in Figure 0.3, and no significant differences compared to the negative control (cells in the absence of any drug or peptide) were observed. While the peptides were expected to have an effect on the number of cells as reported by Debnath et al. [255], no differences were observed in this experiment.

However, compared to their studies, it is important to emphasise that the concentrations used were much higher, and the PLL peptides were linear.

Conversely, SKBR3 cells were affected by the presence of the peptides. Indeed, as reported in Figure 0.5, there were drastic reductions in terms of the number of cells. In particular, the target peptide (TGen3K) achieved the best dose-dependent result, similar to the value obtained with Herceptin (positive control). This suggests that the target sequence may have effectively interacted with the HER2 receptor, but it was necessary to have an adequate number of amino acids. In fact, the targeting sequence (-KCCYSL) alone did not yield satisfactory results in terms of cell count. It is argued that the relatively small size of the hexapeptide does not prevent the translocation of the receptor that is instead inhibited by the relatively larger sizes of both the monoclonal antibody Herceptin and by the TGen3K. Furthermore, this experiment highlighted the ability of the hyperbranched peptides to interact with the cell membrane and interfere with cell proliferation. It is important to note that the reduction in the number of cells did not correlate with an induction of toxicity. As indicated by the lactate dehydrogenase (LDH) cytotoxicity test, no signs of cellular intolerance were observed. For this reason, it can be said that the antiproliferative activity prevailed over the apoptotic activity.

1.2.3 Peptides as Carriers

Dendrimers have a 3D structure that allows them to transport drugs, and their chemical and physical characteristics can be modified to adapt to the cargo's requirements. Additionally, due to the numerous positive charges provided by primary amines, dendrimers can readily complex with negatively charged nucleic acids [383].

Nucleic acids can be classified into various types, including DNA, plasmid DNA, siRNA, microRNA, mRNA, and others. Generally, the aim is to internalise nucleic acids to modulate the synthesis of proteins responsible for a disease or carcinogenic development [384]. However, there are several barriers, both systemic and intracellular, that complicate the effective delivery of nucleic acids. These barriers arise from the immune system's defence mechanisms, which recognise nucleic acids as pathogen. To address these concerns, various carriers have been designed to protect nucleic acid-based cargoes from the extracellular environment [385].

In this thesis, branched peptides were used to increase the percentage of transfected nucleic acids within cells. Different results were obtained depending on the type of nucleic acid complexed.

1.2.3.1 Peptides Complexed with DNA

Peptides were complexed with DNA, and the complexes were characterised by analysing their size and binding strength. Subsequently, they were transfected into cells.

Regarding the size, when the peptide is conjugated to DNA and lipid, it fluctuates between 50 and 200 nm; however, there is a significant reduction in size, especially when considering RGen3K. The PDI is also halved, dropping from 0.417 and 0.465 to values around 0.2/0.25.

Then, gel electrophoresis and complexation with PicoGreen were conducted to assess the complex stability. DNA complexes with peptides (PDs) at various concentrations were prepared, and the results were compared with the same complexes in the presence of a small amount of lipids. It was observed that branched peptides were more effective at compacting DNA strands compared to their linear counterparts. This behaviour may be attributed to the different spatial arrangements

between linear and branched peptides. The branched peptides allow for better exposure of positive charges, leading to improved binding with the negatively charged DNA.

Furthermore, the presence of lipids, such as DOTMA:DOPE, altered the nucleic acid binding. As shown in Figure 0.7, the presence of lipids weakened the DNA complexation ability. However, this weakening of the bond should not necessarily be considered negative. On the contrary, in the transfection experiment with pDNA (gWIZ-Luc), the presence of lipids was necessary to enhance the transfection capacity of the complex. This is because, as reported by Zuhorn et al. 2005 [386], the lipid helper (DOPE) is required to facilitate endosomal escape. It is known that poly-lysine peptides do not have tertiary amines capable of disrupting endosome membrane and subsequent release of exogenous material into the cytoplasm. Therefore, the action of the lipid helper is necessary, as it weakens the endosomal vesicle membrane, increasing the amount of material released into the cytoplasm. In the case of SKBR3 (HER2+) transfection, the selectivity of the targeting sequence towards the HER2 receptor was also evident, but the transfection values of TGen3K were surpassed by the SGen3K peptide. As described in Chapter 4, even though the amino acid sequences of the scrambled sequence are the same but arranged differently, they may have a better spatial arrangement, allowing for improved transfection. This highlights how small modifications can yield significant advantages.

1.2.3.2 Peptides Complexed with siRNA

SiRNA, despite being composed of nucleic acids like DNA, behaves differently due to its shorter length and, consequently, reduced flexibility. Regarding size, the formation of complexes consisting of siRNA, lipids, and different charge ratio of peptides has yielded much less oscillatory values.

As seen in Figure 0.1, starting from the second charge ratio, there are values hovering around 80-100 nm. The behaviour of the complex in the presence of siRNA instead of DNA also varies, and the polydispersity index value changes. In this case, it can be observed that it increases with an increase in peptide concentration.

Furthermore, the complexation of siRNA, due to its higher rigidity, proved to be different from LPDs and PDs. Indeed, it became clear that the branched structure was more effective in binding interfering nucleic acid. In contrast to DNA complexes, lipids did not show any difference in siRNA packaging, both in gel electrophoresis and PicoGreen experiments.

This behaviour was also reflected in siRNA transfection. Confocal microscopy was used to compare the ability to internalise and translate TRPM8 siRNA. This nucleic acid interferes with cell proliferation, but did not modulate N-Cadherin protein transcription, which is responsible for cytoskeletal remodelling [387]. The presence of lipids did not lead to any improvement, as it did with DNA complexation.

As seen in Figure 0.8, both RGen3K and TGen3K have reduced the number of cells compared to the negative control. This aligns with the results obtained in Chapter 3. Specifically, RGen3K has demonstrated its ability to have an anti-proliferative effect on both HER2+ and HER2- cells, and this pattern persists when complexed with siRNA (TRPM8 and control). RGen3K demonstrates a significant reduction in cell numbers, hinting at a potential synergistic effect induced by arginine at the base of the molecular tree, which may lead to apoptosis in Breast Cancer cells. Leveraging a different mechanism, TGen3K exhibits a similar activity in both cell types (MDA-MB-231 and SKBR3), although to a lesser extent. This may be due to the choice of the target sequence, which was designed to mimic the structure of Trastuzumab, which binds to the HER2 receptor on the cell membrane. Consequently, once the sequence has recognised and bound to the

receptor, TGen3K is unable to be internalised and release the siRNA. In contrast, RGen3K, devoid of the sequence, is free to activate the anti-proliferative pathway, and upon internalisation, it can release the siRNA into the cytoplasmic environment.

However, despite a similarity in the proliferation results described in Chapter 3 and Chapter 5, it is evident that the RGen3K:siRNA and TGen3K:siRNA complexes are much more effective with both non-overexpressing MDA-MB-231 cells and SKBR3 (HER+ cells). This difference may be attributed to the size of the peptides and LPR alone. In fact, the peptides alone have a diameter of 482 nm, whereas when complexed with siRNA, they reduce to approximately 80 nm. As described in other studies [388], size becomes a critical factor that can interfere with receptor target recognition and complex internalisation.

In general, these results highlight how small peptides can have similar efficacy to much larger molecules like antibodies. This can be a significant advantage both for the pharmaceutical industry and the production of peptide-based materials and for patients as well. The considerably smaller structure simplifies synthesis and timelines, reducing the cost of the drug and facilitating its availability in the market.

1.2.4 Nanocarriers:siRNA complexes into Alginate Microcarriers

Microparticles have larger dimensions compared to nanoparticles and cannot directly transport drugs or nucleic acids into the cytoplasm due to their size. However, they can serve as protective carriers for nanoparticles, increasing the chances of internalisation [389].

In this thesis, microfluidics was explored for the preparation of alginate microparticles. Alginate is a commonly used polymer in the pharmaceutical field due to its biocompatibility with the human body. To

form the gel, a cation, calcium in this case, must be released into the solution to initiate cross-linking. Several techniques were proposed in this thesis to facilitate cross-linking, and different efficiencies were observed.

As evident in Chapter 6, various modifications were made to optimise the preparation of microparticles. Initially, a comparison was made between the traditional bulk preparation method and microfluidic preparation. As reported in Section 6.5, starting from a method developed at York University, several modifications were made to obtain microparticles more suitable for administration in biological tissues, making them biocompatible. Therefore, was eliminated the ion exchange resin, used to modify and monitor the release of a negatively charged molecule called phenol red. From the results, it emerged that the absence of the resin improved spherical shape of the microparticles. Furthermore, the reduced viscosity allowed the use of a smaller needle (from 18G to 27G). The absence of resin also led to reduced retention of the dye, Phenol Red, as visible in Figure 0.8. However, the reduced retention can still be considered an advantage as microparticles need to protect the cargo while allowing its release for therapeutic effects. Moreover, the absence of resin did not affect the microparticles' ability to respond to the external pH, as shown in Figure 0.8 and Figure 0.11.

At the same time, the amount of phenol red was also reduced (1:100), making it no longer necessary to use alcohol to facilitate the solubilisation of the negatively charged molecule. Phenol red was crucial for visually determining its release from the microparticles, so it was used as a mock molecule to mimic the release of negatively charged molecules. Thus, it was used as a platform to identify improvements or deteriorations in new approaches introduced to make the microparticles more suitable from a pharmaceutical perspective."

Other modifications were made to improve the formulation. For example, an attempt was made to eliminate the calcium bath for gelation and gel formation. Alginate was covalently modified with the peptide RGen3K to introduce positive charges, allowing cations to electrochemically bind with alginate anions following pH changes. However, this experiment did not result in bead formation, possibly due to the pKa values. The microparticles of modified alginate with RGen3K molecules only formed in the presence of calcium chloride. Additionally, efforts were made to decrease the calcium concentration, but the results were inconclusive.

Finally, the characterisation of microparticles produced without resin and using the bulk technique highlighted the limitation in size reduction. Despite the optimisations for microparticle preparation, it was not possible to achieve diameters below 1 mm. It is not entirely clear whether this large size is an advantage or a disadvantage. Large sizes have been shown to reduce blood flow, limiting nutrient supply to tumor masses [390]. However, some studies suggest that tumors may adapt and become more aggressive in low-oxygen environments [391].

Microfluidics allowed for size improvement of microparticles, with further room for enhancement. The first microfluidic method was designed to be comparable to the bulk method but in the presence of an oily phase to preform alginate droplets inside the microfluidic chip and allow gelation to occur in a calcium bath. It was demonstrated that the presence of a surfactant is necessary to prevent unstable droplets from aggregating. The surfactant improved dimensional characteristics but also rendered the droplets stable in the oily phase, leading to challenges during emulsion breaking and agglomerate formation (Section 6.4.3). The second microfluidic method, known as in-chip gelation, involves gelation occurring within the microfluidic chip, resulting in pre-formed beads instead of droplets. Consequently, manipulation of the emulsion during

phase separation in the collection bath did not lead to agglomerate formation, as reported in Section 6.4.2.2. Geometrical considerations were also found to be crucial.

Furthermore, in-chip gelation offered stability, even for "fragile" molecules like nucleic acids. As observed in experiments regarding the release of TGen3K:siRNA, initial release was minimal, indicating that the microbeads effectively protected the TGen3K:siRNA complex. However, over the subsequent 24 hours, when the microparticles were stored under conditions mimicking the human body, they demonstrated the ability to release the nanometric complex completely. This can be considered an advantage in the industrial and clinical settings as it allows for a reduction in the amount of encapsulated drug, which would mostly be concentrated within the target cells.

Microparticles have much larger dimensions compared to nanoparticles and cannot directly transport drugs or nucleic acids into the cytoplasm due to their diameter. However, they can protect nanoparticles from the extracellular environment, increasing the chances of internalisation.

In this thesis, microfluidics was explored for the preparation of alginate microparticles. Alginate is a commonly used polymer in the pharmaceutical field due to its biocompatibility with the human body. To form the gel, a cation, in this case, calcium, must be released into the solution to initiate cross-linking. Several techniques were proposed in this thesis to create the cross-link, and different efficiencies were observed.

1.3 IN SUMMARY

This project has highlighted several innovations that can benefit both patients and the pharmaceutical industry. First, a new molecule called TGen3K was synthesised, featuring a hyperbranched peptide structure that allows for increased therapeutic drug payload and a high number of positive charges capable of binding to the phosphate group of nucleic acids [392]. To this branched structure, an hexapeptide sequence (LSYCCK) was added, which, as described in other studies, has been found to be selective for the HER2 receptor [250,251]. As discussed in Chapter 3 and 5, significant reductions in cell numbers were observed. In this case, it was revealed that the peptides could activate anti-proliferative pathways even without any drugs attached to them. When bound to a siRNA molecule, the effects were further accentuated, possibly due to the smaller size of the complexes that allowed for effective interaction with the receptor. Similarly, RGen3K, a hyperbranched molecule without a target sequence, also showed equally interesting results. Although non-selective, it exhibited an anti-proliferative effect on both HER2+ and HER2- cells when combined with siRNA. This highlighted a different pathway, one that, unlike TGen3K, cannot bind to the receptor and is thus free to be internalised, inducing the anti-proliferative effect. Consequently, considering future anti-tumor therapy, it would be interesting to combine TGen3K and RGen3K to induce a synergistic effect, given both the selectivity for the receptor and the non-selectivity that allows for an anti-proliferative effect. This approach would not only target the majority of tumor cells that express the target receptor but also the small minority of tumor cells that could uncontrollably grow due to the lack of the target receptor.

Moreover, smaller molecules have a less complex chemical structure compared to monoclonal antibodies, which means they can be synthesized more quickly. The synthesis of large protein molecules like antibodies typically requires much longer and more complex production processes. The synthesis of smaller molecules usually requires less starting material and fewer production steps than monoclonal antibodies. This can result in lower production costs.

Furthermore, the design of smaller selective molecules can be more flexible and adaptable to the specific needs of the application. It is easier to make chemical modifications to smaller molecules to optimise their selectivity. Additionally, they are generally more stable and easier to store and transport compared to antibodies, which may require stricter storage conditions.

A second line of attack could also be added through the presence of microparticles. Thanks to the optimisations developed in this project, these microparticles reach sizes similar to those of blood vessels that form following angiogenesis around tumor masses. Consequently, the microparticles can block blood flow, thereby cutting off nutrient support and arresting the growth of the tumor mass. Simultaneously, they can release nanoparticles into the extracellular environment, facilitating recognition by the receptor or internalisation into the cytoplasm.

This project has designed a pharmaceutical model that can target the tumor on multiple levels. Furthermore, preparation via microfluidics has enabled the production of microparticles with suitable dimensions for the pharmaceutical context and provides a method suitable for large-scale handling without cargo loss. This could lead to a significant reduction in production costs, adding to the numerous advantages already brought by microfluidics.

1.4 FUTURE WORK

Several experiments can be conducted in the future. First and foremost, it would be interesting to perform Western blotting and PCR analyses to determine the actual amount of protein (N-Cadherin) produced by cells following transfection with the TGen3K:siRNA complex. Flow cytometry and/or Hoescht Propidium Iodide and Annexin V staining of the cells could also provide key information about any arrest of the cell cycle and of occurring apoptosis processes. Additionally, identifying the localisation of the complex after internalisation would help understand how much of it is internalised and how much can overcome the endosomal membrane barrier. This could be done using inhibitors of the different cell internalisation pathways to identify the one mostly responsible for the dendrimer/nucleic acid internalisation.

Furthermore, testing the complexes *in vivo* would be necessary. Lastly, it would be essential to repeat the TGen3K:siRNA complex release analysis from the alginate microparticle polymer mesh. This would help confirm reproducibility and reduce intervals for supernatant collection to understand the release kinetics over time. *in vitro* tumoroid models where cells are tested when organised in 3D spheroid masses could also provide more information about the ability of the dendrimer/nucleic acid complexes to penetrate tumoral masses independently from the tissue microcirculation.

REFERENCES

1. Schork, N. J. Personalized medicine: Time for one-person trials. *Nature* **520**, 609–611 (2015).
2. CardioPulse Articles. *Eur. Heart J.* **36**, 1842–1843 (2015).
3. Ramaswami, R., Bayer, R. & Galea, S. Precision Medicine from a Public Health Perspective. *Annu. Rev. Public Health* **39**, 153–168 (2018).
4. Calderaro, J. *et al.* Histological subtypes of hepatocellular carcinoma are related to gene mutations and molecular tumour classification. *J. Hepatol.* **67**, 727–738 (2017).
5. Carlberg, C. & Velleuer, E. Multi-step Tumorigenesis and Genome Instability BT - Cancer Biology: How Science Works. in (eds. Carlberg, C. & Velleuer, E.) 41–53 (Springer International Publishing, 2021). doi:10.1007/978-3-030-75699-4_4.
6. Zhu, X., Li, S., Xu, B. & Luo, H. Cancer evolution: A means by which tumors evade treatment. *Biomed. Pharmacother.* **133**, 111016 (2021).
7. Alhmoud, J. F., Woolley, J. F., Al Moustafa, A.-E. & Malki, M. I. DNA Damage/Repair Management in Cancers. *Cancers* vol. 12 (2020).
8. Weston A, H. C. Multistage Carcinogenesis. *Holland-Frei Cancer Med. 6th Ed.*
9. Klaunig, J. E. Chapter 8 - Carcinogenesis. in (eds. Pope, C. N. & Liu, J. B. T.-A. I. to I. T.) 97–110 (Academic Press, 2020). doi:https://doi.org/10.1016/B978-0-12-813602-7.00008-9.
10. Parsa, N. Environmental factors inducing human cancers. *Iran. J. Public Health* **41**, 1–9 (2012).
11. Huang, M. *et al.* Do multiple environmental factors impact four cancers in women in the contiguous United States? *Environ. Res.* **179**, 108782 (2019).
12. Plante, I. Chapter 2 - Dimethylbenz(a)anthracene-induced mammary tumorigenesis in mice. in *Carcinogen-driven mouse models of oncogenesis* (eds. Galluzzi, L. & Buqué, A. B. T.-M. in C. B.) vol. 163 21–44 (Academic Press, 2021).
13. Compton, C. Cancer Initiation, Promotion, and Progression and the Acquisition of Key Behavioral Traits BT - Cancer: The Enemy from Within: A Comprehensive Textbook of Cancer's Causes, Complexities and Consequences. in (ed. Compton, C.) 25–48 (Springer International Publishing, 2020). doi:10.1007/978-3-030-40651-6_2.
14. Pitot, H. C. & Dragan, Y. P. Facts and theories concerning the mechanisms of carcinogenesis. *FASEB J.* **5**, 2280–2286 (1991).
15. Kaliberov, S. A. & Buchsbaum, D. J. Chapter seven--Cancer treatment with gene therapy and radiation therapy. *Adv. Cancer Res.* **115**, 221–263 (2012).
16. Gupta, G. P. & Massagué, J. Cancer Metastasis: Building a Framework. *Cell* **127**,

679–695 (2006).

17. Peng, F. *et al.* Regulated cell death (RCD) in cancer: key pathways and targeted therapies. *Signal Transduct. Target. Ther.* **7**, 286 (2022).

18. Marks, F., Fürstenberger, G. & Müller-Decker, K. Tumor Promotion as a Target of Cancer Prevention BT - Cancer Prevention. in (eds. Senn, H.-J. & Kapp, U.) 37–47 (Springer Berlin Heidelberg, 2007).

19. Biava, P. *Il cancro e la ricerca del senso perduto*. (2008). doi:10.1007/978-88-470-1074-1.

20. Anderson, M. W., Reynolds, S. H., You, M. & Maronpot, R. M. Role of proto-oncogene activation in carcinogenesis. *Environ. Health Perspect.* **98**, 13–24 (1992).

21. Glenfield, C. & Innan, H. Gene Duplication and Gene Fusion Are Important Drivers of Tumourigenesis during Cancer Evolution. *Genes* vol. 12 (2021).

22. Fortunato, A. *et al.* Natural Selection in Cancer Biology: From Molecular Snowflakes to Trait Hallmarks. *Cold Spring Harb. Perspect. Med.* **7**, a029652 (2017).

23. Gurung, A. B. & Bhattacharjee, A. Significance of Ras Signaling in Cancer and Strategies for its Control. *Oncol. Hematol. Rev.* **11**, 147 (2015).

24. Sebolt-Leopold, J. S. Development of anticancer drugs targeting the MAP kinase pathway. *Oncogene* **19**, 6594–6599 (2000).

25. Bahar, M. E., Kim, H. J. & Kim, D. R. Targeting the RAS/RAF/MAPK pathway for cancer therapy: from mechanism to clinical studies. *Signal Transduct. Target. Ther.* **8**, 455 (2023).

26. Deininger, P. Genetic instability in cancer: caretaker and gatekeeper genes. *Ochsner J.* **1**, 206–209 (1999).

27. Haase, D. *et al.* TP53 mutation status divides myelodysplastic syndromes with complex karyotypes into distinct prognostic subgroups. *Leukemia* **33**, 1747–1758 (2019).

28. Griffin, R. *et al.* Differential prognosis of single and multiple TP53 abnormalities in high-count MBL and untreated CLL. *Blood Adv.* **7**, 3169–3179 (2023).

29. Hanahan, D. & Weinberg, R. A. Hallmarks of Cancer: The Next Generation. *Cell* **144**, 646–674 (2011).

30. Yun, J., Li, Y., Xu, C.-T. & Pan, B.-R. Epidemiology and Rb1 gene of retinoblastoma. *Int. J. Ophthalmol.* **4**, 103–109 (2011).

31. Marković, L., Bukovac, A., Varošanec, A. M., Šlaus, N. & Pećina-Šlaus, N. Genetics in ophthalmology: molecular blueprints of retinoblastoma. *Hum. Genomics* **17**, 82 (2023).

32. Djelloul, S. *et al.* Enterocyte differentiation is compatible with SV40 large T expression and loss of p53 function in human colonic Caco-2 cells: Status of the pRb1 and pRb2 tumor suppressor gene products. *FEBS Lett.* **406**, 234–242 (1997).

33. Anderson, N. M. & Simon, M. C. The tumor microenvironment. *Curr. Biol.* **30**, R921–R925 (2020).

34. Bosman, F. T. & Stamenkovic, I. Functional structure and composition of the extracellular matrix. *J. Pathol.* **200**, 423–428 (2003).

35. Huang, J. *et al.* Extracellular matrix and its therapeutic potential for cancer treatment. *Signal Transduct. Target. Ther.* **6**, 153 (2021).

36. Schlich, M. *et al.* Anionic liposomes for small interfering ribonucleic acid (siRNA) delivery to primary neuronal cells: Evaluation of alpha-synuclein knockdown efficacy. *Nano Res.* **10**, 3496–3508 (2017).

37. Liberti, M. V & Locasale, J. W. The Warburg Effect: How Does it Benefit Cancer Cells? *Trends Biochem. Sci.* **41**, 211–218 (2016).

38. Liao, M. *et al.* Targeting the Warburg effect: A revisited perspective from molecular mechanisms to traditional and innovative therapeutic strategies in cancer. *Acta Pharm. Sin. B* (2023) doi:https://doi.org/10.1016/j.apsb.2023.12.003.

39. Gatenby, R. A. & Vincent, T. L. An evolutionary model of carcinogenesis. *Cancer Res.* **63**, 6212–20 (2003).

40. Jiang, X. *et al.* The role of microenvironment in tumor angiogenesis. *J. Exp. Clin. Cancer Res.* **39**, 204 (2020).

41. Yance, D. R. & Sagar, S. M. Targeting Angiogenesis With Integrative Cancer Therapies. *Integr. Cancer Ther.* **5**, 9–29 (2006).

42. Negrini, S., Gorgoulis, V. G. & Halazonetis, T. D. Genomic instability — an evolving hallmark of cancer. *Nat. Rev. Mol. Cell Biol.* **11**, 220–228 (2010).

43. Jesinger, R. A. Breast Anatomy for the Interventionalist. *Tech. Vasc. Interv. Radiol.* **17**, 3–9 (2014).

44. Ellis, H. & Mahadevan, V. Anatomy and physiology of the breast. *Surg.* **31**, 11–14 (2013).

45. Darlington, A. J. Anatomy of the Breast BT - Digital Mammography: A Holistic Approach. in (eds. Hogg, P., Kelly, J. & Mercer, C.) 3–10 (Springer International Publishing, 2015). doi:10.1007/978-3-319-04831-4_1.

46. Weigelt, B. *et al.* Refinement of breast cancer classification by molecular characterization of histological special types. *J. Pathol.* **216**, 141–150 (2008).

47. Sutton, E. J. *et al.* Breast cancer molecular subtype classifier that incorporates MRI features. *J. Magn. Reson. Imaging* **44**, 122–129 (2016).

48. Siegel, R., Naishadham, D. & Jemal, A. Cancer statistics, 2013. *CA. Cancer J. Clin.* **63**, 11–30 (2013).

49. Patel, A., Unni, N. & Peng, Y. The Changing Paradigm for the Treatment of HER2-Positive Breast Cancer. *Cancers (Basel).* **12**, 2081 (2020).

50. Moasser, M. M. The oncogene HER2: its signaling and transforming functions and

its role in human cancer pathogenesis. *Oncogene* **26**, 6469–6487 (2007).

51. Yin, L., Duan, J.-J., Bian, X.-W. & Yu, S. Triple-negative breast cancer molecular subtyping and treatment progress. *Breast Cancer Res.* **22**, 61 (2020).

52. Roskoski, R. The ErbB/HER family of protein-tyrosine kinases and cancer. *Pharmacol. Res.* **79**, 34–74 (2014).

53. Hart, V., Gautrey, H., Kirby, J. & Tyson-Capper, A. HER2 splice variants in breast cancer: investigating their impact on diagnosis and treatment outcomes. *Oncotarget* **11**, (2020).

54. Cavallaro, P. A. *et al.* Peptides Targeting HER2-Positive Breast Cancer Cells and Applications in Tumor Imaging and Delivery of Chemotherapeutics. *Nanomaterials* vol. 13 (2023).

55. Liang, H.-F., Zhang, X.-Z., Liu, B.-G., Jia, G.-T. & Li, W.-L. Circular RNA circ-ABCB10 promotes breast cancer proliferation and progression through sponging miR-1271. *Am. J. Cancer Res.* **7**, 1566–1576 (2017).

56. Ding, L. *et al.* The Roles of Cyclin-Dependent Kinases in Cell-Cycle Progression and Therapeutic Strategies in Human Breast Cancer. *International Journal of Molecular Sciences* vol. 21 (2020).

57. Nahta, R. Molecular Mechanisms of Trastuzumab-Based Treatment in HER2-Overexpressing Breast Cancer. *ISRN Oncol.* **2012**, 428062 (2012).

58. Pohlmann, P. R., Mayer, I. A. & Mernaugh, R. Resistance to Trastuzumab in Breast Cancer. *Clin. Cancer Res.* **15**, (2009).

59. Depowski, P. L., Rosenthal, S. I. & Ross, J. S. Loss of Expression of the PTEN Gene Protein Product Is Associated with Poor Outcome in Breast Cancer. *Mod. Pathol.* **14**, (2001).

60. Cerma, K. *et al.* Targeting PI3K/AKT/mTOR Pathway in Breast Cancer: From Biology to Clinical Challenges. *Biomedicines* vol. 11 (2023).

61. Irene, R. R. *et al.* p95HER2–T cell bispecific antibody for breast cancer treatment. *Sci. Transl. Med.* **10**, eaat1445 (2018).

62. Gajria, D. & Chandarlapaty, S. HER2-amplified breast cancer: mechanisms of trastuzumab resistance and novel targeted therapies. *Expert Rev. Anticancer Ther.* **11**, 263–275 (2011).

63. Hunter, F. W. *et al.* Mechanisms of resistance to trastuzumab emtansine (T-DM1) in HER2-positive breast cancer. *Br. J. Cancer* **122**, 603–612 (2020).

64. Swain, S. M., Shastry, M. & Hamilton, E. Targeting HER2-positive breast cancer: advances and future directions. *Nat. Rev. Drug Discov.* **22**, 101–126 (2023).

65. Boyraz, B. *et al.* Trastuzumab emtansine (T-DM1) for HER2-positive breast cancer. *Curr. Med. Res. Opin.* **29**, 405–414 (2013).

66. D'Amato, V. *et al.* Mechanisms of lapatinib resistance in HER2-driven breast

cancer. *Cancer Treat. Rev.* **41**, 877–883 (2015).

67. Wahdan-Alaswad, R., Liu, B. & Thor, A. D. Targeted lapatinib anti-HER2/ErbB2 therapy resistance in breast cancer: opportunities to overcome a difficult problem. *Cancer Drug Resist.* **3**, 179–198 (2020).

68. Shajahan, A. N., Dobbin, Z. C., Hickman, F. E., Dakshanamurthy, S. & Clarke, R. Tyrosine-phosphorylated Caveolin-1 (Tyr-14) Increases Sensitivity to Paclitaxel by Inhibiting BCL2 and BCLxL Proteins via c-Jun N-terminal Kinase (JNK)*. *J. Biol. Chem.* **287**, 17682–17692 (2012).

69. Jauhari, S., Singh, S. & Dash, A. K. Chapter 7 - Paclitaxel. in (ed. Brittain Excipients and Related Methodology, H. G. B. T.-P. of D. S.) vol. 34 299–344 (Academic Press, 2009).

70. Stinchcombe, T. E. Nanoparticle albumin-bound paclitaxel: a novel Cremphor-EL®-free formulation of paclitaxel. *Nanomedicine* **2**, 415–423 (2007).

71. Niidome, T. & Huang, L. Gene Therapy Progress and Prospects: Nonviral vectors. *Gene Ther.* **9**, 1647–1652 (2002).

72. Stoff-Khalili, M. A., Dall, P. & Curiel, D. T. Gene therapy for carcinoma of the breast. *Cancer Gene Ther.* **13**, 633–647 (2006).

73. Zamore, P. D. RNA Interference: Big Applause for Silencing in Stockholm. *Cell* **127**, 1083–1086 (2006).

74. Eş, I. *et al.* Evaluation of siRNA and cationic liposomes complexes as a model for in vitro siRNA delivery to cancer cells. *Colloids Surfaces A Physicochem. Eng. Asp.* **555**, 280–289 (2018).

75. Petrova, N. S., Zenkova, M. A. & Chernolovskaya, E. L. Structure - Functions Relations in Small Interfering RNAs. in (eds. Andrade, A. O., Pereira, A. A., Naves, E. L. M. & Soares, A. B.) Ch. 8 (IntechOpen, 2013). doi:10.5772/53945.

76. O'Keefe, E. P. siRNAs and shRNAs: Tools for Protein Knockdown by Gene Silencing. *Mater. Methods* **3**, (2013).

77. Bumcrot, D., Manoharan, M., Koteliansky, V. & Sah, D. W. Y. RNAi therapeutics: a potential new class of pharmaceutical drugs. *Nat. Chem. Biol.* **2**, 711–719 (2006).

78. Mintzer, M. A. & Simanek, E. E. Nonviral Vectors for Gene Delivery. *Chem. Rev.* **109**, 259–302 (2009).

79. Dul, M. *et al.* Hydrodynamic gene delivery in human skin using a hollow microneedle device. *J. Control. Release* **265**, 120–131 (2017).

80. Rosazza, C., Meglic, S. H., Zumbusch, A., Rols, M.-P. & Miklavcic, D. Gene Electrotransfer: A Mechanistic Perspective. *Curr. Gene Ther.* **16**, 98–129 (2016).

81. André, F. & Mir, L. M. DNA electrotransfer: its principles and an updated review of its therapeutic applications. *Gene Ther.* **11**, S33–S42 (2004).

82. Do Minh, A., Sharon, D., Chahal, P. & Kamen, A. A. 1.26 - Cell Transfection☆. in (ed.

Moo-Young, M. B. T.-C. B. (Third E.) 383–390 (Pergamon, 2019). doi:https://doi.org/10.1016/B978-0-444-64046-8.00023-9.

83. Kanefuji, T. *et al.* Hemodynamics of a hydrodynamic injection. *Mol. Ther. - Methods Clin. Dev.* **1**, 14029 (2014).

84. Ziv, R., Steinhardt, Y., Pelled, G., Gazit, D. & Rubinsky, B. Micro-electroporation of mesenchymal stem cells with alternating electrical current pulses. *Biomed. Microdevices* **11**, 95 (2008).

85. Wei, Z. *et al.* A Laminar Flow Electroporation System for Efficient DNA and siRNA Delivery. *Anal. Chem.* **83**, 5881–5887 (2011).

86. Sun, W. H. *et al.* In vivo cytokine gene transfer by gene gun reduces tumor growth in mice. *Proc. Natl. Acad. Sci.* **92**, 2889–2893 (1995).

87. Praveen, B. B., Stevenson, D. J., Antkowiak, M., Dholakia, K. & Gunn-Moore, F. J. Enhancement and optimization of plasmid expression in femtosecond optical transfection. *J. Biophotonics* **4**, 229–235 (2011).

88. Ma, N., Ashok, P. C., Stevenson, D. J., Gunn-Moore, F. J. & Dholakia, K. Integrated optical transfection system using a microlens fiber combined with microfluidic gene delivery. *Biomed. Opt. Express* **1**, 694–705 (2010).

89. Robbins, P. D. & Ghivizzani, S. C. Viral Vectors for Gene Therapy. *Pharmacol. Ther.* **80**, 35–47 (1998).

90. Bulcha, J. T., Wang, Y., Ma, H., Tai, P. W. L. & Gao, G. Viral vector platforms within the gene therapy landscape. *Signal Transduct. Target. Ther.* **6**, 53 (2021).

91. Walther, W. & Stein, U. Viral Vectors for Gene Transfer. *Drugs* **60**, 249–271 (2000).

92. Wu, N. & Ataai, M. M. Production of viral vectors for gene therapy applications. *Curr. Opin. Biotechnol.* **11**, 205–208 (2000).

93. Ramamoorth, M. & Narvekar, A. Non viral vectors in gene therapy- an overview. *J. Clin. Diagn. Res.* **9**, GE01-GE6 (2015).

94. Mohammed, A. R., Weston, N., Coombes, A. G. A., Fitzgerald, M. & Perrie, Y. Liposome formulation of poorly water soluble drugs: optimisation of drug loading and ESEM analysis of stability. *Int. J. Pharm.* **285**, 23–34 (2004).

95. Faraji, A. H. & Wipf, P. Nanoparticles in cellular drug delivery. *Bioorg. Med. Chem.* **17**, 2950–2962 (2009).

96. De Jong, W. H. & Borm, P. J. A. Drug delivery and nanoparticles:applications and hazards. *Int. J. Nanomedicine* **3**, 133–149 (2008).

97. Aminu, N. *et al.* The influence of nanoparticulate drug delivery systems in drug therapy. *J. Drug Deliv. Sci. Technol.* **60**, 101961 (2020).

98. Mitchell, M. J. *et al.* Engineering precision nanoparticles for drug delivery. *Nat. Rev. Drug Discov.* **20**, 101–124 (2021).

99. Grimm, L. J., Rahbar, H., Abdelmalak, M., Hall, A. H. & Ryser, M. D. Ductal

Carcinoma in Situ: State-of-the-Art Review. *Radiology* **302**, 246–255 (2021).

100. Zielińska, A. *et al.* Polymeric Nanoparticles: Production, Characterization, Toxicology and Ecotoxicology. *Molecules* **25**, 3731 (2020).

101. Maeda, H., Wu, J., Sawa, T., Matsumura, Y. & Hori, K. Tumor vascular permeability and the EPR effect in macromolecular therapeutics: a review. *J. Control. Release* **65**, 271–284 (2000).

102. Thorpe, P. E. Vascular Targeting Agents as Cancer Therapeutics. *Clin. Cancer Res.* **10**, 415 LP – 427 (2004).

103. Choi, C. H. J., Alabi, C. A., Webster, P. & Davis, M. E. Mechanism of active targeting in solid tumors with transferrin-containing gold nanoparticles. *Proc. Natl. Acad. Sci.* **107**, 1235–1240 (2010).

104. Digiacomo, L., Pozzi, D., Palchetti, S., Zingoni, A. & Caracciolo, G. Impact of the protein corona on nanomaterial immune response and targeting ability. *WIREs Nanomedicine and Nanobiotechnology* **12**, e1615 (2020).

105. Gref, R. *et al.* 'Stealth' corona-core nanoparticles surface modified by polyethylene glycol (PEG): influences of the corona (PEG chain length and surface density) and of the core composition on phagocytic uptake and plasma protein adsorption. *Colloids Surfaces B Biointerfaces* **18**, 301–313 (2000).

106. Treuel, L. & Nienhaus, G. U. Toward a molecular understanding of nanoparticle–protein interactions. *Biophys. Rev.* **4**, 137–147 (2012).

107. Owens, D. E. & Peppas, N. A. Opsonization, biodistribution, and pharmacokinetics of polymeric nanoparticles. *Int. J. Pharm.* **307**, 93–102 (2006).

108. Immordino, M. L., Dosio, F. & Cattel, L. Stealth liposomes: review of the basic science, rationale, and clinical applications, existing and potential. *Int. J. Nanomedicine* **1**, 297–315 (2006).

109. Patel, H. M. Serum Opsonins and Liposomes: Their Interaction and Opsonophagocytosis. *Crit. Rev. Ther. Drug Carrier Syst.* **9**, 39–90 (1992).

110. Wu, J., Akaike, T. & Maeda, H. Modulation of Enhanced Vascular Permeability in Tumors by a Bradykinin Antagonist, a Cyclooxygenase Inhibitor, and a Nitric Oxide Scavenger. *Cancer Res.* **58**, 159 LP – 165 (1998).

111. Kim, C. S., Duncan, B., Creran, B. & Rotello, V. M. Triggered nanoparticles as therapeutics. *Nano Today* **8**, 439–447 (2013).

112. Xing, Q. *et al.* Light-responsive amphiphilic copolymer coated nanoparticles as nanocarriers and real-time monitors for controlled drug release. *J. Mater. Chem. B* **2**, 1182–1189 (2014).

113. Fukumura, D. & Jain, R. K. Tumor microvasculature and microenvironment: Targets for anti-angiogenesis and normalization. *Microvasc. Res.* **74**, 72–84 (2007).

114. Yang, Q. & Lai, S. K. Anti-PEG immunity: emergence, characteristics, and unaddressed questions. *Wiley Interdiscip. Rev. Nanomed. Nanobiotechnol.* **7**, 655–

677 (2015).

115. Parodi, A. *et al.* Synthetic nanoparticles functionalized with biomimetic leukocyte membranes possess cell-like functions. *Nat. Nanotechnol.* **8**, 61–68 (2013).

116. G. Sonavane, K. T. and K. M. G. So"Biodistribution of colloidal gold nanoparticles after intravenous administration: effect of particle size," Colloids and Surfaces B: Biointerfaces.

117. Macdonald, R. L. Nanoparticles and Microparticles. *Neurosurgery* **62**, 152–159 (2015).

118. Dong, X. *et al.* The size-dependent cytotoxicity of amorphous silica nanoparticles: a systematic review of in vitro studies. *Int. J. Nanomedicine* 9089–9113 (2020).

119. Foroozandeh, P. & Aziz, A. A. Insight into Cellular Uptake and Intracellular Trafficking of Nanoparticles. *Nanoscale Res. Lett.* **13**, 339 (2018).

120. Xiao, K. *et al.* The effect of surface charge on in vivo biodistribution of PEG-oligocholic acid based micellar nanoparticles. *Biomaterials* **32**, 3435–3446 (2011).

121. Stillwell, W. Chapter 14 - Membrane Transport. in (ed. Stillwell, W. B. T.-A. I. to B. M.) 305–337 (Elsevier, 2013). doi:https://doi.org/10.1016/B978-0-444-52153-8.00014-3.

122. Yan, X. *et al.* The identification of novel targets of miR-16 and characterization of their biological functions in cancer cells. *Mol. Cancer* **12**, 92 (2013).

123. Chen, I. & Lui, F. *Physiology, Active Transport*. *StatPearls* (2022).

124. Burdick, D., Le Gall, A. H. & Rodriguez-Boulan, E. Vesicular transport: implications for cell polarity. *Biocell* **20**, 343–53 (1996).

125. Xiang, S. *et al.* Uptake mechanisms of non-viral gene delivery. *J. Control. Release* **158**, 371–378 (2012).

126. Alberts B, Johnson A, Lewis J, et al. Transport into the Cell from the Plasma Membrane: Endocytosis. in *Molecular Biology of the Cell. 4th edition.* (ed. Garland Science) (2002).

127. Takei, K. & Haucke, V. Clathrin-mediated endocytosis: membrane factors pull the trigger. *Trends Cell Biol.* **11**, 385–391 (2001).

128. Zanoni, P., Velagapudi, S., Yalcinkaya, M., Rohrer, L. & von Eckardstein, A. Endocytosis of lipoproteins. *Atherosclerosis* **275**, 273–295 (2018).

129. Du, Z., Munye, M. M., Tagalakis, A. D., Manunta, M. D. I. & Hart, S. L. The Role of the Helper Lipid on the DNA Transfection Efficiency of Lipopolyplex Formulations. *Sci. Rep.* **4**, 7107 (2014).

130. Lam, J. K. W. Endosomal Escape Pathways for Non-Viral Nucleic Acid Delivery Systems. in (eds. Liang, W. & Ceresa, B.) Ch. 17 (InTech, 2012). doi:10.5772/46006.

131. Bus, T., Traeger, A. & Schubert, U. S. The great escape: how cationic polyplexes overcome the endosomal barrier. *J. Mater. Chem. B* **6**, 6904–6918 (2018).

132. Wang, Z., Tiruppathi, C., Cho, J., Minshall, R. D. & Malik, A. B. Delivery of nanoparticle-complexed drugs across the vascular endothelial barrier via caveolae. *IUBMB Life* **63**, 659–667 (2011).

133. Williams, T. M. & Lisanti, M. P. The caveolin proteins. *Genome Biol.* **5**, 214 (2004).

134. Jin, H., Heller, D. A., Sharma, R. & Strano, M. S. Size-Dependent Cellular Uptake and Expulsion of Single-Walled Carbon Nanotubes: Single Particle Tracking and a Generic Uptake Model for Nanoparticles. *ACS Nano* **3**, 149–158 (2009).

135. Holzapfel, V. *et al.* Synthesis and biomedical applications of functionalized fluorescent and magnetic dual reporter nanoparticles as obtained in the miniemulsion process. *J. Phys. Condens. Matter* **18**, S2581–S2594 (2006).

136. Abbasi, E. *et al.* Dendrimers: synthesis, applications, and properties. *Nanoscale Res. Lett.* **9**, 247 (2014).

137. Boas, U., Christensen, J. B. & Heegaard, P. M. H. Dendrimers: design, synthesis and chemical properties. *J. Mater. Chem.* **16**, 3785–3798 (2006).

138. Liu, H., Wang, Y., Wang, M., Xiao, J. & Cheng, Y. Fluorinated poly(propylenimine) dendrimers as gene vectors. *Biomaterials* **35**, 5407–5413 (2014).

139. Taranejoo, S., Liu, J., Verma, P. & Hourigan, K. A review of the developments of characteristics of PEI derivatives for gene delivery applications. *J. Appl. Polym. Sci.* **132**, (2015).

140. Joshi, V. G., Dighe, V. D., Thakuria, D., Malik, Y. S. & Kumar, S. Multiple antigenic peptide (MAP): a synthetic peptide dendrimer for diagnostic, antiviral and vaccine strategies for emerging and re-emerging viral diseases. *Indian J. Virol.* **24**, 312–320 (2013).

141. Lyu, Z., Ding, L., Huang, A. Y.-T., Kao, C.-L. & Peng, L. Poly(amidoamine) dendrimers: covalent and supramolecular synthesis. *Mater. Today Chem.* **13**, 34–48 (2019).

142. Chen, S., Huang, S., Li, Y. & Zhou, C. Recent Advances in Epsilon-Poly-L-Lysine and L-Lysine-Based Dendrimer Synthesis, Modification, and Biomedical Applications . *Frontiers in Chemistry* vol. 9 169 (2021).

143. Mlynarczyk, D. T. Dendrimer Structure Diversity and Tailorability as a Way to Fight Infectious Diseases. in (ed. Kocki, T.) Ch. 6 (IntechOpen, 2017). doi:10.5772/67660.

144. Ciolkowski, M. *et al.* Surface modification of PAMAM dendrimer improves its biocompatibility. *Nanomedicine Nanotechnology, Biol. Med.* **8**, 815–817 (2012).

145. Zeng, F. & Zimmerman, S. C. Dendrimers in Supramolecular Chemistry: From Molecular Recognition to Self-Assembly. *Chem. Rev.* **97**, 1681–1712 (1997).

146. Puntoriero, F., Ceroni, P., Balzani, V., Bergamini, G. & Vögtle, F. Photoswitchable Dendritic Hosts: A Dendrimer with Peripheral Azobenzene Groups. *J. Am. Chem. Soc.* **129**, 10714–10719 (2007).

147. Capek, I. Polymer Template-Directed Synthesis BT - Noble Metal Nanoparticles: Preparation, Composite Nanostructures, Biodecoration and Collective Properties.

in (ed. Capek, I.) 317–414 (Springer Japan, 2017). doi:10.1007/978-4-431-56556-7_4.

148. Mishra, B. & Singh, J. Chapter 4 - Novel drug delivery systems and significance in respiratory diseases. in (eds. Dua, K. et al.) 57–95 (Academic Press, 2020). doi:https://doi.org/10.1016/B978-0-12-820658-4.00004-2.

149. Hoffman, A. S. The origins and evolution of "controlled" drug delivery systems. *J. Control. Release* **132**, 153–163 (2008).

150. LANGER, R. & FOLKMAN, J. Polymers for the sustained release of proteins and other macromolecules. *Nature* **263**, 797–800 (1976).

151. Koo, O. M., Rubinstein, I. & Onyuksel, H. Role of nanotechnology in targeted drug delivery and imaging: a concise review. *Nanomedicine Nanotechnology, Biol. Med.* **1**, 193–212 (2005).

152. Calzoni, E. *et al.* Biocompatible Polymer Nanoparticles for Drug Delivery Applications in Cancer and Neurodegenerative Disorder Therapies. *J. Funct. Biomater.* **10**, 4 (2019).

153. Contents. in (eds. Gopi, S., Thomas, S. & Pius, A. B. T.-H. of C. and C.) v–xii (Elsevier, 2020). doi:https://doi.org/10.1016/B978-0-12-817966-6.00028-5.

154. Falde, E. J., Yohe, S. T., Colson, Y. L. & Grinstaff, M. W. Superhydrophobic materials for biomedical applications. *Biomaterials* **104**, 87–103 (2016).

155. Sivan, S. S. *et al.* Encapsulation of Human-Bone-Marrow-Derived Mesenchymal Stem Cells in Small Alginate Beads Using One-Step Emulsification by Internal Gelation: In Vitro, and In Vivo Evaluation in Degenerate Intervertebral Disc Model. *Pharmaceutics* vol. 14 (2022).

156. Vroman, I. & Tighzert, L. Biodegradable Polymers. *Materials* vol. 2 307–344 (2009).

157. Ibrahim, N. K. *et al.* Phase I and Pharmacokinetic Study of ABI-007, a Cremophor-free, Protein-stabilized, Nanoparticle Formulation of Paclitaxel. *Clin. Cancer Res.* **8**, 1038 LP – 1044 (2002).

158. Lengyel, M., Kállai-Szabó, N., Antal, V., Laki, A. J. & Antal, I. Microparticles, Microspheres, and Microcapsules for Advanced Drug Delivery. *Scientia Pharmaceutica* vol. 87 (2019).

159. Lengyel, M., Kállai-Szabó, N., Antal, V., Laki, A. J. & Antal, I. Microparticles, Microspheres, and Microcapsules for Advanced Drug Delivery. *Sci. Pharm.* **87**, 20 (2019).

160. Martínez Rivas, C. J. *et al.* Nanoprecipitation process: From encapsulation to drug delivery. *Int. J. Pharm.* **532**, 66–81 (2017).

161. Adepu, S. & Ramakrishna, S. Controlled Drug Delivery Systems: Current Status and Future Directions. *Molecules* **26**, 5905 (2021).

162. Amar, J. G. & Family, F. Diffusion annihilation in one dimension and kinetics of the Ising model at zero temperature. *Phys. Rev. A* **41**, 3258–3262 (1990).

163. Guenneau, S. & Puvirajesinghe, T. M. Fick's second law transformed: one path to cloaking in mass diffusion. *J. R. Soc. Interface* **10**, 20130106 (2013).

164. Farhadieh, B. Drug Release from Methyl Acrylate–Methyl Methacrylate Copolymer Matrix III: Simultaneous Release of Noninteracting Drug–Excipient Mixtures. *J. Pharm. Sci.* **65**, 1333–1337 (1976).

165. McDougall, R. *et al.* The Nonclinical Disposition and Pharmacokinetic/Pharmacodynamic Properties of N-Acetylgalactosamine–Conjugated Small Interfering RNA Are Highly Predictable and Build Confidence in Translation to Human. *Drug Metab. Dispos.* **50**, 781 LP – 797 (2022).

166. Liu, G. & McEnnis, K. Glass Transition Temperature of PLGA Particles and the Influence on Drug Delivery Applications. *Polymers* vol. 14 (2022).

167. Lao, L. L., Peppas, N. A., Boey, F. Y. C. & Venkatraman, S. S. Modeling of drug release from bulk-degrading polymers. *Int. J. Pharm.* **418**, 28–41 (2011).

168. dos Santos, J., da Silva, G. S., Velho, M. C. & Beck, R. C. Eudragit®: A Versatile Family of Polymers for Hot Melt Extrusion and 3D Printing Processes in Pharmaceutics. *Pharmaceutics* vol. 13 (2021).

169. Siepmann, J. & Siepmann, F. Modeling of diffusion controlled drug delivery. *J. Control. Release* **161**, 351–362 (2012).

170. Kim, S. W., Bae, Y. H. & Okano, T. Hydrogels: Swelling, Drug Loading, and Release. *Pharm. Res.* **9**, 283–290 (1992).

171. Li, Y. & Kohane, D. S. 1.3.8A - Microparticles. in (eds. Wagner, W. R., Sakiyama-Elbert, S. E., Zhang, G. & Yaszemski, M. J. B. T.-B. S. (Fourth E.) 431–451 (Academic Press, 2020). doi:https://doi.org/10.1016/B978-0-12-816137-1.00030-1.

172. Smidsrød, O. & Skja˚k-Br┤k, G. Alginate as immobilization matrix for cells. *Trends Biotechnol.* **8**, 71–78 (1990).

173. Kumar, A. *et al.* Introduction to Alginate: Biocompatible, Biodegradable, Antimicrobial Nature and Various Applications. in (eds. Severo, D. I. A., Mariano, D. A. B. & Vargas, D. J. V. C.) Ch. 5 (IntechOpen, 2023). doi:10.5772/intechopen.110650.

174. Gombotz, W. R. & Wee, S. Protein release from alginate matrices. *Adv. Drug Deliv. Rev.* **31**, 267–285 (1998).

175. Uludag, H., De Vos, P. & Tresco, P. A. Technology of mammalian cell encapsulation. *Adv. Drug Deliv. Rev.* **42**, 29–64 (2000).

176. George, M. & Abraham, T. E. Polyionic hydrocolloids for the intestinal delivery of protein drugs: Alginate and chitosan — a review. *J. Control. Release* **114**, 1–14 (2006).

177. Workman, V. L., Dunnett, S. B., Kille, P. & Palmer, D. D. On-Chip Alginate Microencapsulation of Functional Cells. *Macromol. Rapid Commun.* **29**, 165–170

(2008).

178. Tan, W.-H. T. & Takeuchi, S. Monodisperse Alginate Hydrogel Microbeads for Cell Encapsulation. *Adv. Mater.* **19**, 2696–2701 (2007).

179. Łabowska, M. *et al.* A Review on the Adaption of Alginate-Gelatin Hydrogels for 3D Cultures and Bioprinting. *Materials (Basel).* **14**, 858 (2021).

180. Bialik-Wąs, K., Królicka, E. & Malina, D. Impact of the Type of Crosslinking Agents on the Properties of Modified Sodium Alginate/Poly(vinyl Alcohol) Hydrogels. *Molecules* **26**, 2381 (2021).

181. Minghou, J., Yujun, W., Zuhong, X. & Yucai, G. Studies on the M:G ratios in alginate. *Hydrobiologia* **116**, 554–556 (1984).

182. Mørch, Ý. A., Donati, I., Strand, B. L. & Skjåk-Bræk, G. Effect of Ca2+, Ba2+, and Sr2+ on Alginate Microbeads. *Biomacromolecules* **7**, 1471–1480 (2006).

183. Zhang, C., Grossier, R., Candoni, N. & Veesler, S. Preparation of alginate hydrogel microparticles by gelation introducing cross-linkers using droplet-based microfluidics: a review of methods. *Biomater. Res.* **25**, 41 (2021).

184. Chan, L. W., Lee, H. Y. & Heng, P. W. S. Mechanisms of external and internal gelation and their impact on the functions of alginate as a coat and delivery system. *Carbohydr. Polym.* **63**, 176–187 (2006).

185. Zhang, F., Cheng, G. & Ying, X. Emulsion and macromolecules templated alginate based polymer microspheres. *React. Funct. Polym.* **66**, 712–719 (2006).

186. Lee, B.-B., Bhandari, B. R. & Howes, T. Gelation of an alginate film via spraying of calcium chloride droplets. *Chem. Eng. Sci.* **183**, 1–12 (2018).

187. Leong, J.-Y. *et al.* Advances in fabricating spherical alginate hydrogels with controlled particle designs by ionotropic gelation as encapsulation systems. *Particuology* **24**, 44–60 (2016).

188. Skjåk-Bræk, G., Grasdalen, H. & Smidsrød, O. Inhomogeneous polysaccharide ionic gels. *Carbohydr. Polym.* **10**, 31–54 (1989).

189. Poncelet, D. *et al.* Production of alginate beads by emulsification/internal gelation. I. Methodology. *Appl. Microbiol. Biotechnol.* **38**, 39–45 (1992).

190. Song, H., Yu, W., Gao, M., Liu, X. & Ma, X. Microencapsulated probiotics using emulsification technique coupled with internal or external gelation process. *Carbohydr. Polym.* **96**, 181–189 (2013).

191. Poncelet, D. *et al.* Production of alginate beads by emulsification/internal gelation. II. Physicochemistry. *Appl. Microbiol. Biotechnol.* **43**, 644–650 (1995).

192. Leong, J.-Y., Tey, B.-T., Tan, C.-P. & Chan, E.-S. Nozzleless Fabrication of Oil-Core Biopolymeric Microcapsules by the Interfacial Gelation of Pickering Emulsion Templates. *ACS Appl. Mater. Interfaces* **7**, 16169–16176 (2015).

193. Zhang, W., Sun, X., Fan, X., Li, M. & He, G. Pickering emulsions stabilized by

hydrophobically modified alginate nanoparticles: Preparation and pH-responsive performance in vitro. *J. Dispers. Sci. Technol.* **39**, 367–374 (2018).

194. Paques, J. P., van der Linden, E., van Rijn, C. J. M. & Sagis, L. M. C. Preparation methods of alginate nanoparticles. *Adv. Colloid Interface Sci.* **209**, 163–171 (2014).

195. Galogahi, F. M., Zhu, Y., An, H. & Nguyen, N.-T. Core-shell microparticles: Generation approaches and applications. *J. Sci. Adv. Mater. Devices* (2020) doi:https://doi.org/10.1016/j.jsamd.2020.09.001.

196. Li, W. *et al.* Microfluidic fabrication of microparticles for biomedical applications. *Chem. Soc. Rev.* **47**, 5646–5683 (2018).

197. Gehrmann, S. & Bunjes, H. Instrumented small scale extruder to investigate the influence of process parameters during premix membrane emulsification. *Chem. Eng. J.* **284**, 716–723 (2016).

198. Timko, M. T., Marre, S. & Maag, A. R. Formation and characterization of emulsions consisting of dense carbon dioxide and water: ultrasound. *J. Supercrit. Fluids* **109**, 51–60 (2016).

199. Müller, W. E. G. *et al.* Functional importance of coacervation to convert calcium polyphosphate nanoparticles into the physiologically active state. *Mater. Today Bio* **16**, 100404 (2022).

200. Wolska, E. Fine powder of lipid microparticles – spray drying process development and optimization. *J. Drug Deliv. Sci. Technol.* **64**, 102640 (2021).

201. Akbarzadeh, A. *et al.* Liposome: classification, preparation, and applications. *Nanoscale Res. Lett.* **8**, 102 (2013).

202. Seiffert, S. & Weitz, D. A. Controlled fabrication of polymer microgels by polymer-analogous gelation in droplet microfluidics. *Soft Matter* **6**, 3184–3190 (2010).

203. Tran, K. T. M. & Nguyen, T. D. Lithography-based methods to manufacture biomaterials at small scales. *J. Sci. Adv. Mater. Devices* **2**, 1–14 (2017).

204. Enayati, M., Chang, M.-W., Bragman, F., Edirisinghe, M. & Stride, E. Electrohydrodynamic preparation of particles, capsules and bubbles for biomedical engineering applications. *Colloids Surfaces A Physicochem. Eng. Asp.* **382**, 154–164 (2011).

205. Yilbas, B. S., Al-Sharafi, A. & Ali, H. Chapter 8 - Concluding Remarks. in (eds. Yilbas, B. S., Al-Sharafi, A. & Ali, H. B. T.-S.-C. of S. and W. D. M.) 423–434 (Elsevier, 2019). doi:https://doi.org/10.1016/B978-0-12-814776-4.00008-2.

206. Loo, J. F. C., Ho, A. H. P. & Mak, W. C. Chapter 1 - Printed microfluidic biosensors and their biomedical applications. in (eds. Mak, W. C. & Pui Ho, A. H. B. T.-M. B.) 1–40 (Academic Press, 2023). doi:https://doi.org/10.1016/B978-0-12-823846-2.00001-8.

207. Bloise, N. *et al.* Extra-Small Gold Nanospheres Decorated With a Thiol Functionalized Biodegradable and Biocompatible Linear Polyamidoamine as

Nanovectors of Anticancer Molecules . *Frontiers in Bioengineering and Biotechnology* vol. 8 (2020).

208. Thompson, M. & Scholz, C. Highly Branched Polymers Based on Poly(amino acid)s for Biomedical Application. *Nanomaterials* vol. 11 (2021).

209. Gorzkiewicz, M. *et al.* Poly(lysine) Dendrimers Form Complexes with siRNA and Provide Its Efficient Uptake by Myeloid Cells: Model Studies for Therapeutic Nucleic Acid Delivery. *International Journal of Molecular Sciences* vol. 21 (2020).

210. Anirudha Malik, Sudhir Chaudhary, G. G. and A. T. Dendrimers: A Tool for Drug Delivery. *Adv. Biol. Res. (Rennes).* (2012) doi:http://dx.doi.org/10.5829/idosi.abr.2012.6.4.6254.

211. Shinde, M., Bhalerao, M., Thakre, S., Franklin, J. & Jain, A. Dendrimers- An Excellent Polymer for Drug Delivery System. *Asian J. Pharm. Res. Dev.* **2**, (2014).

212. Shahi, S., Kulkarni, M., Karva, G., Giram, P. & Gugulkar, R. Review Article:DENDRIMERS. *Int. J. Pharm. Sci. Res.* **33**, 187–198 (2015).

213. Svenson, S. & Tomalia, D. A. Dendrimers in biomedical applications—reflections on the field. *Adv. Drug Deliv. Rev.* **57**, 2106–2129 (2005).

214. Najlah, M. & D'Emanuele, A. Crossing cellular barriers using dendrimer nanotechnologies. *Curr. Opin. Pharmacol.* **6**, 522–527 (2006).

215. Nikzamir, M., Hanifehpour, Y., Akbarzadeh, A. & Panahi, Y. Applications of Dendrimers in Nanomedicine and Drug Delivery: A Review. *J. Inorg. Organomet. Polym. Mater.* **31**, 1–16 (2021).

216. Hegde, N., Velingkar, V. & Prabhakar, B. An Update on Design and Pharmacology of Dendritic Poly(l-lysine). *Int. J. Pept. Res. Ther.* **25**, 1539–1562 (2019).

217. Grayson, S. M. & Fréchet, J. M. J. Convergent Dendrons and Dendrimers: from Synthesis to Applications. *Chem. Rev.* **101**, 3819–3868 (2001).

218. Pérez-Ferreiro, M., M. Abelairas, A., Criado, A., Gómez, I. J. & Mosquera, J. Dendrimers: Exploring Their Wide Structural Variety and Applications. *Polymers (Basel).* **15**, (2023).

219. Gupta, V. & Nayak, S. Dendrimers: A Review on Synthetic Approaches. *J. Appl. Pharm. Sci.* 117–122 (2015) doi:10.7324/japs.2015.50321.

220. Sowinska, M. & Urbanczyk-Lipkowska, Z. Advances in the chemistry of dendrimers. *New J. Chem.* **38**, 2168–2203 (2014).

221. Amblard, M., Fehrentz, J.-A., Martinez, J. & Subra, G. Methods and protocols of modern solid phase peptide synthesis. *Mol. Biotechnol.* **33**, 239–254 (2006).

222. Wells, N. J., Basso, A. & Bradley, M. Solid-phase dendrimer synthesis. *Pept. Sci.* **47**, 381–396 (1998).

223. Czarnik, A. W. Solid-phase synthesis supports are like solvents. *Biotechnol. Bioeng.* **61**, 77–79 (1998).

224. Merrifield, R. B. Solid Phase Peptide Synthesis. I. The Synthesis of a Tetrapeptide. *J. Am. Chem. Soc.* **85**, 2149–2154 (1963).

225. Albericio, F. Orthogonal protecting groups for Nα-amino and C-terminal carboxyl functions in solid-phase peptide synthesis. *Pept. Sci.* **55**, 123–139 (2000).

226. Perugini, V., Meikle, S. T., Guildford, A. L. & Santin, M. Hyperbranched poly(ϵ-lysine) substrate presenting the laminin sequence YIGSR induces the formation of spheroids in adult bone marrow stem cells. *PLoS One* **12**, e0187182 (2017).

227. Meikle, S., Perugini, V., Guildford, A. & Santin, M. Synthesis, Characterisation and in vitro Anti-Angiogenic Potential of Dendron VEGF Blockers. *Macromol. Biosci.* **11**, 1761–1765 (2011).

228. Sutcliffe-Goulden, J. L., O'Doherty, M. J. & Bansal, S. S. Solid phase synthesis of [18F]Labelled peptides for positron emission tomography. *Bioorg. Med. Chem. Lett.* **10**, 1501–1503 (2000).

229. FIELDS, G. B. & NOBLE, R. L. Solid phase peptide synthesis utilizing 9-fluorenylmethoxycarbonyl amino acids. *Int. J. Pept. Protein Res.* **35**, 161–214 (1990).

230. Perugini, V. & Santin, M. The Real-Time Validation of the Effectiveness of Third-Generation Hyperbranched Poly(ɛ-lysine) Dendrons-Modified KLVFF Sequences to Bind Amyloid-β1-42 Peptides Using an Optical Waveguide Light-Mode Spectroscopy System. *Sensors* vol. 22 (2022).

231. Miller, K. D. *et al.* Cancer treatment and survivorship statistics, 2019. *CA. Cancer J. Clin.* **69**, 363–385 (2019).

232. Paplomata, E. & O'Regan, R. The PI3K/AKT/mTOR pathway in breast cancer: targets, trials and biomarkers. *Ther. Adv. Med. Oncol.* **6**, 154–166 (2014).

233. Serova, O. V *et al.* Autophosphorylation of Orphan Receptor ERBB2 Can Be Induced by Extracellular Treatment with Mildly Alkaline Media. *International Journal of Molecular Sciences* vol. 20 (2019).

234. Kallioniemi, O. P. *et al.* ERBB2 amplification in breast cancer analyzed by fluorescence in situ hybridization. *Proc. Natl. Acad. Sci.* **89**, 5321–5325 (1992).

235. Wang, F. *et al.* Computational Model to Explore the Endocrine Response to Trastuzumab Action in HER-2/neu Positive Breast Cancer. *Saudi J. Biol. Sci.* **29**, 123–131 (2022).

236. Jin, J.-F. *et al.* The optimal choice of medication administration route regarding intravenous, intramuscular, and subcutaneous injection. *Patient Prefer. Adherence* **9**, 923–942 (2015).

237. Lee, K. B., Dunn, Z. S., Lopez, T., Mustafa, Z. & Ge, X. Generation of highly selective monoclonal antibodies inhibiting a recalcitrant protease using decoy designs. *Biotechnol. Bioeng.* **117**, 3664–3676 (2020).

238. McKeage, K. & Perry, C. M. Trastuzumab. *Drugs* **62**, 209–243 (2002).

239. Scolnik, P. A. mAbs. *MAbs* **1**, 179–184 (2009).

240. Chames, P., Van Regenmortel, M., Weiss, E. & Baty, D. Therapeutic antibodies: successes, limitations and hopes for the future. *Br. J. Pharmacol.* **157**, 220–233 (2009).

241. Martins, F. *et al.* Adverse effects of immune-checkpoint inhibitors: epidemiology, management and surveillance. *Nat. Rev. Clin. Oncol.* **16**, 563–580 (2019).

242. Torka, P., Barth, M., Ferdman, R. & Hernandez-Ilizaliturri, F. J. Mechanisms of Resistance to Monoclonal Antibodies (mAbs) in Lymphoid Malignancies. *Curr. Hematol. Malig. Rep.* **14**, 426–438 (2019).

243. Pintea, I. *et al.* Hypersensitivity reactions to monoclonal antibodies: Classification and treatment approach (Review). *Exp Ther Med* **22**, 949 (2021).

244. Price, L. & Brunt, A. M. Trastuzumab infusion reactions in breast cancer. Should we routinely observe after the first dose? *Eur. J. Hosp. Pharm.* **25**, 331 LP – 333 (2018).

245. Chen, Z. & Ai, D. Cardiotoxicity associated with targeted cancer therapies (Review). *Mol Clin Oncol* **4**, 675–681 (2016).

246. Fischman, A. J., Babich, J. W. & Strauss, H. W. A ticket to ride: peptide radiopharmaceuticals. *J. Nucl. Med.* **34**, 2253–2263 (1993).

247. Landon, A. L., Zou, J. & Deutscher, L. S. Is Phage Display Technology on Target for Developing Peptide-Based Cancer Drugs? *Current Drug Discovery Technologies* vol. 1 113–132 (2004).

248. Bakker, W. H. *et al.* In vivo application of [111In-DTPA-D-Phe1]-octreotide for detection of somatostatin receptor-positive tumors in rats. *Life Sci.* **49**, 1593–1601 (1991).

249. Miao, Y. *et al.* In vivo evaluation of 188Re-labeled alpha-melanocyte stimulating hormone peptide analogs for melanoma therapy. *Int. J. Cancer* **101**, 480–487 (2002).

250. Karasseva, N. G., Glinsky, V. V, Chen, N. X., Komatireddy, R. & Quinn, T. P. Identification and Characterization of Peptides That Bind Human ErbB-2 Selected from a Bacteriophage Display Library. *J. Protein Chem.* **21**, 287–296 (2002).

251. Suga, T., Fuchigami, Y., Hagimori, M. & Kawakami, S. Ligand peptide-grafted PEGylated liposomes using HER2 targeted peptide-lipid derivatives for targeted delivery in breast cancer cells: The effect of serine-glycine repeated peptides as a spacer. *Int. J. Pharm.* **521**, 361–364 (2017).

252. Aina, O. H., Sroka, T. C., Chen, M.-L. & Lam, K. S. Therapeutic cancer targeting peptides. *Pept. Sci.* **66**, 184–199 (2002).

253. Arnold, L. J., Dagan, A., Gutheil, J. & Kaplan, N. O. Antineoplastic activity of poly(L-lysine) with some ascites tumor cells. *Proc. Natl. Acad. Sci.* **76**, 3246–3250 (1979).

254. Szende, B. *et al.* Antitumor effect of lysine-isopeptides. *Cancer Cell Int.* **2**, (2002).

255. Debnath, S., Mukherjee, A., Saha, D., Dash, J. & Chatterjee, T. K. Poly-l-Lysine inhibits VEGF and c-Myc mediated tumor-angiogenesis and induces apoptosis in 2D and 3D tumor microenvironment of both MDA-MB-231 and B16F10 induced mice model. *Int. J. Biol. Macromol.* **183**, 528–548 (2021).

256. Wong, R. S. Y. Apoptosis in cancer: From pathogenesis to treatment. *J. Exp. Clin. Cancer Res.* **30**, (2011).

257. Fulda, S. & Debatin, K.-M. Extrinsic versus intrinsic apoptosis pathways in anticancer chemotherapy. *Oncogene* **25**, 4798–4811 (2006).

258. Westphal, D., Dewson, G., Czabotar, P. E. & Kluck, R. M. Molecular biology of Bax and Bak activation and action. *Biochim. Biophys. Acta - Mol. Cell Res.* **1813**, 521–531 (2011).

259. Handayani, T., Sakinah, S., Nallappan, M. & Pihie, A. H. L. Regulation of p53-, Bcl-2- and caspase-dependent signaling pathway in xanthorrhizol-induced apoptosis of HepG2 hepatoma cells. *Anticancer Res.* **27**, 965–971 (2007).

260. Ribatti, D., Vacca, A. & Dammacco, F. The Role of the Vascular Phase in Solid Tumor Growth: A Historical Review. *Neoplasia* **1**, 293–302 (1999).

261. Lee, S.-M. & Kim, K.-Y. Multi-objective optimization of arc-shaped ribs in the channels of a printed circuit heat exchanger. *Int. J. Therm. Sci.* **94**, 1–8 (2015).

262. Quail, D. F. & Joyce, J. A. Microenvironmental regulation of tumor progression and metastasis. *Nat. Med.* **19**, 1423–1437 (2013).

263. Niu, G. & Chen, X. Vascular endothelial growth factor as an anti-angiogenic target for cancer therapy. *Curr. Drug Targets* **11**, 1000–1017 (2010).

264. Zhang, X. *et al.* Apoptosis and cell proliferation in proliferative retinal disorders: PCNA, Ki-67, caspase-3, and PARP expression. *Curr. Eye Res.* **30**, 395–403 (2005).

265. Debnath, S., Mukherjee, A., Karan, S., Debnath, M. & Chatterjee, T. K. Induction of apoptosis, anti-proliferation, tumor-angiogenic suppression and down-regulation of Dalton's Ascitic Lymphoma (DAL) induced tumorigenesis by poly-l-lysine: A mechanistic study. *Biomed. Pharmacother.* **102**, 1064–1076 (2018).

266. Hoffman, B. & Liebermann, D. A. Apoptotic signaling by c-MYC. *Oncogene* **27**, 6462–6472 (2008).

267. Kumar, S. R. *et al.* In Vitro and In Vivo Evaluation of 64Cu-Radiolabeled KCCYSL Peptides for Targeting Epidermal Growth Factor Receptor-2 in Breast Carcinomas. *Cancer Biother. Radiopharm.* **25**, 693–703 (2010).

268. Fogh, J., Fogh, J. M. & Orfeo, T. One Hundred and Twenty-Seven Cultured Human Tumor Cell Lines Producing Tumors in Nude Mice23. *JNCI J. Natl. Cancer Inst.* **59**, 221–226 (1977).

269. Lacroix, M. & Leclercq, G. Relevance of Breast Cancer Cell Lines as Models for Breast Tumours: An Update. *Breast Cancer Res. Treat.* **83**, 249–289 (2004).

270. Carr, J. R., Park, H. J., Wang, Z., Kiefer, M. M. & Raychaudhuri, P. FoxM1 Mediates

Resistance to Herceptin and Paclitaxel. *Cancer Res.* **70**, 5054–5063 (2010).

271. Park, S., Nedrow, J., Josefsson, A. & Sgouros, G. Human HER2 overexpressing mouse breast cancer cell lines derived from MMTV.f.HuHER2 mice: Characterization and use in a model of metastatic breast cancer. *Oncotarget* **8**, (2017).

272. Lopez-Albaitero, A. *et al.* Overcoming resistance to HER2-targeted therapy with a novel HER2/CD3 bispecific antibody. *Oncoimmunology* **6**, e1267891 (2017).

273. Biri-Kovács, B. *et al.* Structure–Activity Relationship of HER2 Receptor Targeting Peptide and Its Derivatives in Targeted Tumor Therapy. *Biomolecules* vol. 10 (2020).

274. Barrett, T., Ravizzini, G., Choyke, P. L. & Kobayashi, H. Dendrimers in medical nanotechnology. *IEEE Eng. Med. Biol. Mag.* **28**, 12–22 (2009).

275. Zhu, Y., Liu, C. & Pang, Z. Dendrimer-Based Drug Delivery Systems for Brain Targeting. *Biomolecules* vol. 9 (2019).

276. Wang, J., Li, B., Qiu, L., Qiao, X. & Yang, H. Dendrimer-based drug delivery systems: history, challenges, and latest developments. *J. Biol. Eng.* **16**, 18 (2022).

277. Yang, D. H., Kim, H. J., Park, K., Kim, J. K. & Chun, H. J. Preparation of poly-l-lysine-based nanoparticles with pH-sensitive release of curcumin for targeted imaging and therapy of liver cancer in vitro and in vivo. *Drug Deliv.* **25**, 950–960 (2018).

278. Avaritt, B. R. & Swaan, P. W. Internalization and Subcellular Trafficking of Poly-l-lysine Dendrimers Are Impacted by the Site of Fluorophore Conjugation. *Mol. Pharm.* **12**, 1961–1969 (2015).

279. Kamaruzaman, K., Moyle, P. & Toth, I. Peptide-Based Multicomponent Oligonucleotide Delivery Systems: Optimisation of Poly-L-lysine Dendrons for Plasmid DNA Delivery. *Int. J. Pept. Res. Ther.* **23**, (2017).

280. Ferruti, P., Knobloch, S., Ranucci, E., Duncan, R. & Gianasi, E. A novel modification of poly(L-lysine) leading to a soluble cationic polymer with reduced toxicity and with potential as a transfection agent. *Macromol. Chem. Phys.* **199**, 2565–2575 (1998).

281. Granier, F. *et al.* Assessment of Dendrigrafts of Poly-l-lysine Cytotoxicity and Cell Penetration in Cancer Cells. *ACS Appl. Polym. Mater.* **4**, 908–919 (2022).

282. He, J., Xu, S. & Mixson, A. The Multifaceted Histidine-Based Carriers for Nucleic Acid Delivery: Advances and Challenges. *Pharmaceutics* **12**, 774 (2020).

283. Freeman, E. C., Weiland, L. M. & Meng, W. S. Modeling the proton sponge hypothesis: examining proton sponge effectiveness for enhancing intracellular gene delivery through multiscale modeling. *J. Biomater. Sci. Polym. Ed.* **24**, 398–416 (2013).

284. Read, M. L. *et al.* A versatile reducible polycation-based system for efficient delivery of a broad range of nucleic acids. *Nucleic Acids Res.* **33**, e86–e86 (2005).

285. Sun, Z. & Zhou, D. PLL/PAE/DNA ternary complexes with enhanced endosomal escape ability for efficient and safe gene transfection. *New J. Chem.* **40**, 9806–9812 (2016).

286. Kwok, A., Eggimann, G. A., Reymond, J.-L., Darbre, T. & Hollfelder, F. Peptide Dendrimer/Lipid Hybrid Systems Are Efficient DNA Transfection Reagents: Structure–Activity Relationships Highlight the Role of Charge Distribution Across Dendrimer Generations. *ACS Nano* **7**, 4668–4682 (2013).

287. Kudsiova, L. *et al.* Lipopolyplex Ternary Delivery Systems Incorporating C14 Glycerol-Based Lipids. *Mol. Pharm.* **8**, 1831–1847 (2011).

288. Jafari, M., Soltani, M., Naahidi, S., Karunaratne, N. & Chen, P. Nonviral Approach for Targeted Nucleic Acid Delivery. *Curr. Med. Chem.* **19**, 197–208 (2012).

289. Bellefroid, C. *et al.* Systematic study of liposomes composition towards efficient delivery of plasmid DNA as potential application of dermal fibroblasts targeting. *Int. J. Pharm.* **593**, 120122 (2021).

290. Mohammadi, A. *et al.* The discovery and enhanced properties of trichain lipids in lipopolyplex gene delivery systems. *Org. Biomol. Chem.* **17**, 945–957 (2019).

291. Elouahabi, A. & Ruysschaert, J.-M. Formation and Intracellular Trafficking of Lipoplexes and Polyplexes. *Mol. Ther.* **11**, 336–347 (2005).

292. Mok, K. W. C., Lam, A. M. I. & Cullis, P. R. Stabilized plasmid-lipid particles: factors influencing plasmid entrapment and transfection properties. *Biochim. Biophys. Acta - Biomembr.* **1419**, 137–150 (1999).

293. Ramezani, M., Khoshhamdam, M., Dehshahri, A. & Malaekeh-Nikouei, B. The influence of size, lipid composition and bilayer fluidity of cationic liposomes on the transfection efficiency of nanolipoplexes. *Colloids Surfaces B Biointerfaces* **72**, 1–5 (2009).

294. Malaekeh-Nikouei, B., Malaekeh-Nikouei, M., Oskuee, R. K. & Ramezani, M. Preparation, characterization, transfection efficiency, and cytotoxicity of liposomes containing oligoamine-modified cholesterols as nanocarriers to Neuro2A cells. *Nanomedicine Nanotechnology, Biol. Med.* **5**, 457–462 (2009).

295. Patnaik, S. & Gupta, K. C. Novel polyethylenimine-derived nanoparticles for in vivo gene delivery. *Expert Opin. Drug Deliv.* **10**, 215–228 (2013).

296. Ewe, A. *et al.* Storage stability of optimal liposome-polyethylenimine complexes (lipopolyplexes) for DNA or siRNA delivery. *Acta Biomater.* **10**, 2663–2673 (2014).

297. Dizaj, S. M., Jafari, S. & Khosroushahi, A. Y. A sight on the current nanoparticle-based gene delivery vectors. *Nanoscale Res. Lett.* **9**, 1–9 (2014).

298. Rezaee, M., Oskuee, R. K., Nassirli, H. & Malaekeh-Nikouei, B. Progress in the development of lipopolyplexes as efficient non-viral gene delivery systems. *J. Control. Release* **236**, 1–14 (2016).

299. Luo, K. *et al.* Peptide dendrimers as efficient and biocompatible gene delivery

vectors: Synthesis and in vitro characterization. *J. Control. Release* **155**, 77–87 (2011).

300. Hofman, J. *et al.* In Vitro Transfection Mediated by Dendrigraft Poly(L-lysines): The Effect of Structure and Molecule Size. *Macromol. Biosci.* **13**, 167–176 (2013).

301. Lee, H., Jeong, J. H. & Park, T. G. PEG grafted polylysine with fusogenic peptide for gene delivery: high transfection efficiency with low cytotoxicity. *J. Control. Release* **79**, 283–291 (2002).

302. Kudsiova, L. *et al.* Delivery of siRNA using ternary complexes containing branched cationic peptides: the role of peptide sequence, branching and targeting. *Mol. Biosyst.* **12**, 934–951 (2016).

303. Welser, K. *et al.* Gene Delivery Using Ternary Lipopolyplexes Incorporating Branched Cationic Peptides: The Role of Peptide Sequence and Branching. *Mol. Pharm.* **10**, 127–141 (2013).

304. Zhuanglin, S. *et al.* Polymer–Nucleic Acid Interactions. *Top. Curr. Chem.* **375**, (2017).

305. Amarakoon, I. I., Hamilton, C.-L., Mitchell, S. A., Tennant, P. F. & Roye, M. E. Chapter 28 - Biotechnology. in (eds. Badal, S. & Delgoda, R. B. T.-P.) 549–563 (Academic Press, 2017). doi:https://doi.org/10.1016/B978-0-12-802104-0.00028-7.

306. Jiang, J.-Q., Chanseau, C., Alves, I. D., Nlate, S. & Durrieu, M.-C. Dendron-Functionalized Surface: Efficient Strategy for Enhancing the Capture of Microvesicles. *iScience* **21**, 110–123 (2019).

307. Lai, Z. *et al.* Self-Assembling Peptide Dendron Nanoparticles with High Stability and a Multimodal Antimicrobial Mechanism of Action. *ACS Nano* **15**, 15824–15840 (2021).

308. Drexler, C. I., Cyran, J. D. & Webb, L. J. Lipid-Specific Direct Translocation of the Cell-Penetrating Peptide NAF-144–67 across Bilayer Membranes. *J. Phys. Chem. B* **127**, 2002–2010 (2023).

309. No Title.

310. Erbacher, P., Roche, A. C., Monsigny, M. & Midoux, P. The reduction of the positive charges of polylysine by partial gluconoylation increases the transfection efficiency of polylysine/DNA complexes. *Biochim. Biophys. Acta - Biomembr.* **1324**, 27–36 (1997).

311. Patil, M. L., Zhang, M. & Minko, T. Multifunctional Triblock Nanocarrier (PAMAM-PEG-PLL) for the Efficient Intracellular siRNA Delivery and Gene Silencing. *ACS Nano* **5**, 1877–1887 (2011).

312. Brandén, L. J., Mohamed, A. J. & Smith, C. I. E. A peptide nucleic acid–nuclear localization signal fusion that mediates nuclear transport of DNA. *Nat. Biotechnol.* **17**, 784–787 (1999).

313. Chen, J., Gamou, S., Takayanagi, A. & Shimizu, N. A novel gene delivery system using EGF receptor-mediated endocytosis. *FEBS Lett.* **338**, 167–169 (1994).

314. Siegel, D. P. & Epand, R. M. The mechanism of lamellar-to-inverted hexagonal phase transitions in phosphatidylethanolamine: implications for membrane fusion mechanisms. *Biophys. J.* **73**, 3089–3111 (1997).

315. Harvie, P., Wong, F. M. P. & Bally, M. B. Characterization of Lipid DNA Interactions. I. Destabilization of Bound Lipids and DNA Dissociation. *Biophys. J.* **75**, 1040–1051 (1998).

316. Simões, S. *et al.* Mechanisms of gene transfer mediated by lipoplexes associated with targeting ligands or pH-sensitive peptides. *Gene Ther.* **6**, 1798–1807 (1999).

317. Elder, R. M., Emrick, T. & Jayaraman, A. Understanding the Effect of Polylysine Architecture on DNA Binding Using Molecular Dynamics Simulations. *Biomacromolecules* **12**, 3870–3879 (2011).

318. Ducharme, M. & Lapi, S. E. Peptide Based Imaging Agents for HER2 Imaging in Oncology. *Mol. Imaging* **19**, 1536012120960258–1536012120960258 (2020).

319. Rewatkar, P. V, Parekh, H. S. & Parat, M.-O. Molecular Determinants of the Cellular Entry of Asymmetric Peptide Dendrimers and Role of Caveolae. *PLoS One* **11**, e0147491 (2016).

320. Kiss, A. L. & Botos, E. Endocytosis via caveolae: alternative pathway with distinct cellular compartments to avoid lysosomal degradation? *J. Cell. Mol. Med.* **13**, 1228–1237 (2009).

321. Friend, D. S., Papahadjopoulos, D. & Debs, R. J. Endocytosis and intracellular processing accompanying transfection mediated by cationic liposomes. *Biochim. Biophys. Acta - Biomembr.* **1278**, 41–50 (1996).

322. Hong, C. A., Son, H. Y. & Nam, Y. S. Layer-by-layer siRNA/poly(L-lysine) Multilayers on Polydopamine-coated Surface for Efficient Cell Adhesion and Gene Silencing. *Sci. Rep.* **8**, 7738 (2018).

323. Carthew, R. W. & Sontheimer, E. J. Origins and Mechanisms of miRNAs and siRNAs. *Cell* **136**, 642–655 (2009).

324. Zhu, Y., Zhu, L., Wang, X. & Jin, H. RNA-based therapeutics: an overview and prospectus. *Cell Death Dis.* **13**, 644 (2022).

325. Hu, B. *et al.* Therapeutic siRNA: state of the art. *Signal Transduct. Target. Ther.* **5**, 101 (2020).

326. Kulkarni, J. A., Witzigmann, D., Chen, S., Cullis, P. R. & van der Meel, R. Lipid Nanoparticle Technology for Clinical Translation of siRNA Therapeutics. *Acc. Chem. Res.* **52**, 2435–2444 (2019).

327. Zhang, C. *et al.* Modification of Lipid-Based Nanoparticles: An Efficient Delivery System for Nucleic Acid-Based Immunotherapy. *Molecules* vol. 27 (2022).

328. Hoy, S. M. Patisiran: First Global Approval. *Drugs* **78**, 1625–1631 (2018).

329. Yang, J. Patisiran for the treatment of hereditary transthyretin-mediated amyloidosis. *Expert Rev. Clin. Pharmacol.* **12**, 95–99 (2019).

330. Agarwal, S. *et al.* Impact of Serum Proteins on the Uptake and RNAi Activity of GalNAc-Conjugated siRNAs. *Nucleic Acid Ther.* **31**, 309–315 (2021).

331. Syed, Y. Y. Givosiran: A Review in Acute Hepatic Porphyria. *Drugs* **81**, 841–848 (2021).

332. Lamb, Y. N. Inclisiran: First Approval. *Drugs* **81**, 389–395 (2021).

333. Springer, A. D. & Dowdy, S. F. GalNAc-siRNA Conjugates: Leading the Way for Delivery of RNAi Therapeutics. *Nucleic Acid Ther.* **28**, 109–118 (2018).

334. Prakash, T. P. *et al.* Targeted delivery of antisense oligonucleotides to hepatocytes using triantennary N-acetyl galactosamine improves potency 10-fold in mice. *Nucleic Acids Res.* **42**, 8796–8807 (2014).

335. Yonezawa, S., Koide, H. & Asai, T. Recent advances in siRNA delivery mediated by lipid-based nanoparticles. *Adv. Drug Deliv. Rev.* **154–155**, 64–78 (2020).

336. Santos, S. S. *et al.* Peptide dendrimers: drug/gene delivery and other approaches. *Can. J. Chem.* **95**, 907–916 (2017).

337. Luo, K. *et al.* Arginine functionalized peptide dendrimers as potential gene delivery vehicles. *Biomaterials* **33**, 4917–4927 (2012).

338. Alazzo, A. *et al.* Investigating histidinylated highly branched poly(lysine) for siRNA delivery. *J. Mater. Chem. B* **10**, 236–246 (2022).

339. Ochoa, S. V, Casas, Z., Albarracín, S. L., Sutachan, J. J. & Torres, Y. P. Therapeutic potential of TRPM8 channels in cancer treatment . *Frontiers in Pharmacology* vol. 14 (2023).

340. Klauber, T. C. B., Søndergaard, R. V, Sawant, R. R., Torchilin, V. P. & Andresen, T. L. Elucidating the role of free polycations in gene knockdown by siRNA polyplexes. *Acta Biomater.* **35**, 248–259 (2016).

341. Mergler, S. *et al.* Transient Receptor Potential Channel TRPM8 Agonists Stimulate Calcium Influx and Neurotensin Secretion in Neuroendocrine Tumor Cells. *Neuroendocrinology* **85**, 81–92 (2007).

342. Thiery, J. P. Epithelial–mesenchymal transitions in development and pathologies. *Curr. Opin. Cell Biol.* **15**, 740–746 (2003).

343. Lang, S. H. *et al.* Enhanced expression of vimentin in motile prostate cell lines and in poorly differentiated and metastatic prostate carcinoma. *Prostate* **52**, 253–263 (2002).

344. Singh, R., Pervin, S., Karimi, A., Cederbaum, S. & Chaudhuri, G. Arginase Activity in Human Breast Cancer Cell Lines: Nω-Hydroxy-l-arginine Selectively Inhibits Cell Proliferation and Induces Apoptosis in MDA-MB-468 Cells1. *Cancer Res.* **60**, 3305–3312 (2000).

345. Kumar Thimmaraju, M., Trivedi, R., Hemalatha, G., Thirupathy, B. & Mohathasim Billah, A. Microfluidic revolution and its impact on pharmaceutical materials: A review. *Mater. Today Proc.* (2023) doi:https://doi.org/10.1016/j.matpr.2023.03.096.

346. Sun, J., Warden, A. R. & Ding, X. Recent advances in microfluidics for drug screening. *Biomicrofluidics* **13**, 61503 (2019).

347. Ahmed, M. U., Saaem, I., Wu, P. C. & Brown, A. S. Personalized diagnostics and biosensors: a review of the biology and technology needed for personalized medicine. *Crit. Rev. Biotechnol.* **34**, 180–196 (2014).

348. Terry, S. C., Jerman, J. H. & Angell, J. B. A gas chromatographic air analyzer fabricated on a silicon wafer. *IEEE Trans. Electron Devices* **26**, 1880–1886 (1979).

349. Whitesides, G. M. The origins and the future of microfluidics. *Nature* **442**, 368–373 (2006).

350. Manz, A., Graber, N. & Widmer, H. M. Miniaturized total chemical analysis systems: A novel concept for chemical sensing. *Sensors Actuators B Chem.* **1**, 244–248 (1990).

351. Chen, X. Topology optimization of microfluidics — A review. *Microchem. J.* **127**, 52–61 (2016).

352. Brody, J. P., Yager, P., Goldstein, R. E. & Austin, R. H. Biotechnology at low Reynolds numbers. *Biophys. J.* **71**, 3430–3441 (1996).

353. Sohrabi, S., kassir, N. & Keshavarz Moraveji, M. Retracted Article: Droplet microfluidics: fundamentals and its advanced applications. *RSC Adv.* **10**, 27560–27574 (2020).

354. Preetam, S. *et al.* Emergence of microfluidics for next generation biomedical devices. *Biosens. Bioelectron. X* **10**, 100106 (2022).

355. Di Carlo, D. Inertial microfluidics. *Lab Chip* **9**, 3038–3046 (2009).

356. Tice, J. D., Song, H., Lyon, A. D. & Ismagilov, R. F. Formation of Droplets and Mixing in Multiphase Microfluidics at Low Values of the Reynolds and the Capillary Numbers. *Langmuir* **19**, 9127–9133 (2003).

357. Li, B. & Kwok, D. Y. Lattice Boltzmann Model of Microfluidics with High Reynolds Numbers in the Presence of External Forces. *Langmuir* **19**, 3041–3048 (2003).

358. Al-wdan, O. A. *et al.* Insights into microfabrication and implementation of microfluidics in pharmaceutical drug delivery and analysis. *OpenNano* **12**, 100156 (2023).

359. Yang, L. *et al.* Recent Advances in Lipid Nanoparticles for Delivery of mRNA. *Pharmaceutics* vol. 14 (2022).

360. Wang, J. *et al.* Droplet Microfluidics for the Production of Microparticles and Nanoparticles. *Micromachines* **8**, 22 (2017).

361. Håti, A. G. *et al.* Versatile, cell and chip friendly method to gel alginate in microfluidic devices. *Lab Chip* **16**, 3718–3727 (2016).

362. Greijer, A. E. & Wall, E. van der. The role of hypoxia inducible factor 1 (HIF-1) in hypoxia induced apoptosis. *J. Clin. Pathol.* **57**, 1009 LP – 1014 (2004).

363. Vaupel, P., Mayer, A. & Höckel, M. B. T.-M. in E. Tumor Hypoxia and Malignant Progression. in *Oxygen Sensing* vol. 381 335–354 (Academic Press, 2004).

364. Jing, X. *et al.* Role of hypoxia in cancer therapy by regulating the tumor microenvironment. *Mol. Cancer* **18**, 157 (2019).

365. Al Tameemi, W., Dale, T. P., Al-Jumaily, R. M. K. & Forsyth, N. R. Hypoxia-Modified Cancer Cell Metabolism. *Front. Cell Dev. Biol.* **7**, (2019).

366. Thu, B. *et al.* Alginate polycation microcapsules: I. Interaction between alginate and polycation. *Biomaterials* **17**, 1031–1040 (1996).

367. Strand, B. L., Gåserød, O., Kulseng, B., Espevik, T. & Skjåk-Bræk, G. Alginate-polylysine-alginate microcapsules: effect of size reduction on capsule properties. *J. Microencapsul.* **19**, 615–630 (2002).

368. Vankerckhoven *et al.* Opposite Macrophage Polarization in Different Subsets of Ovarian Cancer: Observation from a Pilot Study. *Cells* **9**, 305 (2020).

369. Shieh, H., Saadatmand, M., Eskandari, M. & Bastani, D. Microfluidic on-chip production of microgels using combined geometries. *Sci. Rep.* **11**, 1565 (2021).

370. Chen, Y., Narayan, S. & Dutcher, C. S. Phase-Dependent Surfactant Transport on the Microscale: Interfacial Tension and Droplet Coalescence. *Langmuir* **36**, 14904–14923 (2020).

371. Oveysi, M., Zaker, M. A., Peregrino, G., Bazargan, V. & Marengo, M. Droplet-based fabrication of alginate hydrogel microparticles in presence of surfactants. *Microfluid. Nanofluidics* **27**, 45 (2023).

372. Yasmin, F., Chen, X. & Eames, B. F. Effect of Process Parameters on the Initial Burst Release of Protein-Loaded Alginate Nanospheres. *Journal of Functional Biomaterials* vol. 10 (2019).

373. Cooke, T., Reeves, J., Lanigan, A. & Stanton, P. HER2 as a prognostic and predictive marker for breast cancer. *Ann. Oncol.* **12**, S23–S28 (2001).

374. Tai, W., Mahato, R. & Cheng, K. The role of HER2 in cancer therapy and targeted drug delivery. *J. Control. Release* **146**, 264–275 (2010).

375. Giaquinto, A. N. *et al.* Breast Cancer Statistics, 2022. *CA. Cancer J. Clin.* **72**, 524–541 (2022).

376. Hsu, J. L. & Hung, M.-C. The role of HER2, EGFR, and other receptor tyrosine kinases in breast cancer. *Cancer Metastasis Rev.* **35**, 575–588 (2016).

377. Meric-Bernstam, F. *et al.* Advances in HER2-Targeted Therapy: Novel Agents and Opportunities Beyond Breast and Gastric Cancer. *Clin. Cancer Res.* **25**, 2033–2041

(2019).

378. Hasmann. Chapter 9 - Targeting HER2 by monoclonal antibodies for cancer therapy. in (eds. Ganellin, R., Roberts, S. & Jefferis, R. B. T.-I. to B. and S. M. D. R. and D.) 283–305 (Elsevier, 2013). doi:https://doi.org/10.1016/B978-0-12-397176-0.00009-1.

379. Mezynski, M. J. *et al.* Targeting the PI3K and MAPK pathways to improve response to HER2-targeted therapies in HER2-positive gastric cancer. *J. Transl. Med.* **19**, 184 (2021).

380. Albini, A. *et al.* Cardio-oncology in targeting the HER receptor family: the puzzle of different cardiotoxicities of HER2 inhibitors. *Future Cardiol.* **7**, 693–704 (2011).

381. Symonds, P. *et al.* Low and high molecular weight poly(l-lysine)s/poly(l-lysine)–DNA complexes initiate mitochondrial-mediated apoptosis differently. *FEBS Lett.* **579**, 6191–6198 (2005).

382. Mukherjee, A., Debnath, S., Bhowmik, A. & Biswas, S. DNA interactive property of poly-L-lysine induces apoptosis in MCF-7 cells through DNA interaction. *J. Biochem. Mol. Toxicol.* **37**, e23378 (2023).

383. Chis, A. A. *et al.* Applications and Limitations of Dendrimers in Biomedicine. *Molecules* vol. 25 (2020).

384. Torres-Vanegas, J. D., Cruz, J. C. & Reyes, L. H. Delivery Systems for Nucleic Acids and Proteins: Barriers, Cell Capture Pathways and Nanocarriers. *Pharmaceutics* vol. 13 (2021).

385. Panigaj, M. *et al.* Therapeutic immunomodulation by rationally designed nucleic acids and nucleic acid nanoparticles . *Frontiers in Immunology* vol. 14 (2023).

386. Zuhorn, I. S. *et al.* Nonbilayer phase of lipoplex–membrane mixture determines endosomal escape of genetic cargo and transfection efficiency. *Mol. Ther.* **11**, 801–810 (2005).

387. Kumar, A., Gupta, T., Berzsenyi, S. & Giangrande, A. N-cadherin negatively regulates collective Drosophila glial migration through actin cytoskeleton remodeling. *J. Cell Sci.* **128**, 900–912 (2015).

388. Su, G. *et al.* Size-Dependent Facilitation of Cancer Cell Targeting by Proteins Adsorbed on Nanoparticles. *ACS Appl. Mater. Interfaces* **8**, 30037–30047 (2016).

389. Desai, M. P., Labhasetwar, V., Walter, E., Levy, R. J. & Amidon, G. L. The Mechanism of Uptake of Biodegradable Microparticles in Caco-2 Cells Is Size Dependent. *Pharm. Res.* **14**, 1568–1573 (1997).

390. Hammond, E. M. & Giaccia, A. J. The role of p53 in hypoxia-induced apoptosis. *Biochem. Biophys. Res. Commun.* **331**, 718–725 (2005).

391. Chen, Z., Han, F., Du, Y., Shi, H. & Zhou, W. Hypoxic microenvironment in cancer: molecular mechanisms and therapeutic interventions. *Signal Transduct. Target. Ther.* **8**, 70 (2023).

392. Zheng, M. *et al.* Poly(α-l-lysine)-based nanomaterials for versatile biomedical applications: Current advances and perspectives. *Bioact. Mater.* 6, 1878–1909 (2021).